The copyright of this thesis vests in the author. No quotation from it or information derived from it is to be published without full acknowledgement of the source. The thesis is to be used for private study or non-commercial research purposes only.

Published by the University of Cape Town (UCT) in terms of the non-exclusive license granted to UCT by the author.

University of Cape Town

SURFACE CHARACTERISATION AND FLOTATION BEHAVIOUR OF THE PLATINUM AND PALLADIUM ARSENIDE, TELLURIDE AND SULPHIDE MINERAL SPECIES

By

Natalie Jean Shackleton

University of Cape Town

Thesis Presented for the Degree of
DOCTOR OF PHILOSOPHY

Faculty of Chemical Engineering and Built Environment
UNIVERSITY OF CAPE TOWN

June 2007

"A man can succeed at almost anything for which he has unlimited enthusiasm."

--Charles M. Schwab

University of Cape Town

ACKNOWLEDGEMENTS

I would like to thank and express my sincere gratitude to the following people and institutes;

- Anglo Platinum management for their support during the study and permission to publish the thesis.
- Professor C.T. O'Connor for his guidance and valuable suggestions during the course of this study.
- Dr. V. Malysiak for his guidance during the study.
- Professor D. W. Fuerstenau for his guidance during the initially stages of the study.
- Spectrau (University of Johannesburg) for the XRD analyses and ACeSSS (Division of Information, Engineering & Environment, University of South Australia) for the XPS analyses.
- Professor R. Smart for his interpretation of the XPS results and valuable advice.
- My husband, Andrew, for all his support and encouragement throughout my studies.
- My little boy, Ethan, who gives me so much inspiration.

University of Cape Town

CERTIFICATION BY SUPERVISOR

In terms of paragraph GP 8 of "General rules for the degree of PhD", I, Prof. C.T. O'Connor, as supervisor of the candidate, N.J. Shackleton, certify that I approve of the incorporation in this thesis of material that has been published.

Professor C.T. O'Connor
Faculty of Chemical Engineering and Built Environment
University of Cape Town
Private Bag
Rondebosch
7700

University of Cape Town

TABLE OF CONTENTS

PAGE NO

ACKNOWLEDGEMENTS III

CERTIFICATION BY SUPERVISOR IV

TABLE OF CONTENTS V

LIST OF APPENDICES X

LIST OF FIGURES XI

LIST OF TABLES XVII

NOMENCLATURE XIX

GREEK LETTERS XIX

LIST OF ABBREVIATIONS XX

ABSTRACT XXII

CHAPTER 1 1

LITERATURE REVIEW 1

1.1. Platreef 5

1.2 Mineralogy 7

1.2.1 Platinum and Palladium Sulphides 8

1.2.2 Platinum and Palladium Arsenide 10

1.2.3 Platinum and Palladium Tellurides 11

1.3 Synthesis of the Platinum and Palladium Minerals 14

1.4 Synthetic versus Naturally Occurring Minerals 16

1.5 The Flotation of the PGE Sulphides, Arsenides and Tellurides 17

1.5.1 PGE Sulphides 17

1.5.2 PGE Arsenides 25

1.5.3 PGE Tellurides 27

1.6 Characterisation of the surface of mineral ores using zeta potential determinations, ToF-SIMS and XPS analyses 28

1.6.1 Zeta potential determinations 28

1.6.1.1 Brief description on the theory of zeta potential 28

University of Cape Town

1.6.2 Time of Flight Secondary Ion Mass Spectrometry (ToF-SIMS) *31*
1.6.2.1 Brief description on the theory of ToF-SIMS *31*
1.6.3 X-ray Photoelectron Spectroscopy (XPS) *36*
1.6.3.1 Brief description on the theory of XPS *36*
1.6.4 Research studies using zeta potential, ToF-SIMS and XPS *40*
1.6.4.1 Oxidation studies *40*
1.6.4.2 Copper speciation studies *44*
1.6.4.3 Characterisation of Base metal sulphides *46*
1.6.4.4 Plant related studies *48*
1.6.4.5 General *50*
1.7 Comments Regarding the Literature Review **53**

CHAPTER 2 ..... **54**
OBJECTIVES OF THE RESEARCH **54**

CHAPTER 3 ..... **57**
EXPERIMENTAL METHODS **57**
3.1 Minerals **58**
3.1.1 X-Ray Diffraction (XRD) *60*
3.2 Reagents **62**
3.3 Synthetic Water Composition **62**
3.4 Microflotation Tests **63**
3.4.1 Microflotation Cell Description *63*
3.4.2 Microflotation Procedure *64*
3.5 Surface Characterisation Techniques **66**
3.5.1 Zeta Potential Determinations *66*
3.5.2 Time of Flight Secondary Ion Mass Spectrometry (ToF-SIMS) *66*
3.5.3 X-ray Photoelectron Spectroscopy (XPS) *68*
3.6 HSC Chemistry® Software 69

University of Cape Town

CHAPTER 4 ..... **70**
RESULTS **70**
4.1. MINERALOGICAL CHARACTERISATION **70**
4.1.1 EDS Results **70**
4.1.2 XRD Analysis **77**
4.1.2.1 Rietveld Refinement for Cooperite NS144 and Vysostkite NS148 . *78*
4.1.2.2 Rietveld Refinement for Sperrylite NS145 and NS145 and Palladoarsenide *80*
4.1.2.3 Rietveld Refinement for Moncheite NS142 and NS153 ..... *81*
4.1.2.4 Rietveld Refinement for Merenskyite NS143 and NS152 ..... *82*
4.2 SURFACE ANALYSIS **84**
4.2.1 Zeta Potential Determinations *84*
4.2.2.1 Reproducibility *84*
4.2.2.2 Zeta Potential Determinations for the Individual Reagents used in the Study
4.2.2.2.1 Cooperite and Vysotskite *86*
4.2.2.2.2 Sperrylite and Palladoarsenide *87*
4.2.2.2.3 Moncheite and Merenskyite *89*
4.2.2 ToF-SIMS Analyses *93*
4.2.2.1 Comparative Surface Analysis of Reagent Additions *93*
4.2.2.1.1 Cooperite *93*
4.2.2.1.2 Vysotskite *94*
4.2.2.1.3 Sperrylite *95*
4.2.2.1.4 Palladoarsenide *97*
4.2.2.1.5 Moncheite *98*
4.2.2.1.6 Merenskyite *103*
4.2.2.2 Ethylenediamine (EDA) Addition *104*
4.2.3 XPS Analyses *106*

4.3 MICROFLOTATION TESTWORK **109**
4.3.1 Reproducibility *110*

University of Cape Town

4.3.2 Cooperite *113*
4.3.2.1 Standard Reagent Regime *113*
4.3.3 Vysotskite *113*
4.3.3.1 Standard Reagent Regime *113*
4.3.4 Sperrylite *114*
4.3.4.1 Standard Reagent Regime *114*
4.3.4.2 Collector Screening *116*
4.3.4.3 Varying Size Fraction Flotation *117*
4.3.5 Palladoarsenide *118*
4.3.5.1 Standard Reagent Regime *118*
4.3.6 Moncheite *119*
4.3.6.1 Standard Reagent Regime *119*
4.3.6.2 Effect of Lower Copper Sulphate Concentations *121*
4.3.6.3 Effect of Oxidation *122*
4.3.6.4 Effect of Varying Size Fractions With and Without Pentlandite Conditioning *122*
4.3.7 Merenskyite *125*
4.3.7.1 Standard Reagent Regime *125*
4.3.7.2 Effect of Calcium Ion Concentration *126*
4.3.7.3 Effect of Bismuth on Moncheite and Merenskyite *127*

CHAPTER 5 ..... **131**
DISCUSSION **131**
5.1 MINERALOGICAL CHARACTERISATION **132**
5.2 SURFACE CHARACTERISATION AND FLOTATION BEHAVIOUR OF THE PGE MINERALS **133**
5.2.1 The role of the xanthate collector in the floatability of the PGE minerals *133*
5.2.2 The role of copper sulphate in the floatability of the PGE minerals in the presence of xanthate *143*
5.2.3 Effect of oxidation in the floatability of the PGE minerals *155*
5.2.3.1 Simulatedf oxidation *155*

University of Cape Town

5.2.3.2 Bismuth and surface alteration 158
5.2.3.3 Oxidation from grinding environment 158
5.2.4 Effect of calcium ion concentration 161
5.2.5 Other collectors 162

CHAPTER 6 164
CONCLUSIONS 164

CHAPTER 7 170
LIST OF REFERENCES 170

University of Cape Town

LIST OF APPENDICES

APPENDIX A: Xanthate and Copper Surface Coverage Calculations 182
APPENDIX B: Zeta Potential Determination Procedure..... 184
APPENDIX C: Microflotation Test Procedure..... 185
APPENDIX D: Example of ToF-SIMS Analysis Spreadsheet..... 186
APPENDIX E: XPS Spectra and interpretation for each of the platinum and palladium sulphide, arsenide and telluride mineral species 187

University of Cape Town

LIST OF FIGURES

PAGE NO

Figure 1.1: Simplified geological map of the Bushveld Complex. The green shades represent the Bushveld rocks, the rose shades are the granite cover rocks, the blue and brown shades represent the pre- and post-Bushvels rocks, respectively. The red circular shape near Rustenburg is the Pilansburg alkali complex (Schouwstra et al., 2000)..... 1

Figure 1.2: A typical concentrator flowsheet..... 3

Figure 1.3: Zonal stratigraphy of the Bushveld Complex..... 5

Figure 1.4: Map of the Platreef..... 6

Figure 1.5: Solid state crystal structure for PtS.
"Source: WebElements [http://www.webelements.com/]"..... 8

Figure 1.6: Solid state crystal structure for PdS.
"Source: WebElements [http://www.webelements.com/]"..... 9

Figure 1.7: Solid state crystal structure for PbS.
"Source: WebElements [http://www.webelements.com/]"..... 11

Figure 1.8: Pd-Bi-Te ternary diagram highlighting the variation in composition of PdBiTe particles (black symbols). The known naturally occurring PdBi-tellurides are Michenerite (PdBiTe), Kotulskite (PdTe), Merenskyite ($PdTe_2$), Sobolevskite (Pd(TeSb)Bi), Polarite (Pd(PbTe)Bi), and Froodite ($PdBi_2$). The compositional ranges (normalised in terms of the three components only) of these mineral compositions (Cabri, 2002) are shown by the coloured areas..... 12

Figure 1.9: Solid state crystal structure for $PdTe_2$.
"Source: WebElements [http://www.webelements.com/]"..... 13

Figure 1.10: Solid state crystal structure for $PtTe_2$.
"Source: WebElements [http://www.webelements.com/]"..... 14

Figure 1.11: Log(Conc.)-pH Diagram for metal-water system of Cu(II) activator at a total metal concentration of 1.00E-05M..... 23

Figure 1.12: Potential-pH Diagram for Cu-Ex system at a total concentration of Cu = 1.00E-04M and EX = 1.00E-04M, showing possible stability area of the compound Cu(OH)EX..... 24

University of Cape Town

Figure 1.13: Schematic representation of the electrical double layer and the potential drop across the double layer. 29
Figure 1.14: A schematic diagram of the SIMS process (Physical Electronics, 2006)..... 32
Figure 1.15: ToF-SIMS layout (Physical Electronics, 1997). 33
Figure 1.16: The separation of ions by Time of Flight (Physical Electronics, 1997). 34
Figure 1.17: Schematic representation of the process for obtaining mass spectrum and secondary ion images using ToF-SIMS (de Vaux, 1997). 35
Figure 1.18: Photoelectric effect (Smart et. al, 2006). 37
Figure 1.19: X-ray fluorescence and Auger process..... 38

Figure 3.3: Microflotation apparatus (Wesseldijk et al., 1999). 63
Figure 3.4: Microflotation trial conducted with 1:1 mixtures of moncheite, NS142, and pentlandite. 65
Figure 3.5: Microflotation trial conducted with 1:1 mixtures of moncheite, NS142, and pentlandite. 65
Figure 3.6: Stirred trial conducted with 1:1 mixtures of moncheite, NS142, and pentlandite. 67
Figure 3.7: Stirred trial conducted with 1:1 mixtures of moncheite, NS142, and pentlandite. 67

Figure 4.1: BSE micrograph of Cooperite (NS144). 71
Figure 4.2: BSE micrograph of Vysotskite (NS148)..... 71
Figure 4.3: BSE micrograph of Sperrylite (NS145). 72
Figure 4.4: BSE micrograph of Sperrylite (NS146). 72
Figure 4.5: BSE micrograph of Palladoarsenide (NS147). 73
Figure 4.6: BSE micrograph of Moncheite (NS142)..... 75
Figure 4.7: BSE micrograph of Moncheite (NS153)..... 75
Figure 4.8: BSE micrograph of Merenskyite (NS143)..... 76
Figure 4.9: BSE micrograph of Merenskyite (NS152)..... 76
Figure 4.10: Zeta potential reproducibility curves over a pH range 4-10 for sperrylite..... 85
Figure 4.11: Zeta potential curves over a pH range 6-10 for Cooperite (NS144) treated with no reagents, SIBX, $CuSO_4$, $CuSO_4$+SIBX. 86

University of Cape Town

Figure 4.12: Zeta potential curves over a pH range 6-10 for Vysotskite (NS148) treated with no reagents, SIBX, $CuSO_4$, $CuSO_4$+SIBX. 87
Figure 4.13: Zeta potential curves over a pH range 6-10 for Sperrylite (NS145) treated with no reagents, SIBX, $CuSO_4$, $CuSO_4$+SIBX. 88
Figure 4.14: Zeta potential curves over a pH range 6-10 for Sperrylite (NS146) treated with no reagents, SIBX, $CuSO_4$, $CuSO_4$+SIBX. 88
Figure 4.15: Zeta potential curves over a pH range 6-10 for Palladoarsenide (NS147) treated with no reagents, SIBX, $CuSO_4$, $CuSO_4$+SIBX. 89
Figure 4.16: Zeta potential curves over a pH range 6-10 for Moncheite (NS142) treated with no reagents, SIBX, $CuSO_4$, $CuSO_4$+SIBX. 90
Figure 4.17: Zeta potential curves over a pH range 6-10 for Moncheite (NS153) treated with no reagents, SIBX, $CuSO_4$, $CuSO_4$+SIBX. 91
Figure 4.18: Zeta potential curves over a pH range 6-10 for Merenskyite (NS143) treated with no reagents, SIBX, $CuSO_4$, $CuSO_4$+SIBX. 92
Figure 4.19: Zeta potential curves over a pH range 6-10 for Merenskyite (NS152) treated with no reagents, SIBX, $CuSO_4$, $CuSO_4$+SIBX. 92
Figure 4.20: Copper ions normalised yield for cooperite NS144. 94
Figure 4.21: Xanthate ions normalised yield for cooperite NS144. 94
Figure 4.22: Copper ions normalised yield for vysotskite NS148. 95
Figure 4.23: Xanthate ions normalised yield for vysotskite NS148. 95
Figure 4.24: Copper ions normalised yield for sperrylite NS145 and NS146. 96
Figure 4.25: Xanthate ions normalised yield for sperrylite NS145 and NS146. 96
Figure 4.26: Sulphur ions normalised yield for sperrylite NS145 and NS146. 97
Figure 4.27: Copper ions normalised yield for palladoarsenide NS147. 98
Figure 4.28: Xanthate ions normalised yield for palladoarsenide NS147. 98
Figure 4.29: Copper ions normalised yield for moncheite NS142 and NS153. 99
Figure 4.30: Xanthate ions normalised yield for moncheite NS142 and NS153. 99
Figure 4.31: Sulphur ions normalised yield for moncheite NS142 and NS153. 100
Figure 4.32: Copper ions normalised yield for moncheite NS153 when the $CuSO_4$ concentration was varied. 101

University of Cape Town

Figure 4.33: Xanthate ions normalised yield for moncheite NS153 when the $CuSO_4$ concentration was varied. 101
Figure 4.34: **A** - Ca+Mg+Al+Si ions normalised yield for moncheite NS142 conditioned with and without pentlandite and floated with (mix A) and without (mix B) pentlandite in the presence of xanthate. **B** - Nickel ions normalised yield for moncheite NS142 conditioned with and without pentlandite and floated with (mix A) and without (mix B) pentlandite in the presence of xanthate. **C** - Iron ions normalised yield for moncheite NS142 conditioned with and without pentlandite and floated with (mix A) and without (mix B) pentlandite in the presence of xanthate. **D** - Xanthate ions normalised yield for moncheite NS142 conditioned with and without pentlandite and floated with (mix A) and without (mix B) pentlandite in the presence of xanthate..... 102
Figure 4.35: Copper ions normalised yield for merenskyite NS143 and NS152. 103
Figure 4.36: Xanthate ions normalised yield for merenskyite NS143 and NS152. 103
Figure 4.37: Sulphur ions normalised yield for merenskyite NS143 and NS152. 104
Figure 4.38: Copper ions normalised yield for Pt minerals with and without ethylenediamine addition. 105
Figure 4.39: Copper ions normalised yield for Pd minerals with and without ethylenediamine addition. 106
Figure 4.40: XPS analysis of sperrylite NS145 conditioned with copper sulphate at pH 9. .. 109
Figure 4.41: XPS analysis of sperrylite NS145 conditioned with copper sulphate followed by xanthate at pH 9. 109
Figure 4.42: Sperrylite reproducibility recovery-time curves for concentrates collected at 2, 4, 6, 10 and 20 minute intervals in synthetic water, I = 3.5E-02..... 111
Figure 4.43: Cooperite (NS144) recovery-time curves at pH 9 comparing no reagents, SIBX and $CuSO_4$+SIBX in synthetic water, I = 3.5E-02. 113
Figure 4.44: Vysotskite (NS148) recovery-time curves at pH 9 comparing no reagents, SIBX and $CuSO_4$+SIBX in synthetic water, I = 3.5E-02. 114
Figure 4.45: Sperrylite (NS145) recovery-time curves at pH 9 comparing no reagents, SIBX and $CuSO_4$+SIBX in synthetic water, I = 3.5E-02. 115

University of Cape Town

Figure 4.46: Sperrylite (NS146) recovery-time curves at pH 9 comparing no reagents, SIBX and $CuSO_4$+SIBX in synthetic water, I = 3.5E-02. 115
Figure 4.47: Sperrylite (NS146) total recoveries comparing various collectors. 116
Figure 4.48: Sperrylite (NS146) recovery-time curves at pH 9 comparing differing size fractions with SIBX. 118
Figure 4.49: Palladoarsenide (NS147) recovery-time curves at pH 9 comparing no reagents, SIBX and $CuSO_4$+SIBX in synthetic water, I = 3.5E-02. 119
Figure 4.50: Moncheite (NS142) recovery-time curves at pH 9 comparing no reagents, SIBX and $CuSO_4$+SIBX in synthetic water, I = 3.5E-02..... 120
Figure 4.51: Moncheite (NS153) recovery-time curves at pH 9 comparing no reagents, SIBX and $CuSO_4$+SIBX in synthetic water, I = 3.5E-02..... 120
Figure 4.52: Moncheite (NS153) recovery-time curves at pH 9 comparing $CuSO_4$ concentrations in synthetic water, I = 3.5E-02..... 121
Figure 4.53: Moncheite (NS142 and NS153) recovery-time curves at pH 9 comparing the minerals with and without oxidation in the presence of SIBX in synthetic water, I = 3.5E-02. 122
Figure 4.54: Moncheite (NS142 and NS153) recovery-time curves at pH 9 comparing various size fractions of the minerals in the presence of SIBX in synthetic water, I = 3.5E-02..... 123
Figure 4.55: Moncheite (NS142) recovery-time curves at pH 9 comparing with and without pentlandite in the mixture in the presence of SIBX in synthetic water, I = 3.5E-02..... 123
Figure 4.56: Moncheite (NS142) recovery-time curves at pH 9 comparing size with and without pentlandite in the mixture with SIBX in synthetic water, I = 3.5E-02. .. 124
Figure 4.57: Merenskyite (NS143) recovery-time curves at pH 9 comparing no reagents, SIBX and $CuSO_4$+SIBX in synthetic water, I = 3.5E-02..... 125
Figure 4.58: Merenskyite (NS152) recovery-time curves at pH 9 comparing no reagents, SIBX and $CuSO_4$+SIBX in synthetic water, I = 3.5E-02..... 126
Figure 4.59: Merenskyite (NS153) recovery-time curves at pH 9 comparing a higher calcium concentration in the presence of SIBX. 127

University of Cape Town

Figure 4.60: Moncheite (NS153) and merenskyite (NS152) recovery-time curves at pH 9 with and without bismuth powder ground with the sample in synthetic water, I = 3.5E-02. 128

Figure 5.1: Speciation diagram for ethyl xanthate (EtX) at pH 9. 134
Figure 5.2: Dixanthogen ions normalised yield for the Pt mineral species at pH 9. 135
Figure 5.3: Sperrylite NS145 concentrate mineral map 141
Figure 5.4: Sperrylite NS145 tailings mineral map. 141
Figure 5.5: Sperrylite NS146 concentrate mineral map. 141
Figure 5.6: Sperrylite NS146 tailings mineral map. 141
Figure 5.7: Speciation diagrams at pH 9 for 5.0E-05 M ethyl xanthate and copper. 143
Figure 5.8: Copper speciation diagram for pH 9 over a range of E_h conditions. 145
Figure 5.9: Copper speciation for copper concentration of 5.00E-05M as a function of pH at constant E_h of 300 mV. 145
Figure 5.10: Hydrogen bonding (Copper Ions). 146
Figure 5.11: Hydroxy complex formation (Copper Ions). 146
Figure 5.12: Schematic representation of xanthate adsorption onto copper activated silicate mineral. 147
Figure 5.13: E_h-pH diagram for the copper-water-ethylenediamine (EDA) system at 25°C and 1 atm. Total EDA activity, $\{EDA_T\}$ = 1E-2M; Total dissolved copper activity, $\{Cu_T\}$ = 1E-6M, (Aksu and Doyle, 2000). 153
Figure 5.14: ΔG-diagram (Ellingham) showing the relative stability of Bi, Te, Pd and Pt oxides. 157
Figure 5.15: Speciation diagram for 1.00E-05M Ni^{2+} (Acar and Somasundaran, 1992). 160
Figure 5.16: Speciation diagram for 1.00E-04M Fe^{2+} (Fuerstenau, 1976). 160
Figure 5.17: Speciation diagram for 1.0E-03M Ca^{2+} (Fuerstenau, 1976). 162
Figure 5.18: Speciation diagram for 1.00E-04M Mg^{2+} (Fuerstenau, 1976). 162

University of Cape Town

LIST OF TABLES

PAGE NO

Table 3.1: Hypotheses link to experimental methods. 57
Table 3.2: Platinum and palladium sulphide composition and thermal treatment. 58
Table 3.3: Platinum and palladium arsenide composition and thermal treatment..... 59
Table 3.4: Platinum and palladium telluride composition and thermal treatment. 59
Table 3.5: Surface area of the +38 -38µm size fraction of all the synthesised minerals..... 60
Table 3.6: Synthetic water composition, *I* = 3.5E-02. 62
Table 3.7: Chemical reagents and abbreviations used during the study. 64

Table 4.1: Energy Dispersive Spectroscopy (EDS) results for cooperite and vysotskite 71
Table 4.2: Energy Dispersive Spectroscopy (EDS) results for sperrylite. 73
Table 4.3: Energy Dispersive Spectroscopy (EDS) results for palladoarsenide. 74
Table 4.4: Energy Dispersive Spectroscopy (EDS) results for moncheite. 75
Table 4.5: Energy Dispersive Spectroscopy (EDS) results for merenskyite. 76
Table 4.6: XRD results for cooperite and vysotskite. 77
Table 4.7: XRD results for sperrylite and palladoarsenide. 77
Table 4.8: XRD results for moncheite and merenskyite. 78
Table 4.9: Summary of refinement data for cooperite sample NS144. 79
Table 4.10: Summary of refinement data for vysotskite sample NS148. 79
Table 4.11: Summary of refinement data for sperrylite sample NS145. 80
Table 4.12: Summary of refinement data for sperrylite sample NS146. 81
Table 4.13: Summary of refinement data for moncheite sample NS142. 82
Table 4.14: Summary of refinement data for moncheite sample NS153. 82
Table 4.15: Summary of refinement data for merenskyite sample NS143. 83
Table 4.16: Summary of refinement data for merenskyite sample NS152. 83
Table 4.17: Zeta potential determinations and standard deviations for pH 4, 6, 8, and 10 in synthetic water, I = 3.2E-02. 85
Table 4.18: Summary of the XPS data obtained for the Pt mineral samples. 107
Table 4.19: Summary of the XPS data obtained for the Pd mineral samples. 108

University of Cape Town

Table 4.20: Sperrylite recovery for microflotation tests and standard deviations for concentrates collected at 2, 4, 6,10 and 20 minute intervals in synthetic water, I = 3.5E-02 110
Table 4.21: Reagent concentrations in grams, moles and pseudo-monolayers for all the active ingredients of the chemicals used during the study. 112

Table 5.1: Electrochemical series for Pt, Pd, Bi and Te 156

University of Cape Town

NOMENCLATURE

e	Ion charge
E°	Standard reduction potential
E_h	Oxidation/reduction potential
E_{kin} or E_K	Kinetic energy
E_B	Binding energy
L_o	Effective length of spectrometer
h	Planks constant
m	Ion mass
m_o	Adjacent masses
Δm	Ion mass difference
t	Flight time
t_o	Length of primary ion pulse
Δt	Time difference
v	Ion velocity
V_o	Accelerating potential

GREEK LETTERS

ε	Fluid dielectric constant
η	Dynamic viscosity
κ	Debye-Huckel parameter
ζ	Zeta potential
ν	Frequency of the incident radiation
ϕ	Spectrometer work function
λ_i	Inelastic mean free path (IMFP) of the electron for a particular energy and material
φ	Angle of emission of the electron with respect to the normal sample surfaces

University of Cape Town

LIST OF ABBREVIATIONS

Cooperite (NS144)	PtS – Platinum sulphide
Vysotskite (NS148)	PdS – Palladium sulphide
Moncheite (NS142)	$Pt,Pd(Bi,Te)_2$ – Platinum Palladium Bismuth Telluride
Moncheite (NS153)	$PtTe_2$ – Platinum Telluride
Merenskyite (NS143)	$Pd,Pt\ (Bi,Te)_2$ – Palladium Platinum Bismuth Telluride
Merenskyite (NS152)	$PdTe_2$ – Palladium Telluride
Palladoarsenide (NS147)	Pd_2As – Palladium Arsenide
Sperrylite (NS145)	$PtAs_2$ – Platinum Arsenide
Sperrylite (NS146)	$PtAs_2$ – Platinum Arsenide
a	Particle radius
ATR	Attenuated total internal reflection
COS	Complex oxidised sulphide
$CuSO_4$	Copper sulphate
e^-	Standard reducing agent
EDA	Ethylenediamine
ESCA	Electron spectroscopy for chemical analysis
d	Escape depth of an emitted electron
FTIR	Fourier transform infrared spectroscopy
H^+	Concentration of standard acid
I	Ionic Strength
ICSD	Inorganic Crystal Structure Database
iep	Isoelectric point
IMFP	Inelastic mean free path
IR	Infrared spectroscopy
LIMS	Laser ionisation mass spectrometry
Log(Conc.)	Logarithmic concentration
M	Metal ion
M^+	Metal cation
MS	Metal sulphide
MA	Metal chelates

University of Cape Town

L	Ligand
ML	Metal ligand
pE	Equilibrium potential
PGE	Platinum group elements
PGM	Platinum group minerals
pH_{ie}	Isoeletric point pH
ppm	Parts per million
pzc	Point of zero charge
Rel Std Dev	Relative standard deviation
rpm	Revolutions per minute
SIBX	Sodium iso-butyl xanthate
$SIBX^-$	Xanthate anionic form
$(SIBX)_2$	Xanthate dimer
Std Dev	Standard deviation
ToF-SIMS	Time of flight secondary ion mass spectrometry
UV	Ultraviolet spectroscopy
wt.%	Weighted percent
At.%	Atomic percent
X^-	Xanthate ion
XPS	X-ray photoelectron spectroscopy
XRD	X-ray diffraction

University of Cape Town

ABSTRACT

The Platreef is located in the northern limb of the Bushveld Complex of South Africa. This reef consists of a complex assemblage of rock types, with pyroxenites, serpentinites and calc-silicates being the most abundant. The predominant PGMs are the tellurides, arsenides, alloys and sulphides. The Pt and Pd tellurides contribute between 20-45% of the PGMs present in the Platreef ore followed by the alloys (26%), arsenides (21%) and sulphides (19%). Flotation is used in the processing of the Platreef ore to separate the siliceous gangue from the platinum group minerals (PGM) and base metal sulphides. The PGE arsenide and telluride minerals are considered to be slow floating when compared to other PGMs as there is evidence of them reporting to the tailings.

This thesis aimed to investigate the flotation behaviour of these minerals and presents results which characterise the surface properties of synthetic cooperite (PtS), vysotskite (PdS), sperrylite ($PtAs_2$), palladoarsenide (Pd_2As), moncheite ($PtPd(BiTe)_2$ and $PtTe_2$) and merenskyite ($PdPt(BiTe)_2$ and $PdTe_2$) and attempts to relate the flotation behaviour of the various minerals to these characteristics.

In addressing these questions it was hypothesised that the differences in the floatability between the Pt and Pd arsenide, telluride and sulphide mineral species may be due to one or more of the following effects:

- The hydrophobicity of the synthesised Pt and Pd mineral species may be influenced by their crystal structure, specifically the different crystal planes and/or morphology of the minerals.
- The lower floatability reported for the PGE mineral species may be due the presence of oxidation products on the surface which will influence their floatability.
- When the PGE mineral species are in contact with oxidation products produced during grinding, inadvertent depression may occur due to the presence of precipitating ions.
- Copper sulphate may not be promoting the flotation of the PGE mineral species as it does in the case of the sulphides.
- Oxidation of bismuth and tellurium present in the minerals occurs readily and these passivating layers may influence the flotation response.

University of Cape Town

- Calcium and magnesium ions may have a negative effect on flotation present in the process water of the minerals.

Zeta potential determinations, ToF-SIMS analyses (time of flight secondary ion mass spectrometry) and X-ray photoelectron spectroscopy (XPS) were used to characterise the mineral surface. Microflotation was used to determine the hydrophobicity of the synthetic minerals.

For all the synthetically prepared minerals, except for palladoarsenide, there was good agreement between the measured and calculated crystal structures and they corresponded well to the information contained in the ICSD database. However, the results of this research have not shown that the hydrophobicity of the synthesised Pt and Pd mineral species are related in any way to the crystal structure or resulting planes and/or morphology of the minerals.

In general, it has been shown that the PGE minerals float readily when treated with SIBX and the XPS and ToF-SIMS results showed clearly that xanthate is adsorbed on the mineral surfaces at a higher concentration compared to the copper activated minerals, except for the sperrylite (NS146) and cooperite (NS144) samples. The ToF-SIMS has indicated the presence of dixanthogen on the mineral surfaces studied and it is believed that diaxthogen is the active species for flotation.

Zeta potential determinations have shown that the surface charge differs considerably between the Pt and Pd mineral species which may be due to the significant surface oxidation observed for the Pd minerals. Oxidation of the PGE telluride minerals was shown to negatively affect the flotation performance of the bismuth-rich samples but not the pure Pt and Pd telluride samples. This appears to support the thermodynamically expected hypothesis that bismuth species readily oxidise and that the oxidation products of this reaction negatively affect the floatability of the mineral.

University of Cape Town

Conditioning of moncheite ($PtTe_2$) in the presence of pentlandite reduced the recovery by around 47%. This was associated with pentlandite dissolution products (iron and nickel hydroxy species) being observed to form overlayers on the mineral surfaces thereby inhibiting the adsorption of collector. In addition, further grinding of these samples, with and without pentlandite conditioning, showed a negative effect on the recovery, probably due to the fineness of the particle size distribution and no advantage appeared to be gained from grinding promoting the possible exposure of fresh sites in the sample.

Copper sulphate, the standard activator used in concentrators for the recovery of PGMs by flotation, was found to have a negative effect on the recovery of all of the synthetic PGE mineral samples, with the exception of vysotskite, when compared with the results obtained in the presence of xanthate on its own. It is speculated that the negative effect of copper on the recovery may be due to $Cu(OH)_2$ precipitation on the mineral surfaces. Thus when xanthate ions are subsequently added, most of the active sites are already occupied by the hydrophilic $Cu(OH)_2$ which reduces the degree of xanthate adsorbing directly onto the vacant Pt and Pd mineral surface sites. EDA additions have shown that the copper and copper xanthate species are not strongly bound to the mineral surfaces except for vysotskite. This observation confirms the copper speciation on the mineral surface thereby indicating that the copper is present on the surface as a result of the precipitation of $Cu(OH)_2$ colloids rather than a chemical reaction between the copper and metal ions in the PGE mineral structure.

Further testwork on the PGE telluride mineral samples has shown that the flotation rates as well as the overall recovery for both minerals were negatively affected when ground with bismuth powder, especially for the $PdTe_2$ sample. This result confirms the hypothesis that bismuth is more susceptible to oxidation and that the oxidation products (Bi oxide and hydroxide species) negatively affect the flotation response of the PGE telluride mineral species.

Calcium ions, which are present in process water, did not negatively affect the flotation response of the $PdTe_2$ mineral species.

University of Cape Town

Furthermore, the research showed that in the presence of xanthate, that it is not only the grain size distribution that plays a role in flotation but also the mineral surface chemistry. For example, for the same size distribution of +38 -38µm for the Pt mineral species, the order of flotation rate (in decreasing order) was moncheite, cooperite and sperrylite and for the Pd mineral species, the order of flotation rate was merenskyite, palladoarsenide and vysotskite.

In conclusion it is clear that Pt and Pd arsenide and telluride minerals can be recovered in significant quantities using xanthate as the collector.

Keywords: Microflotation, PGE, surface characterisation, copper activation and SIBX.

University of Cape Town

CHAPTER 1

LITERATURE REVIEW

The recovery of the PGEs in South Africa began in earnest at several of the large gold mines around June 1919. The recovery of platinum group minerals (PGM) improved significantly from 1923 onwards. Today, the Bushveld Complex contains the world's largest deposit of PGMs and Figure 1.1 shows a simplified geological map of the Bushveld Complex.

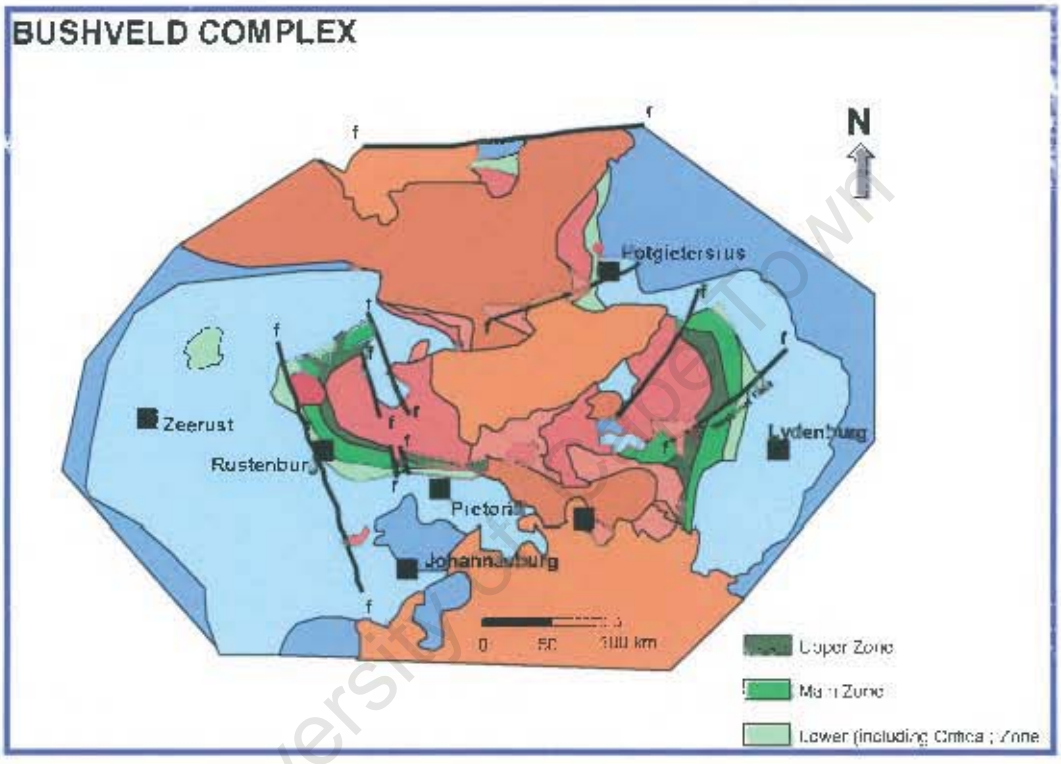

Figure 1.1: Simplified geological map of the Bushveld Complex. The green shades represent the Bushveld rocks, the rose shades are the granite cover rocks, the blue and brown shades represent the pre- and post-Bushveld rocks, respectively. The red circular shape near Rustenburg is the Pilansburg alkali complex (Schouwstra et al., 2000).

The upper Critical Zone of the Bushveld Complex (Figure 1.1) hosts the largest concentration of PGEs in the world. Apart from the Upper Group Chromitite No.2 (UG-2) and Merensky Reef, the Zone also hosts the Platreef mineralisation of the northern limb of the Bushveld Complex (Schouwstra et al., 2000).

University of Cape Town

The Merensky Reef is generally regarded as a uniform reef type; however, large variations occur in reef thickness, reef composition, as well the position of the mineralisation. The Reef comprise approximately equal amounts of dark iron-magnesium silicate minerals (feldspathic pyroxenite) and lighter calcium-aluminium-sodium silicate minerals under- and overlain by thin (5 to 15mm) often discontinuous layers of chromite concentrations. The Merensky Pegmatoid Zone contains the base metal sulphide grains and associated PGM. The Merensky Reef consists predominantly of orthopyroxene (~60%), plagioclase feldspar (~20%), pyroxene (~15%), phlogopite (5%) and occasional olivine. Secondary minerals such as talc, serpentine, chlorite and magnetite have widespread occurrence. The base metal sulphides consist predominantly of pyrrohtite (~40%), pentlandite (~30%) and chalcopyrite (~15%). The major platinum group minerals are cooperite (PtS), braggite [(Pt,Pd)NiS], sperrylite ($PtAs_2$) and PGE alloy. In some areas minerals such as laurite (RuS_2) can be abundant (Schouwstra et al., 2000).

The UG-2 Reef is a platinuferous chromitite layer which, depending on the geographic location within the Complex, is developed some 20 to 400 meters below the Merensky Reef. The UG-2 consists predominantly of chromite (between 60 – 90% by volume) with lesser silicate minerals (5 – 30% pyroxene and 1 – 10% plagioclase). Other minerals present in minor concentrations, can include silicates and oxides and base metal sulphides. Secondary minerals include quartz, serpentine and talc. The Cr_2O_3 content of the UG-2 Reef varies from 30 to 55%. Total PGE varies from locality to locality, but on average range, between 4 and 7g/t. The base metal distribution follows a similar trend to that of the PGE, with most of the values occurring in the bottom and top part of the reef. The base metal content of a typical UG-2 Reef is around 200 – 300ppm Ni, occurring as nickel sulphide and <200ppm copper occurring as copper sulphide. The PGMs present in the UG-2 Reef are highly variable, but generally the UG-2 is characterised by the abundant PGE sulphides [laurite (RuS_2), cooperite (PtS), braggite [(Pt,Pd)NiS], and an unnamed PtRhCuS]. The base metal sulphides consist predominantly of chalcopyrite, pentlandite and pyrrohtite (Schouwstra et al., 2000).

The Platreef is discussed in detail in Section 1.1.

University of Cape Town

Flotation is used for concentrating sulphide and PGE minerals at PGM concentrators. With the depletion of high-grade ore deposits it has become necessary to treat low-grade complex polymetallic ores. This often involves processing of fine particles that are more difficult to float due to their low mass and high surface area amongst others.

In order to maximise the overall valuable minerals recovery from the Bushveld Complex, a better understanding of surface oxidation, collector adsorption and distribution as well as ionic activation of mineral surfaces is needed to maximise valuable minerals recovery.

A typical process circuit used across the South African PGM industry consists of two or three stages of milling. Each comminution stage is followed by flotation (Figure 1.2). Autogenous mills can be used in primary milling circuits while ball mills are employed in secondary milling stages.

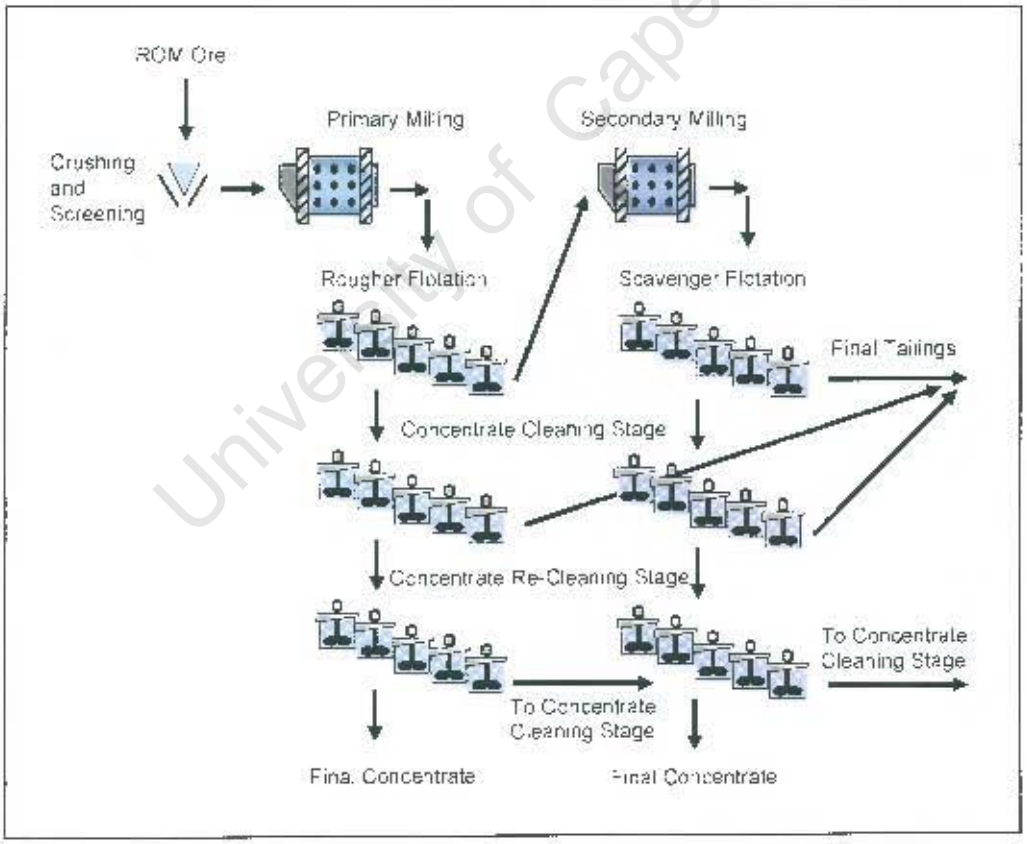

Figure 1.2: A typical concentrator flowsheet.

University of Cape Town

A large variety of flotation circuits are currently used across the industry in South Africa as the primary method for the upgrading of valuable minerals. The roughing and scavenging stages are complemented by a number of cleaning circuits. In the new flotation plants, trends have leaned towards using larger cells. Lately, tank cells (eg. OK150) have been used more extensively. Typically, flotation is carried out at a pH of between 8 and 9, which is the natural pH of the Bushveld Complex ore. Various collectors, depressants and frothers are used. The most common collectors utilised by the PGM industry are xanthates and dithiophosphates. These collectors are typically used for the concentration of sulphide minerals and it is generally accepted that these reagents will also recover the PGE mineral species. In terms of gangue mineral depressants, carboxymethyl cellulose and guar based reagents have been found to be effective in depressing siliceous gangue. In a number of operations, copper sulphate is used as an activator. It is widely speculated that copper sulphate activates the base metal sulphide and PGM minerals. However, the addition of copper sulphate can also contribute to the recovery of gangue minerals due to the inadvertent activation of these minerals (Malysiak, 2003; Shackleton, 2003)

The major loss of PGM in the beneficiation of the Bushveld Complex occurs during the separation of the siliceous gangue from the PGM and sulphide minerals by selective flotation; therefore flotation remains the main metallurgical focus for the South African PGM producers. This may partially be attributed to the belief that the PGMs will behave in a similar way as base metal sulphides in terms of pulp and mineral surface chemistry.

The areas reviewed below focus on the existing knowledge of the Platreef from a geological perspective, as well as the mineralogy of the reef. Flotation of ores, the role of the reagents, and the speciation of the elements of interest were also reviewed. It should be pointed out that there is a limited amount of information available in the published literature in terms of the PGE minerals species and that despite the fact that these minerals are of significant economic importance, very little research has been carried out to date, worldwide, on the recovery of these minerals.

University of Cape Town

1.1 Platreef

The Platreef is located in the northern limb of the Bushveld Complex north of Mokopane (formerly Potgietersrus) in South Africa. This reef consists of a complex assemblage of rock types, with pyroxenites, serpentinites and calc-silicates being the most abundant. Base metal mineralisation and platinum group element (PGE) concentrations are found to be highly irregular, both in value as well as in distribution (Schouwstra et al., 2000). The Potgietersrus or northern limb is partially covered beneath younger Waterberg-aged rocks, with exposures confined to the eastern edge of the limb near Potgietersrus and in the north near Villa Nora (Cawthorn et al., 2002).

The Bushveld Complex shows a range of rock types from dunite and pyroxenite through norite, gabbro and anorthsite to magnetic gabbro and apatite and olivine diorite and so demonstrates the complete differentiation sequence for a basic magma. The use of zonal stratigraphy is more convenient when discussing widely separated areas with similar rock types. The following zonal stratigraphy of the Bushveld Complex is taken from the summary of Eales and Cawthorn, 1996 (Figure 1.3).

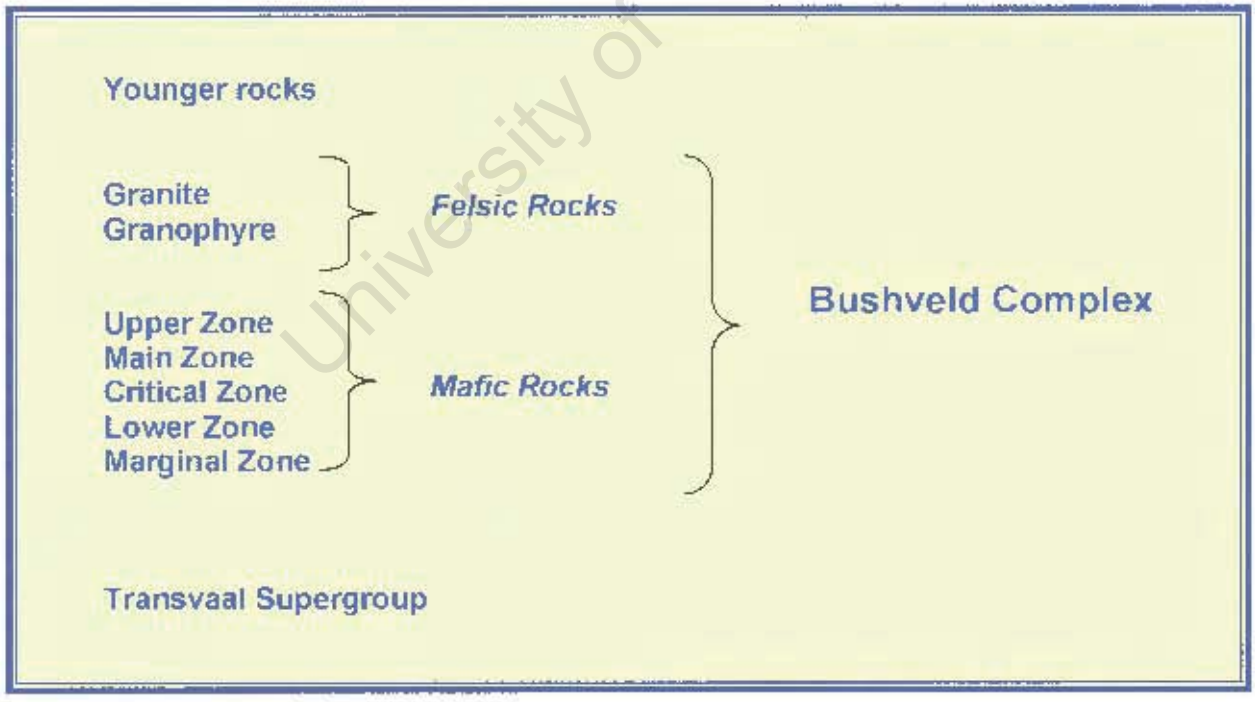

Figure 1.3: Zonal stratigraphy of the Bushveld Complex.

University of Cape Town

The critical zone includes the world's largest platinum bearing ore bodies of which the Platreef is one and will be the only zone discussed below due to its relevance to the study. The critical zone displays spectacular layering of chromitite, norite and anorthsite on all scales from centimetres to tens of meters. Significant lithological and chemical variations prevail along the strike in the critical zone. A variably mineralised (PGE, Cu, Ni) composite pyroxenite zone forms the eastern floor contact of the Potgietersrus limb and is regarded as the local equivalent of the Merensky reef. This pyroxenite zone has been termed the Platreef and has been traced for 35 km along the eastern contact, where it transgresses from the Transvaal Supergroup sedimentary rocks in the south to Archaen granite and gneiss in the north (Figure 1.4).

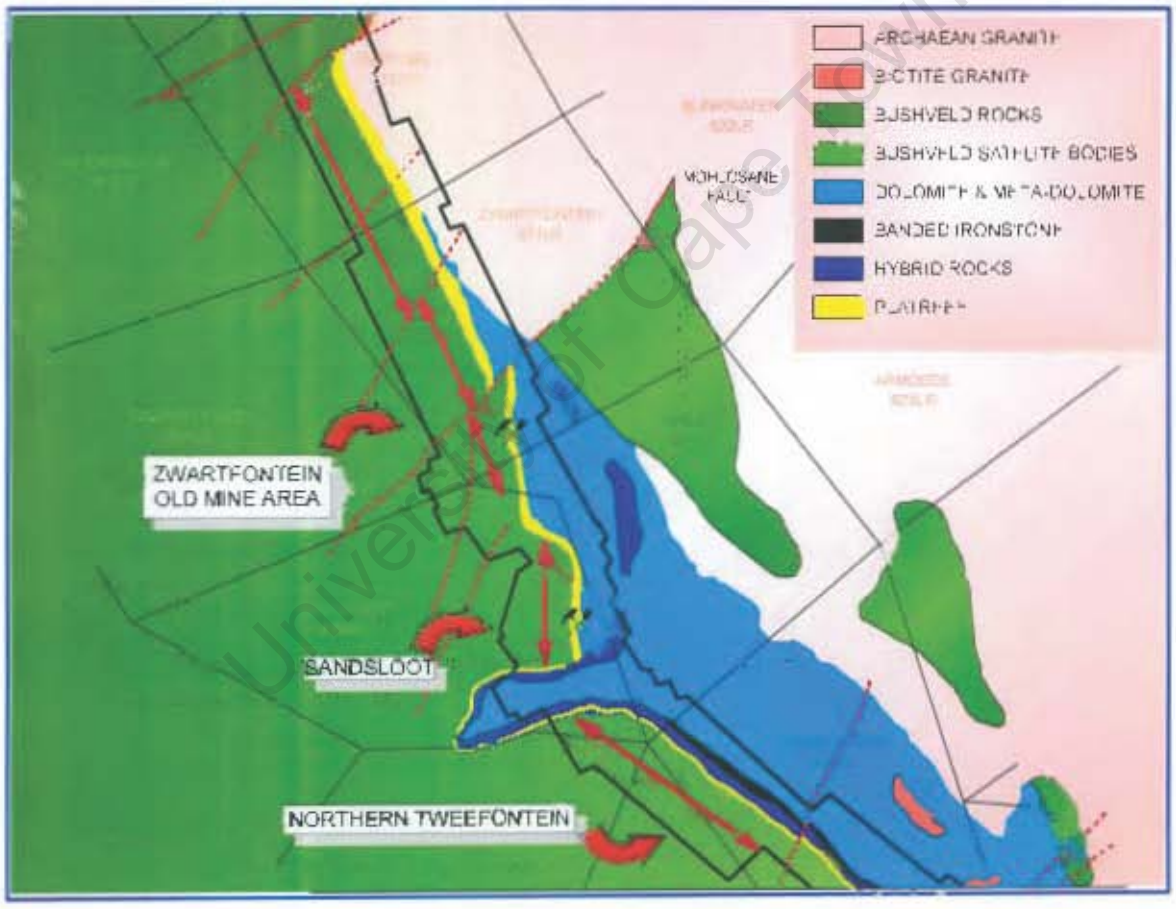

Figure 1.4: Map of the Platreef.

University of Cape Town

The Platreef strikes north – northwest and dips at 40° to the southwest. The pyroxenite sequence varies in thickness from several meters to over 150 m and has an irregular footwall contact and an upper contact with overlying gabbro, norite and anorthosite at the base of the main zone. The Platreef has been divided into three major pyroxenite units, based on texture and mode and the thickness of each unit is variable with some units being totally absent in places;

- The upper pyroxenite termed 'C' reef is usually extremely poor in PGE mineralisation.
- The underlying pyroxenite, termed 'B' reef comprises a coarse-grained pyroxenite with minor intercumulus plagioclase. This phase contains a significant portion of clinopyroxene that can reach 90%. The pyroxenite contains virtually no olivine, minimal chromitite and fair to good grades of disseminated base metal mineralisation.
- The lowermost pyroxenitic phase, known as 'A' reef, comprises a highly feldspathic unit with a marked heterogeneous texture and grain size. Graphic intergrowth of plagioclase feldspar and quartz is frequently noted and the pyroxenite contains disseminated mineralisation and commonly some fairly large blebs of composite base metal sulphide (Cawthorn et al., 2002).

The distribution of mineralisation in the Platreef is variable, but has a strong tendency to be richer on top of the 'B' reef and to decrease gradually downward. The 'A' reef, in general, has lower values than the 'B' reef and may be barren in places. There is a tendency for a limited amount of footwall concentration of sulphides. The 'C' reef is invariably barren of mineralisation (Cawthorn et al., 2002).

University of Cape Town

1.2 Mineralogy

The predominant platinum group minerals (PGM) in the mined area of the Platreef are the PGE tellurides, alloys, arsenides and sulphides. The Pt and Pd tellurides, being the most important, contribute to around 20-30% and up to 45% of the PGMs present in the Platreef ore followed by the alloys (26%), arsenides (21%) and sulphides (19%). Their abundances vary from north to south and from section to section. The major sulphide minerals are pyrrhotite, pentlandite and chalcopyrite (Viljoen and Schürmann, 1998). Non-sulphide

gangue minerals consist mainly of pyroxene and feldspar along with quantities of chlorite, tremolite, talc, and mica.

1.2.1 Platinum and Palladium Sulphides

Cooperite is a rare platinum-bearing sulphide mineral. In cooperite, platinum is coordinated with four sulphurs in a square planar arrangement. Sulphurs are tetrahedrally coordinated by four platinum ions. The crystal structure is of PtS type, with strong and directed covalent bonds. *M* (*M* = Pt, Pd) forms four co-planar bonds with *X* (*X* = O, S), which itself is coordinated by four *M* in a distorted tetrahedral environment. Cabri 2002. Figure 1.5 shows the solid state crystal structure for PtS; *"Source: WebElements [http://www.webelements.com/]"*.

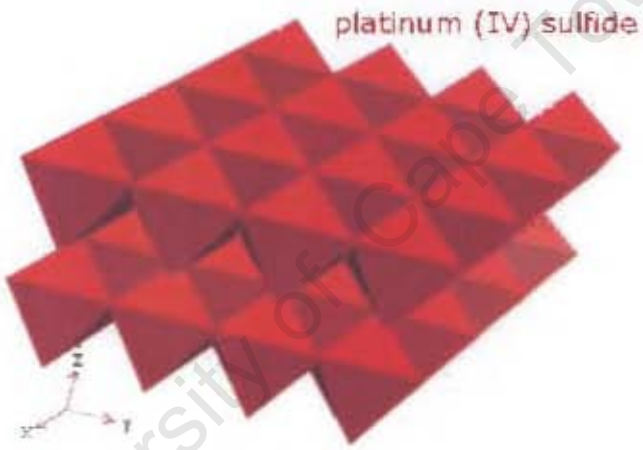

Figure 1.5: Solid state crystal structure for PtS."Source: WebElements [http://www.webelements.com/]"

University of Cape Town

Cooperite crystallography;

- Axial Ratios: a:c = 1:1.75792
- Cell Dimensions: a = 3.47, c = 6.1, Z = 2; V = 73.45 Den(Calc)= 8.45
- Crystal System: Tetragonal - Ditetragonal DipyramidalH-M Symbol (4/m 2/m 2/m) Space Group: P 41/mmc
- X-Ray Diffraction: By Intensity(I/Io): 3.03(1), 1.51(0.8), 1.918(0.7)

The mineral is found in the Bushveld Complex, north of Mokopane (formerly Potgietersrus) in South Africa. It is also present in the Merensky and UG-2 reefs, Bushveld Complex. Cooperite occurs with pentlandite, silicates, chromite, and in complex intergrowths with Pt-Fe alloys (Bannister and Hey, 1932).

Vysotskite has the PdS structure, which has distorted Pd tetrahedral coordination about S, and three distorted square planar environments about the Pd. The square-planar coordination geometries are more regular than previously reported. The mineral is found in the UG-2 Reef, Bushveld Complex, (Cabri, 2002). Figure 1.6 shows the solid state crystal structure for PdS; *"Source: WebElements [http://www.webelements.com/]"*.

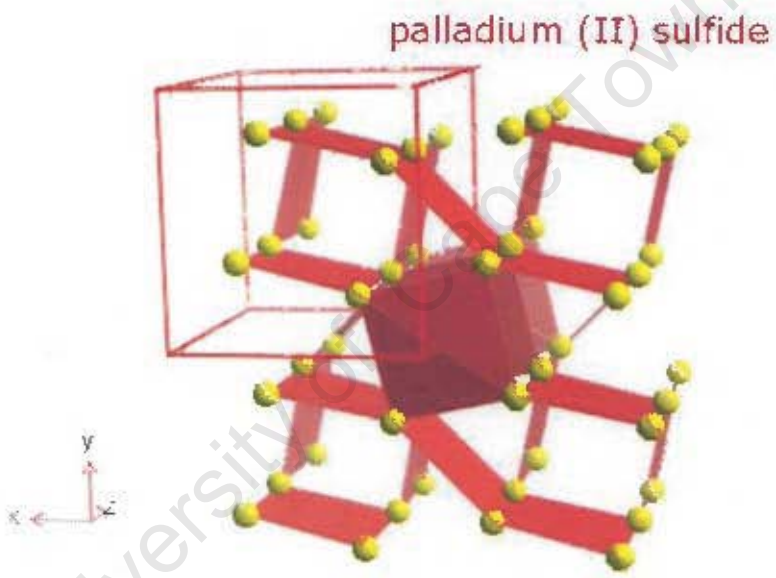

Figure 1.6: Solid state crystal structure for PdS."Source: WebElements [http://www.webelements.com/]"

University of Cape Town

Vysotskite crystallography:

- Axial Ratios: a:c = 1:1.02652
- Cell Dimensions: a = 6.371, c = 6.54, Z = 5; V = 265.46 Den(Calc)= 3.96
- Crystal System: Tetragonal - DipyramidalH-M Symbol (4/m) Space Group: P 41/m
- X-Ray Diffraction: By Intensity(I/Io): 2.86(1), 2.91(1), 2.61(0.8)

1.2.2 *Platinum and Palladium Arsenides*

The PGE arsenides do not have the same variation in composition as seen for the PGE tellurides below (Section 1.2.3). Sperrylite is a rare mineral and besides native platinum, it is the only platinum mineral of any significance of the arsenide group. It is a platinum diarsenide ($PtAs_2$) and has the pyrite-type structure with distorted octahedral coordination around Pt and distorted tetrahedral coordination around As (Cabri, 2002).

Sperrylite has been a major ore mineral in the very productive platinum deposits of the Merensky zone or "reef" of the Bushveld Complex, South Africa, including those of the Rustenburg, Pilanesberg, Lydenburg, and Potgietersrus districts. In general, the mineralogy of these deposits is extremely complex, with the list of associated platinum minerals being quite extensive. There is a large number of inadequately characterised platinum-group phases recorded from the Bushveld Complex (Gait, 1982).

Sperrylite and the well known mineral, pyrite both belong to the Pyrite Group of minerals and share a similar structure. They cannot be mistaken for each other however since pyrite is brassy yellow and sperrylite is tin white in color. The structure of pyrite and sperrylite is analogous to galena with a formula of PbS although galena has a higher symmetry. The difference between the two structures is that the single sulphur atom of galena is replaced by a pair of sulphur atoms in sperrylite. The sulphur pair is covalently bonded together. This pair disrupts the four fold symmetry that a single atom of sulphur would have preserved and thus gives sperrylite a lower symmetry than galena (Gait, 1982). No crystal structure in the solid state has been sourced for sperrylite but Figure 1.7 shows the solid state crystal structure for PbS, which is similar to galena; "*Source: WebElements [http://www.webelements.com/]*".

University of Cape Town

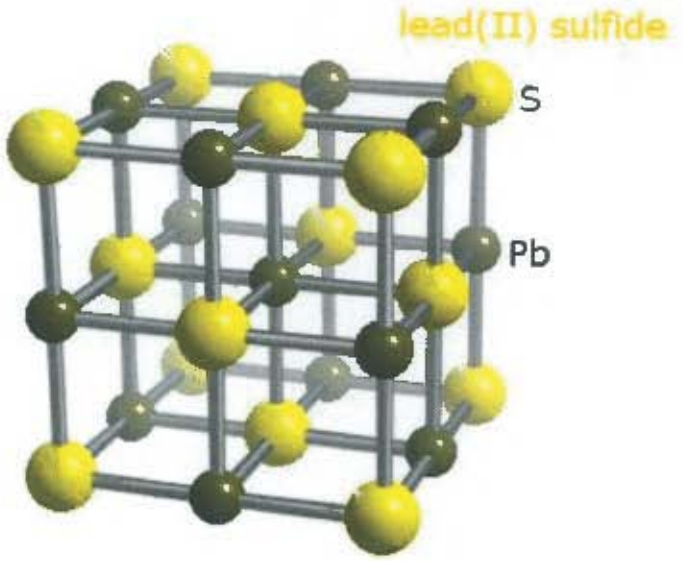

Figure 1.7: Solid state crystal structure for PbS."Source: WebElements [http://www.webelements.com/]"

Sperrylite crystallography;

- Cell Dimensions: a = 5.967, Z = 4; V = 212.46 Den(Calc)= 10.78
- Crystal System: Isometric - DiploidalH-M Symbol (2/m 3) Space Group: P a3
- X-Ray Diffraction: By Intensity(I/Io): 1.801(1), 1.148(0.7), 2.98(0.6)

Crystal structure for palladoarsenide (Pd_2As) is a Fe_2P structure type. No crystal structure in the solid state has been sourced for palladoarsenide.

Palladoarsenide crystallography;

- Axial Ratios: a:b:c =1.092:1:1.2325
- Cell Dimensions: a = 9.25, b = 8.47, c = 10.44, Z = 18; beta = 94° V = 815.96 Den(Calc)= 10.54
- Crystal System: Monoclinic - PrismaticH-M Symbol (2/m) Space Group: P 2/m
- X-Ray Diffraction: By Intensity(I/Io): 2.14(1), 2.21(0.9), 2.6(0.7)

1.2.3 Platinum and Palladium Tellurides

The PGE telluride minerals composition varies considerably and is typically in association with bismuth. Figure 1.8 shows an example of a ternary diagram for a Pd-Te-Bi system,

University of Cape Town

which shows the variation in composition. The solid black triangles represent particles that are depleted in tellurium and bismuth and enriched in palladium. This enrichment may be as a result of the weathering of the ore body (Hey and Malysiak, 2004).

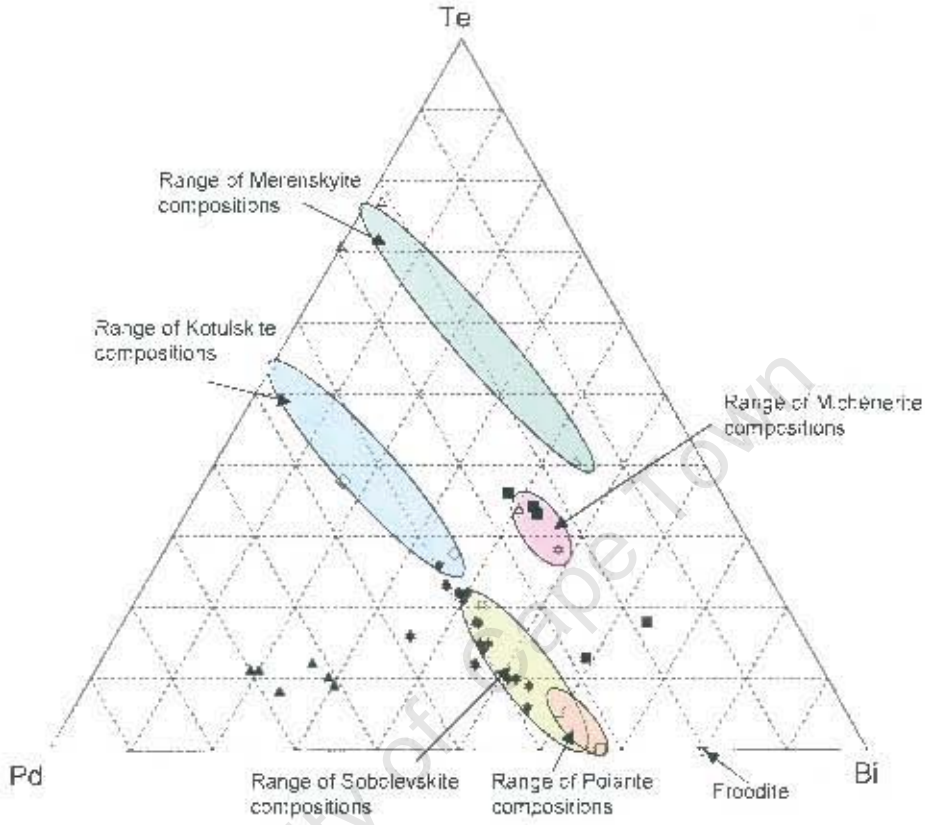

Figure 1.8. Pd-Bi-Te ternary diagram highlighting the variation in composition of PdBiTe particles (black symbols). The known naturally occurring PdBi-tellurides are Michenerite (PdBiTe), Kotulskite (PdTe), Merenskyite ($PdTe_2$) Sobolevskite (Pd(TeSb)Bi), Polarite (Pd(PbTe)Bi), and Froodite ($PdBi_2$). The compositional ranges (normalised in terms of the three components only) of these mineral compositions (Cabri, 2002) are shown by the coloured areas.

The crystal structure for synthetic merenskyite ($PdTe_2$) is layered, with the layering along the [001] direction, similar to that of $Cd(OH)_2$. Figure 1.9 shows the solid state crystal structure for $PtTe_2$; *"Source: WebElements [http://www.webelements.com/]"*.

University of Cape Town

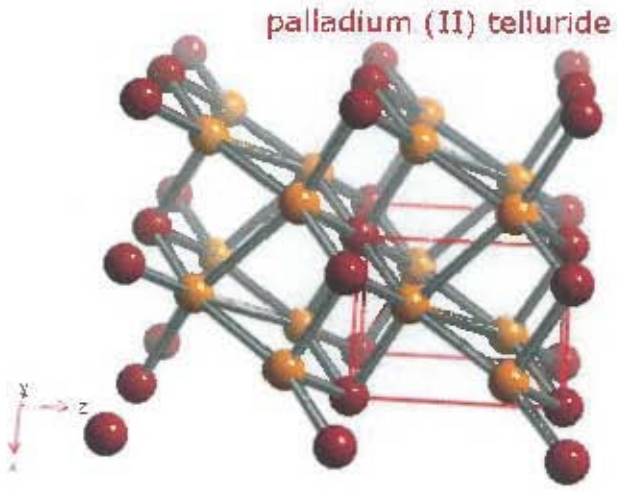

Figure 1.9: Solid state crystal structure for $PdTe_2$."Source: WebElements [http://www.webelements.com/]"

Merenskyite crystallography;

- Axial Ratios: a:c = 1:1.28833
- Cell Dimensions: a = 3.978, c = 5.125, Z = 1; V = 70.24 Den(Calc)= 9.14
- Crystal System: Trigonal - Ditrigonal PyramidalH-M Symbol (3m) Space Group: P 3m1
- X-Ray Diffraction: By Intensity(I/Io): 2.92(1), 2.1(0.6), 3.07(0.3)

The crystal structure for moncheite ($PtTe_2$) is a layer-lattice structure similar to that of brucite (Cabri, 2002). Figure 1.10 shows the solid state crystal structure for $PtTe_2$: *"Source: WebElements [http://www.webelements.com/]".*

University of Cape Town

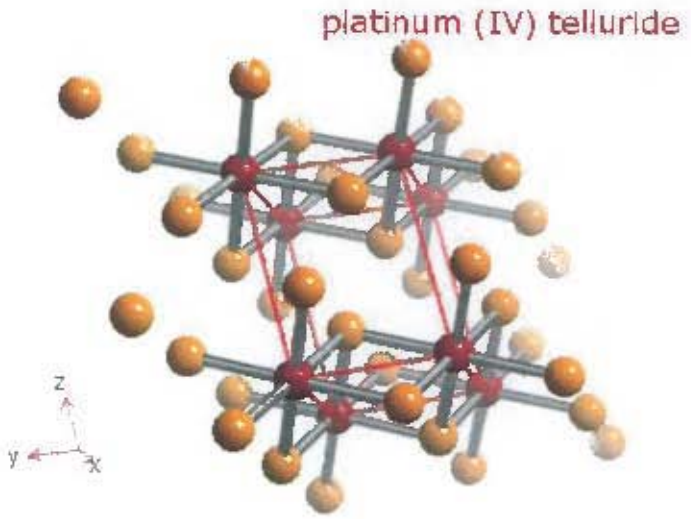

Figure 1.10: Solid state crystal structure for $PtTe_2$."Source: WebElements [http://www.webelements.com/]"

Moncheite Crystallography;

- Axial Ratios: a:c = 1:1.306
- Cell Dimensions: a = 4.049, c = 5.288, Z = 1; V = 75.08 Den(Calc)= 10.37
- Crystal System: Trigonal - Hexagonal ScalenohedralH-M Symbol (3 2/m) Space Group: P 3m1
- X-Ray Diffraction: By Intensity(I/Io): 2.93(1), 2.11(0.8), 2.02(0.7)

1.3 Synthesis of the Platinum and Palladium Minerals

The availability of natural cooperite, vysotskite, sperrylite, palladoarsenide, moncheite and merenskyite is limited due to the low content and small grain size of the Pt and Pd sulphide, arsenide and telluride minerals found in the ore body and hence the only realistic way to study the flotation behaviour of these minerals is to synthesise the mineral and to assume that the synthetic sample generally reflects the behaviour of the naturally occurring mineral. At the very least if all the minerals are synthesised in a similar manner the relative effects of various parameters on their behaviour will be valid.

University of Cape Town

Glasstone (1946) describes metallic alloys where the fused metals are frequently miscible and on cooling the liquid, the two components may either;

- each separate in the pure state
- form a continuous series of solid solutions
- form two solid solutions because of partial miscibility of the solids or
- combine to produce intermetallic compounds

X-ray examination has shown that in solid solutions, the atoms of one metal replace those of the other, at random, in the space lattice; provided the two metals have the same lattice structure and their atoms do not differ appreciably in size then, as a general rule, a continuous series of solid solutions is possible. If one atom is larger than the other, its introduction to the lattice will result in a strain, and a given concentration will be reached when further introduction of foreign atoms will no longer be possible; each element will then have a limited solubility in the other. Sometimes miscibility occurs with two metals that normally have different space lattices; eg. Nickel has a faced-centred cubic and chromium, a body-centred cubic structure. Nickel will dissolve in solid chromium to the extent of 37 atomic %, the alloys being body-centred. Any attempt to increase the proportion of nickel results in a change to the face-centred type of lattice characteristic of pure nickel. Although the two metals are completely miscible the solid solutions do not have the same structures.

There are a few papers describing the synthesis of the PGE arsenide, telluride and sulphide minerals with the aim of studying them mineralogically. The focus of these papers are on the identification, structures, properties and phase relationships of the minerals, viz. Groeneveld Meijer (1955) reported on the synthesis, structures and properties of platinum metal tellurides. The paper describes the synthesis by dry and wet fusion methods and characterisation of the minerals using x-ray and optical methods. Verryn and Merkle (1999) discuss the results obtained on experimental investigations in a dry system PtS-PdS-NiS at 1100°C. Synthetic cooperite, braggite and vysotskite phases were observed at various temperatures profiles. Pikl et al., (1999) and Merkle et al., (1999) described Raman spectroscopic identification of synthetic braggite, comparing the results obtained for braggite to cooperite and vysotskite, respectively.

University of Cape Town

1.4 Synthetic versus Naturally Occurring Minerals

It is important to know whether the synthetically prepared mineral behaves in a similar manner to that found in nature. This is not always possible to test due to size and distribution of these minerals in the ore. A few studies have been carried out comparing synthetic and naturally occurring minerals and one which is of particular relevance to this study is by Shamaila, 2007 where batch flotation tests were carried out using natural ores spiked with the synthetic PGE tellurides and arsenides. The flotation responses of, specifically, synthetic moncheite($Pt(BiTe)_2$), merenskyite($Pd(BiTe)_2$) and sperrylite($PtAs_2$) spiked into various ore types was investigated. The synthetic PGMs were prepared to a size range approximating that of liberated PGMs in a 60% -75µm feed to float. They were spiked to a flotation feed of a Platreef ore sample previously batch ground to 60% -75µm and conditioned for 30 minutes before reagent addition and flotation using a 4.5litre D12 Denver flotation cell. The results showed similarities in the flotation response observed between synthetic and natural PGMs and support the use of synthetic minerals in simulating the flotation behaviour of naturally occurring PGMs. It can also be deduced that if sufficiently liberated the naturally occurring PGMs should be able to float as well as the synthetic PGMs which by definition are fully liberated.

Cabri et al., (1975) reported on a study where natural specimens of palladoarsenide and sperrylite were compared to synthetically prepared ones. It was reported that the natural minerals were more difficult to characterise due to their diffraction patterns being generally weaker compared to those of the synthetically prepared material. The natural palladoarsenide, however, was equivalent to the low-temperature polymorph of the synthetic Pd_2As originally defined by Bergizov et al., (1974).

In another study, Forssberg and Jonsson (1981) carried out experiments that have shown that relatively large amounts of heavy metal ions can adsorb on both synthetic and natural pyrrhotite in an acidic pH. The possible cause is the presence of iron vacancies in the crystal lattice, as indicated by the chemical formula of pyrrhotite, $Fe_{1-x}S$. The vacancies can be filled by metal ions of suitable size. Pyrrhotite releases fairly large quantities of Fe^{2+} and Fe^{3+} ions under oxidising conditions. This can adversely affect the adsorption of heavy metals.

University of Cape Town

Synthetic samples showed a higher specific adsorption, probably due to pores, which give them a higher adsorption rate.

1.5 The Flotation of the PGE Sulphides, Arsenides and Tellurides

Flotation is used to separate the valuable minerals from the siliceous gangue, with selective separation achieved by the adsorption of a collector onto the surface of the platinum group and sulphide minerals. PGM flotation research has mainly focused on the flotation of base metal sulphides due to the association of the PGMs with these minerals, even though, in the Platreef there is a lack of sulphide-associated PGM and they account for <20% of the PGMs present (Howell et al., 2005).

A study carried out by Penberthy et al., (1999) on the recovery of platinum group elements (PGE) from a UG-2 reef showed that PGMs associated with liberated base metal sulphides have been identified as the fastest floating species. In the flotation feed of a normal UG-2 Reef, 17% of the total PGM was associated with the base metal sulphides. Although the liberated PGMs (63% in the flotation feed) were difficult to predict due to their small grain size, they did float and reported to the concentrates but at a slower flotation rate compared to that of the base metal sulphides. The rank of PGM (liberated) flotation rate was, in decreasing order, braggite, cooperite, malanite, ferroplatinum and lastly other non-sulphide platinum mineral phases and laurite. The non-sulphide platinum mineral phases refer to Pt and/or Pd tellurides, PGE arsenides and sulpharsenides, e.g. PtAsS excluding Pt-Fe alloys.

1.5.1 PGE Sulphides

The effect of oxidation on base metal sulphides, surface alteration, reagent adsorption and base metal sulphide flotation has been studied extensively. However, very little research has been carried out on the PGE sulphide minerals which may be due; firstly, that the majority of these minerals are located in South Africa and are therefore not of interest to the worldwide community; secondly, the research performed on PGE type minerals are in-house which is not available to the public domain due to confidentiality.

Surface oxidation is one of the most important factors that influence the flotation selectivity and recovery in the processing of complex sulphide ores. The degree of

University of Cape Town

oxidation determines whether the sulphide mineral surface will be hydrophobic or hydrophilic. Evidence from the combination of techniques has now shown that the mechanisms of oxidation are considerably more complex than those represented by simple reactions such as;

$$MS + xH2O + {}^{1}/_{2}xO2 \rightarrow M_{1-x}S + xM(OH)_2 \quad (1)$$

The chemical nature of the $M_{1-x}S$ product, the spatial distribution of the oxidation products, dissolved and reprecipitated species, other higher oxidation products and interactions with other dissolved species all complicate the real situation (Smart et al., 2003).

Moderate oxidation of the surface of sulphide minerals has been shown to be beneficial for the adsorption of collectors and the formation of hydrophobic sulphur species, excessive oxidation is detrimental to the effective separation of these minerals. Oxidation arises from the dissolution of minerals and grinding media and dissolved metal ions hydrolyse and sulphide ions oxidise. These ions can re-adsorb on the mineral surfaces or react with each other or the dissolved gas molecules before precipitation (Clarke et al., 1995).

It is well established (Smart et al., 2003), that the surface products of excessive oxidation have a profound effect on surface hydrophobicity. Mild oxidation however, appears to be necessary for the flotation of sulphide minerals and is often a requirement for self-induced flotation by the formation of hydrophobic sulphur species. On the other hand, excessive oxidation inhibits flotation by forming surface layers of oxide, hydroxide and oxy-hydroxide species. The rate of oxidation of sulphide minerals depends on the surface area available for reaction, the partial pressure of oxygen, the type and composition of the sulphide mineral, solution pH and temperature (Ralston, 1991).

Xanthates are one of the major classes of collectors used in flotation of sulphide minerals. They have been successfully employed in the industry to separate sulphides from gangue minerals such as silicates. These collectors adsorb on sulphide through a mixed potential

University of Cape Town

mechanism which involves the anodic oxidation of the collector and cathodic reduction of oxygen. The anodic oxidation of xanthate either involves xanthate chemisorption, metal xanthate formation or catalytic oxidation to dixanthogen, which is dependent on the minerals involved. Yoon and Basilio (1993) discuss the four classes of electrochemical mechanisms involving xanthate. The first mechanism, which is referred to as the under potential deposition or chemisorption, is the formation of a monolayer of the thiol oxidation product at potentials below the thermodynamic potential for the metal thiol compound formation. In the catalytic oxidation mechanism, the mineral provides a passage for the transfer of electrons from the site where the collector is oxidised to the site where oxygen is reduced but does not participate in the reaction itself. The third mechanism, the mineral participates in the adsorption process to form a metal thiol compound on the surface. The mechanism for formation of the metal thiol complex can be viewed as an electrochemical reaction, viz.

$$MS \rightarrow M^2 + S^\circ + 2e \text{ (E)}, \qquad (2)$$

and a chemical reaction (C), viz.

$$M^{2+} + 2X^- \rightarrow MX_2 \qquad (3)$$

in which X represents a thiol collector. The overall adsorption mechanism can be represented by an electrochemical reaction (EC):

$$MS + 2X^- \rightarrow MX_2 + S^\circ + 2e \qquad (4)$$

The electrochemical reaction mechanism occurs when the mineral is sufficiently oxidised to liberate metal ions to form metal-xanthates. The mineral oxidation is controlled by the electrochemical potential (E_h), while the chemical step is controlled by the stability constant (pK) of the metal-thiol compound. The fourth mechanism involves a metathetical substitution of the oxidation product on a mineral surface by a thiol collector. The mechanism does not directly involve a charge transfer process but the oxidation products

University of Cape Town

are formed by an electrochemical process. These mechanisms are discussed due to their relevance to this study.

The presence of metal ions in solution can have a major influence on the flotation and separation of sulphide minerals. Metal ion contamination of surfaces is frequently suspected of playing a detrimental role in selective flotation.

Copper activation has been reviewed a number of times over the last thirty years by ,interalia, Finkelstein and Allison (1976), Fuerstenau (1982) and Wang et al., (1989). More recently Finkelstein (1997) gave an in depth review of current theories on copper activation. The main emphasis of the review is the effect on sphalerite, with a few references to pyrrhotite and other sulphides. There has been no significant study of copper activation of PGE sulphide minerals.

Finkelstein and Allison (1976) suggested that, in addition to ion exchange for copper activation, there is an oxidation - reduction reaction in which Cu(II) is reduced to Cu(I) and the sulphide of the mineral is oxidised. The activation of sulphide minerals with Cu^{2+} and other cations induces collectorless flotation, i.e. the minerals become hydrophobic and can be floated without the addition of a conventional collecting reagent. It has been demonstrated that the floatability of copper acitivated sphalerite at neutral and mildly alkaline pH values is significantly depressed with respect to that of more acidic or more alkaline conditions.

Most of the observations and conclusions made to date have been based on classical chemical methods of measuring adsorption. Recently more studies have been conducted using instrumental techniques (Auger, XPS, ToF-SIMS) to identify surface species before and after copper activation. One of the major concerns related to information from these techniques is that they are ex-situ techniques and the surface can be significantly altered depending on the methods used to prepare the sample prior to analysis. In particular hydrolysis and oxidation products that are reversibly adsorbed on the surface can easily be

University of Cape Town

removed by washing procedures prior to analysis, and are alternatively easily deposited on the surface from the solution when the samples are dried prior to analysis.

There is further controversy with regards to the form of the oxidised sulphide generally referred to as COS (complex oxidised sulphide) which is formed as a result of the oxidation – reduction reaction involved in copper activation. It is either a polysulphide or a metal deficient lattice. Finkelstein (1997) argues that the difference between the two forms is not merely about semantics, but rather about the difference between a localised increase in sulphur concentration (polysulphide) and a homogeneous distribution over an entire lattice. Finkelstein (1997) concludes that depending on the conditions either or both can be formed.

Ralston et al., (1981) found that as the pH of the solution increased, the amount of elemental sulphur on the surface of sphalerite decreased with no elemental sulphur being detected above pH 7.5. Under normal flotation conditions employed, which are alkaline, elemental sulphur species are not expected, and the oxidation of the sulphide surface would result in the formation of sulphoxy compounds.

Perry et al., (1984), using Auger spectroscopy, found for copper activation of sphalerite that patches of copper rich islands are formed only after a few monolayers of evenly distributed copper have been adsorbed. Prestidge et al., (1994), using XPS, found that the copper is not evenly distributed for the same mineral.

Finkelstein (1997) discussed the kinetics and reaction mechanisms in depth. It is generally accepted that the reaction takes place in two stages, a rapid stage where a few monolayers are deposited on the surface and then a slower stage where the rate is controlled by diffusion into the sulphide lattice.

One of the findings highlighted by Finkelstein (1997) as being of importance for the application of metal activation to flotation is the extent to which the "lattice cations, the adsorbed cations and the induced acceptor states are mobile". Activation and oxidation of

University of Cape Town

the surfaces results in a surface layer that is significantly different in chemical composition from the bulk. The surface is described as being metastable and alters significantly with time. The implication of this is that the surface, which defines floatability, may change significantly during the passage through the flotation circuit. The time between activation and collector adsorption could therefore be used to improve the selectivity of flotation. With time the copper adsorbed on, say, pyrrhotite may diffuse into the bulk, leaving a surface without copper.

An important component in understanding copper activation is a thorough knowledge of the ionic species in the water used. The temperature, pH, E_h and ions present in the aqueous environment will dictate the chemistry of activation.

Wang et al., (1989) reviewed the aqueous and surface chemistry in the flotation of sulphide minerals. It is well known that heavy metal ions undergo a series of pH-controlled hydrolysis reactions in a binary metal cation-water system. For example in the case of Cu(II), the following reactions occur spontaneously:

$Cu^{2+} + OH \leftrightarrow Cu(OH)^{+}$ (initial hydrolysis) (5)

$2Cu^{2+} + 2OH \leftrightarrow Cu_2(OH)_2^{2+}$ (dimer formation) (6)

$Cu^{2+} + 2OH \leftrightarrow Cu(OH)_2$ (aq) (7)

$Cu^{2+} + 2OH \leftrightarrow Cu(OH)_2$ (s) (precipitation) (8)

$Cu^{2+} + 3OH \leftrightarrow Cu(OH)_3^{-}$ (9)

$Cu^{2+} + 4OH \leftrightarrow Cu(OH)_4^{2-}$ (10)

The distribution of these species at varying pH values can be calculated from their equilibrium constants. Free metal ions dominate only at very acidic pH values. At highly alkaline pH, their dominant species metal hydroxides. In medium pH range, the systems are highly complicated by the formation of soluble hydroxyls and even dimers. Thus,

University of Cape Town

different interactions between the mineral surface and metal ions should be expected, depending on the solution pH and total metal ion concentration.

Numerous speciation diagrams are available in the literature (Figure 1.11). Most of this data is produced at 25°C rather than the higher temperatures (~40°C) often typical of flotation circuits.

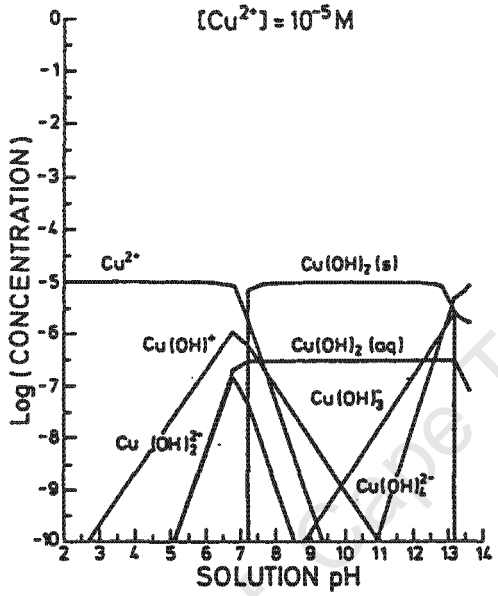

Figure 1.11: Log(Conc.)-pH Diagram for metal-water system of Cu(II) activator at a total metal concentration of 1.00E-05M

From Figure 1.11 it is evident that at the pH typical of Platreef ore flotation circuits, namely pH 9, the Cu species present in decreasing order are $Cu(OH)_2$ (s) >>$Cu(OH)_2$ (aq) > $Cu(OH)_3^-$> $Cu(OH)^+$> $Cu(OH)_4^{2-}$> $Cu_2(OH)_2^{2+}$. The addition of copper sulphate at pH 9 is therefore expected to produce a copper hydroxide precipitate.

Wang et al. (1989) have studied the stability of the ternary Fe(III)-OH-EX complexes and have shown that the intermediate pH depression of pyrite in its flotation with xanthate is very strongly correlated with the presence of ternary compounds. They have also shown that these ternary compounds are not strongly hydrophobic; however, if excess collector is present, they will be associated on the mineral surfaces and make the mineral particle sufficiently hydrophobic for flotation. The stability of Cu(OH)EX(s) would be expected to lie between that of $Cu(EX)_2$(s) and that of $Cu(OH)_2$(s). The equilibrium potential (pE) vs.

University of Cape Town

pH diagram of the Cu-EX-H_2O system at a total concentration of 1.00E-04 M copper and ethyl xanthate is shown in Figure 1.12.

Low pE values represent a reducing environment while high pE values an oxidising environment. The pE scale is intended to represent the concentration of the standard reducing agent (the e^-) analogously to the pH scale representing the concentration of standard acid (H^+). The pE values are obtained from reduction potentials by dividing E° by 0.059. Hence, for example, the pE value of 5 indicates an E° value of 0.295V.

The stability constants were taken from Kakovskii (1957) and Kakovskii and Arashkevich (1968) and that of Cu(OH)EX(s) was estimated. From Figure 1.12 it can be seen that there is a large area of stability for Cu(OH)EX(s), thus if the redox potential of the system falls into this area flotation will be inhibited.

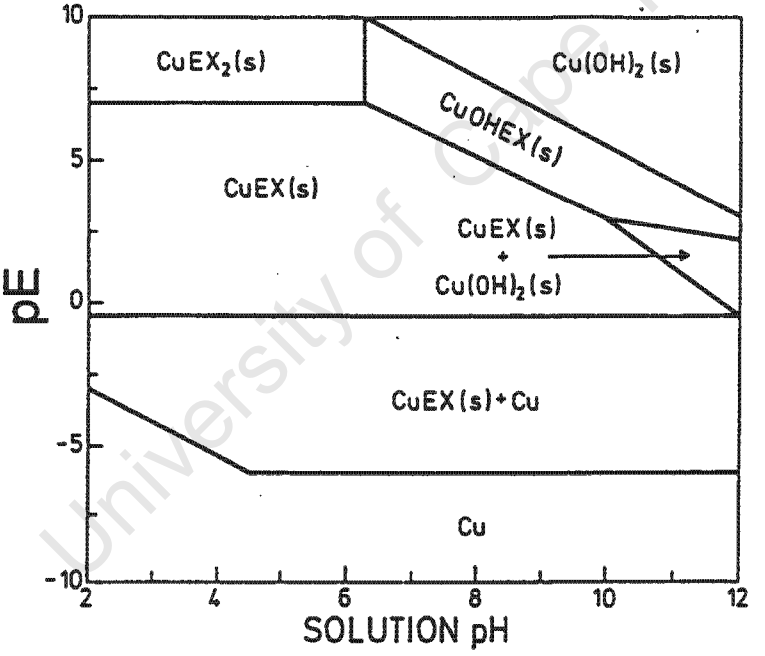

Figure 1.12: pE-pH Diagram for Cu-Ex system at a total concentration of Cu = 1.00E-04M and EX = 1.00E-04M, showing possible stability area of the compound Cu(OH)EX.

University of Cape Town

Notwithstanding the literature review above, many questions remain regarding the issue of copper activation. In particular, little attention has been paid to the aspect of copper activation on PGE sulphides.

1.5.2 PGE Arsenides

There does not appear to be any published research dealing with the oxidation of sperrylite surfaces and its effect on flotation. Nakazawa et al., (1986) described how nickel arsenide minerals were slow floating due to the oxidation of the mineral surfaces.

The reaction of sulphydryl collectors with the surface of sperrylite was studied by Volyanskii et al., (1985). Their conclusions were that potassium butyl xanthate is absorbed on the mineral surface in the form of dixanthide (oxidised form of xanthate, KX_2). In addition, they showed that sodium butyl dithiophosphate is also adsorbed (both in molecular and ionic form) on the surface of sperrylite. They suggested that varying the liquid phase pH may be a way of regulating the sulphydryl collector adsorption on the surface and thereby regulating the floatability of the mineral to a certain extent.

Unlike the PGE arsenides, the base metal arsenide, arsenopyrite (FeAsS), has been extensively studied. Most of the investigations to date have dealt with the separation of arsenopyrite from pyrite (Wang et al., 1992; Qiming et al., 1993; Monte et al., 2002). These studies have shown that the oxidised surface properties of these minerals can be utilised in developing methods for effective separation of these minerals. The oxidation product layer of pyrite consists mainly of sulphate and ferric hydroxide while the arsenopyrite surfaces, under moderately oxidising environment, are covered by stable, thick layers of oxidation products composed of ferric hydroxide and arsenate (AsO_4) on the outer surfaces.

The floatability of nickel arsenide was studied by Iwasaki et al., (1986) by salting a sample with synthetic nickel arsenide for bench flotation tests. The results indicated that oxidation by air virtually inhibited the flotation of nickel arsenide but, the use of nitrogen during grinding and flotation combined with copper activation restored its floatability.

University of Cape Town

Copper activation followed by sulphidising helped the recovery of the sulphide minerals and cursory analyses of the flotation products showed that the precious metal recoveries improved by the proposed flotation procedure.

Investigations describing the effect of xanthate, dithiocarbamate and copper sulphate on arsenopyrite surface alteration and floatability which may be applicable to PGE arsenide flotation have also been reported. Adsorption of isopropyl xanthate ions onto arsenopyrite and its effect on flotation has been studied by, amongst others, Valdivieso et al., (2003). They have shown that adsorption occurred first as isopropyl dixanthogen through an anodic oxidation reaction of the xanthate ions on arsenopyrite, with no effect on zeta potential of arsenopyrite, and then as isopropyl xanthate ions through hydrophobic bonding with the dixanthogen adsorbed at the arsenopyrite/aqueous solution interface, increasing negatively the zeta potential of arsenopyrite. Microflotation studies showed that arsenopyrite floated well due to the dixanthogen mineral surface coverage. This observation is consistent with a previous study by Allison et al., (1972). Who reported that the anodic oxidation reaction of xanthate ions to dixanthogen lead to a hydrophobic arsenopyrite surface.

O'Connor et al., (1990) tested various alkyl functional groups of collectors and showed that the best separations of arsenopyrite from pyrite were obtained using sodium isobutyl dithiophosphate and a mixture of 10%:90% sodium cyclohexyl : n-propyl dithiocarbamate. This reagent combination gave a recovery of 74.8% arsenopyrite and 8.4% pyrite with grades of 38% arsenopyrite and 11.6% pyrite, respectively.

In terms of copper activation of arsenopyrite, a number of studies have dealt with the mechanisms and products of Cu(II) activation. Abeidu et al., (1980) suggested that Cu(II) reacts preferentially with the arsenic sites on arsenopyrite surface to form an insoluble copper arsenide, either Cu_3As or Cu_3As_2. However, Wang et al., (1992) reported that the formation of copper arsenide is kinetically unfavourable, since the formation of these compounds requires a change of structure. As demonstrated in their electrochemical and XPS studies, the surfaces of arsenopyrite are readily oxidised to arsenate. Cu(II) then

University of Cape Town

reacts with the surface arsenate groups to form copper arsenate and arsenite [e.g. $Cu_3(AsO_4)_2$, $CuOHAsO_2$, $Cu(AsO_4)_2$] depending on the degree of surface oxidation and solution pH. All the copper arsenate and arsenite compounds have very low solubility and will remain on the mineral surface.

From the other base metal arsenides, cobalt arsenide was studied by Formanek and Lauvernier (1963). They reported that cobalt arsenides were quite sensitive to conditioning and the presence of a few percent iron necessitated copper activation with amyl xanthate as collector for flotation.

1.5.3 PGE Tellurides

It is well established that the surface products from excessive oxidation have a profound effect on mineral surface alteration which in turn has an effect on the flotation of those minerals and the Pd-Te-Bi system is no exception. Elvy et al., (1996) reported on the oxidation of the minerals in the Pd-Te-Bi system. This oxidation led to the formation of layers of tellurium and/or bismuth oxide covering the palladium-rich substrate.

Recently, Vermaak et al., (2004), described the electrochemical and Raman spectroscopic studies of the interaction of ethyl xanthate with Pd-Bi-Te. The study investigates whether the lack of collector interaction with the palladium bismuth tellurides is the reason for the poor flotation recoveries observed in practical applications. The results of the investigation showed that dixanthogen was present on the mineral surfaces when the surfaces were anodically polarized. This suggests that the poor flotation recovery of the Pd-Bi-Te minerals from flotation feeds cannot be attributed to a lack of interaction of the collector with the surface.

Separation of pyrite and gold tellurides by selective flotation was described by Yan and Hariyasa (1997). Flotation tests were carried out to test the natural floatability of the tellurides in the North Kalgoorlie samples and at natural pH, the tellurides floated readily with the addition of frother only. This recovery could be enhanced by the further addition of an activator and xanthate while some dithiophosphate collectors decreased the natural floatability of the tellurides.

University of Cape Town

1.6 Characterisation of the surface of mineral ores using zeta potential determinations, ToF-SIMS and XPS analyses

This section briefly describes the various surface analysis techniques as well as the applications related to these techniques in an attempt to show that the data from these analyses provide vital information in the understanding of flotation processes.

1.6.1 Zeta potential determinations

1.6.1.1 Brief description on the theory of zeta potential

Fuerstenau (1982) has reviewed these general concepts of the mineral-water interface and the electrical double layer. There are two factors which are important regarding the mineral-water interfaces, namely; the interaction of water molecules with the mineral surface, both in liquid and gaseous environments and the electrical double layer at the solid-water interface. Orientated water layers at mineral surfaces have a significant effect on the wettability of solids and also the nature of adsorption at an interface and the electrical double layer can affect the flotation process in many ways, e.g. flocculation and dispersion of mineral suspensions are controlled by the double layer, a high surface charge can inhibit the chemisorption of chemically adsorbing collectors, slime coatings are determined by electrical double layer interactions and flotation kinetics relate directly to the effect of double layers on the kinetics of the film thinning.

The electrical double layer develops upon immersion of a mineral in an aqueous solution, since charged species will migrate across the mineral/water interface until equilibrium conditions are established and the mineral surfaces will acquire a charge with respect to the aqueous phase. As a result, a region of electrical homogeneity forms at the mineral/water interface. The excess (positive and negative) charge fixed at the mineral surface is exactly balanced by the diffuse region of equal but opposite charge on the liquid side. The surface charge and diffuse region constitute the electrical double layer. Figure 1.13 shows a schematic representation of the electrical double layer and the potential drop across the double layer.

University of Cape Town

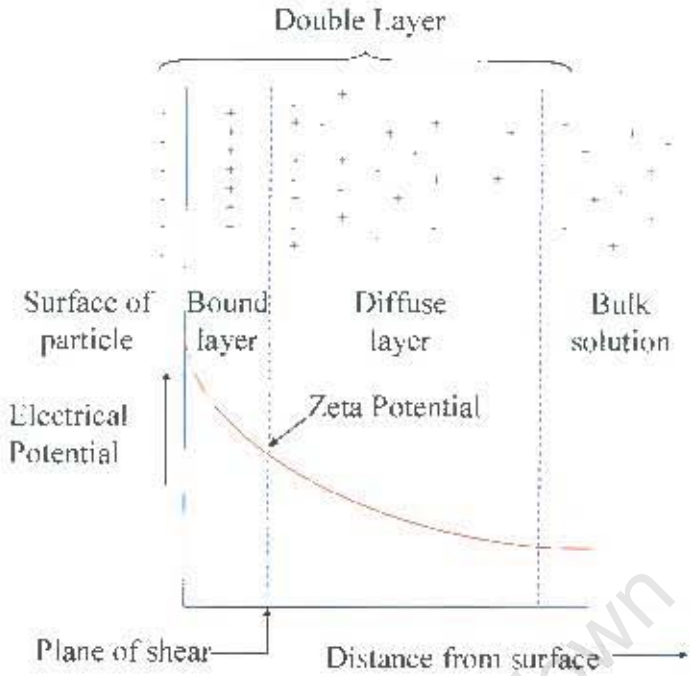

Figure 1.13: Schematic representation of the electrical double layer and the potential drop across the double layer.

The electrical charge on a mineral surface can be generated by a number of mechanisms, including chemisorption, preferential dissolution of surface ions, selective adsorption of ions and mineral lattice substitution. Ionic species play a predominant role in establishing the nature of the double layer. Ions that give rise to the surface charge are called potential-determining ions and are special to each mineral. Ions that are adsorbed only to maintain electro-neutrality in the system are called counter ions and any kind of electrolyte ions can function as counter ions. The first layer of counter ions lies at a distance from the surface in the Stern plane and this distance is determined by the ionic radius. The surface charge is generally a complex function of the ionic strength and the activity of potential-determining ions in solution. It is given by the difference in adsorption of positive and negative potential-determining ions. The definition of surface charge: requires that all positive and negative potential-determining ions be adsorbed onto the surface and not occur in the diffuse layer. At the point of zero charge (pzc), the adsorption densities of potential-determining ions are equal. The pzc of a mineral is the single most important parameter that describes the double-layer phenomenon at the mineral-water interface. The importance of the pzc resides

University of Cape Town

on the fact that the sign of the surface charge has a major effect on the adsorption of all ions and particularly those ions charged oppositely to the surfaces. If an ion present in a solution functions as a counter ion to maintain electro-neutrality and if it adsorbs only by electrostatic attraction, it is called an indifferent ion. Some ions exhibit surface activity in addition to electrostatic attraction and these ions are called surface active counter ions and flotation collectors generally fall into this category.

The two most commonly used methods in flotation chemistry research for the evaluation of electrokinetic potentials are electrophoresis and streaming potential. Electrophoresis involves the measurement of the rate at which fine particles move in an electric field, whereas evaluation of streaming potentials is based on the measurement of the potential setup when a liquid is forced through a bed of particles. From the appropriate theory, one evaluates the potential at the slipping plane, which is generally considered to be just outside the Stern plane. The potential at the slipping plane is referred to as the zeta potential and is generally assumed to approximate the Stern layer potential. Besides the electrokinetic phenomena themselves, electrokinetic techniques provide a method for measuring the electrical effects due to adsorption. In addition to controlling collector adsorption, the double layer controls the stability of suspensions and the kinetics of bubble-particle contact (Aplan and Fuerstenau, 1962).

It is customary to interpret electrokinetic data in terms of ζ-potential. This is the potential of the slipping plane between the moving and stationary phase, when the liquid far away from the interface is considered to be at zero potential.

When an electrical field is applied across an electrolyte, charged particles suspended in the electrolyte are attracted towards the electrode of opposite charge. Viscous forces acting on the particles tend to oppose this movement. When equilibrium is reached between these two opposing forces, the particles move with constant velocity and this phenomenon is called electrophoretic mobility. The velocity of a particle is related to the dielectric constant and viscosity of the suspending liquid and to the

University of Cape Town

electrical potential at the boundary between the moving particle and the liquid (Malvern Instruments Training Manual, 1996).

Zeta potential is related to the electrophoretic mobility by the Henry equation (Hunter, 1993):

$$u_E = \frac{\zeta\varepsilon}{1.5\,\eta} f(\kappa a) \qquad (11)$$

where u_E is the electrophoretic mobility, ε is the fluid dielectric constant, ζ is the zeta potential, η is the dynamic viscosity, κ is the Debye-Huckel parameter and a is the particle radius. For large particles in more concentrated electrolyte solutions $\kappa a >> 1$ and $f(\kappa a) = 1.5$. This transforms Henry's equation (11) into Smoluchowski's equation (12):

$$u_E = \frac{\zeta\varepsilon}{\eta} \qquad (12)$$

At 25°C this reduces to:

$$\zeta = 12.85 \times u_E \text{ (mV)} \qquad (13)$$

1.6.2 Time of Flight Secondary Ion Mass Spectrometry (ToF-SIMS)

1.6.2.1 Brief description on the theory of ToF-SIMS

Benninghoven (1975) describes secondary ion mass spectroscopy (SIMS) as positively and negatively charged atomic and molecular particles that are emitted from a surface during ion bombardment and are mass analysed. These secondary ions give important information about the chemical composition and structure of the solid surface. The SIMS technique is widely employed for bulk, thin film and surface analysis. Time of flight SIMS (ToF-SIMS) is the dominant experimental variant of *static SIMS* that emerged as a technique of potential importance in surface science.

University of Cape Town

Conceptually the process is very simple and is shown is Figure 1.14 (Vickerman, 2001).

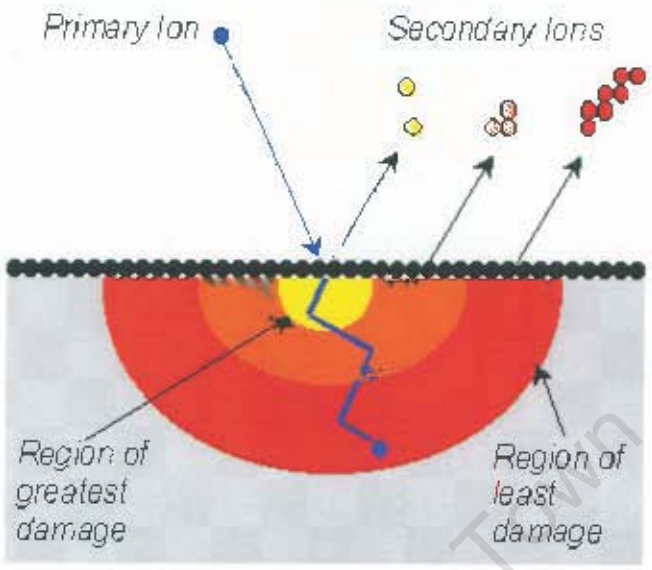

Figure 1.14: A schematic diagram of the SIMS process (Physical Electronics, 2006)

The ToF-SIMS uses a pulsed primary ion beam to desorb and ionize species from a sample surface. The primary ion dose is low ($<10^{12}$ ions/cm^2) and it uses short pulses of <1ns. In other words, less than 1 in 1000 surface atoms or molecules is struck by a primary ion. The actual desorption is caused by a "collision cascade" i.e.: collisions occurring between the atoms of the solid. The term "secondary ions" is used to distinguish them from the primary bombarding ions. A small percentage of the secondary ions are charged and can therefore be extracted by an electric field (accelerating field) into a mass spectrometer. The kinetic energy (E_{kin}) of the ions can be expressed as;

$$E_{kin} = eV_o = \frac{1}{2}mv^2 \qquad (14)$$

where V_o is the accelerating potential, m the mass of the ion and e its charge. Lighter ions have higher velocities than the heavier ions and will therefore arrive at the detector first. The mass separation is obtained by the flight time (t) from the

University of Cape Town

sample to the detector. This can be determined using equation 15 where L_o is the effective length of the spectrometer.

$$t = L_o/v = L_o\,(m/2eV_o)^{1/2} \qquad (15)$$

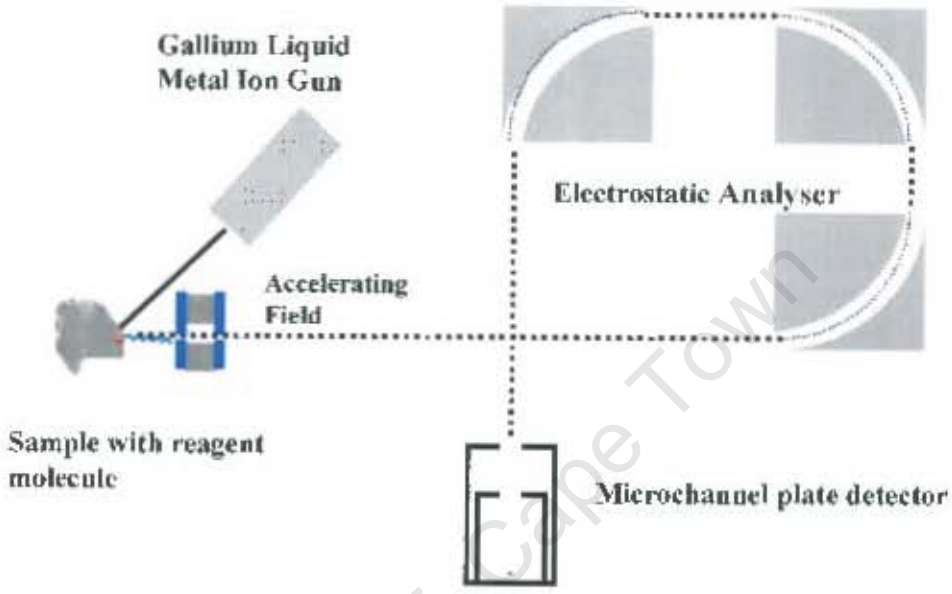

Figure 1.15: ToF-SIMS layout (Physical Electronics, 1997).

The mass spectra are recorded by measuring the time difference between pulsing the primary ion gun and the arrival of secondary ions on a fast dual microchannelplate detector at the spectrometer by means of a multistop time-to-digital converter (TDC) (Figure 1.15). Neighbouring masses m_o and $m_o+\Delta m$ can only be resolved if the relationship between time width and separation are correct. Using equation (16) it can be shown that for small mass differences the relationship between flight times and mass resolution is given by

$$m/\Delta m = t_o/2\Delta t \qquad (16)$$

From equation (19) it can be seen that in order to obtain high mass resolution, a short primary ion pulse (t_o) has to be used (Figure 1.16).

University of Cape Town

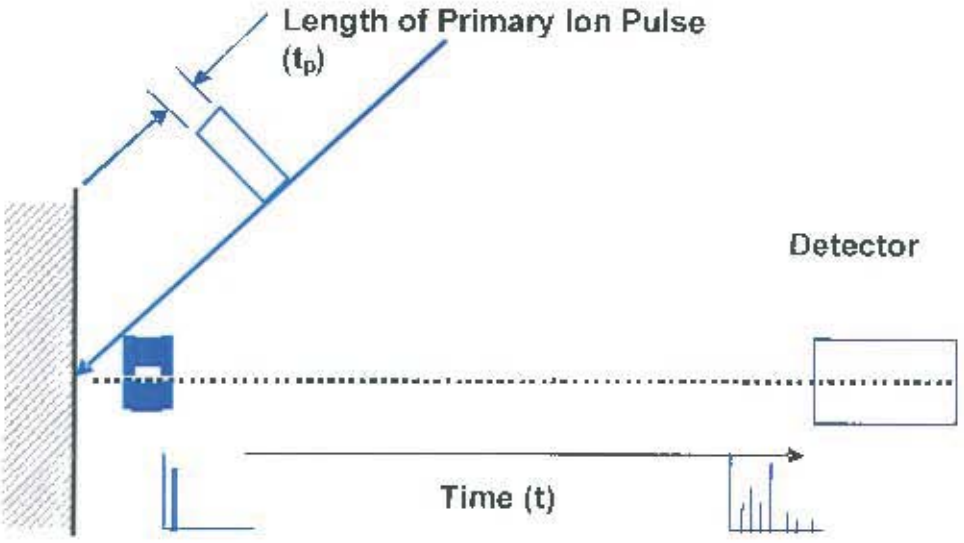

Figure 1.16: The separation of ions by Time of Flight (Physical Electronics, 1997).

The energy transferred when a primary ion impacts with the sample surface results in fragmentation of the original surface in the vicinity of the impact, resulting in the release of atomic species. Further away from the impact site, higher mass molecular species are released as a result of the energy transferred by the impact throughout the substrate. A heavy energetic primary ion cannot be stopped immediately by the first atoms it encounters and will therefore continue into the surface until it has lost all its energy due to elastic scattering off atomic cores and inelastic scattering off electronic shells and free electrons. The ions that are collided with will recoil and displace other atoms, which will in turn collide with other atoms, setting up a complex sequence of collisions. Some atoms will be permanently displaced from their positions while others will return elastically to their original lattice positions. The collision cascade will eventually result in the surface atoms being displaced (Schueler, 1992; Reich, 1997).

The PHI TRIFT II^{NT} instrument used during this study operates in the static SIMS regime. The term static refers to the number of primary ions impacting the surface per unit area. The static SIMS regime is accepted to be about 10^{12}–10^{13} primary ions/cm^2. The density of a silicon surface is approximately 10^{15} atoms/cm^2. The PHI TRIFT II^{NT} ToF-SIMS features state of the art primary ion gun technology, including a

focused liquid metal ion gun with three orders of magnitude range of beam current, from 20 nA (fast spectroscopy) to 20 pA (high lateral resolution, 0.1 μm analytical probe). The ToF-SIMS is capable of analysing small features of interest on both conducting and insulating samples due to automatic electron charge compensation (Reich, 1997).

An image is generated by rastering a finely focused beam across the sample surface. The entire mass spectrum is acquired from every pixel in the image. The mass spectrum and secondary ion images are used to determine the composition and distribution of the sample constituents (Physical Electronics, 2006). Figure 1.17 shows a schematic representation of the process for obtaining mass spectrum and secondary ion images.

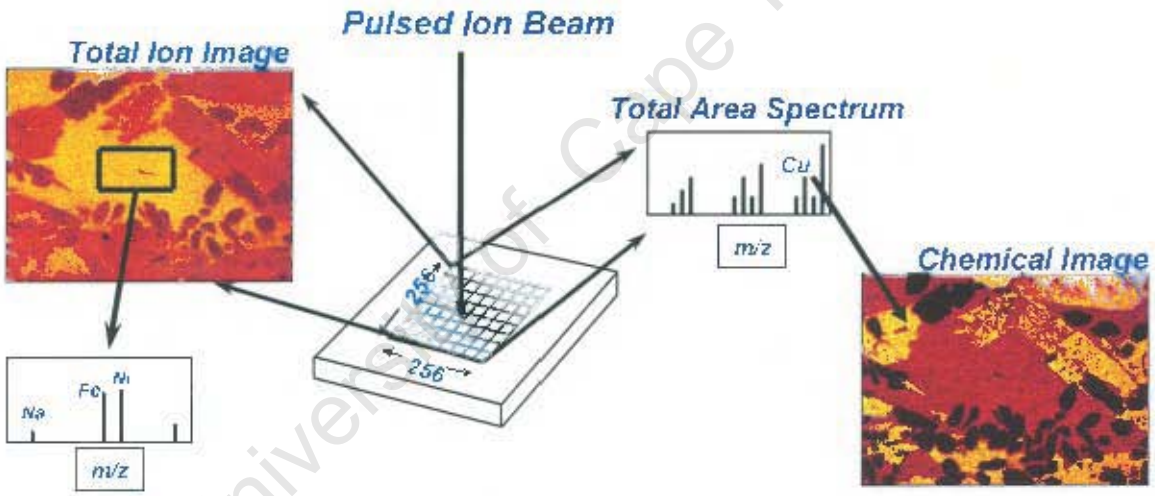

Figure 1.17: Schematic representation of the process for obtaining mass spectrum and secondary ion images using ToF-SIMS (Physical Electronics, 1997).

The ToF-SIMS is capable of shallow sputter depth profiling where an ion gun is operated in direct current (DC) mode for sputtering, and the same ion gun or second gun is operated in pulsed mode for data acquisition. Depth profiling by ToF-SIMS allows monitoring of all species of interest simultaneously, with high mass resolution (Physical Electronics, 2006).

University of Cape Town

1.6.3 X-ray Photoelectron Spectroscopy (XPS)

1.6.3.1 Brief description on the theory of XPS

Surface analysis by X-ray Photoelectron Spectroscopy (XPS) involves irradiating a solid *in vacuo* with monoenergetic soft x-rays and analysing the emitted electrons by energy. The spectrum is obtained as a plot of the number of detected electrons per energy interval versus their kinetic energy. Each element has a unique spectrum. The spectrum from a mixture of elements is approximately the sum of the peaks of the individual constituents. Because the mean free path of electrons in solids is very small, the detected electrons originate from only the top few atomic layers. Quantitative analysis can be obtained from peak heights or peak area, and identification of chemical states often can be made from the exact measurement of peak positions and separations, as well as from certain spectral features (Moulder et al. 1995).

XPS was developed in the mid 1960s by K. Siegbahn and his research group. K. Siegbahn was awarded the Nobel Prize for Physics in 1981 for his work in XPS. Siegbahn (1990) has described the fundamentals of XPS as well as new trends. The phenomenon is based on the photoelectric effect outlined by Einstein in 1905 where the concept of the photon was used to describe the ejection of electrons from a surface when photons impinge upon it.

The photoelectric effect which was discovered by Hertz in 1887, lead to the development of the X-ray photoelectron spectrometer. Hertz discovered that some metallic metals emitted electrons from their surfaces when exposed to light. This phenomenon is now commonly known as the photoelectric effect and is described by equation 17.

$$E_K = h\nu - E_B - \phi \qquad (17)$$

Where E_K is the kinetic energy of the photoelectrons emitted from the sample into continuum, h is Plank's constant, ν is the frequency of the incident radiation, E_B is the

University of Cape Town

binding energy of the photoelectron and ϕ is the spectrometer work function of the material being examined.

The adsorption of energy, in the form of a photon, by a material gives rise to the ejection of an electron from that atom into continuum (Figure 1.18). The binding energy may be regarded as the energy difference between the initial static and the final state after a photoelectron has left the atom.

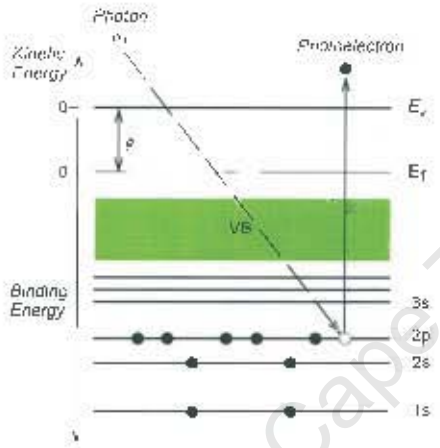

Figure 1.18: Photoelectric effect (Smart et.al., 2006).

The atom left in the excited state may then relax via two processes: X-ray fluorescence or the Auger process. The Auger electron and process of emission is named after Pierre Auger. These processes involve an electron from an outer energy level filling the core hole. The resulting energy difference between these two levels is then emitted via a photon, or, alternatively the excess energy may be transferred to another electron (Auger electron) ejecting it from the atom.

University of Cape Town

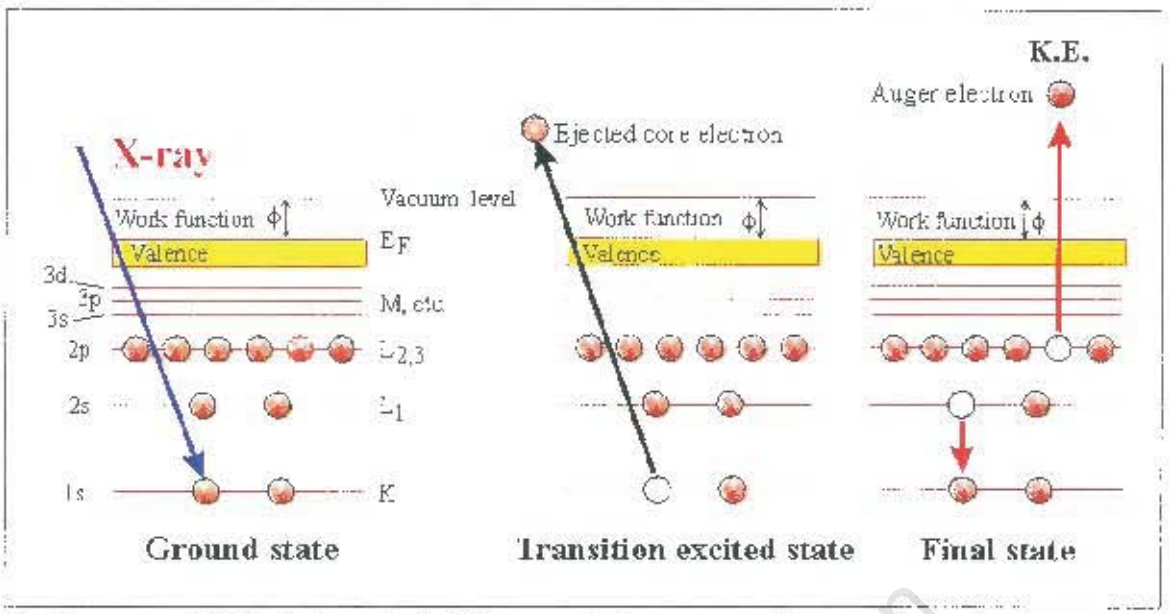

Kinetic energy (K.E.) is independent of the x-ray photon energy. However, in the binding energy (B.E.) scale. Auger peak positions depend on the x-ray source

Figure 1.19: X-ray fluorescence and Auger process.

Both photoelectrons and Auger electrons appear in the XPS spectra. Complicating features derived from these transitions also appear in the XPS spectra, e.g. secondary electrons, initial and final state shake-ups and shake-offs, intrinsic and extrinsic plasmons, plasmon gain peaks and satellite peaks which all assist in the identification of peaks (Figure 1.19).

The XPS technique was developed to detect and analyse the photoelectrons emitted from materials. The initial function of XPS was to determine the atomic structure, however, the chemical shifts in the spectra brought about the development of electron spectroscopy for chemical analysis (ESCA). Chemical shift is the change in the binding energy of a core electron of an element due to a change in the chemical bonding of that element, i.e. the interaction of core electrons with electrostatic potential from valence electrons. This occurs by a change in oxidation state, lattice sites (coordination, defects), electron density changes and interfacial fields.

University of Cape Town

From a qualitative view, core binding energies are determined by the electrostatic interaction between it and the nucleus, and reduced by the electrostatic shielding of the nuclear charge from all other electrons in the atom (including valence electrons). Removal or addition of electronic charge as a result of changes in bonding will alter the shielding, i.e.

- Withdrawal of valence electron charge: - increase in binding energy (BE)
- Addition of valence electron charge: - decrease in BE

Photoemission process can be thought of as the following 3 steps:

- Photon absorption and ionisation (initial state effects)
- Response of atom and creation of photoelectron (final state effects)
- Transport of electron to surface (extrinsic effects)

XPS is a surface sensitive technique capable of analysing up to a depth of 4 nm. The depth analysis (escape depth) is dependent on the inelastic mean free path (IMFP) of the emitted photons. The IMPF of an electron moving in a solid is the average distance travelled by the electron before it looses energy via undergoing an inelastic collision. The escape depth of a photoelectron depends on its path within the solid and its angle of emission to the surface (equation 18). Electrons emitted perpendicular to the surface has the maximum escape depth.

$$d = \lambda \cos \varphi \qquad (18)$$

Where d is the escape depth of an emitted electron, λ_i is the IMFP of the electron for a particular energy and material, and φ is the angle of emission of the electron with respect to the normal sample surfaces.

Sampling depth is defined as the depth at which 95% of all photoelectrons are scattered by the time they reach the surface. For electrons emitted perpendicular to the surface, 63% of the signal originates from 1 λ, 86% originates from 2 λ, and 95% originates from within 3 λ, as the signal from below the surface is proportional to $e^{-1/\lambda}$.

University of Cape Town

Decreasing the angle of the detector relative to the surface decreases the sampling depth allowing more surface sensitive analysis. Angle-resolved XPS is commonly used to study optically flat materials, due to its ability to detect changes in chemical speciation at various depth analyses.

1.6.4 Research studies using zeta potential, ToF-SIMS and XPS

There are many examples in the literature of papers describing the use of these surface techniques to give a general insight into flotation responses. A few examples of such investigations are reported here to illustrate this type of research with reference to the current study but are by no means exhaustive.

1.6.4.1 Oxidation studies

Xanthate adsorption on selected sulphides in the virtual absence and presence of oxygen was study by Fuerstenau et al., (1989), using zeta potential measurements. The results showed that oxygen was adsorbed more readily than xanthate onto the galena surface and that it effectively blocks the xanthate ion from adsorbing onto the lead sites. Hence, in the absence of oxygen or very little oxygen, xanthate adsorbs at mono layer coverage only and adsorption is independent of pH. In the presence of oxygen, multi-layers of xanthate are noted on the surface and these multi-layers comprised of precipitated lead xanthate in a 1:2 coordination of lead to xanthate.

Mycroft et al., (1990) studied the electrochemical oxidation of pyrite surfaces in near-neutral aqueous chloride solutions using XPS and Raman spectroscopy. The results displayed the presence of a polysulphide species not previously identified which forms over a potential range of 150-750 mV. According to the Pourbaix diagram, these polysulphide species are metastable in this region, and seem to be intermediates in the production of sulphur.

Mycroft et al., (1994) examined the distribution of oxidised species with depth on air-oxidised pyrrhotite. The results have shown that at the surface of the

University of Cape Town

alteration zone of the mineral, a thin iron oxide zone forms. This layer overlays the second alteration zone, a sulphur rich zone with a composition of FeS_2 at the top of the zone. The sulphur to iron ratio decreases to bulk pyrrhotite with increasing depth. Only minor amounts of thiosulphate and sulphates were detected in the study. The formation of the iron oxy-hydroxide layer appears to drive the diffusion of iron from the underlying iron sulphide. The depletion of iron from this zone produces the sulphur rich or polysulphide rich layer. XPS evidence presented shows that disulphide and polysulphide accumulate in the zone, along with minor amounts of elemental sulphur and oxy-sulphur species, all of which are products of monosulphide oxidation.

Knipe et al., (1994) carried out a XPS study of water adsorption on iron sulphide minerals. Samples of natural pyrrhotite and pyrite were fractured within the analytical chamber of the XPS. Theses mineral surfaces were exposed, in the absence of oxygen, to the various doses of D_2O. XPS was performed between each water dose to investigate the interaction of the iron sulphide surfaces with water vapour. Recorded Fe and S photoelectron spectra showed no evidence of oxidation products on either mineral. Conclusions were that pyrrhotite and pyrite interact with water via fundamentally different processes. Pyrrhotite reaction involves the donation of electron charge through Fe vacancies, whereas the water species detected on pyrite interact with the Fe *3d* molecular orbital, and it is suggested that hydrogen bonding with the disulphide moiety may be important.

The effect of oxidation on the collectorless flotation of chalcopyrite was studied by Fairthorn et al., (1996) using zeta potential measurements and XPS. The results show that iron and to a lesser extent copper dissolve from the chalcopyrite lattice leaving a metal deficient sulphur rich surface and these metals reabsorb or precipitate as hydroxide species on the chalcopyrite surface. The hydrophobicity of the surface and therefore the chalcopyrite flotation are controlled by these two processes.

University of Cape Town

Schaufuß et al., (1998) studied the incipient oxidation of fractured pyrite surfaces in air. Synchrotron and conventional XPS was used to study the initial oxidation of pyrite. The synchrotron radiation significantly enhanced the surface sensitivity obtained and allowed the detection of intermediate sulphur species. It has been shown that the surface components that are directly exposed to atmospheric gases undergo oxidation to sulphate, whereas the bulk sulphur mainly forms 'electron deficient' disulphides. These results were used to propose an oxidation mechanism including the oxidation of different iron as well as sulphur sites.

Smart et al., (1999) used the XPS to study sulphide mineral surfaces under different conditions of preparation, oxidation and reaction. This paper presents evidence for the assignment of components of the S *2p* XPS spectra to metal-deficient sulphide surfaces, polysulphides and elemental sulphur.

The correlation between the surface composition and collectorless flotation of chalcopyrite was examined by Zachwieja et al., (1998). The flotation response of air-oxidised chalcopyrite in alkaline solutions in the absence of a collector has been correlated with the surface composition as determined by XPS. Iron-oxygen species are removed from the surface of the oxidised mineral during conditioning in nitrogen-saturated alkaline solution to leave an iron-deficient sulphide lattice at the solid/liquid interface. The floatability of the conditioned mineral is consistent with the sulphur-rich sulphide lattice being hydrophobic. Oxidised chalcopyrite surfaces subjected to an applied reducing potential became sulphur-deficient and were un-floatable.

Smart et al., (2000) performed SIMS studies on oxidation products and polysulphide formation in reacted sulphide surfaces. This paper compared the data obtained using SIMS and XPS. Tests were carried out on air-oxidised galena, solution oxidised galena, statistical analysis of oxidised ground galena particles, polysulphide identification in troilite/pyrrhotite/pyrite comparison. The SIMS results appeared to directly reflect the surface chemistry of the metal and

University of Cape Town

the sulphur species and were not consistent with the recombination or fragmentation of secondary neutral or ionic species. The results strongly suggested increasing polymerisation of S-S species with increasing oxidation in accordance with the XPS assignment to polysulphide of increasing chain length.

O'Dea et al., (2000) studied the interaction of xanthate with galena using Static SIMS. Three xanthate fragments together with O and S negative images were compared. Oxidised galena surfaces had relatively low concentrations of adsorbed xanthate compared to freshly cleaved galena surfaces at both low and high xanthate concentrations which was apparently due to surface oxidation products passivating against continuing dissolution.

Smart et al., (2003) studied the oxidation and collector adsorption in sulphide mineral flotation using XPS. They studied surface speciation as a function of time, pH, E_h and collector adsorption related to mineral flotation. The study revealed that the mechanisms of oxidation are considerably more complex than those represented by simple reactions such as:

$$MS + xH_2O + 1/2xO_2 \rightarrow M_{1-x}S + xM(OH)_2 \qquad (19)$$

The chemical nature of the $M_{1-x}S$ products, spatial distribution of the oxidation products and the interaction with other dissolved species all complicate the real situation. It was found that hydroxide products were not formed uniformly over the surface of the sulphide mineral and the chemical form of the metal-deficient or sulphide rich surface was highly variable. The results also indicated that collector adsorption occurred in many different modes, i.e.; on specific surface sites, colloidal precipitation from solution, the detachment of small sulphide particles from larger particle surfaces, the detachment of small oxide/hydroxide particles, removal of adsorbed and amorphous oxidised surface layers, inhibition of oxidation, disaggregation of larger particles and patch wise or face-specific coverage.

University of Cape Town

Smart et al., (2003) described surface analytical studies of oxidation and collector adsorption in sulphide mineral flotation. The initial surfaces and oxidation products were studied using various techniques including XPS and ToF-SIMS. Changes to surface speciation were followed as a function of time, pH, E_h, and collector adsorption related to mineral flotation. The results showed that oxidation products are formed in different processes, viz. metal deficient sulphides, polysulphides and sulphur; oxidised fine sulphide particles; colloidal hydroxide particles and flocs; continuous surface layers of varying depth; sulphate and carbonate species; isolated and patch wise and face-specific oxide, hydroxide and hydroxycarbonate development. The actions of collector molecules have been identified in several modes, viz. adsorption to specific sites; colloidal precipitation from solution; detachment of small sulphide particles from larger particle surfaces; detachment of small oxide/hydroxide particles; removal of adsorbed and amorphous oxidised surface layers; inhibition of oxidation; disaggregation of larger particles; and patch wise or face-specific coverage.

University of Cape Town

1.6.4.2 Copper speciation studies

Van der Laan et al., (1992) studied the oxidation state variations in copper minerals with Cu *2p* XPS. Divalent and monovalent spectra were presented. Divalent Cu gave a narrow, single line due to excitation into the empty *3d* density of stats, whereas monovalent Cu gave a broad band at higher energy due to transitions to the empty metal *s* and ligand states. The differences in the spectra can be used to distinguish between the two-oxidation states, which have been applied to copper sulphide tetrahedrite complexes.

Laajalehto et al., (1995) examined copper sulphide surfaces using synchrotron radiation XPS. The conventional XPS excitation is not very sensitive for sulphur emission, because of the high kinetic energy of S *2p* or S *2s* photoelectrons. The synchrotron allows the choice of excitation energy within a large energy

range and the high intensity available in the synchrotron storage ring allows a choice of the excitation energy, which yields an optimum kinetic energy for excited photoelectrons, from a point of surface sensitivity. Hence, the inelastic mean free path of S *2p* photoelectrons is about 15 atomic layers for AL*Kα* excitation which can be reduced to ~1.5 atomic layers for synchrotron radiation. The results showed a surface core level shift of sulphur bonded to copper in planar CuS_3 coordination observed in the S *2p* spectrum for CuS. The behaviour was different for other copper sulphide studied.

Nagaraj and Brinen (1995) studied the adsorption of sulphide collectors on pyroxene. SIMS and XPS were used to study the interaction between pyroxene and xanthate and thionocarbamate at pH 9. No collector adsorption was evident on untreated pyroxene. Collector adsorption was observed only after pyroxene that had been treated with Cu(II) ions and then with collector. XPS results showed that copper on pyroxene was reduced from cupric to cuprous upon collector adsorption suggesting the formation of a cuprous complex of the collector. The SIMS imaging suggested that the copper adsorption occurs at copper sites on the surface.

Gerson et al., (1998) described the mechanism of copper activation of sphalerite using data obtained from SIMS, XAFS and XPS. The model proposed that, on surface adsorption of Cu, the Zn(II) atoms are replaced by Cu(II) atoms which are reduced in situ to Cu(I). This reduction is accompanied by the oxidation of the three neighbouring S atoms to an oxidation state of approximately -1.5. On bulk adsorption of Cu atoms into the sphalerite lattice a distorted trigonal planar configuration is achieved through the breakage of a formally tetrahedral Zn-S bond. The breakage of this bond results in a 3-fold coordinated Cu plus one S 3-fold coordinated to Zn atoms. The breakage of this bond leads to a greater reduction of the Cu than on surface adsorption and also oxidation of the 3-fold coordinated S atom to approximately -0.5 oxidation state.

University of Cape Town

Fornasiero and Ralston (2005) have investigated the effect of surface oxide/hydroxide products on the collectorless flotation of copper-activated sphalerite using zeta potential measurements and XPS. An optimum copper concentration for maximum sphalerite flotation was identified, beyond which flotation decreased. The decrease in flotation coincided with the precipitation of copper hydroxide in neutral to mildly alkaline pH conditions. The hydrophobic polysulphide and hydrophilic copper hydroxide species were the main surface species influencing sphalerite flotation.

The depression mechanisms of sodium bisulphite in the xanthate-induced flotation of copper activated sphalerite were researched by Khmeleva et al., (2006). They used batch flotation, XPS and ToF-SIMS surface techniques and FTIR to identify the mechanisms of interaction of sulphite ions with both collector and the sphalerite surface. The data has suggested that copper xanthate decomposition on the surface of the activated sphalerite and the decomposition of the hydrophobic copper-sulphide species on the shalerite surface are the active mechanisms for sphalerite depression by sodium bisulphite.

University of Cape Town

1.6.4.3 Characterisation of base metal sulphides

A few examples of mineral characterisation have been included to demonstrate the ability of the surface analysis techniques, in particular, XPS. Pentlandite has been used as an example since there was no evidence of this type research performed on PGE type minerals.

Buckley and Woods (1991) used XPS to investigate the surface oxidation of pentlandite. The XPS spectra indicated that the initial reaction on exposure to air is the removal of iron from the pentlandite lattice to form a hydrated iron oxide overlayer and leave a metal ion-deficient pentlandite in addition to a restructured nickel-iron sulphide. Further oxidation resulted in some nickel being transferred to the oxide. Pentlandite behaved in a similar manner to that

established for pyrrhotite, indicating that the iron in pentlandite is preferentially removed on anodic oxidation to leave a metal deficient sulphide layer. The formation of sulphate was also indicated on scans to high potentials in basic media.

Legrand et al., (1997) describes the surface characterisation of pentlandite by XPS. Natural pentlandite was used for the study. The Fe *2p*, Ni *2p*, S *2p* and O *1s* spectra were discussed. The main feature of interest was found in the S *2p* spectrum where two major doublets were found, one with a S $2p_{2/3}$ binding energy of 161.44 eV and the other at 162.19 eV. These doublets are interpreted as being due to sulphur in a 4 coordinate environment and a 5 coordinate environment, respectively. They obtained a ratio of 1:2.5 for the two species, in agreement with the theoretical ratio of 1:3 predicted from the pentlandite structure. Natural pentlandite samples were exposed to deionised water for 1.5 and 6 hours. The pentlandite surfaces were oxidised to give surfaces that were rich in iron oxy-hydroxide species depleted in nickel and sulphur.

Legrand et al., (1998) also characterised millerite because of its relationship to pentlandite. Millerite only contains one metal and is not as complicated as pentlandite and studying its surface may be useful in understanding some of the possible reactions that pentlandite can undergo under various conditions. The millerite Ni *2p* and S $2p_{2/3}$ binding energies are reported as 853.1 and 161.7 +/- 0.2 eV, respectively. Millerite exposed to air and water for 24 hours will react to form various species; namely, hydroxy nickel and oxysulphur nickel species (mainly hydrated $NiSO_4$). The sulphur in NiS is oxidised to polysulphide and oxysulphur species (mainly sulphate), while nickel oxidation remains Ni(II). Similar reactions occur in air and water. Oxidation products either form islands or very thin layers at the millerite surface.

University of Cape Town

Nesbitt et al., (2001) studied the fivefold and sixfold coordinated sulphur in pyrrhotite with evidence for millerite and pyrrhotite surface species. Collection of S *2p* XPS spectra of millerite using conventional XPS and a synchrotron photon source, demonstrated the presence of one surface species on millerite and spectral deconvolution indicates a second surface contribution. Core level shift is attributed to a surface monomeric species (S^{2-}) wheras the second contribution is probably a surface dimeric species (S_2^{2-}). Surface dimers indicate surface reconstruction of millerite surfaces upon cleavage.

1.6.4.4 Plant related studies

A number of plant studies were examined showing how surface chemistry surveys play a role in establishing problems in the plant and how to overcome them.

The flotation of a copper and lead-zinc sulphide ore from Mt. Isa has been studied by Grano et al., (1990), in the absence and presence of specific collectors and depressants over a range of grinding and flotation E_h conditions. XPS was used to determine the surface composition of the flotation products. The results show that a substantial portion of the iron sulphide minerals is naturally floatable due to a surface coating of graphite carbon formed during ore genesis. Flotation of both ores showed a strong dependency on E_h. The collector selectivity removes ferric hydroxides and carbonates from the surface of the chalcopyrite. Grinding in an oxidising environment reduced selectivity due to an increased flotation of the iron sulphide minerals.

Kristall et al., (1994) examined the flotation of sphalerite in the Murchison zinc concentrator. XPS was used to examine samples taken during the pulp chemical survey where important chemical changes occurring during preconditioning (aerated) and conditioning sections of the plant were monitored. XPS results for sulphur showed an increase in the proportion of sulphur occurring as sulphate through preconditioning which is a result of sulphide

University of Cape Town

mineral oxidation. The results for zinc showed an increase in the amount of zinc hydroxide species present through preconditioning, which were not necessarily adsorbed on the sphalerite surface as shown by XPS of the sample after solution replacement. Direct evidence for pyrite oxidation through preconditioning was provided by the XPS, which showed an increase in the amount of oxidised ion, relative to pyrite. There was evidence for modification of the sphalerite surface to form a metal deficient surface. Conditioning the sample with lime to a pH of 11.5 revealed a clean sphalerite surface indicating the dispersion of zinc hydroxides at high pH and this enhanced flotation kinetics and recovery of sphalerite contained in other ore bodies.

Smart and Judd (1994) showed during a surface analysis survey how the poor performance in the re-flotation circuit at Olympic Dam Operation was related to ineffective operation of the Lasta filter. Samples were collected when the circuit was performing well and when the circuit was performing poorly. Surface analysis on these samples showed significant differences that could be related to plant performance. Maintaining the specified pressures and wash volumes were found to be critical to optimum filter operation.

The detection and control of calcium sulphate precipitation in the lead circuit of the Hilton concentrator of Mount Isa mines limited in Australia was studied by Grano et al., 1996. They used XPS to identify the presence of an overlayer of precipitated calcium sulphate at the surface of the sulphide minerals. There was a decrease in surface concentration of calcium sulphate on the concentrates compared to the tailing samples, which suggested that the flotation process was selective against minerals, which have calcium sulphate predominating at the surface thereby reducing the galena flotation rate. Methods to control calcium sulphate precipitation were discussed.

University of Cape Town

1.6.4.5 General

This section considers a variety of studies including the effect of collectors, gangue minerals and surface passivating layers originating from water sources.

Mackenzie and O'Brien (1969) used zeta potential determinations to investigate the adsorption of nickel and cobalt ions from aqueous solution onto the quartz surface. They concluded that Ni^{2+} and Co^{2+} are only weakly adsorbed onto the quartz surface and that $NiOH^+$ and $CoOH^+$ were the main Ni (II) and Co (II) ionic species adsorbed. They suggested that the adsorption of these ions might involve a combination of Coulombic forces between the negative $Si\text{-}O^-$ sites at the quartz surface and the positive $NiOH^+$ and $CoOH^+$ ions as well as hydrogen bonding between the OH groups of the hydroxide complex and the Si-OH and $Si\text{-}O^-$ groups at the quartz surface; i.e. the latter being the dominant mechanism. They also pointed out that positively charged $Ni(OH)_2$ and $Co(OH)_2$ colloids could explain the positive zeta potential values at high pH values (less than 11).

Fuerstenau (1975) investigated the role of metal ion hydrolysis in oxide and silicate flotation systems. Electrophoretic data showed that a greater charge was left at the surface after hydroxy complex adsorption than was present prior to adsorption. Either of the two mechanisms could account for this phenomenon, namely, hydrogen bonding between the hydroxy complex and an oxide site, or water formation from the hydroxyl of the hydroxy complex and adsorbed hydrogen ions. In the case of water formation, he suggested that the hydrogen ion could adsorb onto oxide sites while hydroxyl ion could adsorb onto silicon sites. Adsorption of hydroxy complexes, such as $CuOH^+$, could occur by splitting out water. In the presence of collector, this could lead to collector adsorption onto this site.

Fuerstenau et al., (1977) also studied the mechanism of pyroxene (augite, diopside) flotation with potassium oleate. Electrophoretic data indicated that the

University of Cape Town

hydroxy complexes $FeOH^+$, $MgOH^+$, and $CaOH^+$ were responsible for the flotation of these pyroxenes.

Hodgson and Agar (1989) carried out electrochemical studies to determine a possible effect of Ca^{2+}, $S_2O_3^{2-}$ and SO_4^{2-} ions on pentlandite and pyrrhotite floatability and xanthate interactions. It was found that these ions were significantly surface active at the normal process pH. It was concluded that these ions would influence the extent of X^- adsorption by the sulphide minerals as well as control the onset of hydrophobicity. $S_2O_3^{2-}$ and Ca^{2+} ions competed with xanthate for adsorption on the surface sites of pentlandite, whereas only Ca^{2+} increased the xanthate dosage required rendering pyrrhotite hydrophobic. The calcium ions adsorbed onto the surface sulphur sites, sulphate also being adsorbed onto the Fe sites. The $S_2O_3^{2-}$ ion was considered to be coordinated onto surface via the oxidised Fe sites or the Ca (S_2) product. Iron and polysulphides were considered to be surface-active forms, which form part of the pyrrhotite surface. Ca^{2+} cations can chemisorb onto the pentlandite surface, replacing metal ions at the pentlandite surface. The initial oxidation reaction for pentlandite is pH independent and to be of the following form

$$Fe_{4.5}Ni_{4.5}S_8 \rightarrow (Fe_{4.5-x}Ni_{4.5-x}S_8) + xFe^{2+} + xNi^{2+} + 4xe \qquad (20)$$

Presence of Ca^{2+} ions modifies this reaction by replacing the metal cation at the surface.

Kartio et al., (1992) described a technique for XPS measurements of volatile adsorbed layers with particular application to the studies of sulphide flotation. Desorption and reactions with atmospheric gases prior to the measurement are avoided by repeated exposure of the sample to an inert atmosphere at room temperature followed by cooling to liquid nitrogen temperature and subsequent evacuation to spectrometer temperature. This method was applied to pyrite treated in aqueous potassium ethyl xanthate solutions. The presence of

University of Cape Town

dixanthogen adsorption layers on FeS_2 was observed by XPS and confirmed using infrared and electrochemical measurements.

Static SIMS measurements of galena mineral surfaces after diisobutyl dthiophosphinate adsorption show the presence of a 1:1 complex of the reagent and lead. No evidence was found for the possibility of S-S bonding between PbS and dithiophosphinate. This assignment was not only based on the observed mass but on the observed isotope ratio (Brinen and Nagaraj, 1994).

A statistical comparison of hydrophobic and hydrophilic species on galena and pyrite particles in flotation concentrates and tails was carried out using the evidence from ToF-SIMS data (Piantadosi and Smart, 2001). The data showed that there was approximately 12 times more collector on galena compared to pyrite. Galena particles in the concentrate showed less calcium, lead hydroxide and oxy-sulphur species on their surfaces compared to the tailings particles. Reduced collector adsorption and increased hydrophilic species concentrations inhibited the flotation of pyrite.

Goh et al., (2005) has shown that ToF-SIMS has the ability to differentiate between monolayer and multilayer thiol collector adsorption in sulphide systems.

The above literature review has summarised the type of information that can be obtained using various combinations of zeta potential, ToF-SIMS and XPS characterisation techniques with particular reference to flotation processes. This information is fundamental in nature and provides an in-depth knowledge of the nature of mineral surfaces with respect their surface charge, top monolayer, as well as a few nanometers into the surface, and surface speciation.

1.7 Comments Regarding the Literature Review

There is very little published literature relating to the PGE arsenides, tellurides and sulphides in terms of their flotation properties, in general, or their behaviour relative to copper activation

University of Cape Town

and/or xanthate adsorption on the mineral surfaces. As mentioned above, however, the mechanisms contributing to the flotation of the PGE minerals are of considerable interest at operating circuits treating Platreef type ore and hence the importance of this present study.

University of Cape Town

CHAPTER 2

OBJECTIVES OF THE RESEARCH

As described in Chapter 1 the Bushveld Complex, located in the northern limb of the Bushveld Complex north of Mokopane (formerly Potgietersrus) in South Africa, contains platinum, palladium, rhodium, ruthenium, iridium, osmium, gold, as well as copper, nickel and cobalt in economically recoverable quantities.

Platinum group minerals (PGM) flotation research has mainly focused on the flotation of base metal sulphides since generally PGMs are associated with sulphides. Anecdotally it has also been somewhat naively assumed that all PGMs would have a similar flotation response to the base metal sulphides. However, in the Platreef, there is a lack of sulphide-associated PGMs and they account for <20% of the PGMs present (Howell et al., 2005).

It has also been proposed that the Pt and Pd arsenide and telluride minerals in the Platreef ore are slow floating when compared to other PGE minerals. This has been concluded on the basis of the relative amounts reporting in the feed and tailings. The key questions that are addressed in the thesis relate to determining whether the Pt and Pd arsenide and telluride are indeed slow floating and, if this is found to be the case, to what extent this can be related to the surface characteristics of the minerals.

It is hypothesised in this study that the flotation behaviour of the minerals could be influenced by a range of factors which include the following:

- The hydrophobicity of the synthesised Pt and Pd mineral species may be influenced by the crystal planes and/or morphology of the minerals. There are papers (Vaughan et. al., 1997; Nesbitt et al., 1998) that refer to the cleavage surface of the minerals which suggest that for S-rich surface stoichiometries for ZnS, the [111] surface, becomes more stable, whereas for the S-poor compositions, the [111] surface, has the lowest energy. The synthesis procedure may influence the dominant crystal planes and/or morphology present in the mineral.

University of Cape Town

- There are indications that the PGE arsenide and telluride mineral species are slow floating as they are evident in the tailings. The lower floatability observed for the PGE mineral species may be due the presence of oxidation products (air induced oxidation) which will influence their floatability. Due to the nobility of platinum this is only likely to occur for the palladium mineral species.
- When the PGE mineral species are in contact with oxidation products produced during grinding, inadvertent depression may occur due to precipitating ions, for example, from pentlandite, $NiOH^+$ and $FeOH^+$.
- It is widely known (Finkelstein, 1997) that copper sulphate is used as a promoter of the base metal sulphide minerals. It is also speculated that it will promote the flotation of the PGE mineral species. It is proposed that since these tests were carried out in a frothless environment this would eliminate any effect copper sulphate may have on froth structure.
- Bismuth and tellurium readily oxidise and these passivating oxide layers may influence the flotation response.
- It is well known (Malysiak, 2003) that calcium and magnesium ions can have a negative effect on flotation and since process water contains these ions it is proposed that changing the ionic strength of the synthetic water will impact on the flotation response of the PGE minerals.

Thus the objectives of this research are

- To determine whether the crystal structure and/or composition or surface structure and/or composition of the various Pt and Pd mineral species resulting in their not being hydrophobic or amenable to collector adsorption.
- To examine whether the Pt and Pd mineral species readily oxidise and whether the oxidation products affect the mineral surface composition and floatability.
- To determine if the oxidation products from other minerals and grinding media inadvertently affect the mineral surface composition and thus floatability by precipitation onto the mineral surfaces.
- To investigate whether the Pt and Pd mineral species are not amenable to copper activation because they have differing crystal structures compared, for example, to

University of Cape Town

sulphides like pentlandite as there are no sulphur atoms available to which copper may bond.

- To examine whether the PGE mineral surfaces become passivated by Bi and Te oxide and hydroxide species which may reduce the floatability of the Pt and Pd mineral species.
- To evaluate whether the ion species in the pulp affect the PGE mineral surfaces which will impact on the floatability of the Pt and Pd mineral species, e.g. Ca and Mg ions passivating the mineral surfaces.

University of Cape Town

CHAPTER 3

EXPERIMENTAL METHODS

This research proposes that there is a difference in the floatability between the Pt and Pd arsenide, telluride and sulphide mineral species as a result of one or more of the following hypothesis listed in Table 1. Table 1 illustrates the experimental methods that will be used to evaluate each hypothesis listed.

Table 3.1: Hypotheses link to experimental methods.

Hypotheses	*Experimental Method*
• Differing crystal structure/composition or surface structure/composition of the various Pt and Pd mineral species resulting in their being not hydrophobic or amenable to collector adsorption.	XRD – crystal structure ToF-SIMS – surfaces composition Zeta potential – adsorption studies
• The Pt and Pd mineral species readily oxidise and the oxidation products negatively affect the mineral surface composition and floatability. • Similarly, oxidation products from other minerals and grinding media also negatively affect the mineral surface composition and floatability by precipitation onto the mineral surfaces. • The Pt and Pd mineral species are not amenable to copper activation because they have differing crystal structures compared, for examples, to sulphides like pentlandite as there are no sulphur atoms available for the copper to bond to. • Passivation of the mineral surfaces by Bi and Te oxide and hydroxide species is occurring which reduces the floatability of the Pt and Pd mineral species. • Ion species in the pulp as well as the pH, affect mineral surfaces which impacts on the floatability of the Pt and Pd mineral species, e.g. Ca and Mg ions passivating the mineral surfaces.	Microflotation – flotation recovery and kinetics XPS – surface composition and speciation ToF-SIMS – surfaces composition Zeta potential – adsorption studies

University of Cape Town

3.1 Minerals

The PGE minerals were synthesised using at methods developed by Anglo Research. The methods involved the weighing of stoichiometric amounts of the pure metal powders which are finely ground for each mineral species and transferred to a quartz ampoule. The evacuated, sealed ampoule was heated in a vertical furnace then cooled to ambient temperature. Details of the materials and thermal treatment conditions are shown in Tables 3.2 – 3.4. The pure platinum and palladium sponge (99.95%) was obtained from Anglo Platinum's Precious Metal Refiners (PMR), tellurium, bismuth and arsenic was supplied by Alfa Aesar at > 99.9% purity. Other chemicals used in this study were of analytical grade and the gases were of instrument grade.

Table 3.2: Platinum and palladium sulphide composition and thermal treatment.

Mineral	*Stoichiometric Composition Selected*	*Thermal Treatment*	*Product Produced*
Cooperite (NS144) PtS	$Pt_{2.00}S_{2.00}$ (34.35g Pt, 5.65g S)	Ampoule heated to 1000°C at a rate of 20°/min, held for 96 hours, then allowed cooling naturally at a rate of 10°/min. Break tube, regrind, reseal and reheat to 1000°C at a rate of 20°/min, held for 96 hours, then allowed cooling naturally at a rate of 10°/min	40g @ >99% purity
Vysotskite (NS148) PdS	$Pd_{8.00}S_{8.00}$ (30.74g Pd, 9.26g S)	Ampoule heated to 800°C at a rate of 20°/min, held for 30 minutes and subjected to a controlled linear slow-cooling down to 350°C over 60 hours.	40g @ 97.4% purity

University of Cape Town

Table 3.3: Platinum and palladium arsenide composition and thermal treatment.

Mineral	*Stoichiometric Composition Selected*	*Thermal Treatment*	*Product Produced*
Sperrylite (NS145) ***$PtAs_2$***	$Pt_{4.00}As_{8.00}$ (33.93g Pt, 26.06g As)	Ampoule heated to 800°C at a rate of 10°/min, held for 6 hours then slowly cooled to ambient temp at a rate of 5°/min.	60g @ 90.6% purity
Sperrylite (NS146) ***$PtAs_2$***	$Pt_{4.00}As_{8.00}$ (33.93g Pt, 26.06g As)	Ampoule heated to 800°C at a rate of 10°/min, held for 12 hours then slowly cooled to ambient temp at a rate of 5°/min.	60g @ 93.5% purity
Palladoarsenide (NS147) ***Pd_2As***	$Pd_{2.65}As$ (44.38g Pd, 15.62g As)	Ampoule heated to 800°C at a rate of 10°/min, held for 12 hours then slowly cooled to ambient temp at a rate of 5°/min.	60g @ >95% purity

Table 3.4: Platinum and palladium telluride composition and thermal treatment.

Mineral	*Stoichiometric Composition Selected*	*Thermal Treatment*	*Product Produced*
Moncheite (NS142) ***$PtPd(BiTe)_2$***	$Pt_{0.94}Pd_{0.06}Bi_{0.5}Te_{1.50}$ (23.46g Pt, 0.06g Pd, 11.22g Bi, 24.4g Te)	Ampoule heated to 1150°C at a rate of 20°/min, held for 15 minutes then slowly cooled to ambient temp at a rate of 10°/min. The sample was further treated by heating the ampoule to 1150°C at a rate of 20°/min, held for 15 minutes then slowly cooled to 480°C and held at that temp for 4 weeks then slowly cooled to ambient temp at a rate of 10°/min.	60g @ 86.9% purity
Merenskyite (NS143) ***$PdPt(BiTe)_2$***	$Pd_{0.92}Pt_{0.08}Bi_{0.18}Te_{1.82}$ (15.3g Pd, 2.44g Pt, 7.15g Bi, 35.08g Te)	Ampoule heated to 800°C at a rate of 20°/min, held for 30 minutes and subjected to a controlled linear slow-cooling down to 350°C over 60 hours then slowly cooled to ambient temp at a rate of 10°/min.	60g @ 97.1% purity
Moncheite (NS153) ***$PtTe_2$***	$Pt_{1.00}Te_{2.00}$ (20g Pt, 40g Te)	Ampoule heated to 1150°C at a rate of 20°/min, held for 30 minutes, and subjected to a controlled linear slow-cooling down to 350°C over 60 hours then slowly cooled to ambient temp at a rate of 10°/min.	60g @ 75.7% purity
Merenskyite (NS152) ***$PdTe_2$***	$Pd_{1.00}Te_{2.00}$ (20g Pd, 40g Te)	Ampoule heated to 800°C at a rate of 20°/min, held for 30 minutes and subjected to a controlled linear slow-cooling down to 350°C over 60 hours then slowly cooled to ambient temp at a rate of 10°/min.	60g @ 68.7% purity

University of Cape Town

The PGE minerals that were produced were not all homogeneous even though the methods for the preparation and thermal treatment of the material were followed meticulously. The final product was sent for mineralogical analysis to verify the homogeneity of the sample.

All mineral samples were stored under argon and freshly ground in an agate just prior to each experiment. The products were screened to obtain size fractions of –25µm for zeta potential determinations and +38 – 106µm for microflotation tests.

Using the BET method, the surface area of the +38 -106µm size fraction of all the synthesised minerals was determined. The results are shown in Table 3.5.

Table 3.5: Surface area of the +38 – 106µm size fraction of all the synthesised minerals.

Mineral	*Surface area of the +38 – 106µm size fraction (m^2/g)*	*Mineral*	*Surface area of the +38 – 106µm size fraction (m^2/g)*
Cooperite (NS144) PtS	0.077	***Vysotskite (NS148) PdS***	0.068
Sperrliyte (NS145) $PtAs_2$	0.04	***Palladoarsenide (NS147) Pd_2As***	0.26
Sperrliyte (NS146) $PtAs_2$	0.06		
Moncheite (NS142) $PtPd(BiTe)_2$	0.20	***Merenskyite (NS143) $PdPt(BiTe)_2$***	0.13
Moncheite (NS153) $PtTe_2$	0.22	***Merenskyite (NS152) $PdTe_2$***	0.14

3.2 X-Ray Diffraction (XRD)

The aim of the XRD investigation is to identify the phases present in the samples and to analyse the X-Ray diffractograms by means of the Rietveld method to obtain further crystallographic information. Quantitative phase analysis (Rietveld Quantification) is a

University of Cape Town

powerful method for determining the quantities of crystalline and amorphous components in multiphase mixtures. The amorphous phase is calculated by difference.

Powder XRD was employed during this investigation. XRD data was collected utilising a PANanalytical X'Pert Pro diffractometer with X'Cellerator detector using the following diffractometer settings:

Start Position [°2Th.]	4.000
End Position [°2Th.]	110.000
Steop Size [°2Th.]	0.0170
Scan Step Time [s]	100.6952
PSD Mode	Scanning
PSD Length [°2Th.]	2.12
Divergence Slit Size [°]	0.2500
Specimen Length [mm]	10.00
Measurement Temperature [°C]	25.00
Anode Material	Cu
K-Alpha1 [Å]	1.54060
K-Alpha2 [Å]	1.54443
K-Beta [Å]	1.39225
K-A2 / K-A1 Ratio	0.50000
Generator Settings	40mA, 40kV

University of Cape Town

A search-match routine based on peak and profile data and utilising the PDF2 database was used to identify the best fitting phases in the database. The search was limited so that only phases containing the expected elements were displayed. The elements H, O and Si were added to the list of possible elements; this was done to include phases that were formed by oxidation, hydration or contamination from the vessel. The SemiQuant values from the database only give a rough indication of the amount of each phase present in the samples. The SemiQuant values are normalised and if the sample contains an amorphous component, this quantification method will lead to overestimated values.

The crystal structure data related to the best-fitting phases were retrieved from the ICSD database (Inorganic Crystal Structure Database) and imported into the PANanalytical HighScore Plus software. In certain cases, where substitutions of elements were known to exist,

atoms were added to the structure. The Rietveld parameters were subsequently refined to a point where agreement between the calculated and observed pattern were as good as possible.

3.2 Reagents

During the study, water with a specific conductance of 0.7µS cm^{-1} and a surface tension of 72.8 mN m^{-1} at 20°C, produced by a MILLI-RO PLUS apparatus, was used to prepare synthetic water (*I* = 3.5E-02). High purity argon (Afrox) was used during storage to minimise mineral oxidation. Purified collector, sodium isobutyl xanthate, was obtained from SENMIN. Other chemicals were of analytical grade quality. Copper sulphate (Saarchem) was used as activator. Sodium carbonate (Saarchem) and hydrochloric acid (Riedel-de Haen) were used for pH adjustment.

3.3 Synthetic Water Composition

Water with a specific conductance of 0.7µS cm^{-1} was modified by the addition of various chemical compounds of analytical grade quality (Table 3.6) to produce synthetic process water [*I* (Ionic strength) = 3.5E-02]. The synthetic water contained amounts of key ions similar to those typically found in circuit water (Ca^{2+} 80ppm, Mg^{2+} 80ppm, Na^{+}135ppm, Cl^{-} 270ppm, SO_4^{2-} 250ppm, NO_3^{-} 135ppm, CO_3^{2-} 40ppm, TDS 990ppm).

Table 3.6: Synthetic water composition, I = 3.5E-02.

Chemical Compound	Formula	Mass(g) in 1 litre	Mol/dm^3
Calcium chloride (BDH Chemicals)	$CaCl_2.2H_2O$	0.147	0.001
Calcium nitrate (BDH Chemicals)	$Ca(NO_3)_2.4H_2O$	0.236	0.001
Magnesium sulphate (Saarchem)	$MgSO_4.7H_2O$	0.615	0.0025
Magnesium nitrate (BDH Chemicals)	$Mg(NO_3)_2.6H_2O$	0.107	0.0004
Sodium chloride (Saarchem)	NaCl	0.356	0.0061
Sodium carbonate (Saarchem)	Na_2CO_3	0.058	0.0005

University of Cape Town

3.4 Microflotation Tests

Mineral recovery in a microflotation cell can be used as an indicator of hydrophobicity in a given chemical and electrochemical system. Small-scale flotation experiments have been found to be a useful tool to investigate the relative hydrophobicity and hence potential flotation behaviour of the various constituents of the ore. A study of the effect of reagent adsorption on a specific mineral can be carried out, since the influence of froth phase and hydrodynamics in the pulp phase are not present.

3.4.1 Microflotation Cell Description

The cell consists of a conical tapered cylindrical tube with air introduced through a needle at the base of the cell. Mineral loaded bubbles rise through the cell and are deflected off the cone at the top of the cell, after which they burst, resulting in the minerals dropping into the concentrate launder. After a set time the needle is removed and the particles in the launder are collected as a concentrate. During the study, flotation was carried out by introducing air at a flowrate of 5 cm^3/min. The mean bubble size diameter was 0.96mm (Bradshaw and O'Connor, 1996). The peristaltic pump speed was kept constant and set to maintain a good particle suspension. The microflotation apparatus used during the study is shown in Figure 3.1.

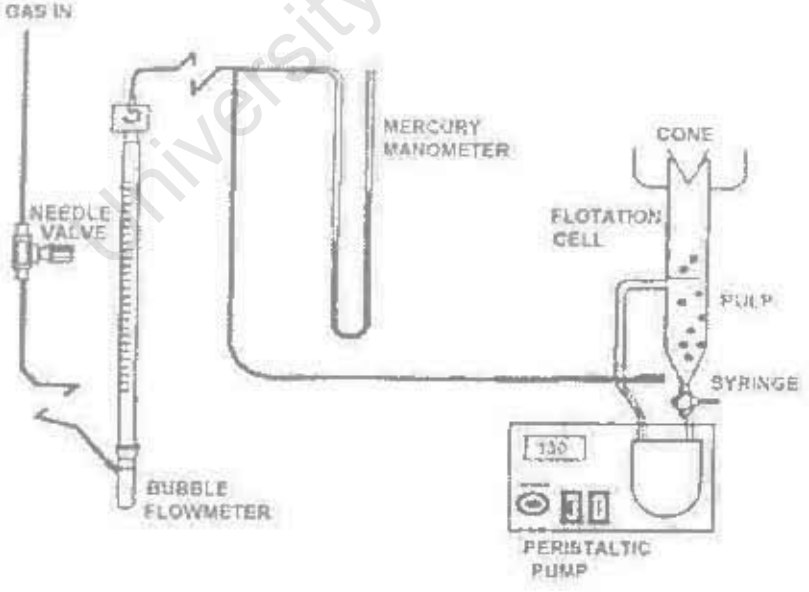

Figure 3.1: Microflotation apparatus (Wesseldijk et al., 1999).

University of Cape Town

3.4.2 Microflotation Procedure

Microflotation tests were conducted in synthetic water. A 2g sample was added to 250ml of the required solution, which had been adjusted to the desired pH. The desired pH was maintained throughout flotation by adjusting with either sodium carbonate or hydrochloric acid. Concentrates were collected at time intervals of 2, 4, 6, 8 and 20 minutes. The floated and non-floated fractions were allowed to dry in air and weighed. The microflotation products were weighed, thus enabling the recovery of each individual mineral to be determined. The reagents used during the study are listed in Table 3.7, which includes the reagent abbreviations.

Table 3.7: Chemical reagents and abbreviations used during the study.

Chemical Reagent	Abbreviation
Copper Sulphate	$CuSO_4$
Sodium isobutyl xanthate	SIBX
Senkol 65	DTC
Ethlylenediamine	EDA
Hydrochloric acid	HCl
Sodium carbonate	Na_2CO_3
Sodium hydroxide	NaOH

During the tests, various combinations of reagents were investigated at concentrations of 5.00E-05M unless otherwise stated. These were SIBX, [$CuSO_4$ + SIBX], [$CuSO_4$ + EDA + SIBX], [$CuSO_4$ + SIBX + EDA], DTC, [SIBX + DTC], [$CuSO_4$ + DTC], Senkol 65, [SIBX + Senkol 65] and [$CuSO_4$ + Senkol 65]. The sequence of reagent addition was as indicated by the sequence of reference in brackets. Conditioning periods for the reagents tested were 2 minutes for SIBX and DTC and 5 minutes for $CuSO_4$ and EDA.

Further microflotation trials were conducted to test the hypothesis that oxidation products from other minerals negatively affect the mineral surface composition and floatability by precipitation onto the PGE mineral surfaces where 1:1 mixtures of moncheite, NS142, and

University of Cape Town

pentlandite were floated using SIBX. The two trials, A and B, are described in Figures 3.2 and 3.3.

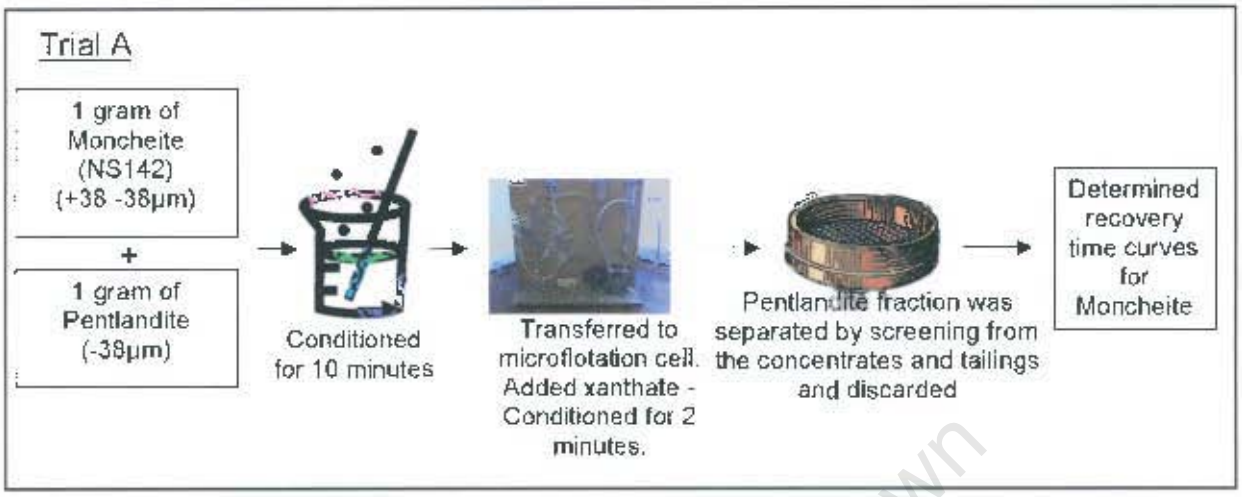

Figure 3.2: Microflotation trial conducted with 1:1 mixtures of moncheite, NS142, and pentlandite.

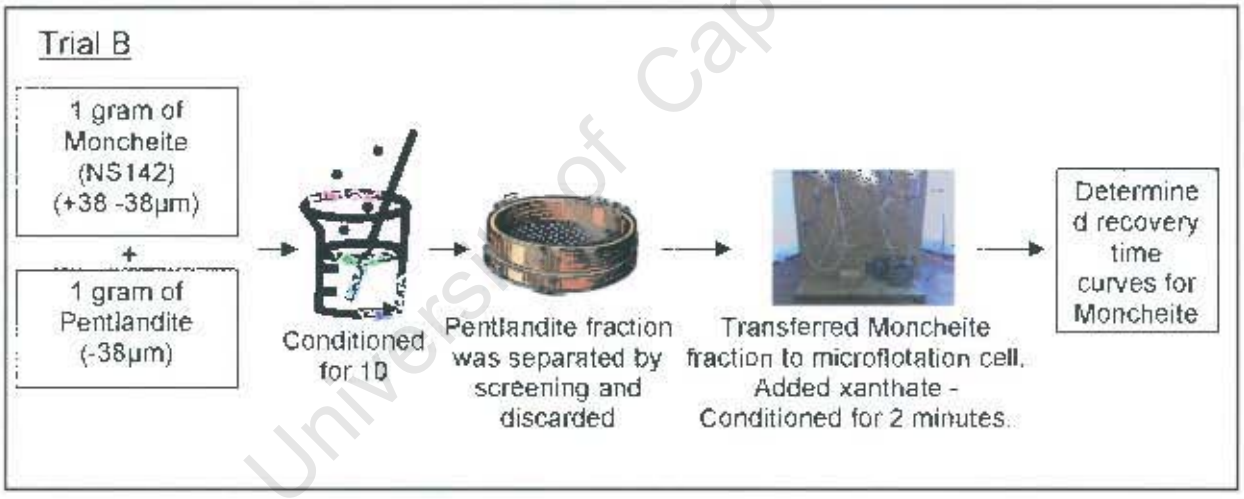

Figure 3.3: Microflotation trial conducted with 1:1 mixtures of moncheite, NS142, and pentlandite.

Another set of experiments involved a 10 minute conditioning period of 1:1 mixtures of moncheite (NS142) and pentlandite, where varying size fractions of moncheite and pentlandite were used for the mixtures, i.e. -10µm, -10 +38µm and +38 -38µm size fractions in synthetic water. After conditioning, the pentlandite fraction was removed by screening and discarded. The moncheite fractions were combined and floated in the

University of Cape Town

presence of xanthate and the products were screened to obtain the recovery for each size fraction. The results of these experiments are presented on Section 4.3.6.4.

3.5 Surface Characterisation Techniques

3.5.1 Zeta Potential Determinations

Zeta potential determinations are used to study the electrokinetic phenomena at mineral-collector interfaces. This information can thus be used to assist in predicting flotation behaviour of a mineral in an aqueous system. This technique has been described in Section 1.6.1. In this study, the zeta potential determinations were carried out on dilute dispersions of the individual minerals studied using a Malvern Zetasizer 4. The instrument gives the electrophoretic mobility from which the zeta potential was calculated using the Smoluchowski equation. The zeta potential determinations were carried out at pH 6, 8 and 10 at 25°C using synthetic water as the background electrolyte. During the experiments, the effect of SIBX (5.00E-05M) and $CuSO_4$ (5.00E-05M) on the mineral surface alteration was investigated. A mineral sample weighing 0.17g was dispersed in 120cm^3 of synthetic water and the pH was adjusted to the desired value. Conditioning of the mineral for zeta potential determinations was carried out for 20 minutes. The pH was checked prior to taking the reading. The E_h was allowed to vary naturally.

3.5.2 Time of Flight Secondary Ion Mass Spectrometry (ToF-SIMS)

ToF-SIMS analysis is known to be a technique used to determine the occurrence of atomic/molecular species on the surface of mineral samples. This technique has been described in Section 1.6.2. In this study, mineral mixtures, which were conditioned in synthetic water in the presence of the desired reagents, were analysed using ToF-SIMS PHI TRIFT II^{NT} instrument operating in the static SIMS regime (10^{12}–10^{13} primary ions/cm^2) at Anglo Research – Germiston Campus).

ToF-SIMS analysis was carried out on stirred trial products (samples were conditioned in synthetic water (pH 9) for 1 minute prior to reagent addition; conditioning periods for the reagents tested were 2 minutes for SIBX at a concentration 5.00E-05M and 5 minutes for

University of Cape Town

$CuSO_4$ at a concentration of 5.00E-05M and ethylenediamine (EDA) at a concentration of 5.00E-05M.

Further stirred trials were conducted with 1:1 mixtures of moncheite, NS142, and pentlandite. As mentioned in Section 3.4.2, the rationale for these trials is to test the hypothesis that oxidation products from other minerals negatively affect the mineral surface composition and floatability by precipitation onto the PGE mineral surfaces. These two trials, A and B, are described in Figures 3.4 and 3.5 below.

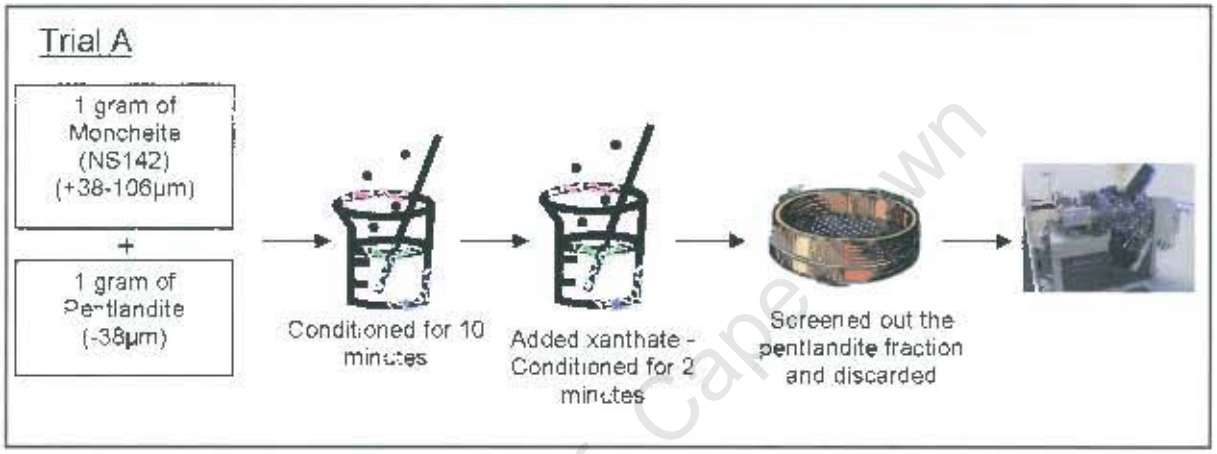

Figure 3.4: Stirred trial conducted with 1:1 mixtures of moncheite, NS142, and pentlandite.

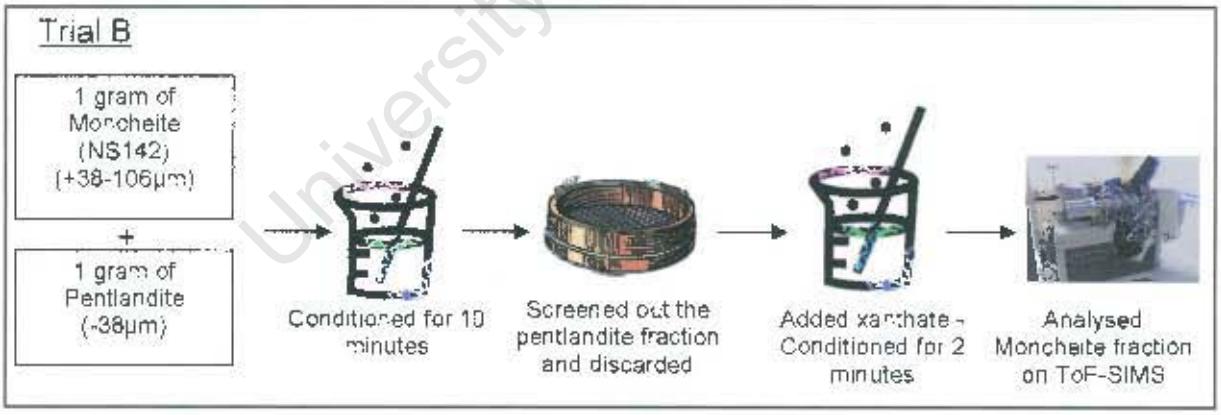

Figure 3.5: Stirred trial conducted with 1:1 mixtures of moncheite, NS142, and pentlandite.

The samples were filtered and washed with water (conductivity 0.7µmS cm^{-1}), adjusted to the desired pH, to remove any physically attached ions. All samples were dried in an argon atmosphere at ambient temperature. The 15 kV bunched, 600pA gallium beam was used

University of Cape Town

throughout the investigation unless otherwise stated. Ten areas (300X300µm) of each mineral were imaged and analysed for the elements of interest in the positive and negative SIMS modes. The data obtained were evaluated using Statistica. The intensities obtained are normalised for the elements of interest and presented as a normalised yield.

3.5.3 X-ray Photoelectron Spectroscopy (XPS)

X-ray Photoelectron Spectroscopy (XPS) is a quantitative spectroscopic technique that measures the empirical formula, chemical state and electronic state of the elements that exist within a material. XPS is a surface chemical analysis technique that can be used to analyse the chemistry of the surface of a material in its "as received" state, or after some treatment such as: fracturing, cutting or scraping in air or UHV to expose the bulk chemistry, ion beam etching to clean off some of the surface contamination, exposure to heat to study the changes due to heating, exposure to reactive gases or solutions, exposure to ion beam implant, exposure to UV light, for example. This technique has been described in detail in Section 1.6.3. The XPS analyses were carried out with a Kratos Axis Ultra spectrometer using a monochromatic Al Kalpha source (15 mA, 14 kV). The instrument work function was calibrated to give a binding energy (BE) of 83.96 eV for the Au 4f7/2 line for metallic gold and the spectrometer dispersion was adjusted to give a BE of 932.62 eV for the Cu 2p3/2 line of metallic copper. Binding energy accuracy is ±0.025 eV. The Kratos charge neutraliser system was used on all specimens. Survey spectra were collected with a pass energy of 160 eV and an analysis area of 300-700 lm. High-resolution spectra were obtained using either a 20 eV or 40 eV pass energy and an analysis area of 300-700 lm. Spectra were analysed using CasaXPS software (version 2.2.107). The samples were prepared according to the following sequence where a new ground sample was used at each stage and XPS measurements were carried out at each stage for the synthetic minerals.

- Sample 1 - Conditioned for 1 minute in synthetic water (pH 9); settled, the supernatant was decanted, the solid was washed with pH 9 adjusted deionised water (NaOH); two sedimentation/decantation cycles were carried out.
- Sample 2 - Conditioned for 1 minute in synthetic water (pH 9); then conditioned for 5 minutes with 5.00E-05M $CuSO_4$; settled, the supernatant was decanted, the solid was

University of Cape Town

washed with pH 9 adjusted deionised water (NaOH); two sedimentation/decantation cycles were carried out.

- Sample 3 - Conditioned for 1 minute in synthetic water (pH 9); then conditioned for 5 minutes with 5.00E-05M $CuSO_4$, then conditioned for 2 minutes with 5.00E-05M sodium isobutyl xanthate; settled, the supernatant was decanted, the solid was washed with pH 9 adjusted deionised water (NaOH), two sedimentation/decantation cycles were carried out.
- Sample 4 - Conditioned for 1 minute in synthetic water (pH 9); then condition for 2 minutes with 5.00E-05M sodium isobutyl xanthate; settled, the supernatant was decanted, the solid was washed with pH 9 adjusted deionised water (NaOH), two sedimentation/decantation cycles were carried out.

It should be noted that the decantation and washing processes were carried out in such a manner that would mimimise the removal of any physically adsorbed species from the surfaces. Immediately after the preparation of each sample, the solution was degassed (oxygen) with argon bubbling, capped, frozen in liquid nitrogen and stored frozen until the XPS analysis. Immediately after thawing each sample, a spatula end was used to place concentrated slurry from the bottom of the tube on to conductive sticky tape on an XPS stub. A tissue edge was used to remove excess solution by capillary action still leaving the mineral surfaces covered without exposure to air. This sample was placed in the XPS fore-vacuum within 3 minutes and the remaining solution evaporated.

University of Cape Town

3.6 HSC Chemistry® Software

HSC Chemistry® is designed for various kinds of chemical reactions and equilibria calculation. Version 4.1 of the software was used to obtain the ΔG-diagram (Ellingham). The program uses an extensive thermochemical database which contains enthalpy (H), entropy (S) and heat capacity (C) data for more than 15000 chemical compounds. The ΔG-diagram module presents the basic thermochemical data for the given species in graphical format as a function of temperature. The ΔG-diagram (Ellingham) shows the relative stability of various oxides, sulphates, chlorides, etc.

CHAPTER 4
RESULTS

4.1. MINERALOGICAL CHARACTERISATION

4.1.1 EDS Results

Energy dispersive spectroscopy (EDS) was used to characterise and check the homogeneity of the synthetic samples that were produced. Figures 4.1 - 4.9 show the back scattered electron (BSE) micrographs for the products produced. These figures depict the different phases found in the products and are described in Tables 4.1 - 4.5.

Synthesis of cooperite (PtS), named NS144, was performed by weighing stoichiometric amounts of the pure material (platinum sponge and sulphur powder) into a silica tube which was evacuated overnight, sealed, the contents mixed and thermally treated. The thermal treatment involved heating the ampoule to 1000°C for 96 hours followed by natural cooling to ambient temperature. The ampoule was broken and the melt was reground to a fine powder, transferred to a silica ampoule which was evacuated overnight, sealed and thermally treated. The thermal treatment involved heating the ampoule to 1000°C for 96 hours followed by natural cooling to ambient temperature. Figure 4.1 presents a BSE micrograph of cooperite which shows a homogeneous product. Table 4.1 displays the EDS results obtained.

Synthesis of vysotskite (PdS), termed NS148 involved weighing stoichiometric amounts of the pure material (palladium sponge and sulphur powder) into a silica tube which was evacuated overnight, sealed and thermally treated. The thermal treatment involved heating the ampoule to 800°C, holding at that temperature for 30 minutes, and then subjected to a controlled linear slow cooling to 350°C over 60 hours. The furnace was then switched off and cooling allowed to occur naturally to ambient temperature. The Back Scattered Electron (BSE) micrograph of this sample is shown in Figure 4.2. Please note that in Figure 4.2 the black colour represents part of the polished section matrix and not the mineral. Table 4.1 displays the EDS results which show the percentages obtained for the three phases observed.

University of Cape Town

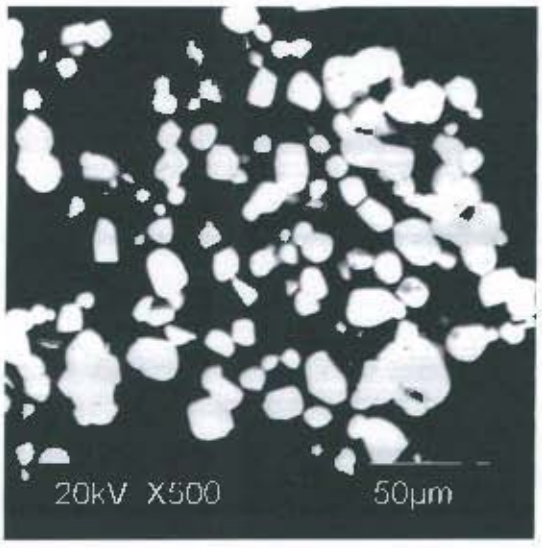

Figure 4.1: BSE micrograph of Cooperite (NS144).

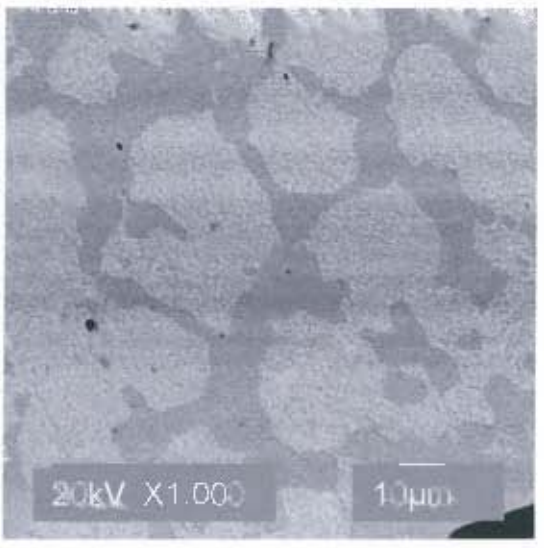

Figure 4.2: BSE micrograph of Vysotskite (NS148).

Table 4.1: Energy Dispersive Spectroscopy (EDS) results for cooperite and vysotskite.

Sample	Expected Phase	Composition	EDS Results
NS 144	***Cooperite***	85.9% Pt 14.1% S	86% Pt, 14% S
NS 148	***Vysotskite***	76.9% Pd 23.1% S	Bright Phase: 78% Pd, 22% S Intermediate Phase: 89% Pd, 11% S Dark Phase: 92% Pd, 8% S

Synthesis of the sperrylite ($PtAs_2$) samples (60g) involved weighing stoichiometric amounts of the pure material (platinum sponge and arsenic powder) into a silica tube which was evacuated overnight, sealed, the contents mixed and thermally treated. The thermal treatment of the first sample (NS145) involved heating the ampoule to 800°C for 6 hours followed by natural cooling to ambient temperature (Vermaak, 2005). The ampoule could not be heated sufficiently enough to melt the contents due to the high partial pressure of arsenic in sperrylite (Weast et al., 1981). This product was loosely sintered and very porous; when characterised mineralogically, showed Pt specks with a size range of 2–5 µm within the sperrylite phase. Many studies have described methods where re-grinding and/or leaving the charge at temperature for extended periods of time improves homogeneity of the melt [Groeneveld Meijer, 1955; Makovicky et al., 1992; Vermaak et al., 2004]. This product was then further treated by grinding the material to a fine powder and transferring to a silica tube, which was evacuated overnight, sealed and the contents mixed. The ampoule was again

University of Cape Town

thermally treated by heating to 800°C and keeping at that temperature for 1 week followed by natural cooling to ambient temperature. The mineralogical composition of this product had not altered and still contained pure Pt phases as illustrated by the bright specks in Figure 4.3. Therefore a second sample (NS146) was prepared in the same manner except that the thermal treatment involved heating the ampoule to 800°C for 12 hours followed by natural cooling to ambient temperature. This product (Figure 4.4) contained much fewer Pt specks (bright particles) compared to the case of NS145 and was less porous. Clearly, the longer initial heating time at 800°C yielded a more homogeneous product whereas re-treatment of the first sample for 1 week did not alter the sample composition. Please note that in Figure 4.3 and 4.4 the black colour represents part of the polished section matrix and not the mineral. Further samples were produced for another application using the same thermal treatment method as described for NS146 and similar products were produced which behaved in the same manner during microflotation which show the robustness of the thermal treatment method.

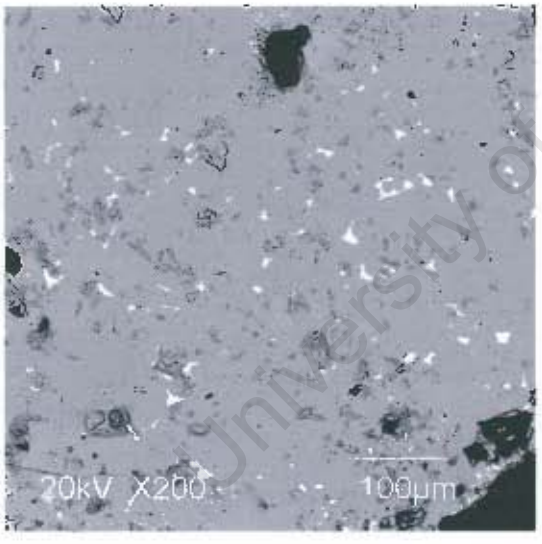

Figure 4.3: BSE micrograph of Sperrylite (NS145).

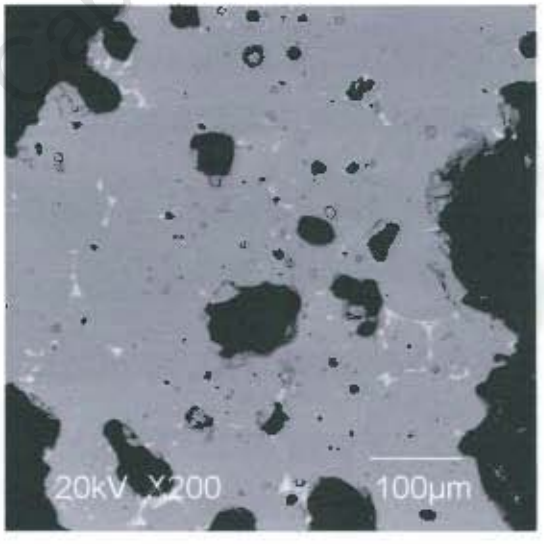

Figure 4.4: BSE micrograph of Sperrylite (NS146).

Table 4.2 below shows the composition obtained for each sample from the Energy Dispersive Spectroscopy (EDS) results obtained from the scanning electron microscope investigation. It should be noted that in the case of sample NS146 the Pt specks are relatively much richer in arsenic relative in the case of NS145.

University of Cape Town

Table 4.2: Energy Dispersive Spectroscopy (EDS) results for sperrylite.

Sample	Expected Phase	Composition	EDS Results
NS145	***Sperrylite***	56.6% Pt 43.4% As	55.9% Pt, 44.1% As (99.8% Pt, 0.2% As for the Pt specks in the sample)
NS146	***Sperrylite***	56.6% Pt 43.4% As	57.5% Pt, 42.5% As (97.5% Pt, 2.5% As for the Pt specks in the sample)

Synthesis of palladoarsenide (60g sample) was performed by weighing stoichiometric amounts of the pure material (palladium sponge and arsenic powder) into a silica tube which was evacuated overnight, sealed. the contents mixed and thermally treated. The thermal treatment method for palladoarsenide is the same as described for sperrylite, NS146. Figure 4.5 presents a BSE micrograph of palladoarsenide (NS147) which shows that two phases are present and Table 4.3 displays the EDS results which show the percentages obtained for the two phases. Please note that in Figure 4.5 the black colour represents part of the polished section matrix and not the mineral.

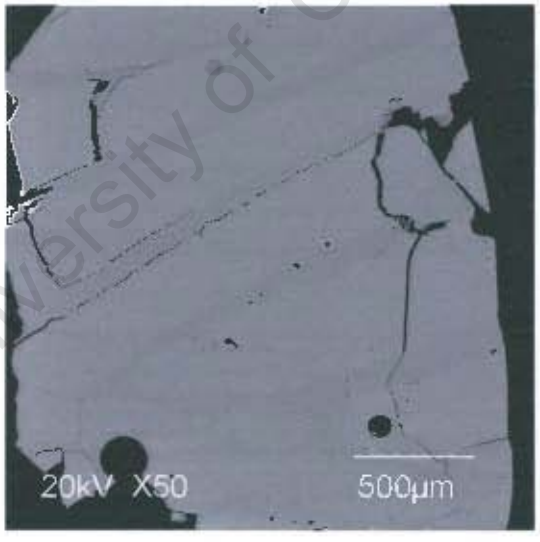

Figure 4.5: BSE micrograph of Palladoarsenide (NS147).

University of Cape Town

Table 4.3: Energy Dispersive Spectroscopy (EDS) results for palladoarsenide.

Sample	Expected Phase	Composition	EDS Results
NS147	***Palladoarsenide***	73.9% Pd 26.1% As	Dark phase: 62% Pd, 38% As Light Phase: 69.9% Pd, 30.1% As

Synthesis of moncheite $PtPd(BiTe)_2$, termed NS142, was prepared by placing stoichiometric amounts of the pure components, viz. platinum and palladium sponge and bismuth and tellurium powder, into a silica tube which was evacuated overnight, sealed, the contents mixed and thermally treated. The thermal treatment involved heating the ampoule to 1150°C, holding at that temperature for 15 minutes and then switching off the furnace and allowing cooling to ambient temperature. Due to its inherent inhomogeneity this product was further treated by grinding the material to a fine powder and transferring to a silica tube, which was evacuated overnight and sealed. The ampoule was thermally treated by heating to 1150°C and then cooling to 480°C, holding at that temperature for 4 weeks, switching off the furnace and allowing cooling to ambient temperature. The Back Scattered Electron (BSE) micrograph of this sample is shown in Figure 4.6.

A second sample of moncheite $PtTe_2$ viz. NS153, was prepared in the same manner as NS142 except that after being thermally treated by heating to 1150°C, the sample temperature was held at that temperature for 30 minutes, and then subjected to a controlled linear slow cooling to 350°C over 60 hours. Thereafter the furnace was switched off and the sample allowed to cool naturally to ambient temperature. The Back Scattered Electron (BSE) micrograph of this sample is shown in Figure 4.7. Please note that in Figure 4.6 and 4.7 the black colour represents part of the polished section matrix and not the mineral.

University of Cape Town

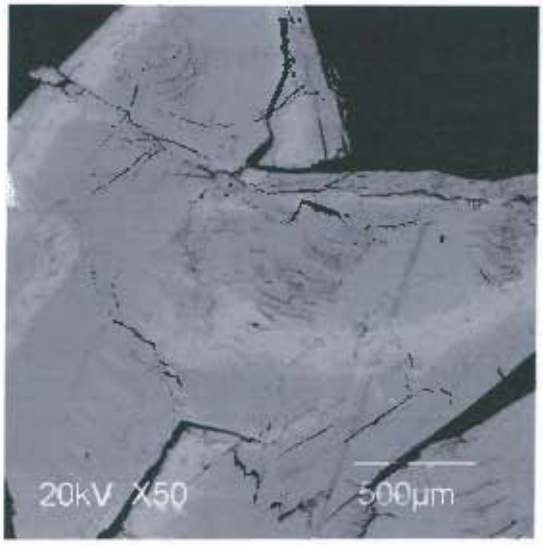

Figure 4.6: BSE micrograph of Moncheite (NS142).

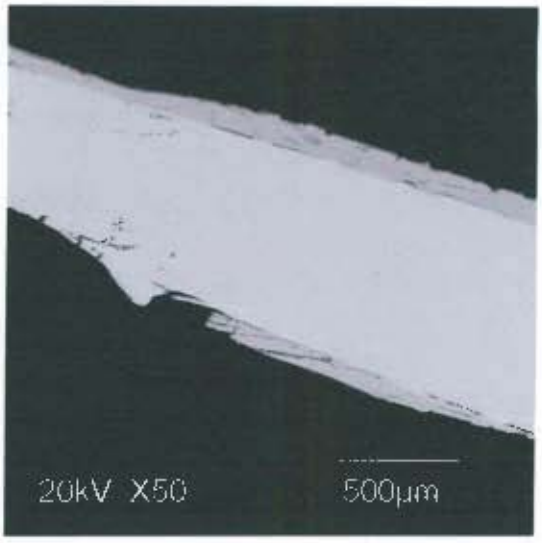

Figure 4.7: BSE micrograph of Moncheite (NS153)

Table 4.4 shows the compositions obtained for each of these samples from the Energy Dispersive Spectroscopy (EDS) results obtained from the scanning electron microscope investigation.

Table 4.4: Energy Dispersive Spectroscopy (EDS) results for moncheite.

Sample	*Expected Phase*	*Composition*	*EDS Results*
NS 142	***Moncheite***	18.9% Bi 41.3% Te 0.14% Pd 39.6% Pt	Bright Phase: 39.6% Bi, 22.2% Te, 1.2% Pd, 37% Pt Intermediate Phase: 36.7% Bi, 24.1% Te, 0% Pd, 39.2% Pt Dark Phase: 6.4% Bi, 52.5% Te, 0% Pd, 41.2% Pt
NS 153	***Moncheite***	66.7% Te 33.3% Pt	58% Te, 42% Pt

Synthesis of merenskyite $PdPt(BiTe)_2$, termed NS143, was prepared by placing stoichiometric amounts of the pure components, viz. platinum and palladium sponge and bismuth and tellurium powder, into a silica tube which was evacuated overnight, sealed, the contents mixed and thermally treated. The thermal treatment involved heating the ampoule to 800°C, holding at that temperature for 30 minutes, and then subjected to a controlled linear slow cooling to 350°C over 60 hours. As for NS153 the furnace was then switched off and

University of Cape Town

cooling allowed to occur naturally to ambient temperature. The Back Scattered Electron (BSE) micrograph of this sample is shown in Figure 4.8.

A second sample of merenskyite $PdTe_2$, viz. NS152, was prepared in a manner identical to NS143. The Back Scattered Electron (BSE) micrograph of this sample is shown in Figure 4.9. Please note that in Figure 4.8 and 4.9 the black colour represents part of the polished section matrix and not the mineral.

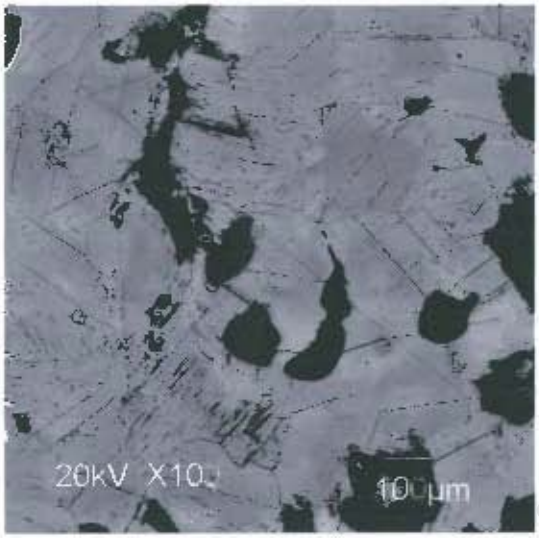

Figure 4.8: BSE micrograph of Merenskyite (NS143).

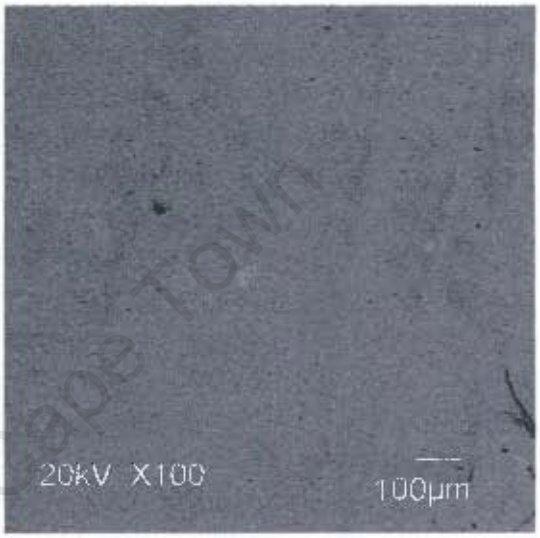

Figure 4.9: BSE micrograph of Merenskyite (NS152).

Table 4.5 shows the compositions obtained for each of these samples from the Energy Dispersive Spectroscopy (EDS) results obtained from the scanning electron microscope investigation.

Table 4.5: Energy Dispersive Spectroscopy (EDS) results for merenskyite.

Sample	*Expected Phase*	*Composition*	*EDS Results*
NS 143	***Merenskyite***	11.9% Bi 58.5% Te 25.5% Pd 4.1% Pt	Bright Phase: 11.3% Bi, 59.2% Te, 23.6% Pd, 6% Pt Intermediate Phase: 8.9% Bi, 63.5% Te, 24.2% Pd, 3.4% Pt Dark Phase: 11.7% Bi, 57.9% Te, 24.3% Pd, 6.1% Pt
NS 152	***Merenskyite***	66.7% Te 33.3% Pd	72.2% Te, 27.8% Pd

University of Cape Town

4.1.2 XRD Analysis

XRD analyses were performed to quantify the mineral phases as well as to determine the crystal structure of the synthesised minerals and to compare it to those found in nature. In all cases, the phases that were expected to be present in the sample could be positively identified; however, none of the samples were pure. The individual XRD and Rietveld refinement results for all the synthetic samples are detailed below in Tables 4.6 – 4.16.

Table 4.6: XRD results for cooperite and vysotskite.

Sample	Expected phase	Identified phases	Rietveld Quantification (%)
NS144	**Cooperite (PtS)**	Cooperite Impurity	Unknown
NS148	**Vysotskite (PdS)**	Vysotskite Palladium Sulphide	97.4 2.65

Table 4.7: XRD results for sperrylite and palladoarsenide.

Sample	Expected phase	Identified phases	Rietveld Quantification (%)
NS145	**Sperrylite $PtAs_2$**	Sperrylite Platinum Quartz	90.6 4.5 4.8
NS146	**Sperrylite $PtAs_2$**	Sperrylite Platinum Quartz	93.5 4.5 2.0
NS147	**Palladoarsenide Pd_2As**	Palladoarsenide	-

University of Cape Town

Table 4.8: XRD results for moncheite and merenskyite.

Sample	Expected phase	Identified phases	Rietveld Quantification (%)
NS142	**Moncheite $PtPd(BiTe)_2$**	Moncheite	86.9
		Platinum Telluride	12.3
		Bismuth Tellurium Oxide	0.8
NS153	**Moncheite $PtTe_2$**	Moncheite	75.7
		Tellurium	23.1
		Paratellurite	1.2
NS143	**Merenskyite $PdPt(BiTe)_2$**	Merenskyite	97.1
		Tsumoite	1.7
		Michenerite	1.2
NS152	**Merenskyite $PdTe_2$**	Merenskyite	68.7
		Kotulskite	31.3

4.1.2.1 Rietveld Refinement for Cooperite NS144 and Vysostkite NS148

The most similar crystal structure for cooperite was retrieved from the ICSD database ref 031 131 and no atoms were added to the structure. The refinement procedure resulted in a surprisingly bad agreement between the measured and the calculated profiles. The peak positions are good, but the intensity agreements are bad. The problem might be related to preferred orientation and therefore, the sample should be milled in a micronising mill, side-loaded and re-analysed. A summary of the data obtained from the refinement is given in Table 4.9, but accuracy is not expected to be high.

The crystal structure most similar to vysotskite and palladium sulphide was retrieved from the ICSD database ref 061 063 and ref 0032 053, respectively. No atoms were added to either structure. The refinement procedure resulted in reasonably good agreement between the measured and the calculated profiles. A summary of the data obtained from the refinement is given in Table 4.10.

University of Cape Town

Table 4.9: Summary of refinement data for cooperite sample NS144.

Refinement Data	Relevant parameters of Cooperite
Formula sum	$Pt_{2.00}S_{2.00}$
Formula mass g/mol	454.3000
Density (calculated) g/cm³	10.2446
Weight fraction/ %	100.000000
Space group (No.)	P 42/m m c (131)
Lattice parameters	
a/ Å	3.47099(4)
b/ Å	3.47099(4)
c/ Å	6.11124(6)
alpha/ °	90
beta/ °	90
gamma/ °	90
R (Bragg)/ %	18.83510

Table 4.10: Summary of refinement data for vysotskite sample NS148.

Refinement Data	Relevant parameters of Vysotskite	Relevant parameters of Palladium Sulphide
Formula sum	$Pd_{8.00}S_{2.00}$	$Pd_{32.00}S_{14.00}$
Formula mass g/mol	1107.6800	3853.6400
Density (calculated) g/cm³	6.7315	8.9823
Weight fraction/ %	97.4(3)	2.65(8)
Space group (No.)	P 42/m (84)	I -4 3 m (217)
Lattice parameters		
a/ Å	6.42938(4)	8.9308(4)
b/ Å	6.42938(4)	8.9308(4)
c/ Å	6.60926(6)	8.9308(4)
alpha/ °	90	90
beta/ °	90	90
gamma/ °	90	90
R (Bragg)/ %	4.84577	11.05858

University of Cape Town

4.1.2.2 Rietveld Refinement for Sperrylite NS145 and NS145 and Palladoarsenide NS147

The crystal structures most similar to sperrylite, platinum and quartz were retrieved from the ICSD database, ref 043 104, ref 076 153 and ref 079 634, respectively. No atoms were added to the sperrylite structure. For palladoarsenide, it was possible to identify palladoarsenide as the main phase in the sample from the diffractogram. However, the scan was not good enough for a Rietveld refinement procedure to be performed on this sample and therefore no crystallographic information is available.

The refinement procedure resulted in reasonably good agreement between the measured and the calculated profiles. A summary of the data obtained from the refinement is given in Table 4.11 for NS145 and Table 4.12 for NS146. Very similar results are seen in Table 4.11 and 4.12 with respect to density and space groups for sperrylite. The weight fraction gives the composition of the mineral as shown in Table 4.2.

Table 4.11: Summary of refinement data for sperrylite sample NS145.

Refinement Data	*Relevant parameters of Sperrylite*	*Relevant parameters of Platinum*	*Relevant parameters of Quartz*
Formula sum	$PtAs_{2.00}$	Pt	$SiO_{2.00}$
Formula mass g/mol	1379.7330	780.3600	180.2529
Density (calculated)	10.7796	21.3736	2.6468
g/cm³ Weight fraction/ %	90.6(3)	4.5(1)	4.8(4)
Space group (No.)	P a -3 (205)	F m -3 m (225)	P 31 2 1 (152)
Lattice parameters			
a/ Å	5.96751(3)	3.9283(2)	4.914(1)
b/ Å	5.96751(3)	3.9283(2)	4.914(1)
c/ Å	5.96751(3)	3.9283(2)	5.406(2)
alpha/ °	90	90	90
beta/ °	90	90	90
gamma/ °	90	90	120
R (Bragg)/ %	8.66367	4.93460	2.90206

University of Cape Town

Table 4.12: Summary of refinement data for sperrylite sample NS146.

Refinement Data	*Relevant parameters of Sperrylite*	*Relevant parameters of Platinum*	*Relevant parameters of Quartz*
Formula sum	$PtAs_{2.00}$	Pt	$SiO_{2.00}$
Formula mass g/mol	1379.7330	780.3600	180.2529
Density (calculated) g/cm^3	10.7870	21.4209	2.6612
Weight fraction/ %	93.5(3)	4.5(1)	2.0(2)
Space group (No.)	P a -3 (205)	F m -3 m (225)	P 32 2 1 (154)
Lattice parameters			
a/ Å	5.96615(3)	3.9254(2)	3.9254(2)
b/ Å	5.96615(3)	3.9254(2)	3.9254(2)
c/ Å	5.96615(3)	3.9254(2)	3.9254(2)
alpha/ °	90	90	90
beta/ °	90	90	90
gamma/ °	90	90	90
R (Bragg)/ %	7.53097	3.33346	3.33346

4.1.2.3 Rietveld Refinement for Moncheite NS142 and NS153

The most similar crystal structure for moncheite NS142 and NS153 was retrieved from the ICSD database ref 041 385. The structure is for pure moncheite, $PtTe_2$, therefore two atoms were added to the structure (Pd and Bi) for NS142. The site occupancy of Pd was linked to Pt and the site occupancy of Bi was linked to Te. The most similar crystal structure for Pt_2Te_3, Bismuth Tellurium Oxide, tellurium and paratellurite was retrieved from the ICSD database, ref 041 371, ref 085 725, ref 040 042 and ref 025 706, respectively. No atoms were added to these structures.

The refinement procedure resulted in a reasonably good agreement between the measured and the calculated profiles. A summary of the data obtained from the refinement is given in Table 4.13 for NS142 and Table 4.14 for NS153. The weight fraction gives the composition of the mineral as shown in Table 4.4.

University of Cape Town

Table 4.13: Summary of refinement data for moncheite sample NS142.

Refinement Data	Relevant parameters of Moncheite	Relevant parameters of Platinum Telluride	Relevant parameters of Bismuth Tellurium Oxide
Formula sum	$Pt_{0.95}Te_{0.90}Pd_{0.05}Bi_{1.10}$	$Pt_{2.00}Te_{18.00}$	$Bi_{32.00}Te_{32.00}O_{112.00}$
Formula mass g/mo	535.3739	4637.8800	12562.5100
Density (calculated)	11.8414	10.7750	7.5061
g/cm^3 Weight fraction/%	86.9(4)	12.3(4)	0.8(1)
Space group (No.)	P -3 m 1 (164)	R -3 m (166)	P b c n (60)
Lattice parameters			
a/ Å	4.04136(8)	4.0104(6)	22.782390
b/ Å	4.04136(8)	4.0104(6)	5.514000
c/ Å	5.3071(1)	51.31(1)	22.119800
alpha/ °	90	90	90
beta/ °	90	90	90
gamma/ °	120	120	90
R (Bragg)/ %	5.18055	6.29091	6.84145

Table 4.14: Summary of refinement data for moncheite sample NS153.

Refinement Data	Relevant parameters of Moncheite	Relevant parameters of Tellurium	Relevant parameters of Paratellurite
Formula sum	$Pt_{1.00}Te_{2.00}$	$Te_{3.00}$	$Te_{4.00}O_{8.00}$
Formula mass g/mol	450.2900	382.8000	638.3952
Density (calculated) g/cm^3	10.2079	6.2447	6.0426
Weight fraction/%	75.7(3)	23.1(3)	1.2(1)
Space group (No.)	P -3 m 1 (164)	P 31 2 1 (152)	P 41 21 2 (92)
Lattice parameters			
a/ Å	4.02442(8)	4.454000	4.796000
b/ Å	4.02442(8)	4.454000	4.796000
c/ Å	5.2216(2)	5.924000	7.626000
alpha/ °	90	90	90
beta/ °	90	90	90
gamma/ °	120	120	90
R (Bragg)/ %	5.01399	4.33725	3.75821

4.1.2.4 Rietveld Refinement for Merenskyite NS143 and NS152

The most similar crystal structure for merenskyite was retrieved from the ICSD database ref 041 385. The structure is for pure merenskyite, $PdTe_2$, therefore two atoms were added to the structure (Pd and Bi). The site occupancy of Pd was linked to Pt and the site occupancy of Bi

University of Cape Town

was linked to Te. The most similar crystal structure for tsumoite and michenerite was retrieved from the ICSD database, ref 030 525 and ref 070 060, respectively and no atoms were added to these structures. The refinement procedure resulted in a reasonably good agreement between the measured and the calculated profiles. A summary of the data obtained from the refinement is given in Table 4.15 for NS143 and Table 4.16 for NS152.

Table 4.15: Summary of refinement data for merenskyite sample NS143.

Refinement Data	*Relevant parameters of Merenskyite*	*Relevant parameters of Tsumoite*	*Relevant parameters of Minchenerite*
Formula sum	$Pt_{0.10}Te_{1.80}Pd_{0.90}Bi_{0.20}$	$Te_{6.00}Bi_{6.00}$	$Pd_{4.00}Te_{3.00}Bi_{3.00}$
Formula mass g/mol	386.7451	2019.4820	1771.9220
Density (calculated) g/cm³	8.7144	8.2975	10.0454
Weight fraction/%	97.1(8)	1.7(2)	1.2(1)
Space group (No.)	P -3 m 1 (164)	R -3 m 1(164)	P 21 3 (198)
Lattice parameters			
a/ Å	4.0477(2)	4.403332	6.640815
b/ Å	4.0477(2)	4.403332	6.640815
c/ Å	5.1930(4)	24.065150	6.640815
alpha/ °	90	90	90
beta/ °	90	90	90
gamma/ °	120	120	90
R (Bragg)/ %	7.96708	7.09082	5.81689

Table 4.16: Summary of refinement data for merenskyite sample NS152.

Refinement Data	*Relevant parameters of Merenskyite*	*Relevant parameters of Kotulskite*
Formula sum	$Pt_{1.00}Te_{2.00}$	$Pd_{2.00}Te_{2.00}$
Formula mass g/mol	361.6000	468.0000
Density (calculated) g/cm³	8.2767	9.2455
Weight fraction/%	68.7(3)	31.3(4)
Space group (No.)	P -3 m 1 (164)	P 63/m m c (194)
Lattice parameters		
a/ Å	4.0383(2)	4.1394(2)
b/ Å	4.0383(2)	4.1394(2)
c/ Å	5.136130	5.6637(3)
alpha/ °	90	90
beta/ °	90	90
gamma/ °	120	120
R (Bragg)/ %	6.33495	4.38998

University of Cape Town

In summary, the XRD data has shown that for all the synthetic PGE mineral samples the phases that were expected to be present in the sample could positively be identified, however, none of the samples were pure. The most pure samples were sample NS143, which is composed of 97% merenskyite and sample NS148 which is composed of 97% vysotskite. Sample NS144 seemed to be pure cooperite, but an impurity was present which could not be identified and therefore quantification of this sample could not be achieved. X-ray diffraction of sample NS147 produced a very poor diffractogram, with low intensities, a high background and overlapping peaks; Rietveld refinement could not be done on this sample.

The EDS and XRD results for all the synthetic minerals did not highlight differences between the synthetic minerals that would explain the varying results obtained during the surface analyses and microflotation testwork.

University of Cape Town

4.2 SURFACE ANALYSIS

4.2.1 Zeta Potential Determinations

Zeta potential determinations are used to study the electrokinetic phenomena at mineral-collector interfaces. It is believed that this information can thus be used to assist in predicting flotation behaviour of a mineral in an aqueous system.

4.2.1.1 Reproducibility

The aim of the reproducibility tests was to establish the reliability of the zeta potential determination procedure used during the study. Any possible error includes the variability of the mineral samples, the consistency of the Malvern Zetasizer operation as well as the operator's ability to be consistent.

In order to determine the reproducibility and standard deviation, zeta potential determinations were carried out on a sample of sperrylite, in the absence of any reagent addition. The zeta potential determinations and standard deviations for each pH investigated are given in Table 4.17. The results obtained are graphically summarised by zeta potential-pH curves in Figure 4.10.

Table 4.17: Zeta potential determinations and standard deviations for pH 4, 6, 8, and 10 in synthetic water, I = 3.2E-02.

pH	Zeta Potential Determinations (mV)						Mean	Std Dev	Relative Std Dev (%)
	1	2	3	4	5	6			
4	-17.1	-15.6	-16.4	-16.2	-16.8	16.6	-16.6	0.32	1.92
6	-16.8	-16.2	-16.1	-17.1	-16.4	-16.3	-16.5	0.39	2.34
8	-12.7	-13.4	-13.6	-12.9	-12.8	-12.6	-13.0	0.43	3.31
10	-12.3	-12.1	-12.2	-12.9	-13.7	-12.8	-12.7	0.60	4.71

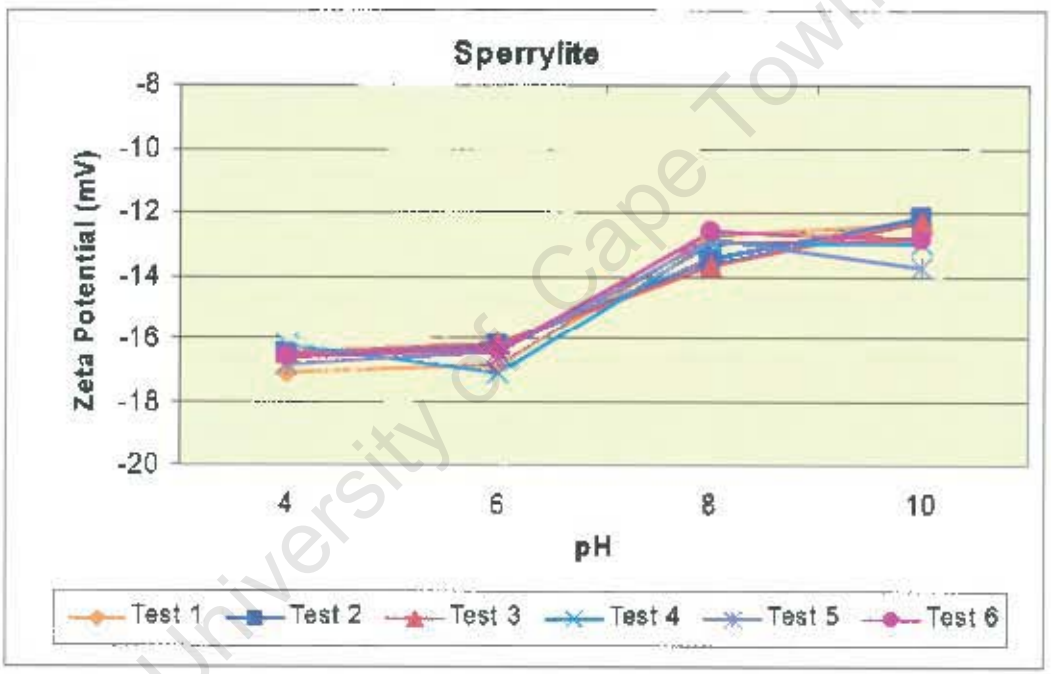

Figure 4.10: Zeta potential reproducibility curves over a pH range 4-10 for sperrylite.

As demonstrated by the zeta potential-pH curves and the low standard deviation for each measured pH, the technique and the procedure used gave reproducible results.

University of Cape Town

4.2.2.2 Zeta Potential Determinations for the Individual Reagents used in the Study

Zeta potential studies were carried out to investigate the effect of copper sulphate and xanthate and combinations of these reagent regimes on the surface charge.

4.2.2.2.1 Cooperite and Vysotskite

In the absence of reagents, the zeta potential for cooperite is around -5mV for the entire pH range studied (Figure 4.11). Cooperite's surface charge is much more positive compared with vysotskite (Figure 4.12) which is around -25mV. In the presence of xanthate there is a small shift in the zeta potential versus pH curves observed for cooperite and vysotskite especially around pH 9. The zeta potential versus pH curve shifts to more positive values when $CuSO_4$ is added compared to the no reagent curve for both PGE sulphide minerals with vysotskite showing a large shift to more positive values. When xanthate is added after the copper sulphate addition; the zeta potential versus pH curve shifts to more negative values. This indicates that xanthate is being adsorbed on the copper covered mineral surfaces.

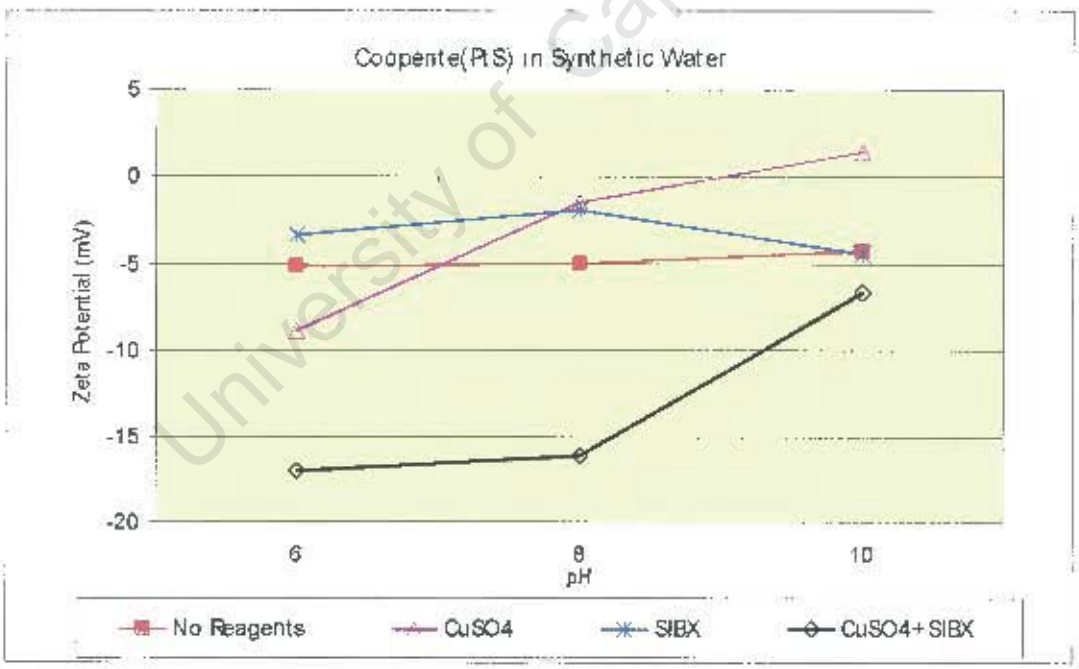

Figure 4.11: Zeta potential curves over a pH range 6-10 for Cooperite (NS144) treated with no reagents, SIBX, $CuSO_4$, $CuSO_4$+SIBX.

University of Cape Town

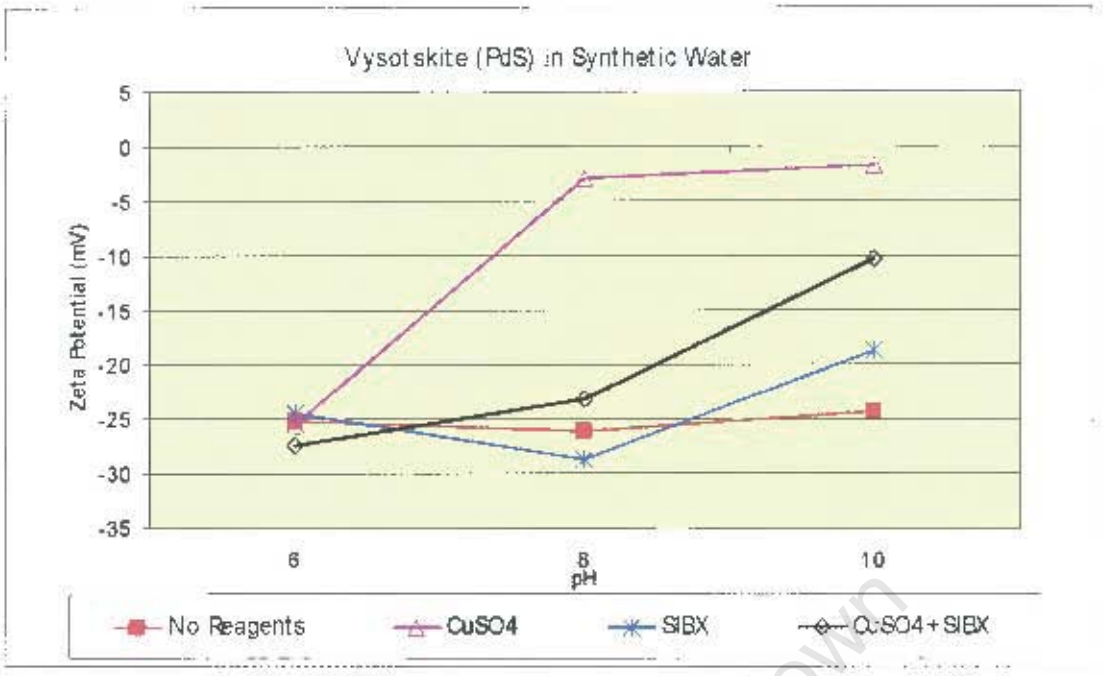

Figure 4.12: Zeta potential curves over a pH range 6-10 for Vysotskite (NS148) treated with no reagents, SIBX, $CuSO_4$, $CuSO_4$+SIBX.

4.2.2.2.2 Sperrylite and Palladoarsenide

In the case of the sperrylite sample, NS145, when $CuSO_4$ is added, the zeta potential versus pH curve shifts to more positive values, compared to the no reagent curve. This shift is attributed to the electrostatic adsorption of the positive Cu(II) ion species, which are predominant below pH 7. At the higher pH of 10 the precipitation of $Cu(OH)_2$ or Cu(OH)X (O'Connor et al., 2005) colloids lead to a slight decrease in zeta potential as observed in Figure 4.13. When SIBX is added and compared to the 'no reagent' curve the zeta potential versus pH curve shifts to more negative values indicating that xanthate is being adsorbed onto the mineral surfaces. When xanthate is added to the copper activated mineral surface, the shift in zeta potential is much larger compared to the xanthate only zeta potential versus pH curve as the precipitated colloidal $Cu(OH)_2$ is likely to be converted to and Cu(I)X colloids (Malysiak, 2003).

The results for sperrylite sample NS146 (Figure 4.14) are very similar to those observed for sperrylite sample NS145, except that there was not much xanthate adsorption onto the mineral surface when xanthate was added and compared to the 'no reagents' curve. These

University of Cape Town

results correspond to those obtained for XPS and ToF-SIMS analyses, which will be discussed in Chapter 5.

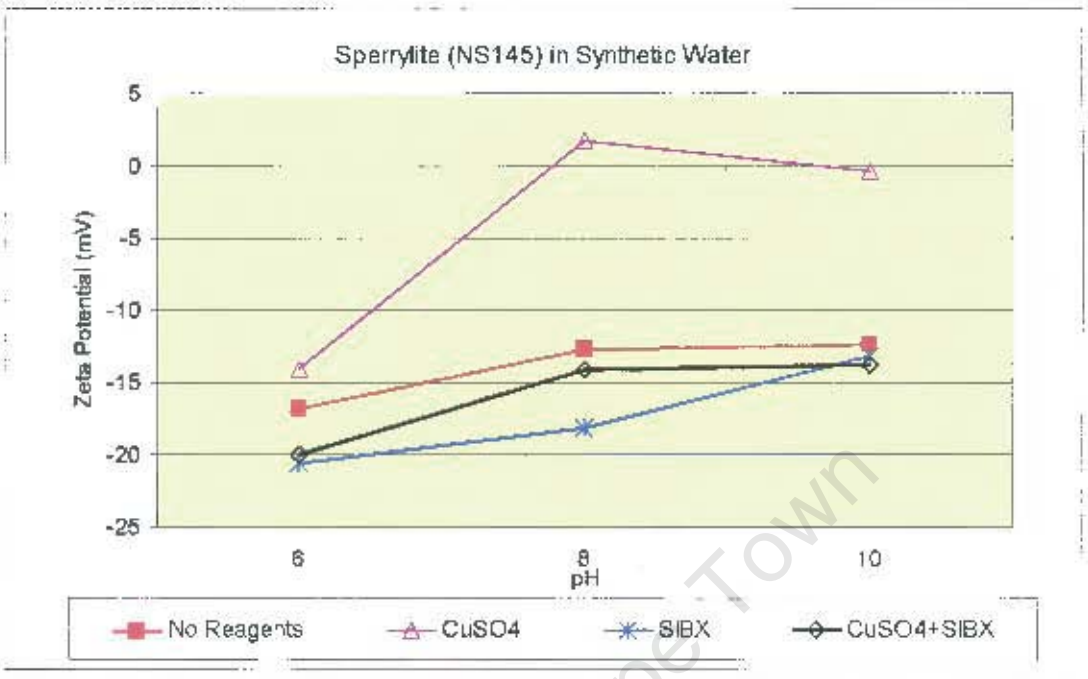

Figure 4.13: Zeta potential curves over a pH range 6-10 for Sperrylite (NS145) treated with no reagents, SIBX, $CuSO_4$, $CuSO_4$+SIBX.

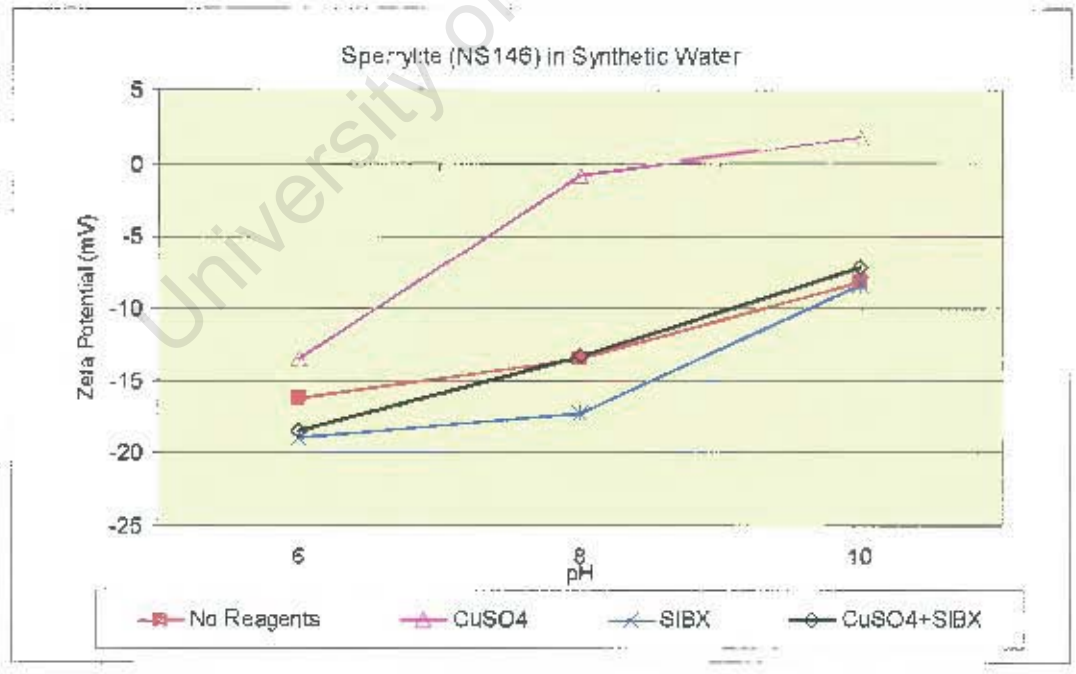

Figure 4.14: Zeta potential curves over a pH range 6-10 for Sperrylite (NS146) treated with no reagents, SIBX, $CuSO_4$, $CuSO_4$+SIBX.

University of Cape Town

The zeta potential data for the palladoarsenide sample NS147 show very different trends compared to those seen for the sperrylite samples. In this case, the palladoarsenide surface charge is fairly neutral for the entire pH range tested (Figure 4.15). The neutral palladoarsenide surface charge rules out the possibility of electrostatic adsorption of positively charged Cu(II) species at the lower pH. Based on the copper speciation diagram (Fuerstenau, 1976), it can be assumed that the $Cu(OH)_2$ colloids are precipitating onto the mineral surface above pH 8. The assumption is supported by a significant shift in the zeta potential versus pH curve in the presence of Cu(II) ions and SIBX, which can be attributed to the conversion of hydrophilic $Cu(OH)_2$ to weakly hydrophobic Cu(I)X species. This is further supported by the significant shift in the zeta potential versus pH curve when comparing the zeta potential data obtained for the copper and SIBX treated palladoarsenide to the SIBX only trial.

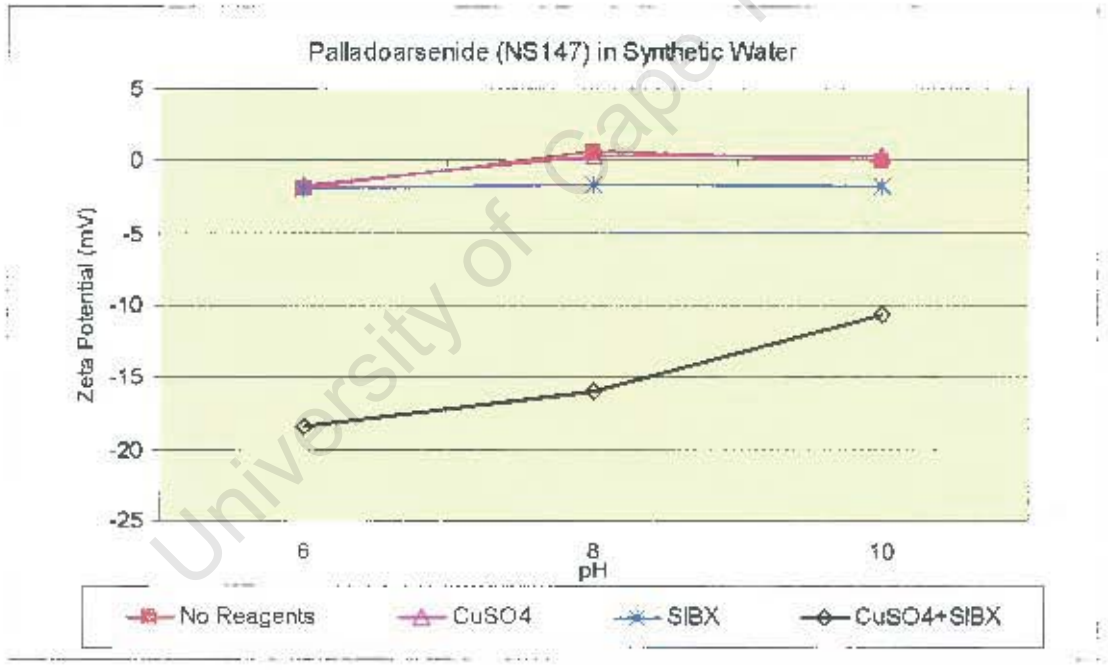

Figure 4.15: Zeta potential curves over a pH range 6-10 for Palladoarsenide (NS147) treated with no reagents, SIBX, $CuSO_4$, $CuSO_4$+SIBX.

4.2.2.2.3 Moncheite and Merenskyite

Figures 4.16 – 4.19 show the zeta potential pH curves for moncheite, NS142 and NS153 and merenskyite, NS143 and NS152, respectively. In the case of the moncheite sample, NS142,

University of Cape Town

the zeta potential versus pH curve shifts to more positive values in the presence of copper ions, compared to the no reagent curve (Figure 4.16). This shift is attributed to the electrostatic adsorption of the positive Cu(II) ion species, which are predominant below pH 7. At the higher pH, the precipitation of $Cu(OH)_2$ colloids lead to a slight decrease in zeta potential as observed in Figure 4.16. When SIBX is added and compared to the no reagents curve, the zeta potential versus pH curve shifts to slightly more negative values indicating that xanthate is being adsorbed onto the mineral surfaces. When xanthate is added in the presence of copper species, the shift in zeta potential is much larger compared to the xanthate only zeta potential versus pH curve indicating that xanthate ions must be adsorbing onto the copper ion activated mineral surfaces. One possible mechanism is a chemical reaction, which involves the formation of Cu(I)-X complexes at pH9. The second mechanism could be electrostatic attraction between the positively charged copper species and the negatively charged xanthate ions.

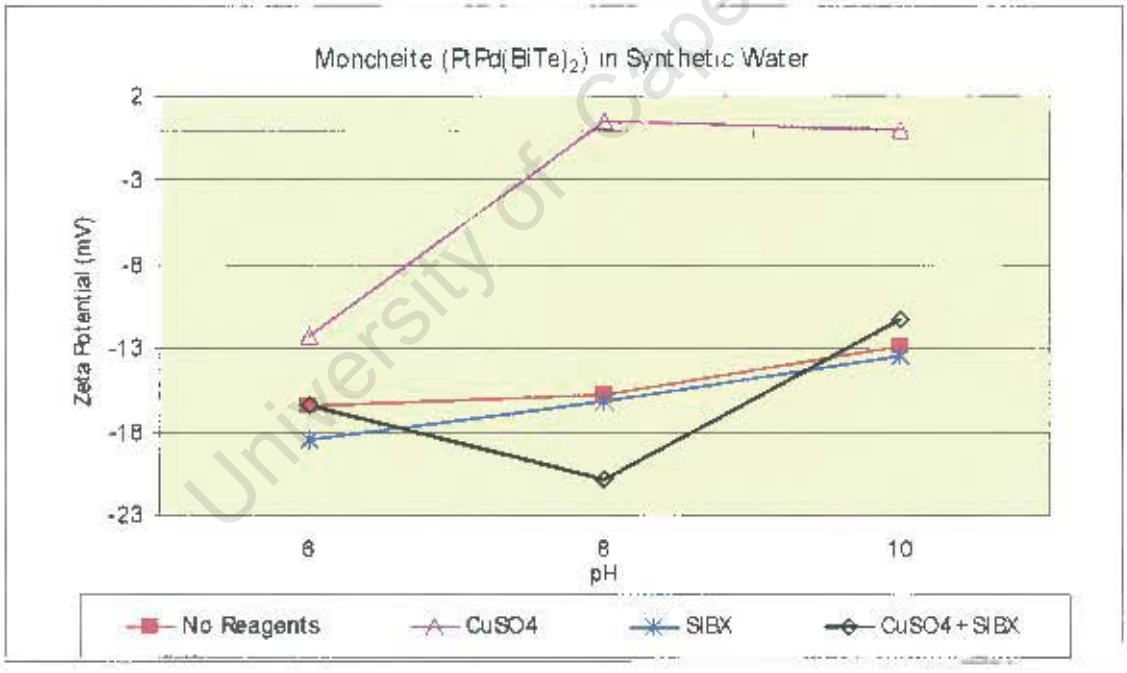

Figure 4.16: Zeta potential curves over a pH range 6-10 for Moncheite (NS142) treated with no reagents, SIBX, $CuSO_4$, $CuSO_4$+SIBX.

The results for moncheite sample NS153 (Figure 4.17) are different from the results obtained for NS142. The sample, NS153, is more negatively charged compared to NS142 when

University of Cape Town

conditioned in synthetic water only. There is copper adsorption on the mineral surfaces when $CuSO_4$ is added as the zeta potential pH curve shifts to more positive values compared to the no reagent trial. The shift in the zeta potential curve is more prominent from pH 8 indicating a higher affinity of the mineral surfaces for the copper species. Xanthate adsorption is shown to be minimal; however, there is xanthate adsorption occurring onto the copper activated mineral surfaces as the zeta potential pH curves shifts to more negative values compared to the $CuSO_4$ addition case but a much smaller shift is observed compared to the result obtained for NS142.

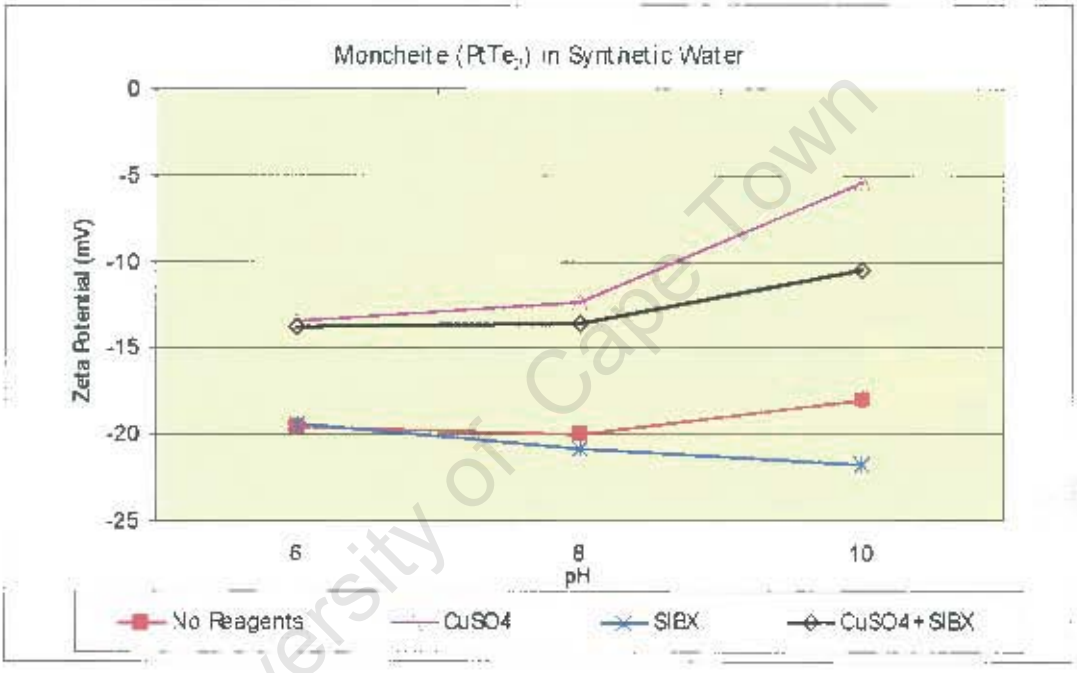

Figure 4.17: Zeta potential curves over a pH range 6-10 for Moncheite (NS153) treated with no reagents, SIBX, $CuSO_4$, $CuSO_4$+SIBX.

University of Cape Town

The merenskyite samples also show differences between the two mineral compositions (Figures 4.18 and 4.19). The more pure mineral, $PdTe_2$, is more negative when conditioned with no reagents. Both samples show very little xanthate adsorption onto the mineral surface compared to the no reagents zeta potential pH curve. In the presence of $CuSO_4$, both samples show copper adsorption onto mineral surfaces due to the positive shift in the zeta potential pH curve compared to the no reagent curve. There is xanthate adsorption onto the

copper activated mineral surfaces for both merenskyite samples as the zeta potential pH curves shifts to more negative values compared to the $CuSO_4$ addition case.

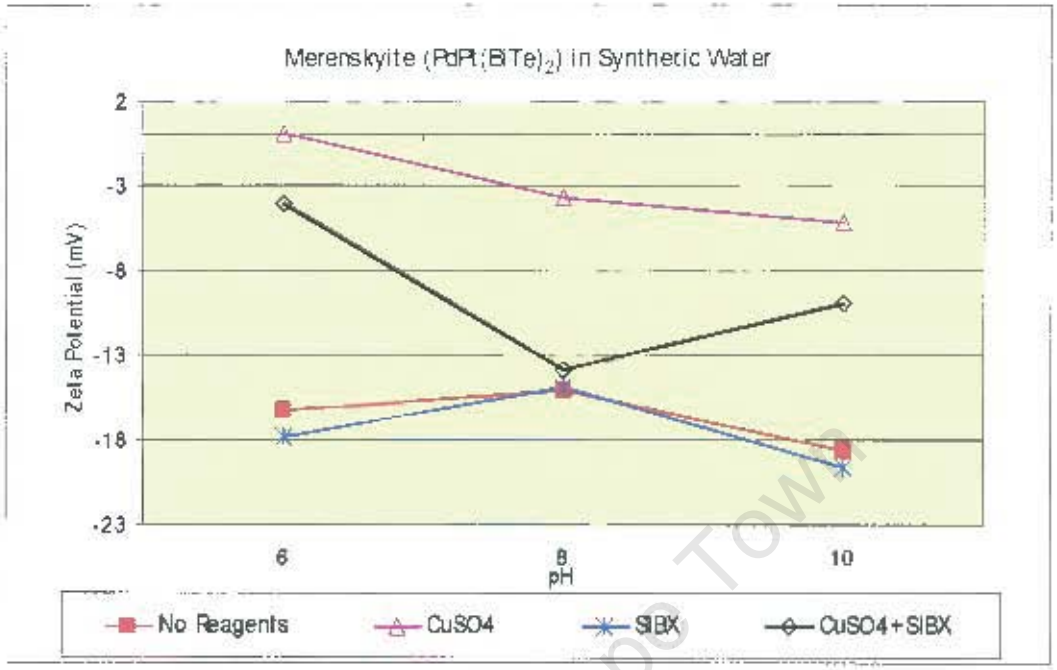

Figure 4.18: Zeta potential curves over a pH range 6-10 for Merenskyite (NS143) treated with no reagents, SIBX, $CuSO_4$, $CuSO_4$+SIBX.

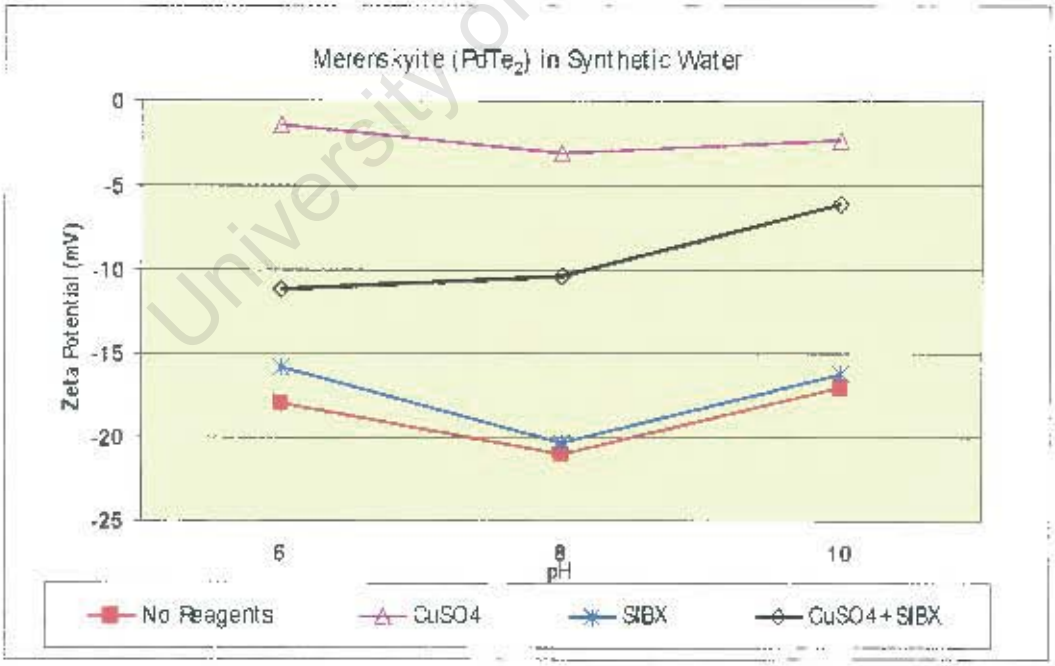

Figure 4.19: Zeta potential curves over a pH range 6-10 for Merenskyite (NS152) treated with no reagents, SIBX, $CuSO_4$, $CuSO_4$+SIBX.

University of Cape Town

In summary, the most striking difference observed is between the Pt and Pd mineral species in the absence of reagents and in the presence of xanthate, where the zeta potential versus pH curves are on opposite ends of the scale for the Pt and Pd sulphides minerals (cooperite and vysotskite) and the Pt and Pd arsenide minerals (sperrylite and palladoarsenide). Another difference observed is between the Pt mineral species where cooperite's surface charge is much more positive compared with the other mineral types. There is also a minimal shift in the zeta potential versus pH curves observed in the presence of xanthate for all mineral species.

The zeta potential results also show that all of the synthetic minerals except for palladoarsenide and cooperite show a significant shift to more positive zeta potential values in the presence of copper sulphate. This indicates the presence of positively charged copper species on the mineral surfaces and/or the formation of neutral $Cu(OH)_2$ colloids which may partially cover the negative mineral surface above pH 7.5. When xanthate is added to the various mineral mixtures after the copper sulphate addition, the zeta potential versus pH curve shifts to more negative values: this includes the curves obtained for palladoarsenide and cooperite. This indicates that xanthate is being adsorbed on the copper 'activated' mineral surfaces.

4.2.2 ToF-SIMS Analyses

ToF-SIMS analysis is a well-established technique in determining the occurrence of atomic/molecular species on the surface of mineral samples. The testwork was carried out with the aim of gaining an understanding of mineral surface alteration and link those to flotation recovery. It must be noted that the ToF-SIMS technique is qualitative; hence the results obtained are to be interpreted as relative effects rather than giving absolute values. The intensities (signals) obtained during analysis are normalised to the total ion yield in positive and negative SIMS for the elements of interest and are presented as normalised yield. The normalised data obtained were then evaluated using Statistica.

University of Cape Town

4.2.2.1 Comparative Surface Analysis of Reagent Additions

4.2.2.1.1 Cooperite

The copper and xanthate ion normalised yields for cooperite are shown in Figures 4.20 and 4.21, respectively. A higher copper ions yield was observed for the $CuSO_4$+SIBX trial compared to the $CuSO_4$ only case. This may be due to a reaction between copper and xanthate in solution which causes precipitation of copper-xanthate colloids onto the mineral surface. The data also shows the presence of xanthate before and after copper sulphate addition and the results show a higher yield of xanthate on the copper activated mineral surfaces compared the xanthate only case (Figure 4.21).

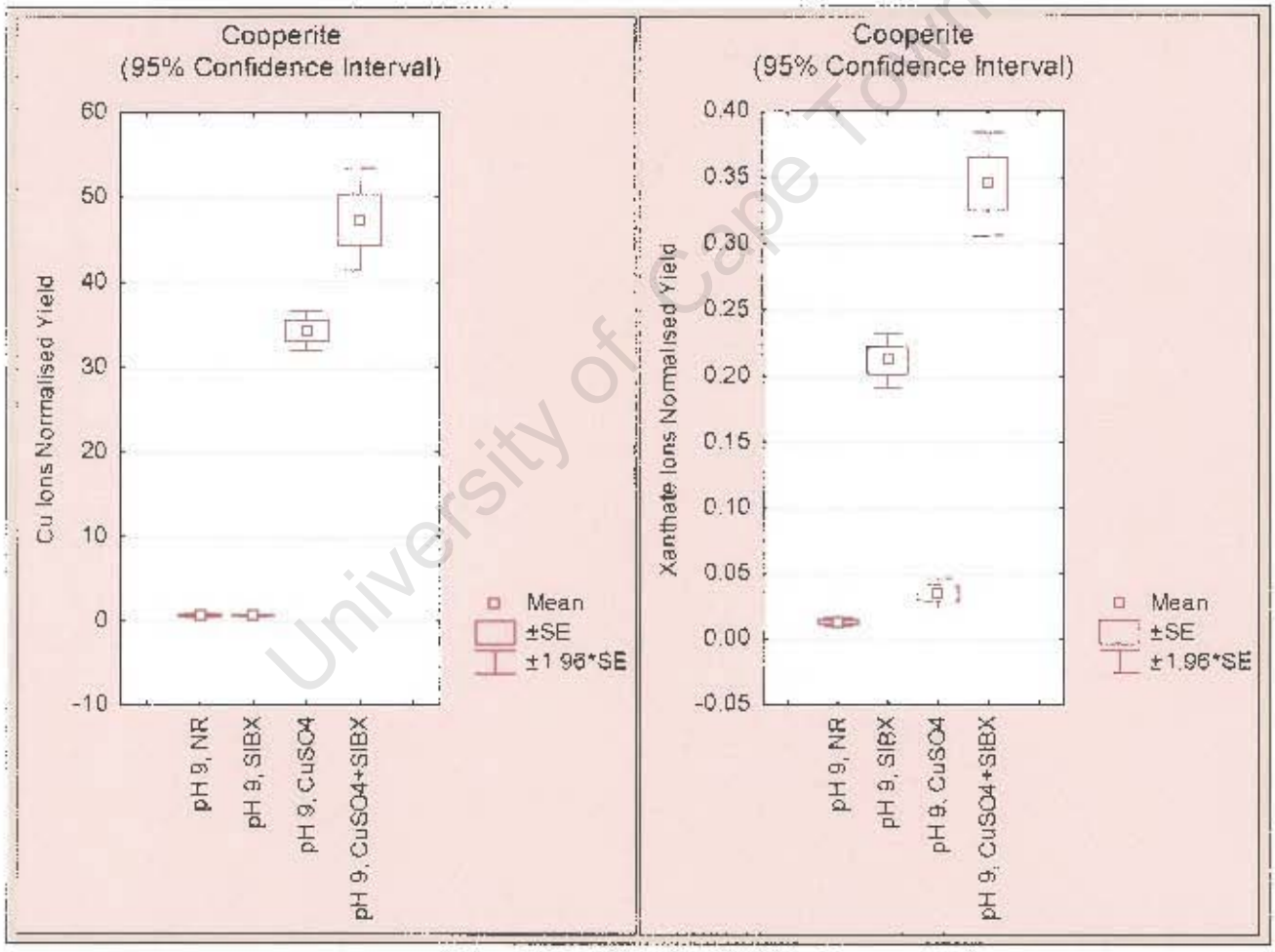

Figure 4.20: Copper ions normalised yield for cooperite NS144.

Figure 4.21: Xanthate ions normalised yield for cooperite NS144.

University of Cape Town

4.2.2.1.2 Vysotskite

Figures 4.22 and 4.23 show the copper and xanthate ion normalised yields for vysotskite, respectively. A high copper yield is observed for the $CuSO_4$ and $CuSO_4$+SIBX trials and the data shows xanthate adsorption before and after copper sulphate addition and as seen for cooperite; a higher adsorption of xanthate on the copper activated mineral surfaces compared the xanthate only case (Figure 4.23).

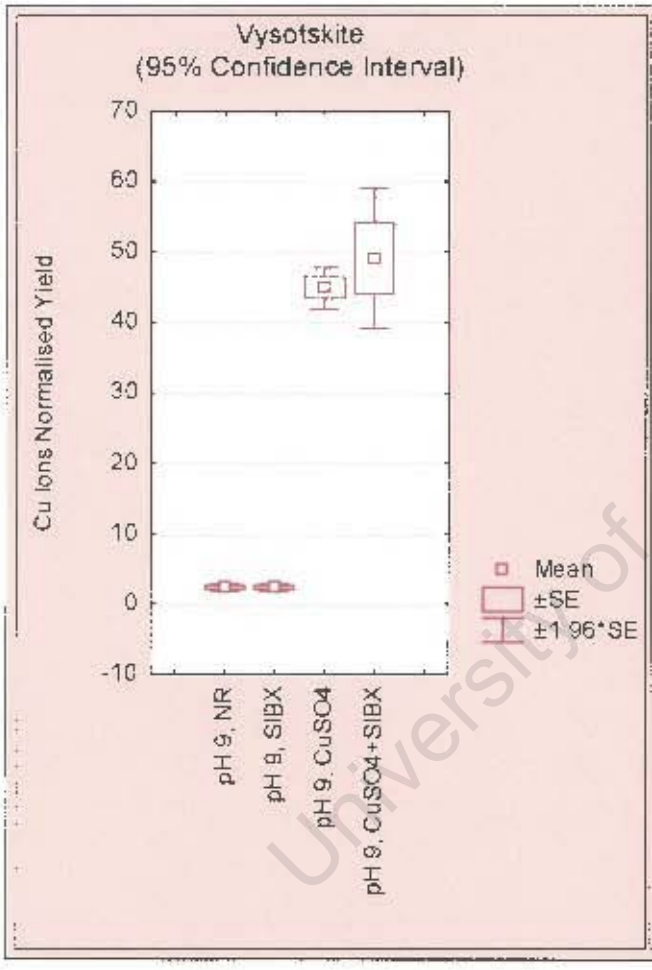

Figure 4.22: Copper ions normalised yield for vysotskite NS148.

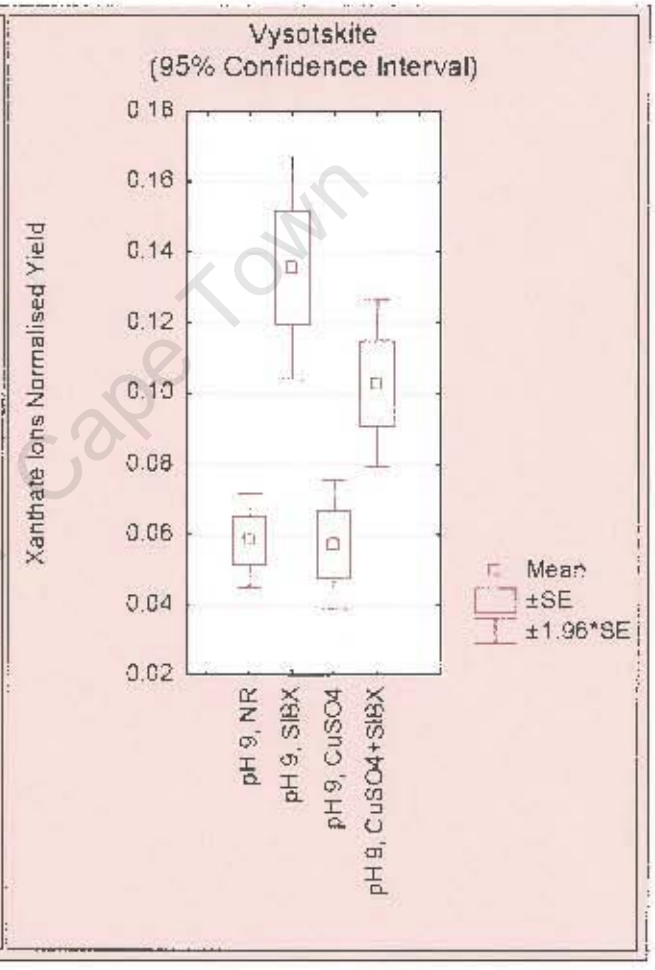

Figure 4.23: Xanthate ions normalised yield for vysotskite NS148.

University of Cape Town

4.2.2.1.3 Sperrylite

The copper and xanthate ion normalised yields for both sperrylite samples are shown in Figures 4.24 and 4.25, respectively. In the case of the sperrylite sample NS145, a higher Cu

yield was observed for the $CuSO_4$ and $CuSO_4$+SIBX trials compared to those results obtained for sperrylite sample NS146. Both sperrylite samples show xanthate adsorption on the copper activated mineral surfaces. In the presence of SIBX only, NS145 shows xanthate adsorption where NS146 does not show any xanthate adsorption. However, the sulphur ion yield, which is also an indicator of xanthate adsorption, shows higher sulphur ions surface concentration for the SIBX and $CuSO_4$+SIBX trials for both samples (Figure 4.26) compared to the no reagents and $CuSO_4$ addition trials.

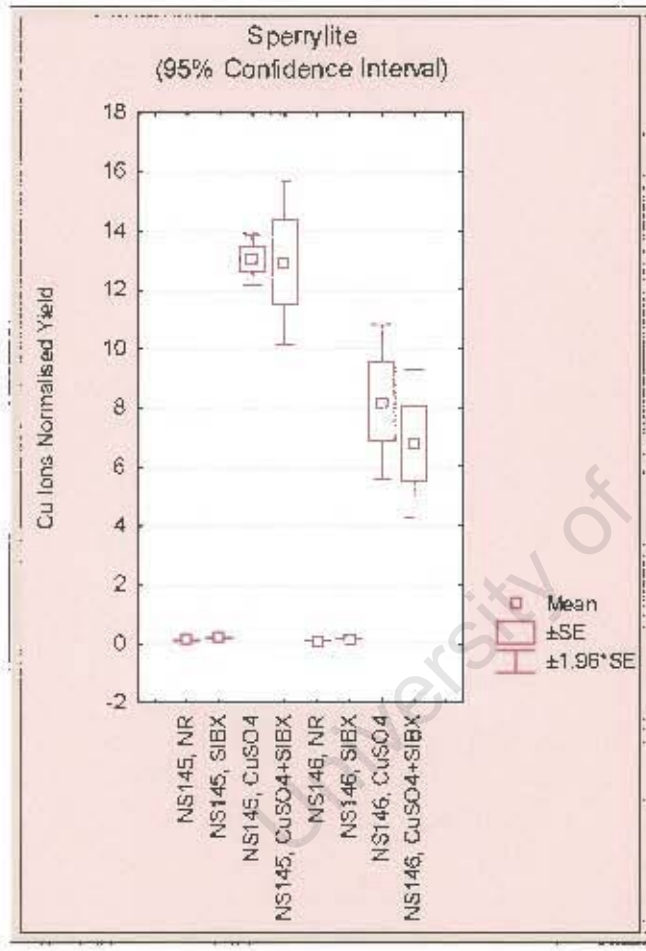

Figure 4.24: Copper ions normalised yield for sperrylite NS145 and NS146.

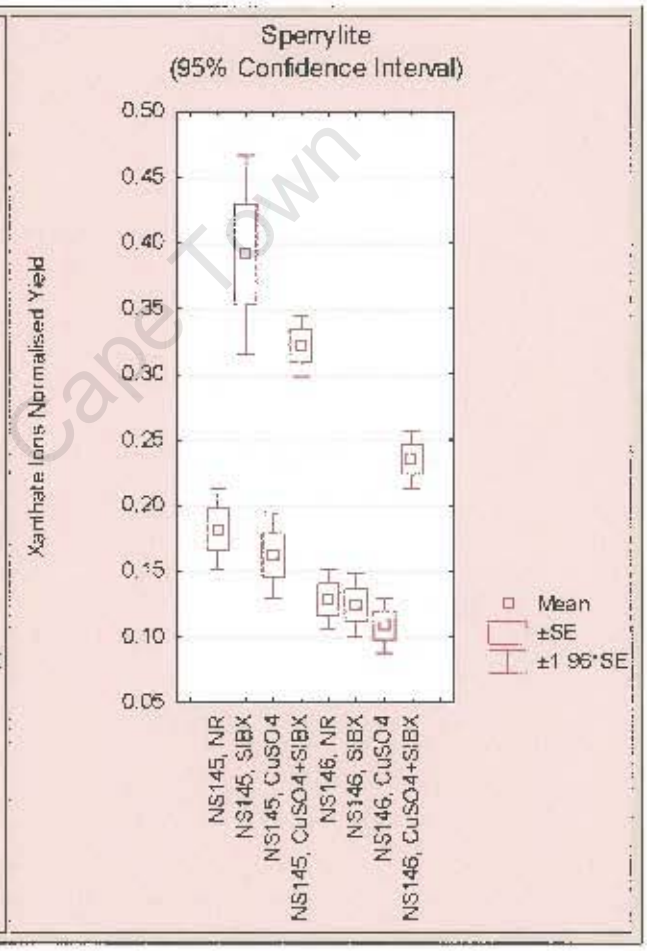

Figure 4.25: Xanthate ions normalised yield for sperrylite NS145 and NS146.

University of Cape Town

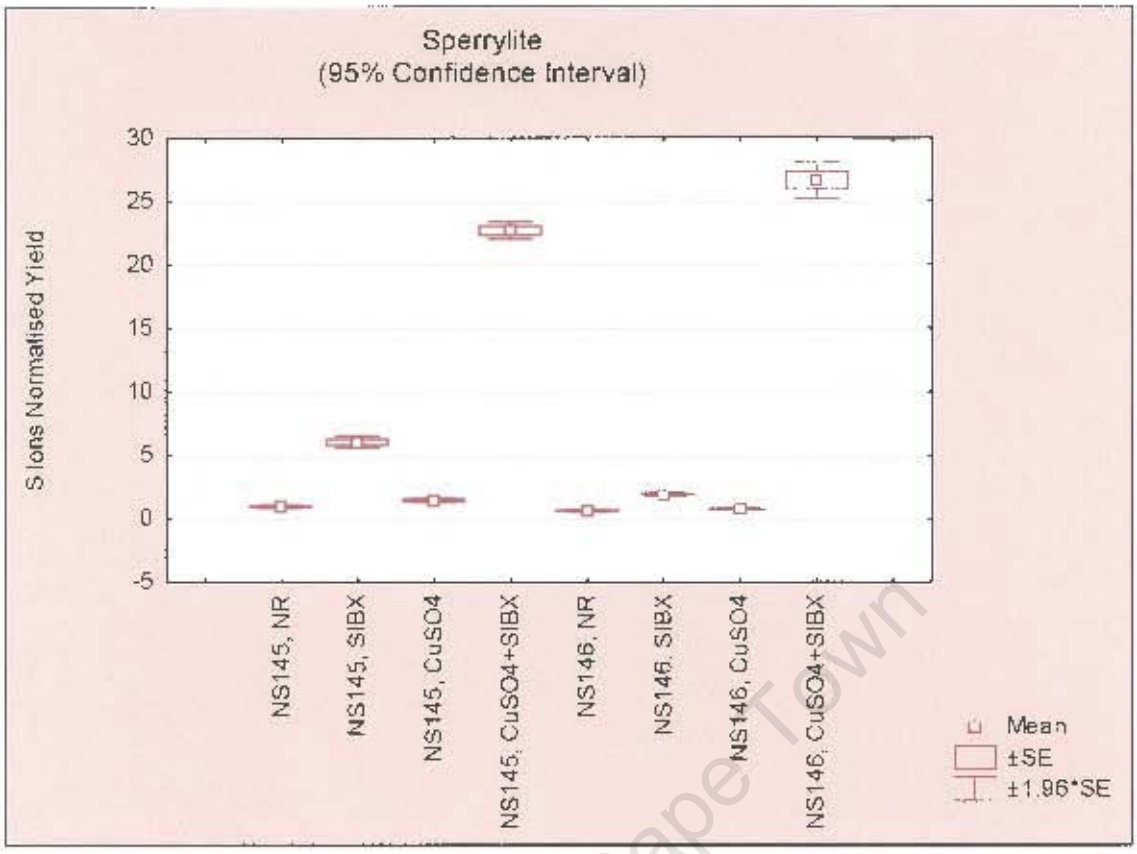

Figure 4.26: Sulphur ions normalised yield for sperrylite NS145 and NS146.

4.2.2.1.4 Palladoarsenide

The copper and xanthate ions normalised yields for palladoarsenide are shown in Figures 4.27 and 4.28, respectively. The results for the palladoarsenide sample NS147 are similar to those observed for the sperrylite sample NS145, i.e., a higher surface coverage of Cu and xanthate ions was observed. The data also shows a reduction in the concentration of the Cu(II) colloids present on the mineral surface when xanthate is added in the presence of $CuSO_4$. The xanthate surface coverage is not significantly different even though there is less copper present on the mineral surface.

University of Cape Town

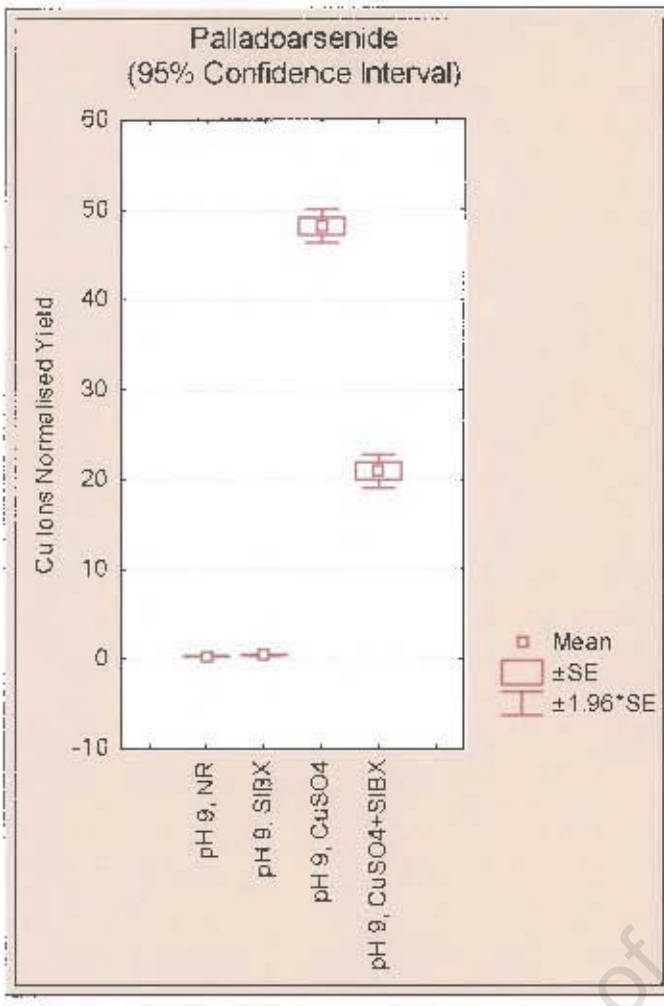

Figure 4.27: Copper ions normalised yield for palladoarsenide NS147.

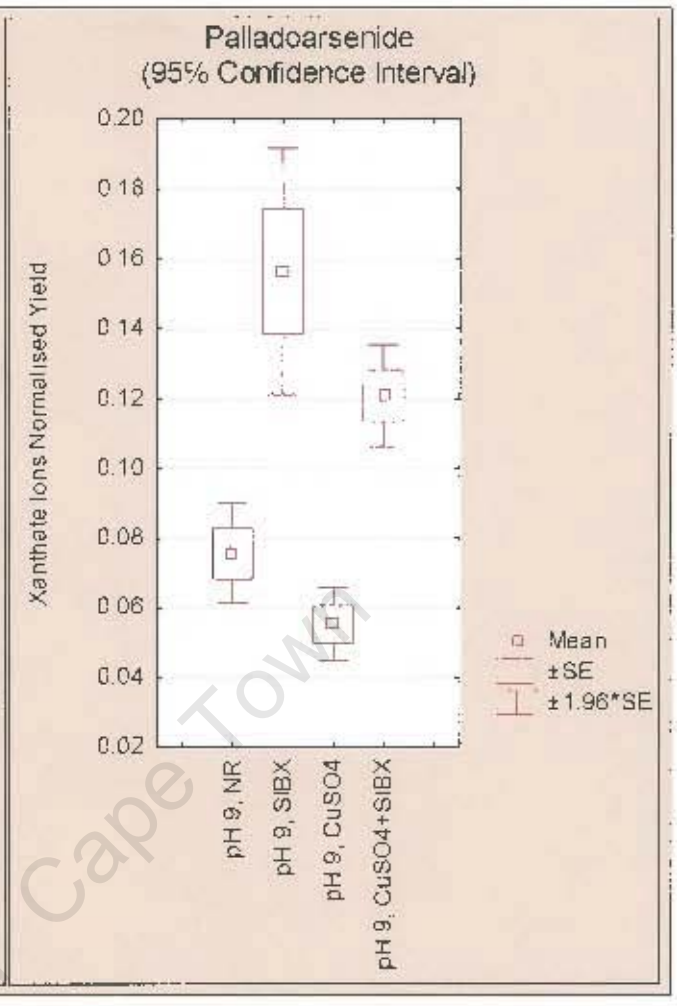

Figure 4.28: Xanthate ions normalised yield for palladoarsenide NS147.

University of Cape Town

4.2.2.1.5 Moncheite

The copper and xanthate ion normalised yield for both moncheite samples are shown in Figures 4.29 and 4.30, respectively. In the case of the moncheite sample NS142, a higher Cu ions yield was observed for the $CuSO_4$ and $CuSO_4$+SIBX trials compared to those results obtained for moncheite sample NS153 (Figure 4.29). Both moncheite samples show xanthate adsorption before and after copper sulphate addition (Figure 4.30).

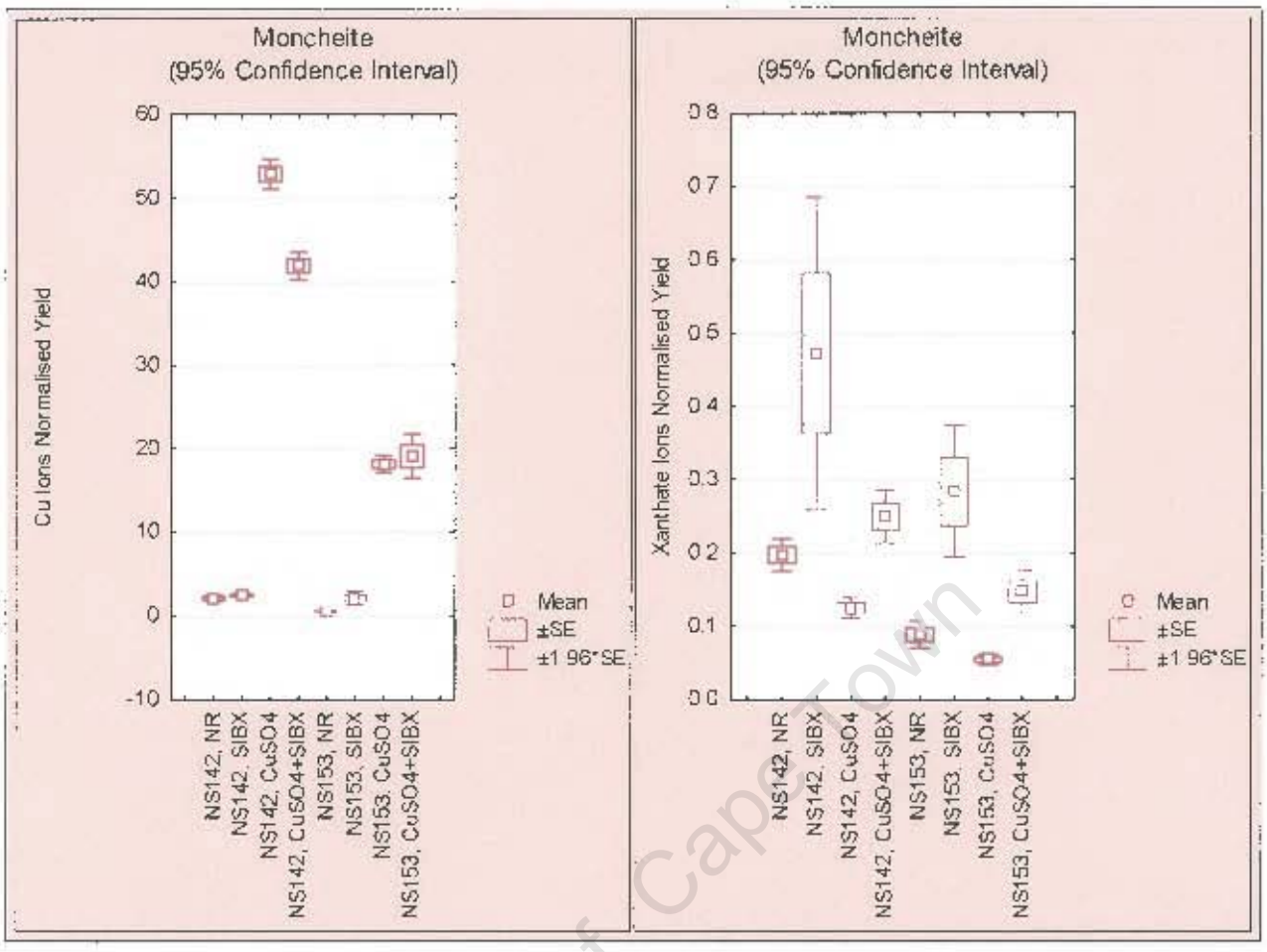

Figure 4.29: Copper ions normalised yield for moncheite NS142 and NS153.

Figure 4.30: Xanthate ions normalised yield for moncheite NS142 and NS153.

The sulphur ions normalised yield, which is also an indicator of xanthate adsorption, shows a much higher sulphur ions surface concentration for moncheite, NS153, compared to moncheite, NS142, for the SIBX and $CuSO_4$+SIBX trials (Figure 4.31).

University of Cape Town

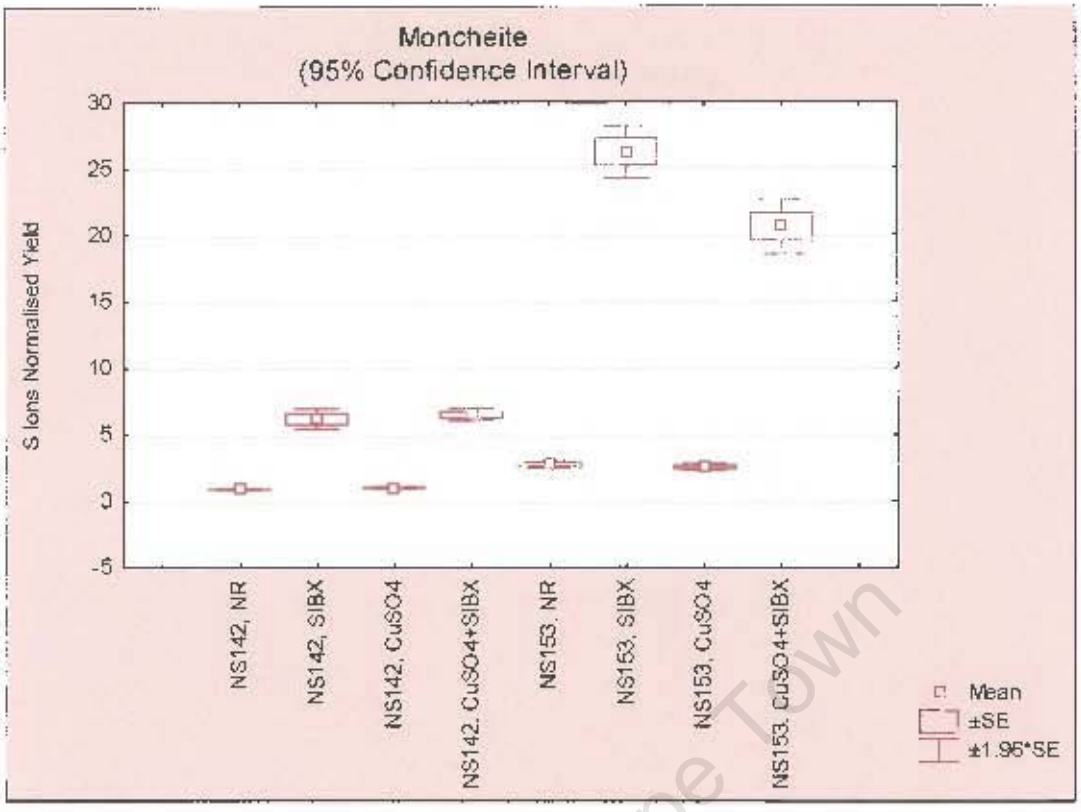

Figure 4.31: Sulphur ions normalised yield for moncheite NS142 and NS153.

The effect of copper sulphate concentration was evaluated due to the reduction in recovery observed with the addition of copper sulphate (5.00E-05M) compared to the xanthate only trial. The surface analyses for these trials are shown in Figures 4.32 and 4.33, for the relative percent copper and xanthate ion surface coverage for the moncheite ($PtTe_2$) sample, respectively. The results show a lower copper ions surface coverage with the reduced copper sulphate addition compared to the standard 5.00E-05M $CuSO_4$ concentration normally used (Figure 4.32. The xanthate surface coverage has significantly increased with the lower copper sulphate (5.00E-06M) addition (Figure 4.33) compared to the 5.00E-05M copper sulphate addition.

University of Cape Town

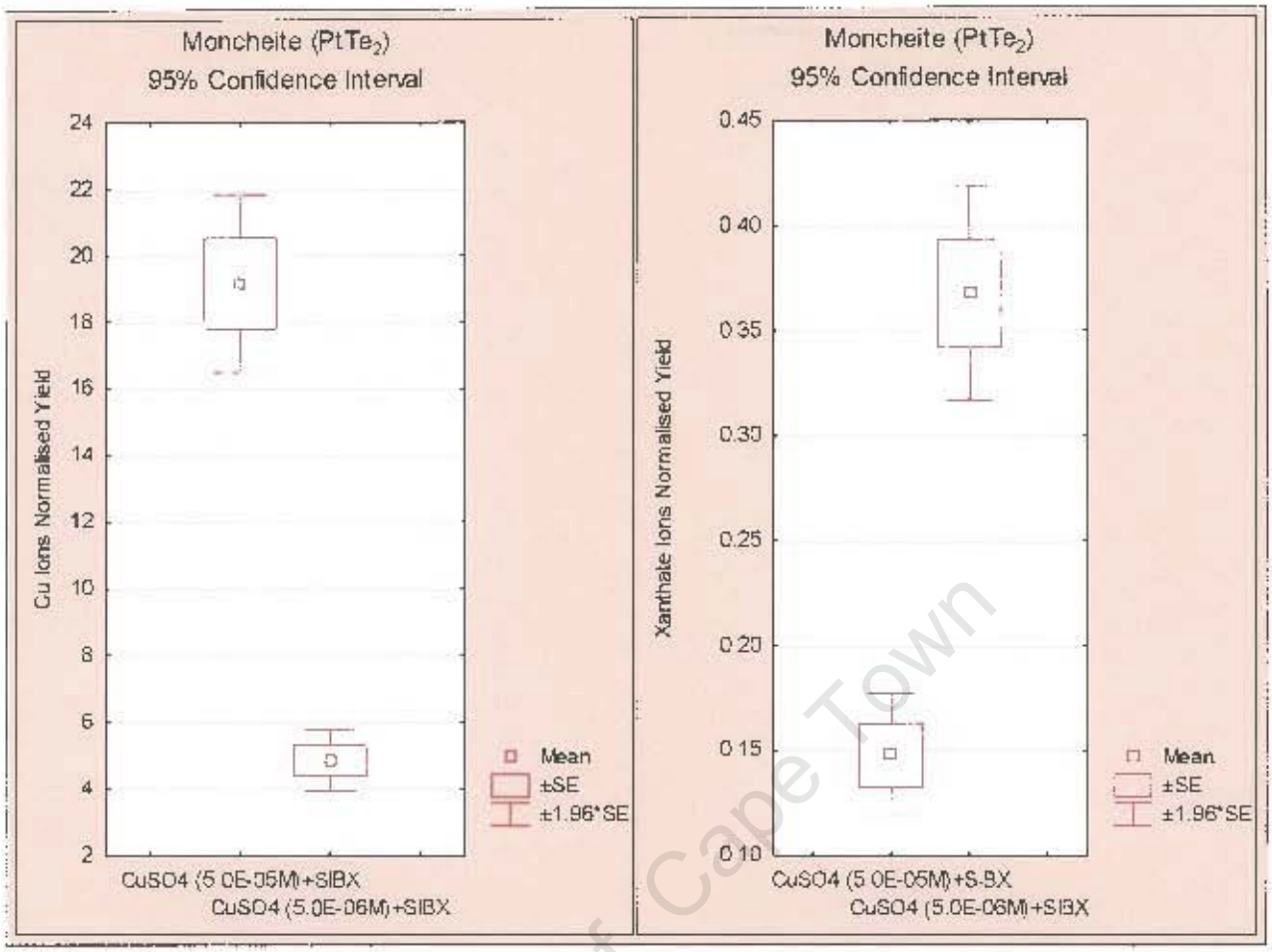

Figure 4.32: Copper ions normalised yield for moncheite NS153 when the $CuSO_4$ concentration was varied.

Figure 4.33: Xanthate ions normalised yield for moncheite NS153 when the $CuSO_4$ concentration was varied.

Figure 4.34 A, B, C and D shows the normalised yield for [Calcium, Magnesium, Aluminum, Silicon], Ni, Fe and xanthate ions, respectively. The results show that when moncheite, NS142, is conditioned in the presence of pentlandite and xanthate (Trial A) the normalised yield of Ca+Mg+Al+Si, Ni and Fe ions increases and the xanthate ion surface concentration decreases compared to the results obtained for moncheite on its own. The test (Trial B) where the pentlandite was removed by screening and discarded before the flotation of the moncheite showed lower surface concentrations of Ca+Mg+Al+Si, Ni and Fe, while the xanthate ion surface concentration increased slightly compared to the trial where pentlandite was floated with moncheite.

University of Cape Town

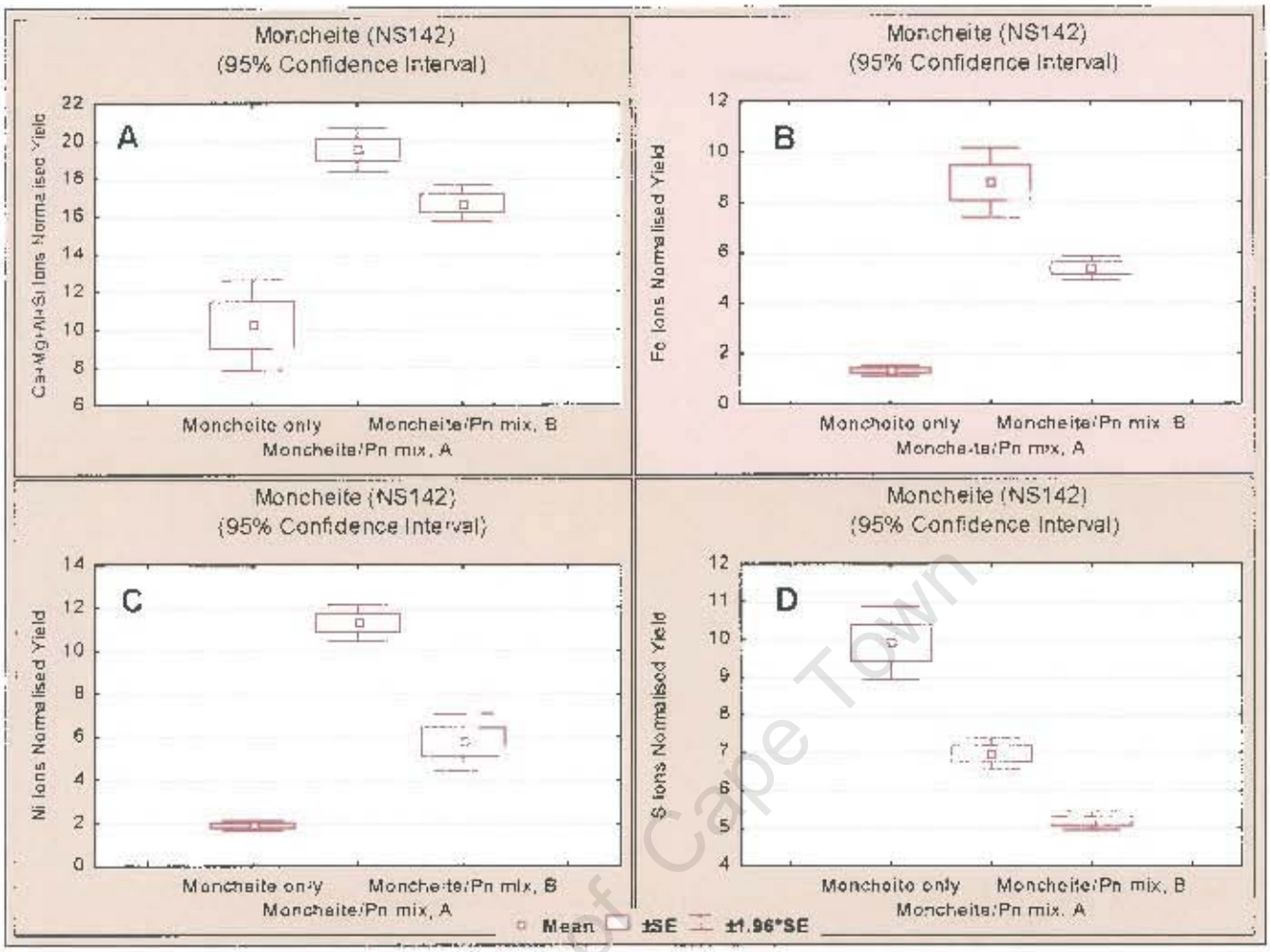

Figure 4.34: A - *Ca+Mg+Al+Si ions normalised yield for moncheite NS142 conditioned with and without pentlandite and floated with (mix A) and without (mix B) pentlandite in the presence of xanthate.*

B - *Nickel ions normalised yield for moncheite NS142 conditioned with and without pentlandite and floated with (mix A) and without (mix B) pentlandite in the presence of xanthate.*

C - *Iron ions normalised yield for moncheite NS142 conditioned with and without pentlandite and floated with (mix A) and without (mix B) pentlandite in the presence of xanthate.*

D - *Xanthate ions normalised yield for moncheite NS142 conditioned with and without pentlandite and floated with (mix A) and without (mix B) pentlandite in the presence of xanthate.*

The effect of oxidation was examined on both moncheite samples and the ToF-SIMS data showed minor surface concentrations of oxidation products (Bi and Te) for NS142 compared to NS153 which showed no oxidation products. The oxidising conditions involved exposing the minerals to 100°C for 7 days with purging of air at regular intervals. These results are

University of Cape Town

consistent with those obtained for the microflotation data which is discussed later in this section.

4.2.2.1.6 Merenskyite

The copper and xanthate ion normalised yield for both merenskyite samples are shown in Figures 4.35 and 4.36, respectively.

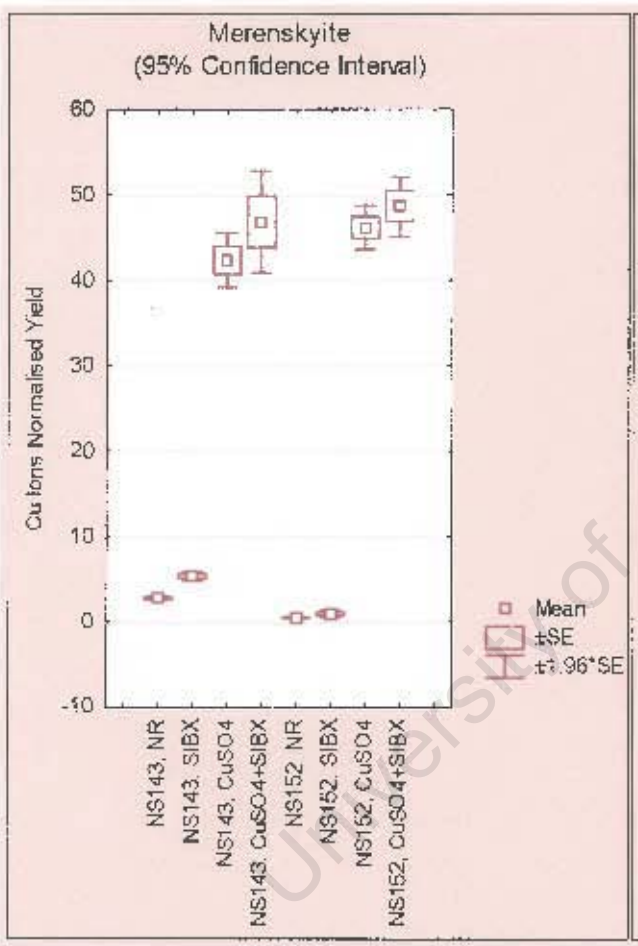

Figure 4.35: Copper ions normalised yield for merenskyite NS143 and NS152.

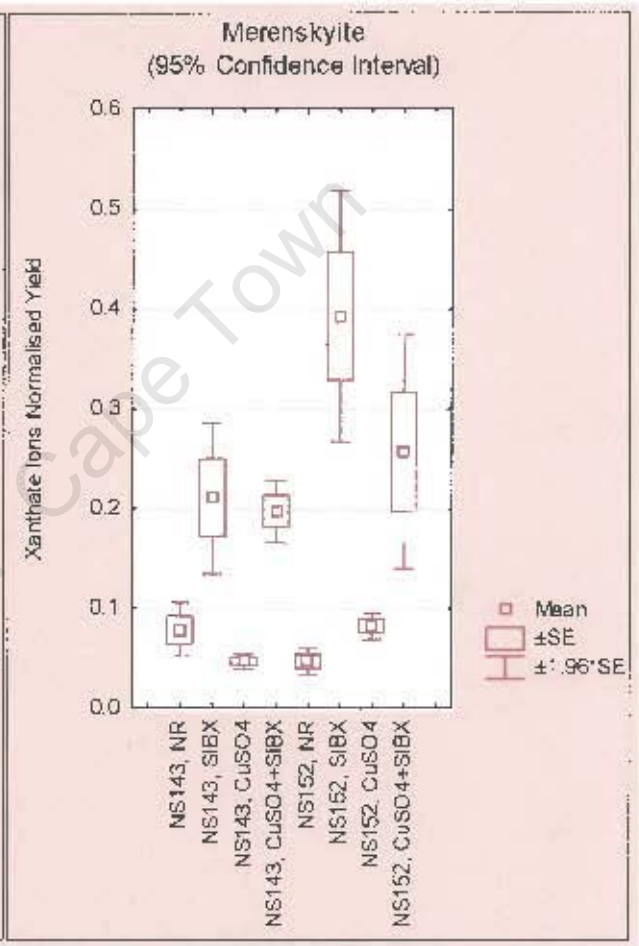

Figure 4.36: Xanthate ions normalised yield for merenskyite NS143 and NS152.

The Cu ions surface coverage was similar for both merenskyite samples (Figure 4.35). Both merenskyite samples show xanthate adsorption before and after copper sulphate addition (Figure 4.36).

University of Cape Town

The sulphur ion normalised yield, which is also an indicator of xanthate adsorption, shows a much higher sulphur ions surface concentration for merenskyite, NS152, compared to the merenskyite, NS143, for the SIBX and $CuSO_4$+SIBX trials (Figure 4.37).

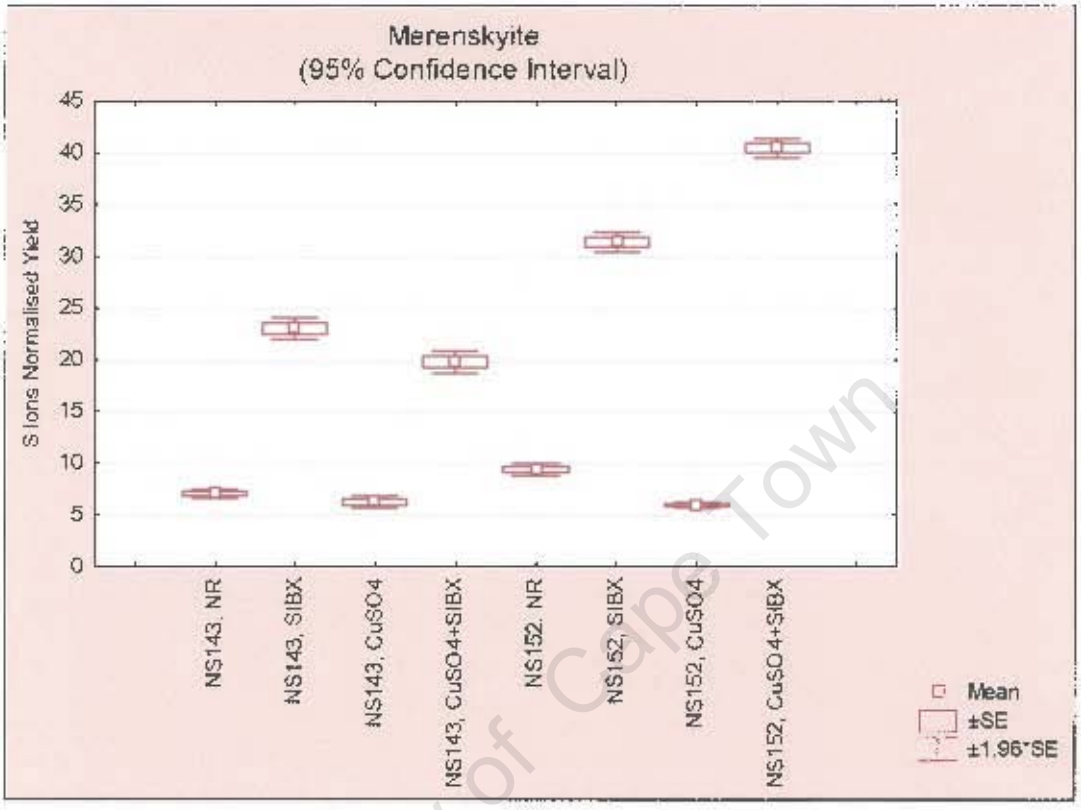

Figure 4.37: Sulphur ions normalised yield for merenskyite NS143 and NS152.

4.2.2.3 Ethylenediamine (EDA) Addition

Further testwork was conducted with the addition of a complexing agent, ethylenediamine (EDA), after the $CuSO_4$ addition and after the $CuSO_4$+SIBX addition, in an attempt to remove any of the unconverted $Cu(OH)_2$ colloids thereby determining the speciation and the bonding mechanism of the copper ions to the mineral surface. Figures 4.38 and 4.39 show the copper normalised yield obtained for the Pt and Pd minerals with and without ethylenediamine addition, respectively. These tests were carried out in synthetic water at pH 9 and all the reagents were added at a concentration of 5.00E-05 M. The ToF-SIMS data shows that when EDA is added to the system, in either sequence, before and after xanthate addition, there is a removal of copper ions from both the sperrylite (NS145 and NS146), moncheite (NS142) and

University of Cape Town

both merenskyite (NS143 and NS152) mineral surfaces. The palladoarsenide (NS147) does not exhibit any copper removal with the addition of EDA for the $CuSO_4$+SIBX+EDA sequence. However, it should be noted that a significantly lower copper normalised yield was observed on the mineral prior to the addition of EDA compared to the sperrylite samples. With the addition of EDA after $CuSO_4$ and prior to SIBX there is removal of the copper hydroxyl species. Moncheite, NS153, does not exhibit any copper removal with the addition of EDA which may be due to the lower initial copper adsorption and thus a higher concentration of copper ions in solution available for reaction with EDA. Both Pt and Pd sulphide minerals do not exhibit any copper removal with the addition of EDA for the $CuSO_4$+SIBX+EDA sequence but cooperite shows copper removal when EDA is added after the $CuSO_4$ addition and prior to SIBX.

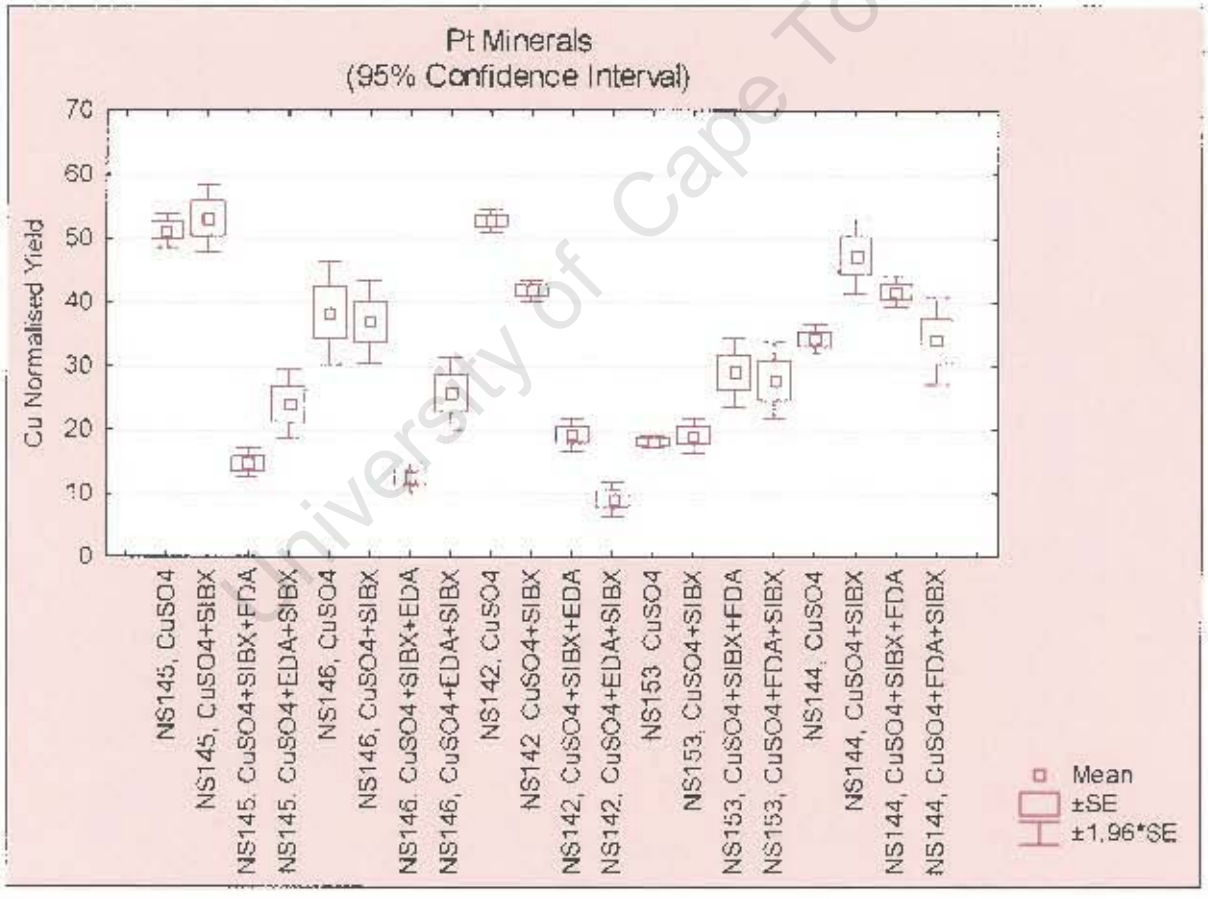

Figure 4.38: Copper ions normalised yield for Pt minerals with and without ethylenediamine addition.

University of Cape Town

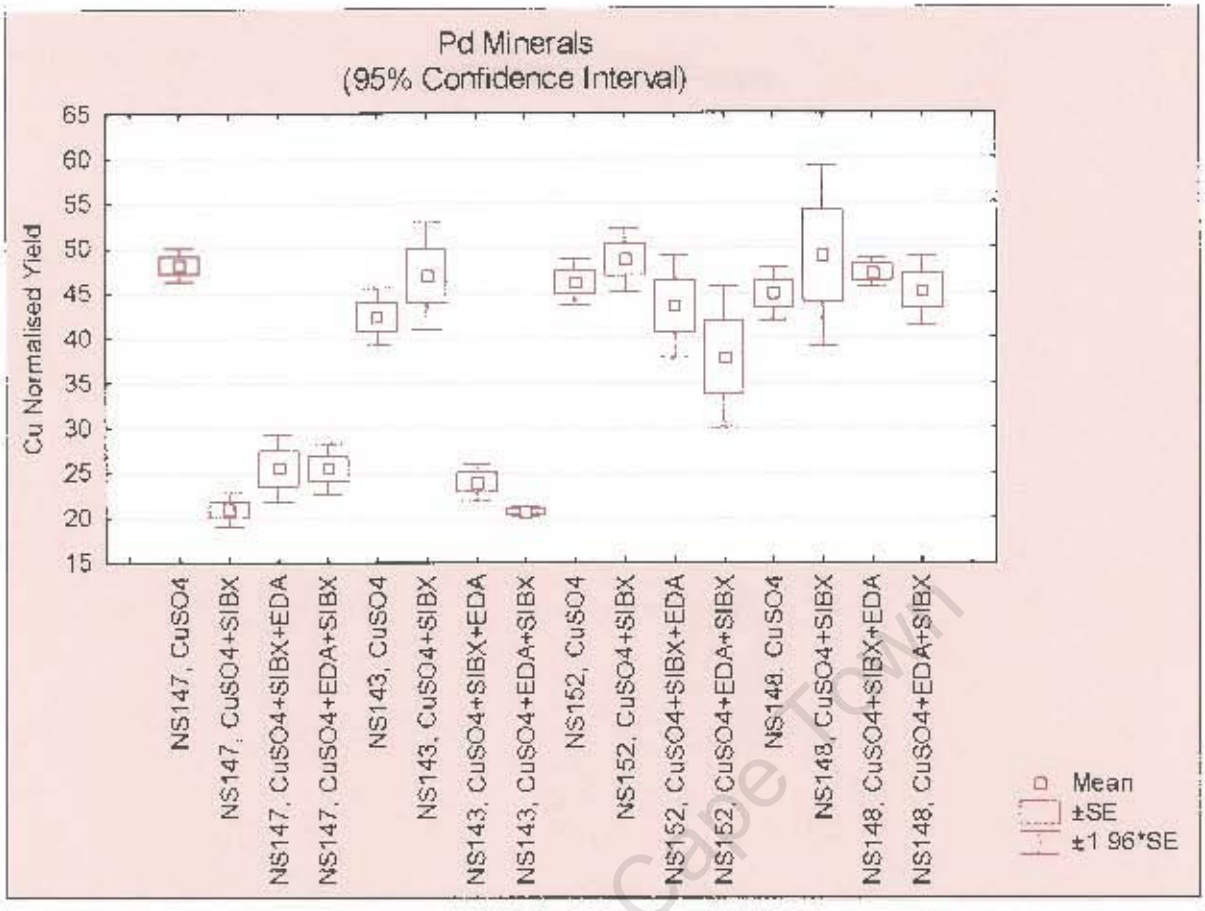

Figure 4.39: Copper ions normalised yield for Pd minerals with and without ethylenediamine addition.

4.2.3 XPS Analyses

XPS studies were carried out to determine the chemical speciation of the species present on the mineral surfaces and the results are summarised hereunder in Table 4.18 for the Pt minerals and Table 4.19 for the Pd minerals. It is interesting to note that the Pd minerals species surfaces are significantly altered and show heavily oxidised surfaces when compared to the Pt mineral species which show minimal oxidation even though they were all stored under an inert atmosphere. The XPS results obtained during copper sulphate addition for $PdTe_2$ (NS152) is not consistent with those observed during the zeta potential, ToF-SIMS and microflotation testwork. This may be due to the extensive oxidation observed for the $PdTe_2$ mineral surface which may have inhibited the adsorption of the copper ions (Table 4.19). Appendix E shows the relevant spectra for the various elements of interest and detailed interpretation of the results.

University of Cape Town

Table 4.18: Summary of the XPS data obtained for the Pt mineral samples.

Sample conditioning step	Sperrylite ($PtAs_2$) NS145	Sperrylite ($PtAs_2$) NS146	Moncheite ($PtPd(BiTe)_2$) NS142	Moncheite ($PtTe_2$) NS153	Cooperite (PtS) NS144
In synthetic water	Ions present in the synthetic water are not strongly adsorbed No oxidation of As observed.	Ions present in the synthetic water are not strongly adsorbed. No oxidation of As observed.	Ions present in the synthetic water are not strongly adsorbed Some oxidation - TeO_4 ion or $Te(OH)_2$) and reduced Bi(I) or Bi(0)	Ions present in the synthetic water are not strongly adsorbed. Some oxidation - TeO_4 ion or $Te(OH)_2$) – This sample appears to be less oxidised after synthetic water conditioning	Specifically adsorbs Mg^{2+}. Limited oxidation from synthetic water
			The ratio of TeO_4 ion or $Te(OH)_2$) is very different between NS142 (35:65) and NS153 (60:40).		
	Pt as Pt(II) and Pt(0)	Pt as Pt(II) and some apparent Pt(0)	Pt as Pt(II)	Pt as Pt(II)	Pt as Pt(II)
With $CuSC_4$ addition	Copper is detected at 3.5 at.% (1.5% is needed for effective copper activation in plant sample). ~80%Cu(II) with ~20% Cu(I).	Cu is detected at 4.6 at.%. ~66% Cu(II) with ~33% Cu(I).	Cu is detected in at 0.8 at.%. 99% of Cu as Cu(II)	Copper is detected at 1.0 at.%. 100% of Cu as Cu(II).	Copper is detected at 1.6 at.%. 100% of Cu as Cu(I).
	Cu(II) as precipitated, probably colloidal, $Cu(OH)_2$.				Adsorption of the Cu(I) has followed the classical mechanism of local reduction with oxidation of adjacent sulphide sites.
With $CuSO_4$+SIBX addition	Cu is present at 3.2 at.%. 100% Cu(I). Strong adsorption of xanthate.	Cu is present at 3.7 at.% 100% Cu(I) Strong adsorption of xanthate.	Cu is present at 0.7 at.% 94% Cu(II) with 6% Cu(I). Some xanthate adsorption (0.3%S). Some production of oxidised dixanthogen.	Cu is present at 0.7 at.%. 64% Cu(II) with 36% Cu(I) Xanthate adsorption (2.8%S). Some production of oxidised dixanthogen. Less oxide / hydroxide after xanthate addition.	Cu is present at 1.6 at.% 100% Cu(I) Xanthate adsorption (5%S increase).
With SIBX addition	There is xanthate adsorption but not as large as with copper activation.	These spectra are closely similar to NS145 with distinct but lower xanthate adsorption compared with copper activation	Xanthate adsorption (0.6%S) For the copper-xanthate system, the area estimate is 240 c/s compared with the xanthate alone at 370 counts.	Xanthate adsorption (3.8%S). More xanthate adsorbed without CuSO4 addition. For the copper-xanthate system, the area estimate is 960 c/s compared with the xanthate alone at 1780 counts	Xanthate adsorption lower (3%S increase) compared with copper activation

University of Cape Town

Table 4.19: Summary of the XPS data obtained for the Pd mineral samples.

Sample conditioning step	Palladoarsenide (Pd_2As) NS147	Merenskyite ($PdPt(BiTe)_2$) NS143	Merenskyite ($PdTe_2$) NS152	Vysotskite (PdS) NS148
In synthetic water	Ions present in the synthetic water are not strongly adsorbed. Heavily oxidised surface	Ions present in the synthetic water are not strongly adsorbed. Extensive oxidation predominantly Te - TeO_4 ion or $Te(OH)_2$) and Bi(V), Bi(III) and as reduced Bi(I)	Ions present in the synthetic water are not strongly adsorbed. Heavily oxidised surface	Ions present in the synthetic water are not strongly adsorbed. Heavily oxidised surface.
	16% unoxidised PdAs, 63% oxidised Pd as PdO or $Pd(OH)_2$ 72% oxidised As(i) and 28% oxidised As(III)	Ratio % of Te ion to TeO_4 and/or $Te(OH)_2$ is 44:56. Ratio % of Bi(V). Bi(III) to Bi(I) is 72:25:3.	Ratio % of Te and charged Te ions to TeO_4 and/or $Te(OH)_2$ is 56.33:11.	18% unoxidised PdS and 82% oxidised PdO
With $CuSO_4$ addition	Copper is detected at 1.2 at.% (1.5% is needed for effective copper activation in plant sample). Pd appears to be entirely oxidised. As shows more oxidation 87% Cu as Cu(II) with 13% of Cu as Cu(I).	Cu is detected in at.1 1 at%. 87% of Cu as Cu(II) with 13% of Cu as Cu(I).	<0.05 at.% copper is detected. Increase in oxidised species (TeO_4 and/or $Te(OH)_2$) from 11 to 20%	Copper is detected at 1.0 at.%. 65% of Cu as Cu(II) with 35% of Cu as Cu(I).
	Cu(II) as precipitated, probably colloidal, $Cu(OH)_2$.			
With $CuSO_4$+SIBX addition	Cu is present at 0.2 at.% - Too low to speciate. Xanthate adsorption (2%S).	Cu is present at 0.9 at%. 70% Cu(II) with 30% Cu(I). Some xanthate adsorption observed	Cu is present at 0.1 at.% - Too low to speciate Xanthate adsorption (0.8%S) Significant changes in Te component – less oxidation products due to surface cleaning by xanthate adsorption.	Cu is present at 1.1 at.%. 78% Cu(I) with 22% Cu(II) Significant increase in PdS component from 12 to 31% due to surface cleaning indicating xanthate adsorption.
With SIBX addition	Xanthate adsorption (2.5%S). Pd remains entirely oxidised. As shows more oxidation.	Xanthate adsorption (0.7%S). For the copper-xanthate system, the area estimate is 316 counts compared with the xanthate alone at 319 counts.	Xanthate adsorption (1.2%S). Changes in Te component – less oxidation products due to surface cleaning by xanthate adsorption. For the copper-xanthate system, the area estimate is 480 c/s compared with the xanthate alone at 130 counts	Xanthate adsorption similar compared with copper activation however, PdS component increase only from 12 to 18%.

University of Cape Town

As an example of the conversion of Cu(II) to Cu(I) with addition of xanthate Figures 4.40 and 4.41 show the Cu *2p* spectra for NS145 with the addition of $CuSO_4$ and with the addition of $CuSO_4$ followed by xanthate, respectively. When xanthate is added after the $CuSO_4$ addition, the chemical state of the copper changed dramatically from between >80% Cu(II) to 100% Cu(I) as seen in the Cu *2p* spectra for NS145. Figure 4.40 clearly shows the satellite peak due to Cu(II) whereas in Figure 4.41 when xanthate is added to the copper activated mineral surface there is no satellite peak which shows that any Cu(II) present on the surface was converted to Cu(I).

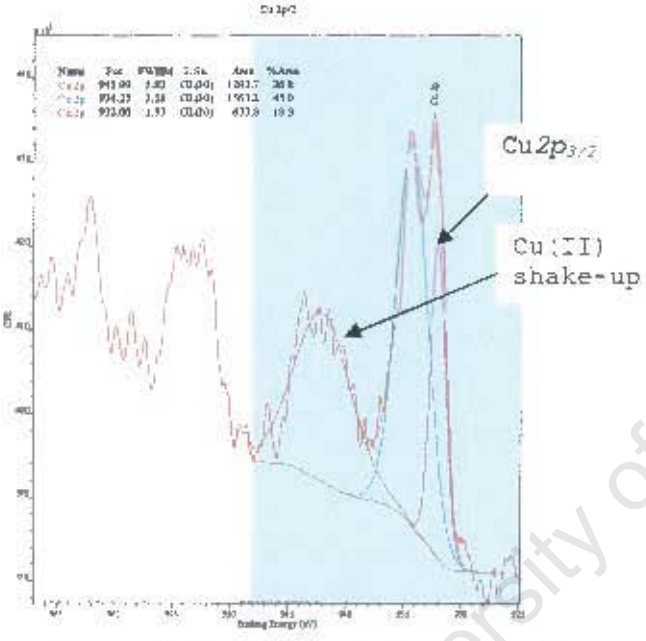

Figure 4.40: XPS analysis of sperrylite NS145 conditioned with copper sulphate at pH 9.

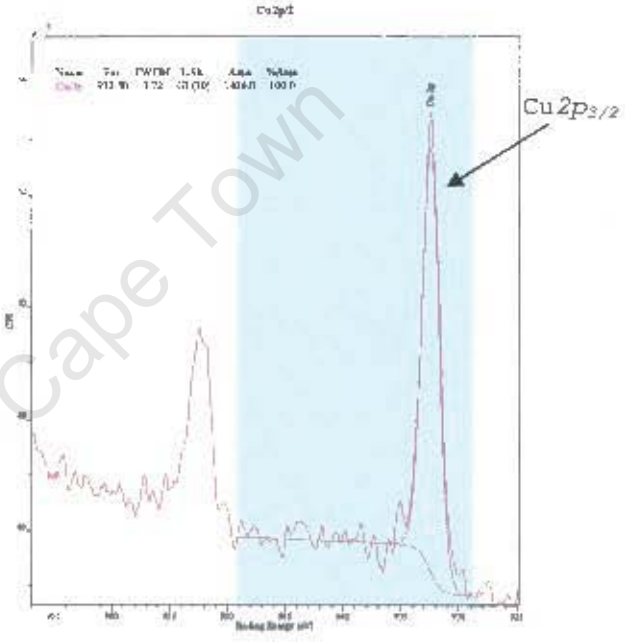

Figure 4.41: XPS analysis of sperrylite NS145 conditioned with copper sulphate followed by xanthate at pH 9.

University of Cape Town

4.3 MICROFLOTATION TESTWORK

Microflotation testwork was performed at pH 9 for all the minerals unless otherwise stated with the aim of linking the trends observed from the surface analysis experiments to floatability. In particular, the effect of xanthate and the subsequent addition of xanthate on copper (II) ion activated mineral surfaces for the PGE minerals were studied. To evaluate the contribution of entrainment and natural floatability, flotation tests were conducted without any reagent addition. In general, entrainment did not contribute significantly to the total recovery of the

minerals studied in the +38 -38µm fraction. These tests were labeled as the standard reagent regime.

4.3.1 Reproducibility

The objective of the reproducibility tests was to evaluate the reliability of the procedure and apparatus used for the microflotation testwork. Any possible error includes the variability of the mineral samples and the operator's ability to be consistent.

In order to determine the reproducibility and standard deviation, the microflotation tests were carried out on a sperrylite sample NS145 in the presence of sodium isobutyl xanthate in synthetic water. Concentrates were collected at 2, 4, 6, 8 and 20 minute intervals and the results are displayed in Table 4.20. The results are also graphically represented in Figure 4.42. As demonstrated by the recovery-time curves and the low standard deviation for each concentrate collected, the procedure and apparatus used gave very reproducible results.

Table 4.20: Sperrylite recovery for microflotation tests and standard deviations for concentrates collected at 2, 4, 6, 8 and 20 minute intervals in synthetic water, I = 3.5E-02.

Time (mins)	Sperrylite Recovery (%)			Mean	Std Dev	Relative Std Dev (%)
	1	2	3			
2	15.1	16.3	15.7	15.7	0.6	3.82
4	29.1	33.1	31.5	31.2	2.03	6.50
6	41.0	40.6	42.0	41.2	0.72	1.74
8	50.1	48.7	49.0	49.3	0.71	1.45
20	73.5	72.1	71	72.2	1.23	1.71

University of Cape Town

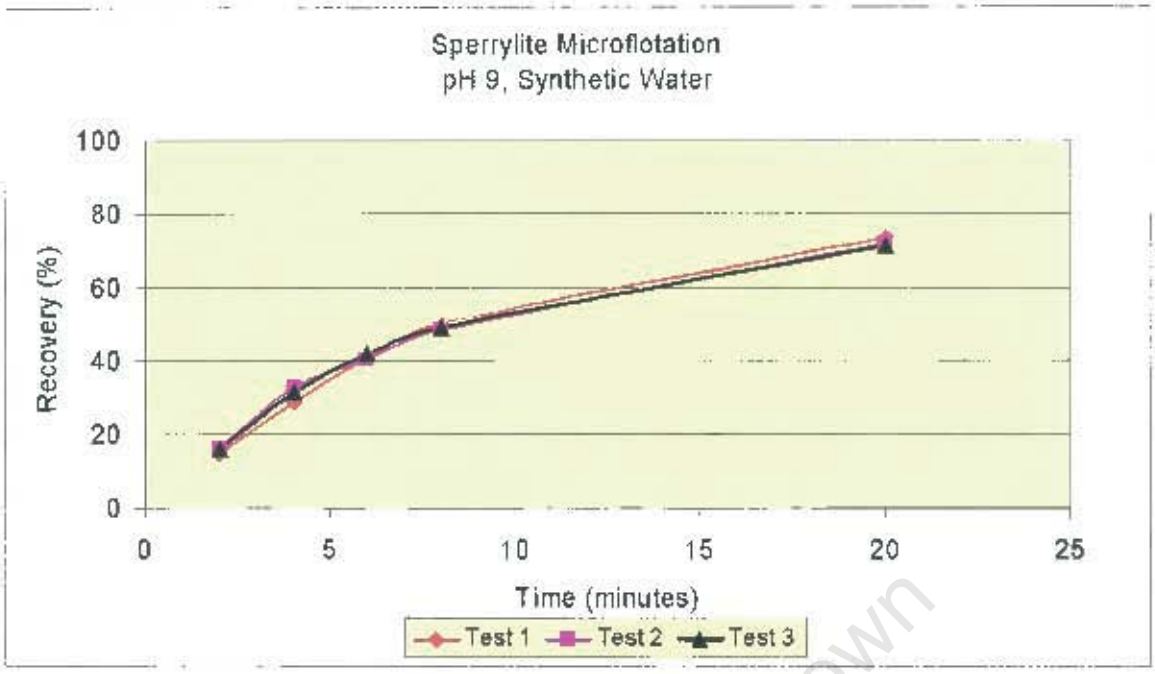

Figure 4.42: Sperrylite reproducibility recovery-time curves for concentrates collected at 2, 4, 6, 8 and 20 minute intervals in synthetic water, I = 3.5E-02.

In Table 4.21, the dosages used for copper sulphate, xanthate and ethylenediamine (EDA) have been converted into grams, moles and psuedo-monolayers for the active ingredients of the reagents for each of the synthetic minerals. The calculation for the copper and xanthate surface coverage can be found in Appendix A.

University of Cape Town

Table 4.21: Reagent concentrations in grams, moles and pseudo-monolayers for all the active ingredients of the chemicals used during the study.

Chemical Reagent	*Gram of Reagent*	*Moles of Reagent*	*Psuedo- monolayer of Reagent*
***Copper Sulphate*, ($CuSO_4$), Mw = 159.6**	0.0008	1.26E-05	**Cooperite NS144 – 20.5** Vysotskite NS148 – **23.2** Sperrylite NS145 – **39.5** Sperrylite NS146 – **26.3** Palladoarsenide NS147 – **6.1** Moncheite NS142 – **7.9** Moncheite NS153 – **7.2** Merenskyite NS143 – **12.1** Merenskyite NS143 – **11.3**
	0.00008	1.26E-06	Moncheite NS142 – **0.79**
***Sodium isobutyl xanthate*, (SIBX), Mw = 172.2**	0.0019	1.28E-05	Cooperite NS144 – **36.9** Vysotskite NS148 – **41.8** Sperrylite NS145 – **71.0** Sperrylite NS146 – **47.4** Palladoarsenide NS147 – **10.9** Moncheite NS142 – **14.2** Moncheite NS153 – **12.9** Merenskyite NS143 – **21.9** Merenskyite NS152 – **20.3**
***Ethylenediamine*, (EDA), Mw = 60.1**	0.00075	1.25E-05	Cooperite NS144 – **20.3*** Vysotskite NS148 – **23.0*** Sperrylite NS145 – **39.1*** Sperrylite NS146 – **26.1*** Palladoarsenide NS147 – **6.0*** Moncheite NS142 – **7.8*** Moncheite NS153 – **7.1*** Merenskyite NS143 – **12.0*** Merenskyite NS152 – **11.2***

* = Atom size of the EDA is based on the copper atom size (20.8 $Å^2$, Gaudin et al. 1959)

The values in Table 4.21 show that copper and xanthate coverage for the sperrylite samples were highest followed by the PGE sulphides, Pd tellurides, Pt tellurides and palladoarsenide. The pseudo-monolayers is an approximation and show that there was sufficient EDA added to the minerals after copper sulphate addition to remove any weakly attached copper species by complexation in solution.

University of Cape Town

4.3.2 Cooperite

4.3.2.1 Standard Reagent Regime

The microflotation data shows a good flotation response of 94% if no reagents are added (Figure 4.43). When xanthate is added, the recovery for cooperite does not improve any further. In the presence of copper sulphate and xanthate, the flotation kinetics is slower and the overall recovery drops to 89%.

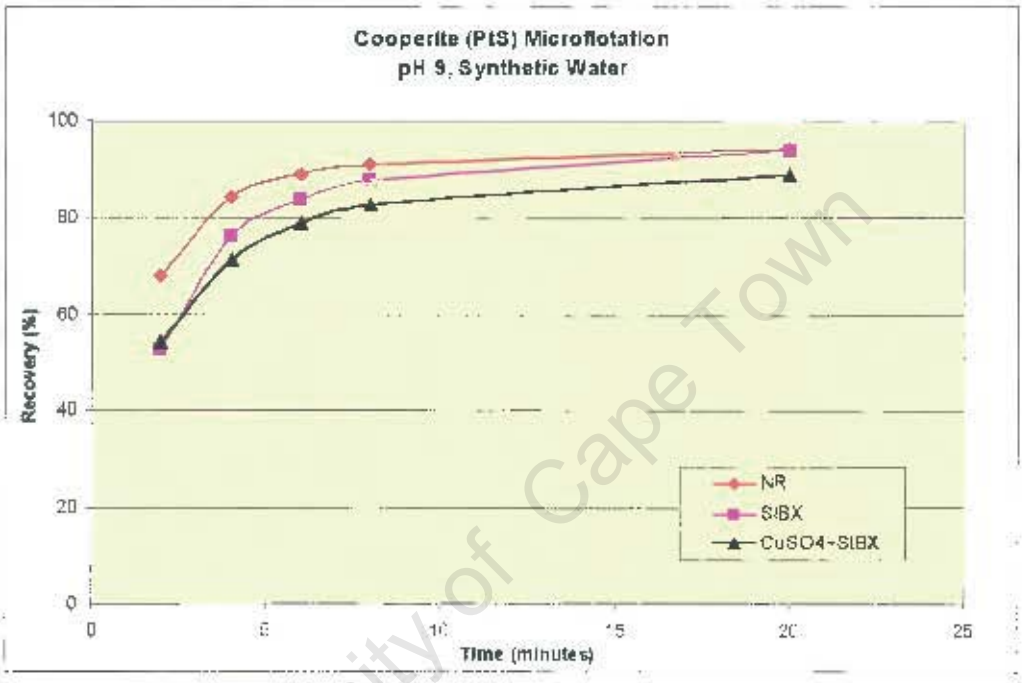

Figure 4.43: Cooperite (NS144) recovery-time curves at pH 9 comparing no reagents, SIBX and $CuSO_4$+SIBX in synthetic water, I = 3.5E-02.

4.3.3 Vysotskite

4.3.3.1 Standard Reagent Regime

Figure 4.44 shows the recovery-time curves for vysotskite (NS148). In the absence of reagents, a moderate flotation recovery of 64% is obtained. In the presence of xanthate, the flotation recovery increased to 95% and with the addition of copper sulphate followed by xanthate the flotation kinetics and recovery increased to 99%.

University of Cape Town

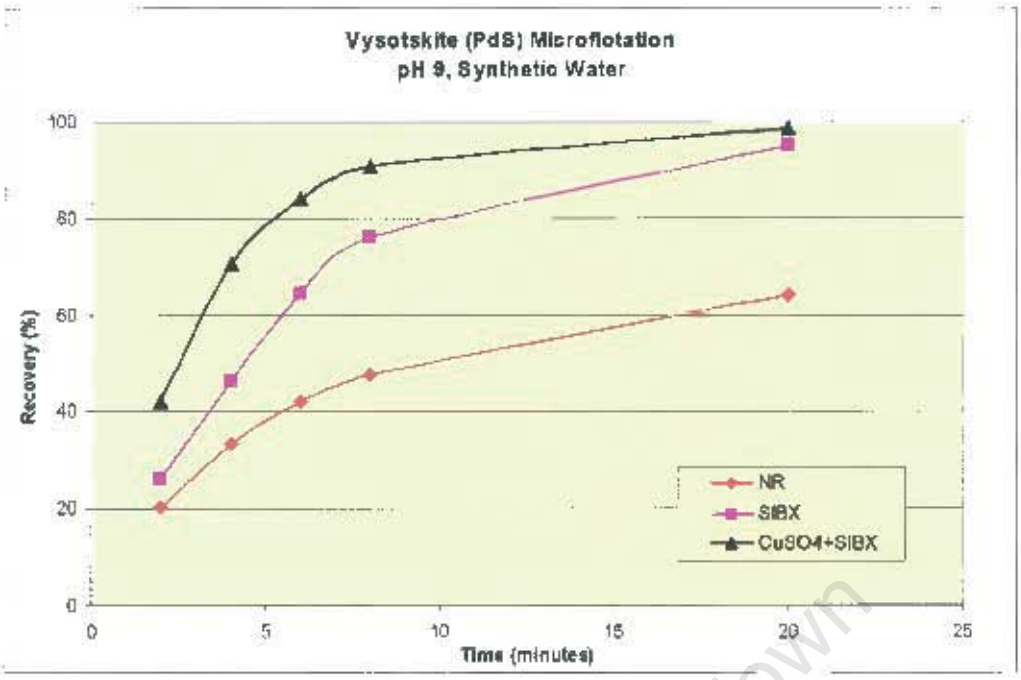

Figure 4.44: Vysotskite (NS148) recovery-time curves at pH 9 comparing no reagents, SIBX and $CuSO_4$+SIBX in synthetic water, I = 3.5E-02.

4.3.4 Sperrylite

4.3.4.1 Standard Reagent Regime

The microflotation data shows that both sperrylite samples have a poor flotation response if no reagents are added: NS145 and NS146 show a recovery of 7.14% and 0.9%, respectively (Figures 4.45 and 4.46). When SIBX, is used as the collector, the recovery for NS145 increases to ~74%, where NS146 gave a recovery of only 1.9%. With the addition of copper sulphate followed by xanthate, the recovery drops off marginally for NS145 (69%) and increases slightly for NS146 (8.5%). These trends are consistent with those observed during the surface analyses, where xanthate adsorption was lower for NS146 compared to NS145, thereby linking the flotation response to the surface chemistry.

University of Cape Town

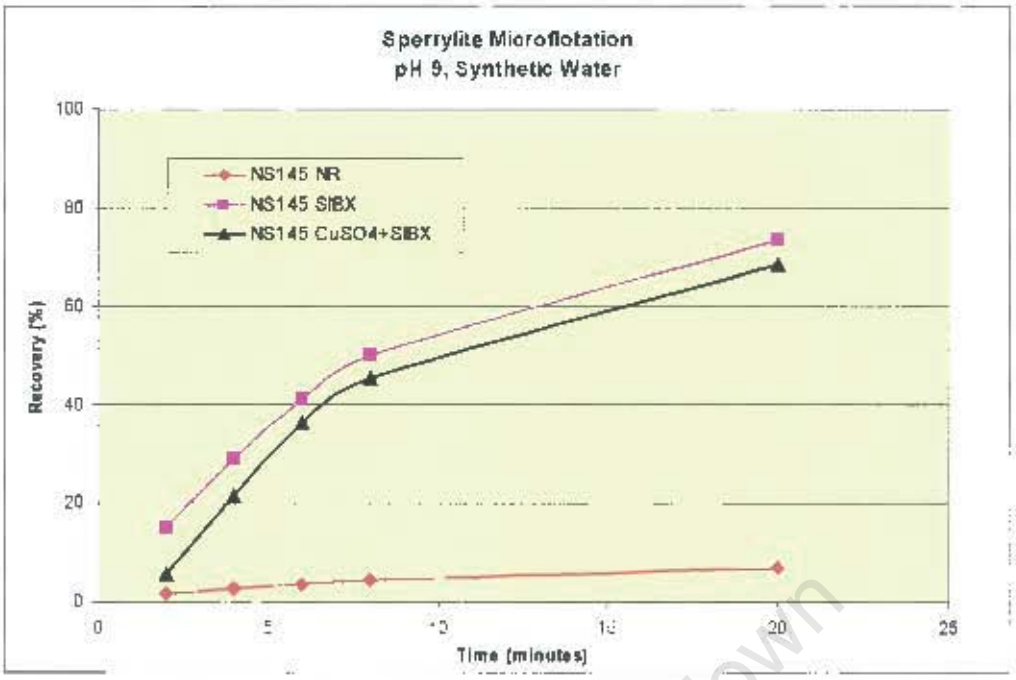

Figure 4.45: Sperrylite (NS145) recovery-time curves at pH 9 comparing no reagents, SIBX and $CuSO_4$+SIBX in synthetic water, I = 3.5E-02.

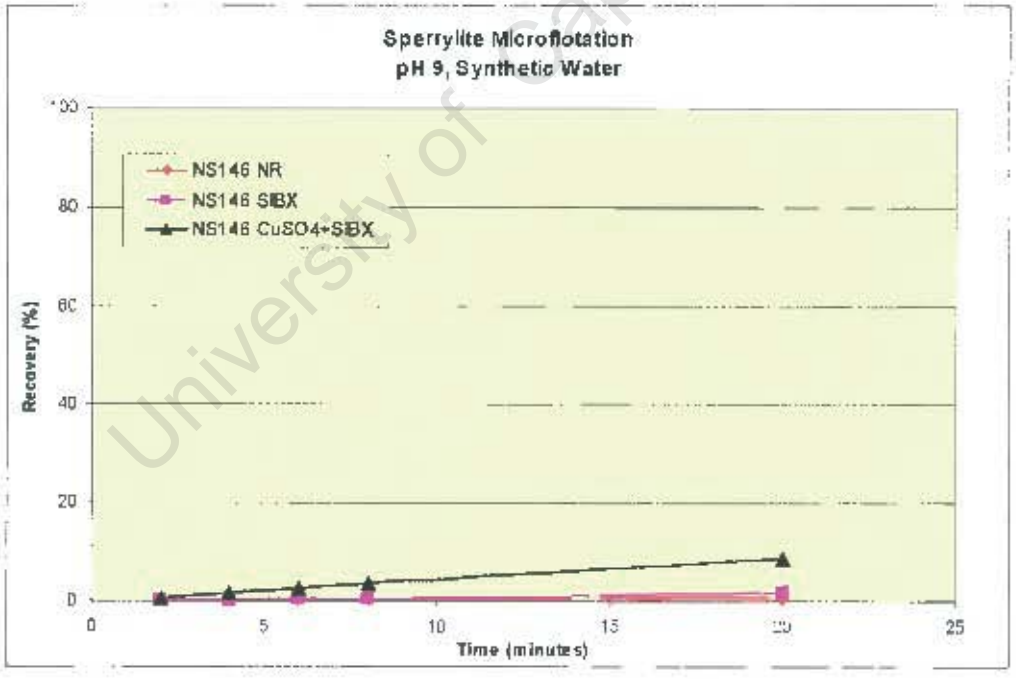

Figure 4.46: Sperrylite (NS146) recovery-time curves at pH 9 comparing no reagents, SIBX and $CuSO_4$+SIBX in synthetic water, I = 3.5E-02.

University of Cape Town

4.3.4.2 Collector Screening

Due to the low recovery obtained for sperrylite NS146 further testwork was conducted in an attempt to improve the flotation response of this mineral. This included collector screening and pH adjustment. Figure 4.47 shows the total recovery when comparing various collectors and combinations of collectors and activator for sperrylite sample NS146. The sample responded slightly better to the addition of Senkol 65 which is a dithocarbonate as the collector compared with SIBX. The dosage for Senkol 65 was 5.00E-5M. The highest recovery (20%) was obtained at double the Senkol 65 and SIBX concentrations. DTC (Dithiocarbamate) was also screened as an alternate collector as it is known to be more specific for PGE minerals but did not improve the flotation response significantly (Nagaraj. et al., 1988).

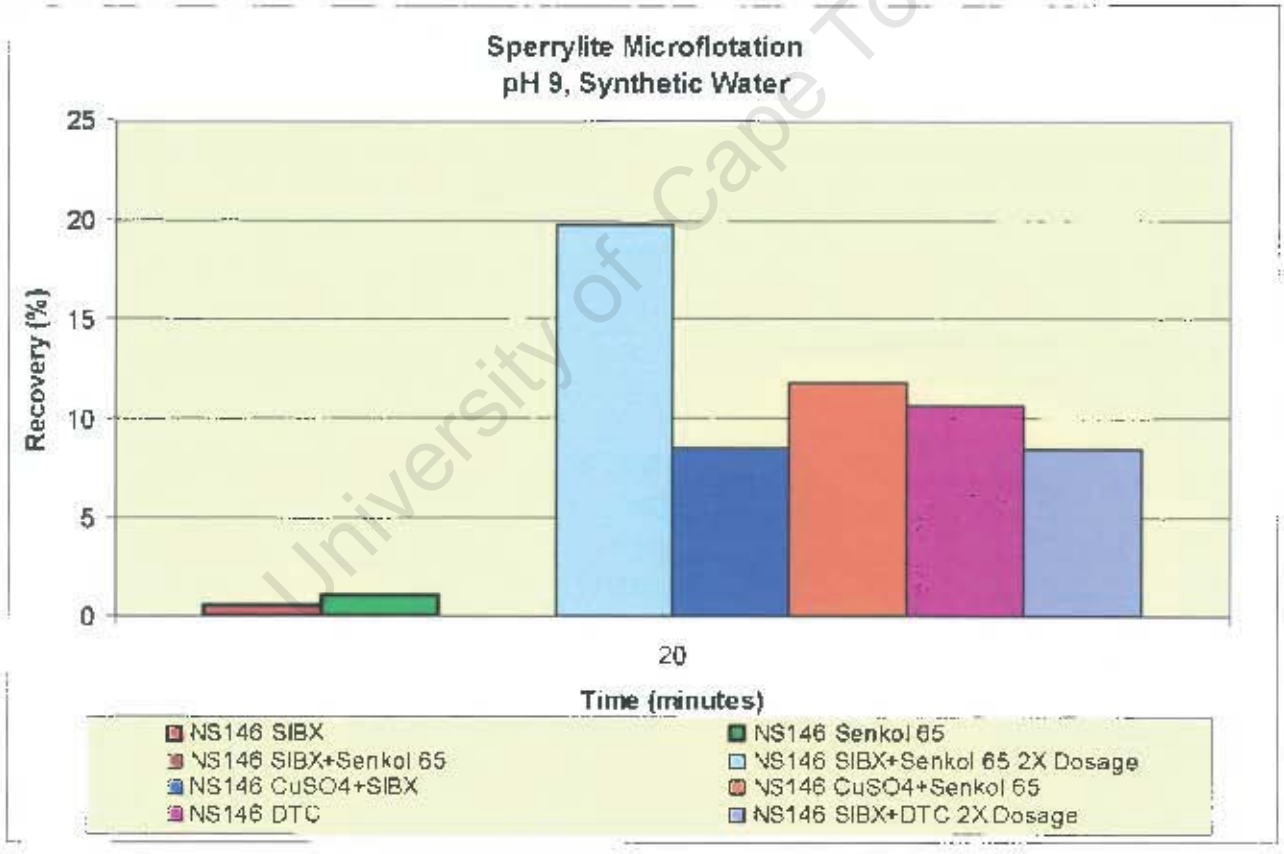

Figure 4.47: Sperrylite (NS146) total recoveries comparing various collectors.

University of Cape Town

In addition, microflotation testwork was carried out at pH 6 with $CuSO_4$+SIBX additions for NS146 and compared to the corresponding pH 9 trial. The results show that the recovery increased from 8.5% for the pH 9 trial (Figure 4.46) to 15% for the pH 6 trial. This is probably due to a lower concentration of $Cu(OH)_2$ colloids, which are predominant above pH 8. When carrying out the microflotation test at pH 10 with SIBX for NS146, the recovery was reduced to 0.59%, which may be due to the high concentration of hydroxide ions on the mineral surface which does not allow much xanthate adsorption due to competition for sites. This trend was also observed during the zeta potential determinations.

4.3.4.3 Varying Size Fraction Flotation

It is well known that poor recoveries can often be ascribed to either the effect of inadequate liberation of the mineral or to particle size effects and therefore these tests were included in the study. With respect to liberation, self-evidently the samples used in the present study are fully liberated in terms of their separation from gangue which is absent. The microflotation trials that were conducted on both sperrylite samples at a -38µm size fraction is shown in Figure 4.48 and these results were compared to those obtained for the +38 -38µm size fraction. The results show that the recovery for NS145 was reduced by 31% for the -38µm fraction and the recovery for NS146 was increased by 35% for the -38µm fraction when compared to the respective +38 -38µm size fractions.

University of Cape Town

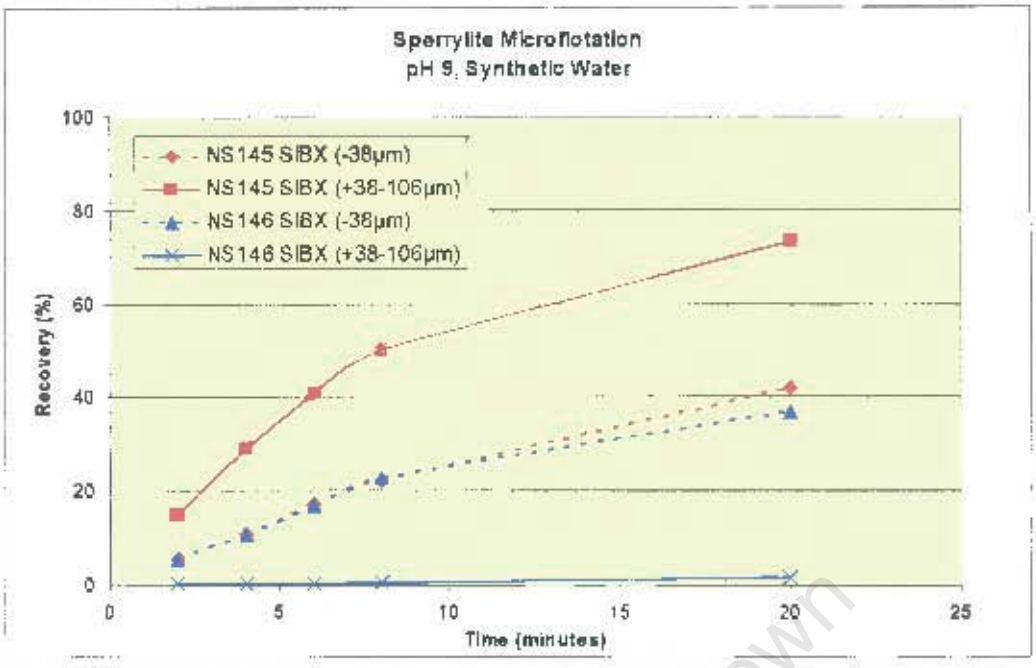

Figure 4.48: Sperrylite (NS146) recovery-time curves at pH 9 comparing differing size fractions with SIBX.

4.3.5 Palladoarsenide

4.3.5.1 Standard Reagent Regime

Figure 4.49 shows the recovery-time curves for palladoarsenide (NS147). NS147 gave a recovery of 27% in the absence of reagents. With the addition of SIBX, NS147 gave a recovery of ~96% and with the addition of copper sulphate followed by xanthate, the recovery dropped off to 67%. The ToF-SIMS data follows similar trends to those seen in the microflotation data where the average xanthate adsorption was higher for the SIBX only case compared to the $CuSO_4$+SIBX case.

University of Cape Town

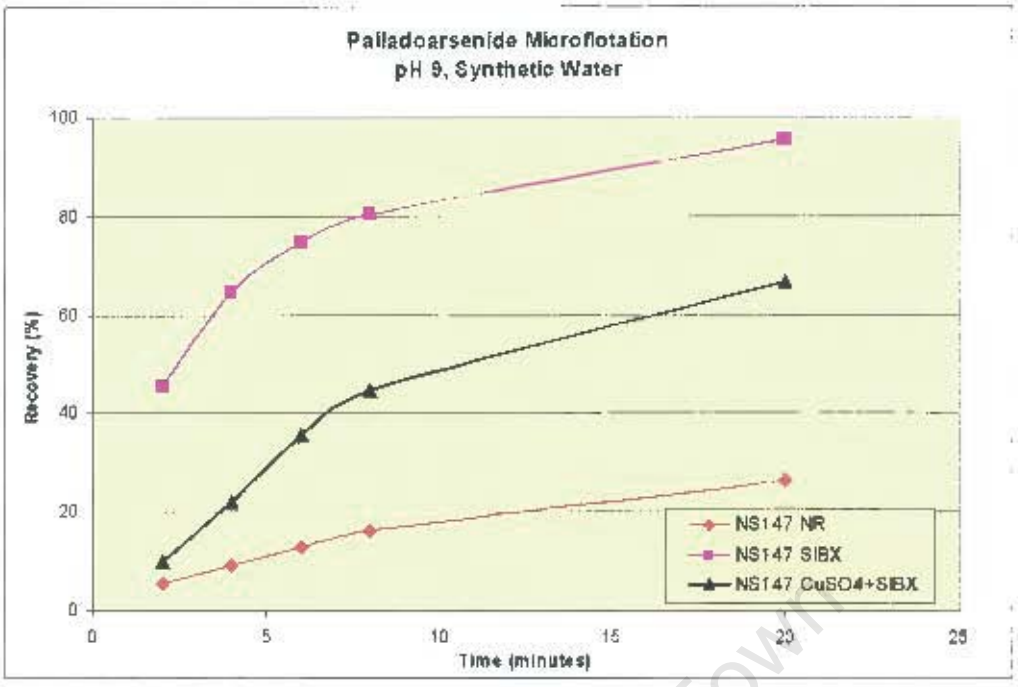

Figure 4.49: Palladoarsenide (NS147) recovery-time curves at pH 9 comparing no reagents, SIBX and $CuSO_4$+SIBX in synthetic water, I = 3.5E-02.

4.3.6 Moncheite

4.3.6.1 Standard Reagent Regime

The microflotation data shows that both moncheite samples have a low to moderate flotation response if no reagents are added. NS142 and NS153 show a recovery of 17.8% and 49%, respectively (Figures 4.50 and 4.51). When SIBX is used as the collector, the recovery for both moncheite samples, NS142 and NS153, increases to >99%. With the addition of copper sulphate followed by xanthate, the recovery drops off compared to the xanthate only trials, i.e.: NS142 and NS153 gave recoveries of 48.5% and 41.3%, respectively. These trends are consistent with those observed during the surface analyses, where xanthate adsorption was lower for both moncheite samples in the presence of $CuSO_4$+SIBX compared to the SIBX only case, thereby linking the flotation response to the surface chemistry.

University of Cape Town

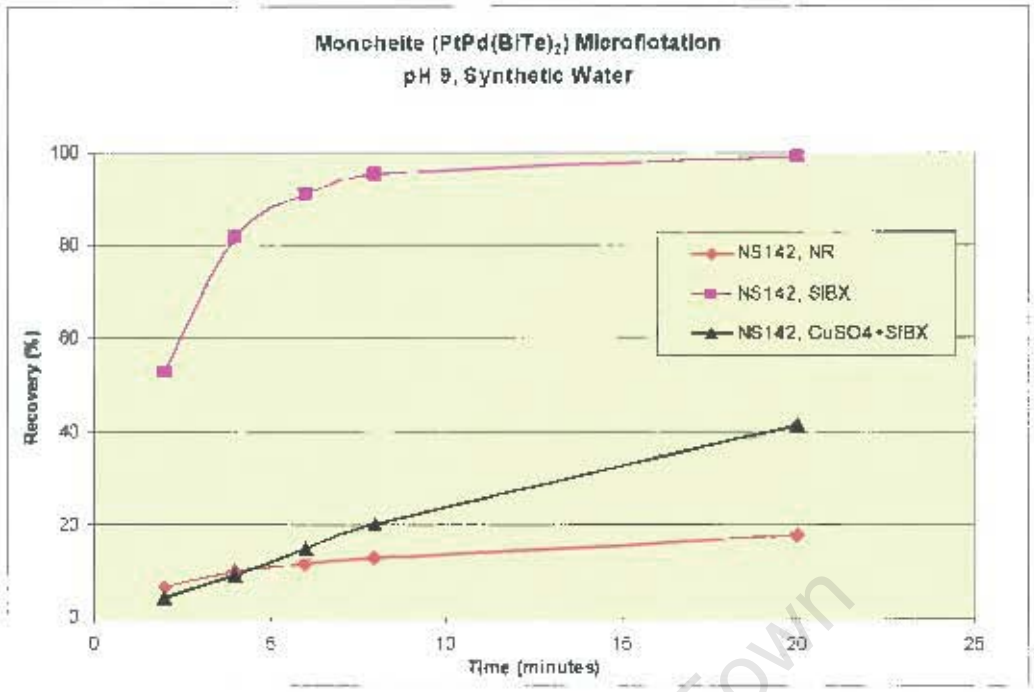

Figure 4.50: Moncheite (NS142) recovery-time curves at pH 9 comparing no reagents, SIBX and $CuSO_4$+SIBX in synthetic water, I = 3.5E-02.

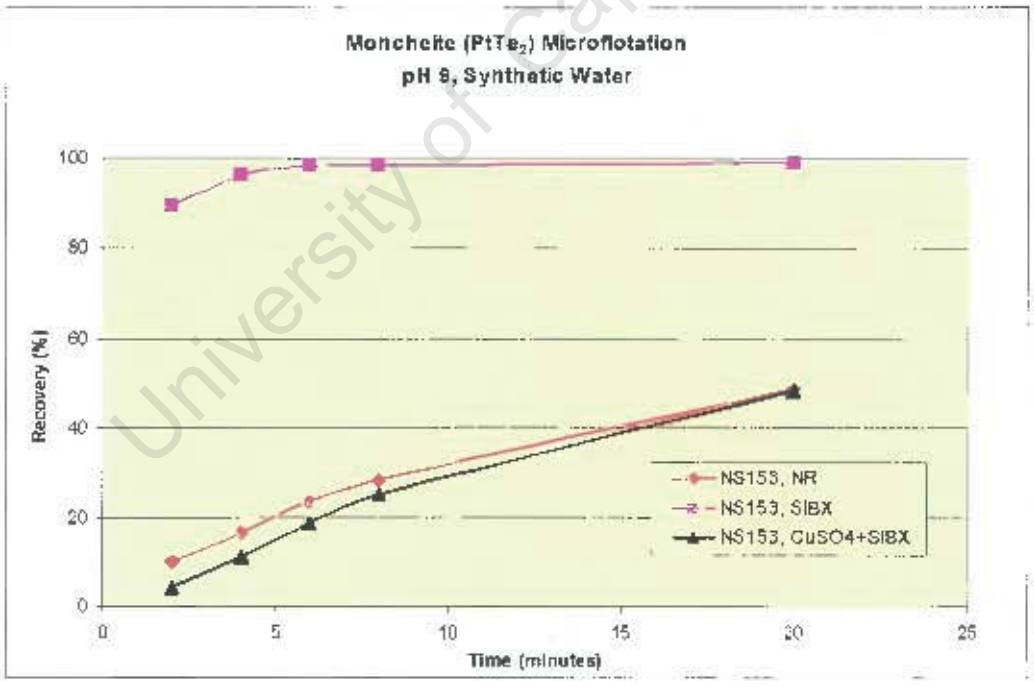

Figure 4.51: Moncheite (NS153) recovery-time curves at pH 9 comparing no reagents, SIBX and $CuSO_4$+SIBX in synthetic water, I = 3.5E-02.

University of Cape Town

4.3.6.2 Effect of Lower Copper Sulphate Concentration

The effect of copper sulphate concentration was evaluated due to the reduction in recovery observed with the addition of copper sulphate (5.00E-05M) compared to the xanthate only trial (Figure 4.52). The results show that the addition of a lower copper sulphate concentration (5.00E-06M) improved the recovery of moncheite (NS153) from around 48% to 93% which shows that the $Cu(OH)_2$ colloids are preventing xanthate adsorption (Figure 4.43). These trends are consistent with those observed during the surface analyses, where xanthate adsorption was higher for the moncheite sample in the presence of a lower $CuSO_4$ concentration of 5.00E-06M compared to the $CuSO_4$ concentration of 5.00E-05M case, thereby linking the flotation response to the surface chemistry.

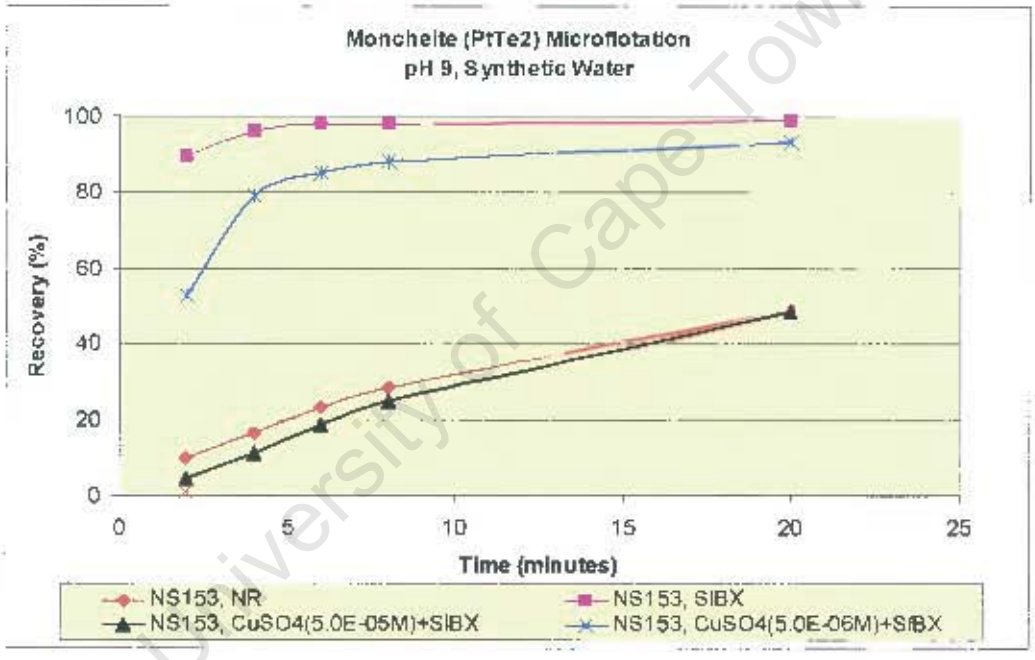

Figure 4.52: Moncheite (NS153) recovery-time curves at pH 9 comparing $CuSO_4$ concentrations in synthetic water, I = 3.5E-02.

Due to the good floatability obtained for both synthetic moncheite samples in the presence of xanthate; testwork was conducted with the aim of evaluating various conditions, which may have a deleterious effect on the flotation response of the synthetic minerals examined. These included; simulated oxidation, oxidation due to grinding environment and size distribution.

University of Cape Town

4.3.6.3 Effect of Oxidation

The effect of oxidation was examined on both moncheite samples and the recovery-time curves are displayed in Figure 4.53. The oxidising conditions involved exposing the minerals to 100°C for 7 days with the purging of air at regular intervals. The results showed that the recovery of the platinum bismuth telluride sample, NS142, was negatively impacted on when exposing the sample to oxidising conditions compared to the platinum telluride sample, NS153, which was unaffected by the oxidising conditions.

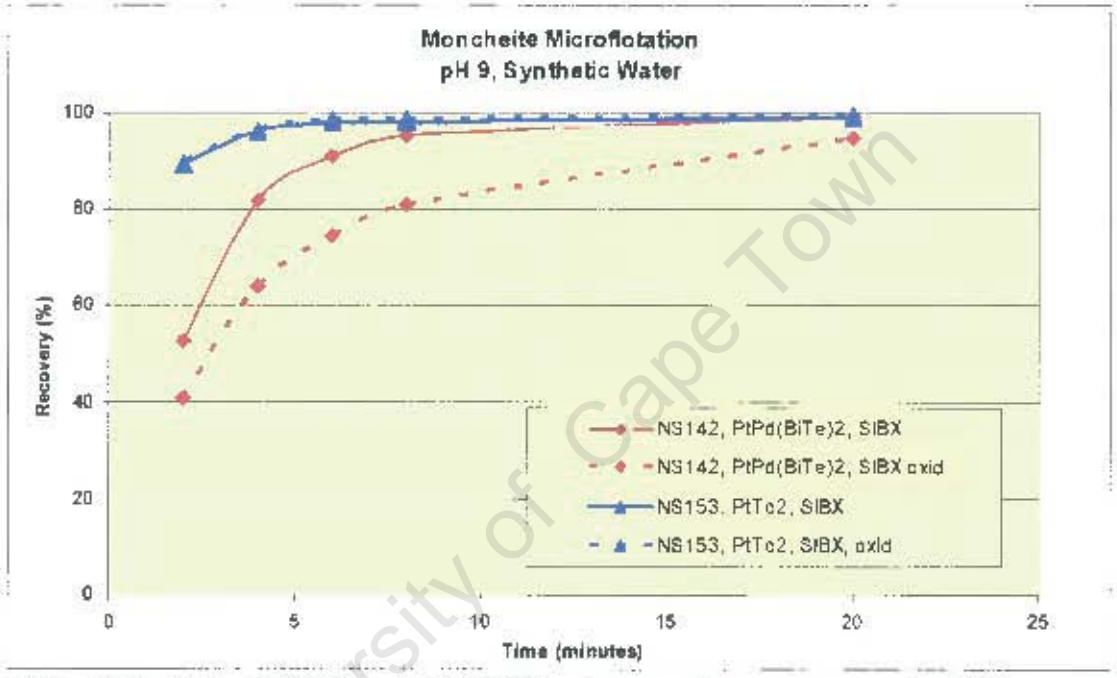

Figure 4.53: Moncheite (NS142 and NS153) recovery-time curves at pH 9 comparing the minerals with and without oxidation in the presence of SIBX in synthetic water, I = 3.5E-02.

University of Cape Town

4.3.6.4 Effect of Varying Size Fractions With and Without Pentlandite Conditioning

Microflotation trials were conducted on both moncheite samples at -10µm, >10µm -38µm size fractions and compared to the +38 -38µm size fraction (Figure 4.54). The data shows that the recovery for both moncheite samples decreases with the decrease in the size fraction size.

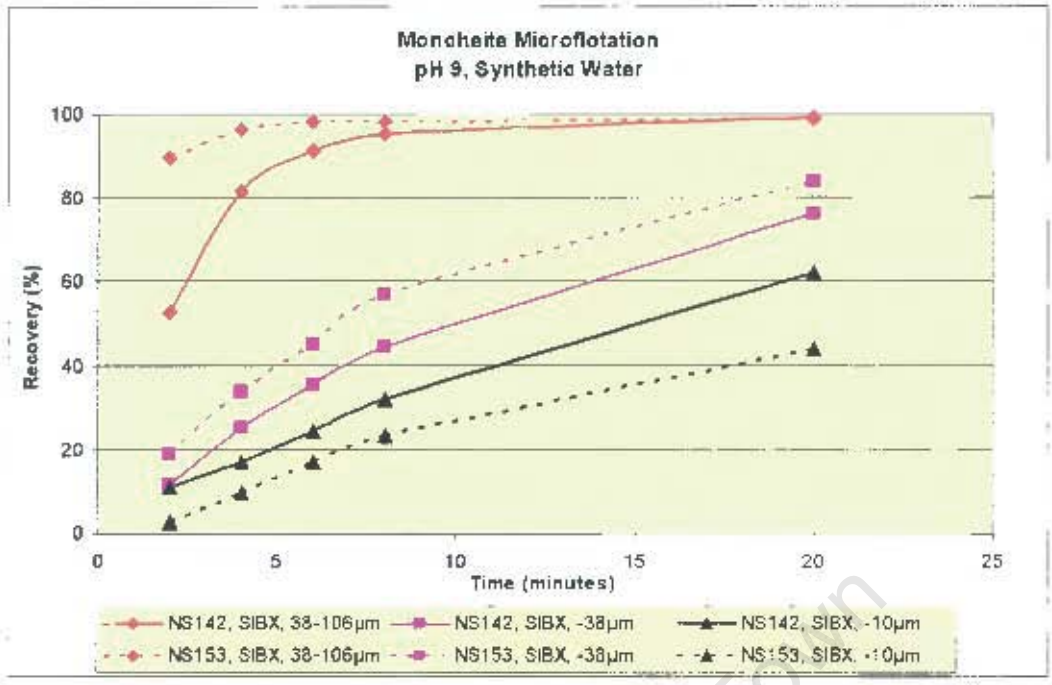

Figure 4.54: Moncheite (NS142 and NS153) recovery-time curves at pH 9 comparing various size fractions of the minerals in the presence of SIBX in synthetic water, I = 3.5E-02.

Further microflotation tests were conducted on the moncheite, NS142, sample with and without conditioning with pentlandite and the results are displayed in Figure 4.55.

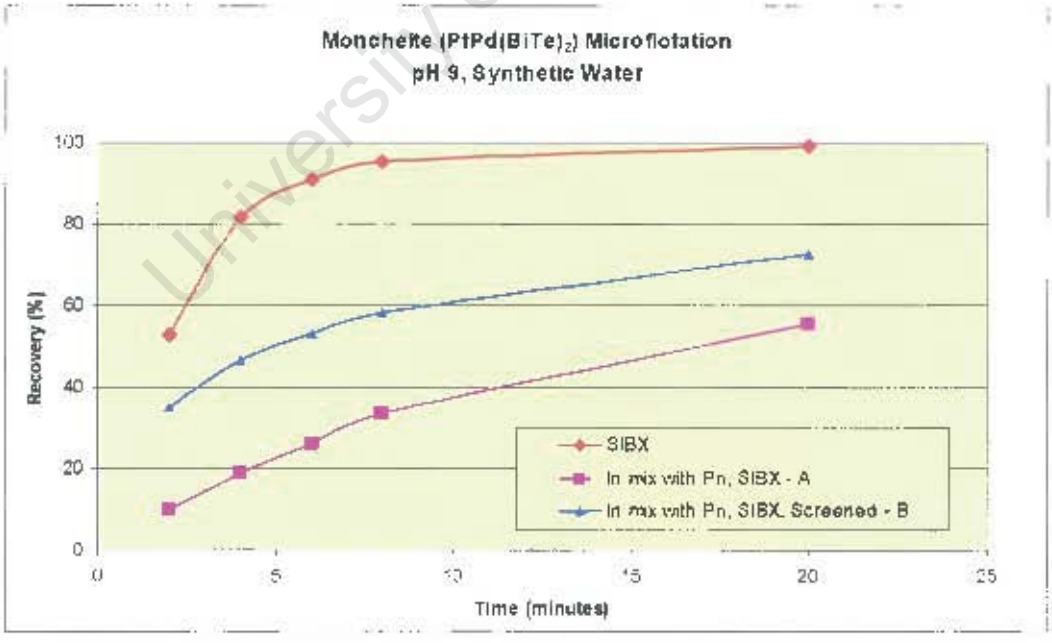

Figure 4.55: Moncheite (NS142) recovery-time curves at pH 9 comparing with and without pentlandite in the mixture in the presence of SIBX in synthetic water, I = 3.5E-02.

University of Cape Town

The results show that when NS142 is conditioned for 10 minutes in the presence of pentlandite and floated together in the presence of xanthate, the recovery of moncheite decreases significantly from >99% to 56% (Trial A). This effect is not as profound when the pentlandite fraction is screened out prior to flotation (Trial B) and the moncheite fraction is floated in the presence of xanthate; the recovery of moncheite decreases from >99% to 73%.

Figure 4.56 shows the comparison of -10µm, +10µm -38µm and +38 -106µm size fractions of moncheite, NS142, with and without conditioning with pentlandite, where the pentlandite fraction was removed by screening prior to flotation. The results show that the recovery of the moncheite is negatively affected when conditioned in the presence of pentlandite for the +10µm -38µm and +38µm -106µm size fractions. The -10µm size fraction showed an improvement in the recovery which may be due to the alteration of the minerals surface charge causing the particles to aggregate.

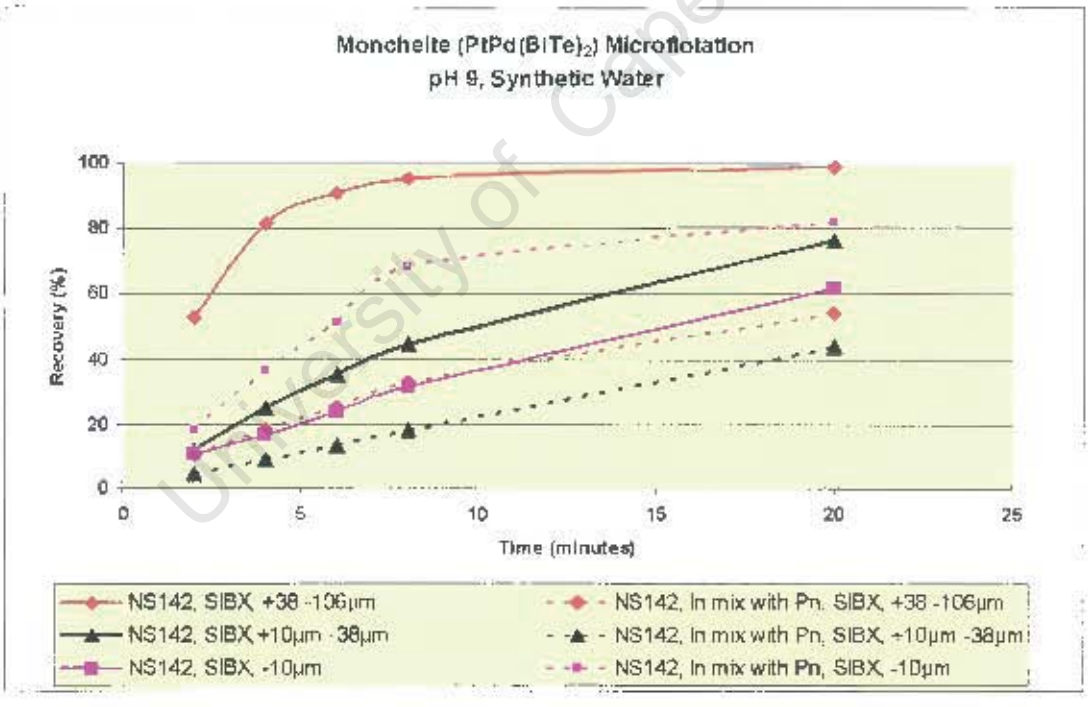

Figure 4.56: Moncheite (NS142) recovery-time curves at pH 9 comparing size with and without pentlandite in the mixture with SIBX in synthetic water, I = 3.5E-02.

University of Cape Town

4.3.7 Merenskyite

4.3.7.1 Standard Reagent Regime

The microflotation data shows that both merenskyite samples have a reasonably good flotation response in the absence of reagents. NS143 and NS152 show a recovery of 75% and 63%, respectively (Figures 4.57 and 4.58). When SIBX is used as the collector, the recovery for both merenskyite samples, NS143 and NS152, increases to >99%. With the addition of copper sulphate followed by xanthate, the flotation kinetics drops off sharply. However, the reduction in the ultimate recovery is not so significant, especially for merenskyite, NS152 compared to the xanthate only trials, i.e.; NS143 and NS152 gave recoveries of 87% and 96%, respectively.

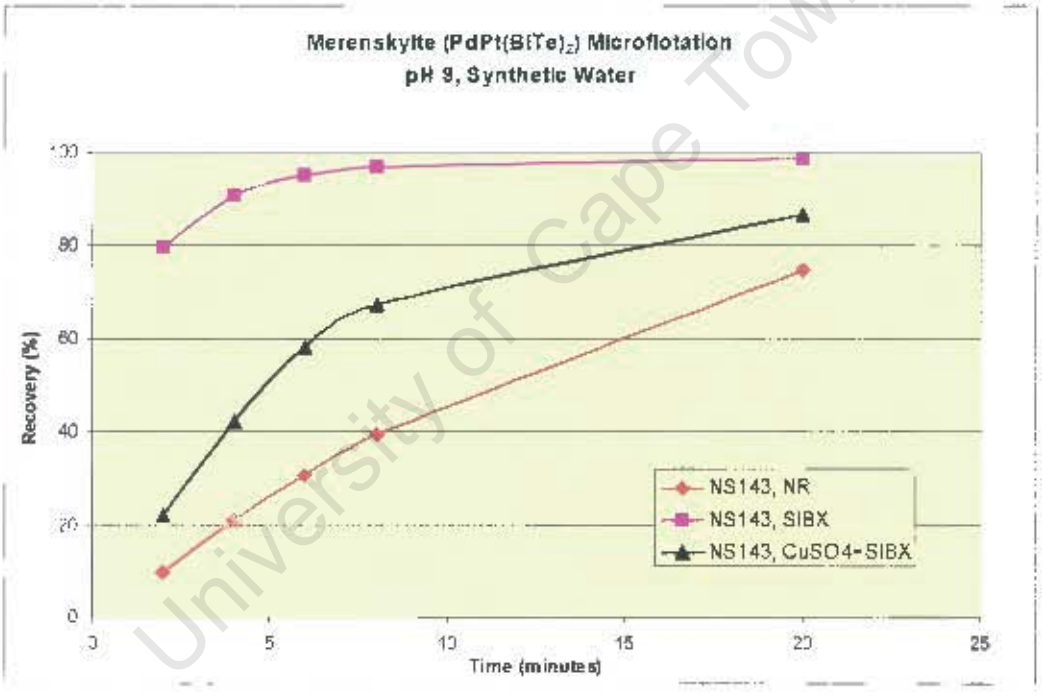

Figure 4.57: Merenskyite (NS143) recovery-time curves at pH 9 comparing no reagents, SIBX and $CuSO_4$+SIBX in synthetic water, I = 3.5E-02.

University of Cape Town

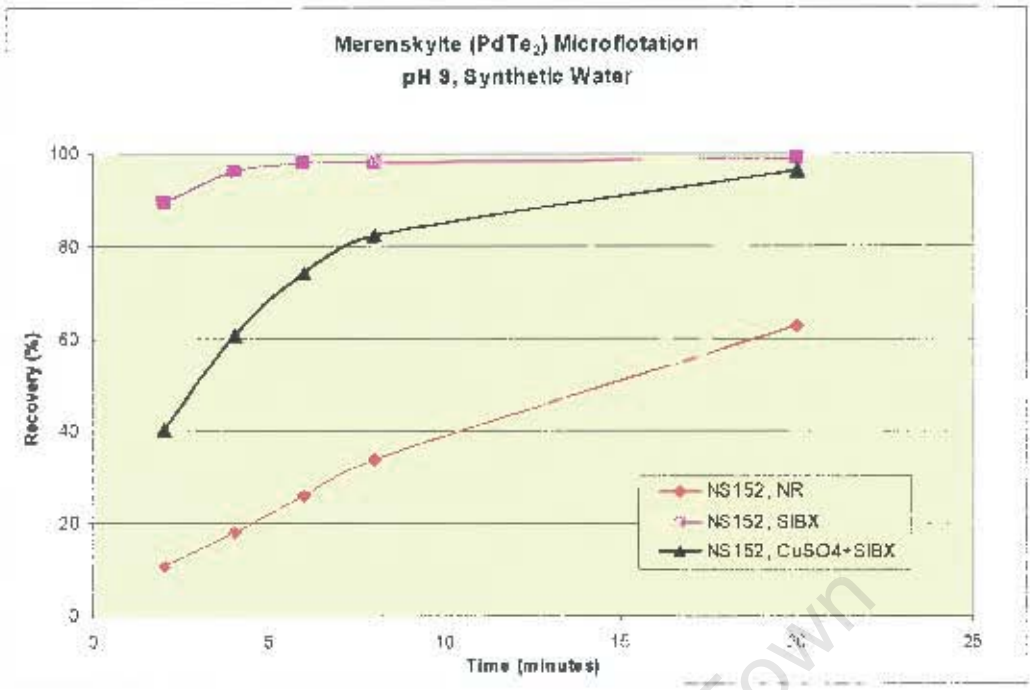

Figure 4.58: Merenskyite (NS152) recovery-time curves at pH 9 comparing no reagents, SIBX and $CuSO_4$+SIBX in synthetic water, I = 3.5E-02.

Once again due to the good floatability obtained for both synthetic merenskyite samples in the presence of xanthate; testwork was conducted with the aim of evaluating various conditions, which may have a deleterious effect on the flotation response of the synthetic minerals examined.

4.3.7.2 Effect of Calcium Ion Concentration

It was proposed that the ion species e.g. Ca ions, present in the pulp affect mineral surfaces which impacts on the floatability of the Pt and Pd mineral species thereby passivating the mineral surfaces. Figure 4.59 shows the data obtained for merenskyite, NS153, when varying the calcium ion concentration in the synthetic water. The results show that increasing the calcium concentration from 80ppm to 500ppm did not negatively affect the flotation response of the merenskyite sample. This is consistent with the ToF-SIMS and XPS data which have also shown that the ions found in synthetic water do not appear to be strongly adsorbed onto the mineral surfaces.

University of Cape Town

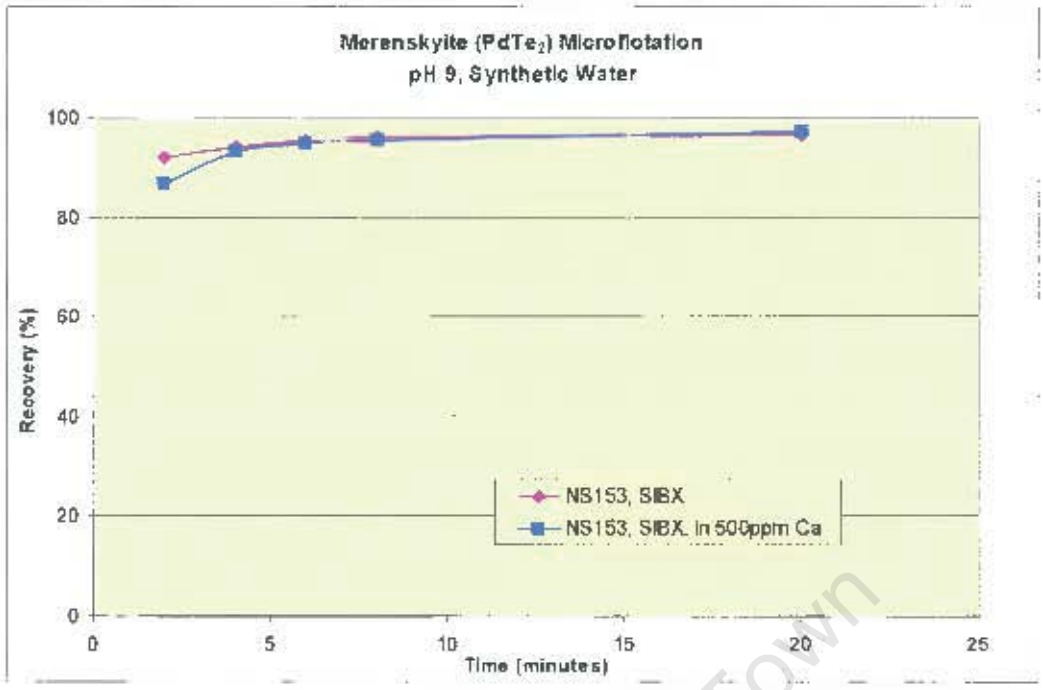

Figure 4.59: Merenskyite (NS153) recovery-time curves at pH 9 comparing a higher calcium concentration in the presence of SIBX.

4.3.7.3 Effect of Bismuth on Moncheite and Merenskyite

This testwork was conducted under the premise that Bi oxidises readily therefore if the pure Pt or Pd telluride samples were ground with Bi powder, a lower flotation response would be expected. The flotation kinetics of the samples with Bi in the structure was lower compared to the pure PGE telluride samples, however the overall recovery was not negatively affected. Figure 4.60 shows the recovery-time curves for moncheite, NS153 and merenskyite, NS152 samples. The results show that when samples of $PtTe_2$ and $PdTe_2$ are ground with bismuth powder the flotation kinetics as well as the overall recovery for both mineral samples is negatively affected, especially for the $PdTe_2$ sample.

University of Cape Town

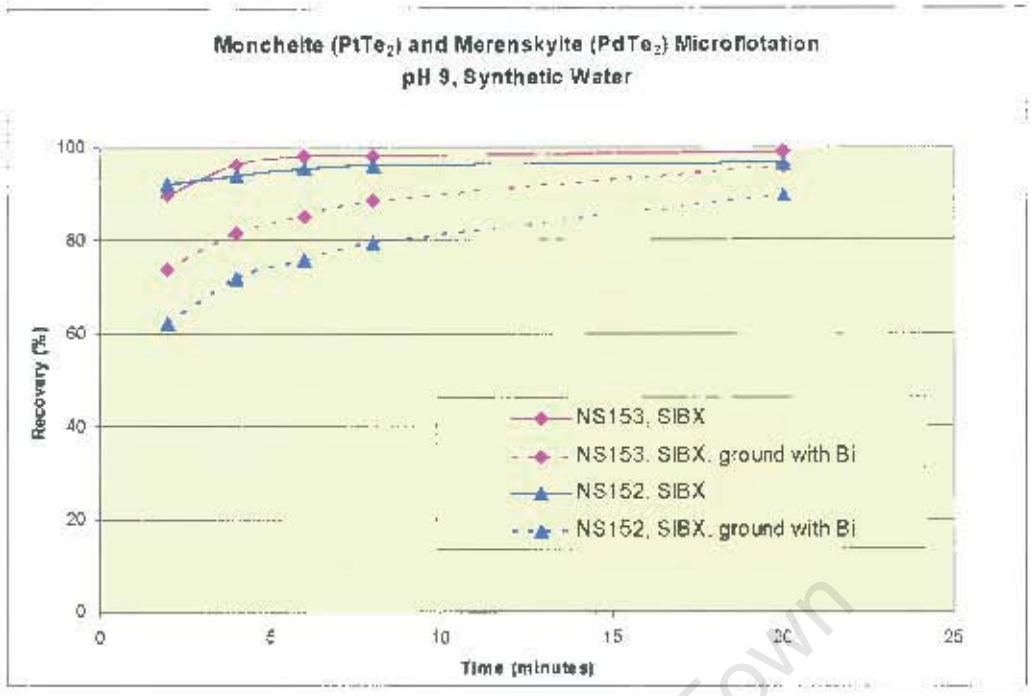

Figure 4.60: Moncheite (NS153) and merenskyite (NS152) recovery-time curves at pH 9 with and without bismuth powder ground with the sample in synthetic water, I = 3.5E-02.

The microflotation data can be summarised as follows for the standard reagent regime:

In the absence of reagents:

- Both sperrylite samples showed a poor flotation response; NS145 and NS146 showed a recovery of 7.14% and 0.9%, respectively.
- The moncheite samples gave a low to moderate flotation response; NS142 and NS153 showed a recovery of 17.8% and 49%, respectively.
- Cooperite showed the best flotation response and obtained a 94% recovery.
- Palladoarsenide (NS147) gave a recovery of 27%.
- Both merenskyite samples showed a reasonably good flotation response, where NS143 and NS152 showed a recovery of 75% and 63%, respectively.
- Vysotskite gave a reasonably good recovery of 64%.

In the presence of xanthate:

- The recovery for sperrylite (NS145) increased to ~74%, where sperrylite (NS146) gave a recovery of only 1.9%.

University of Cape Town

- The recovery for both moncheite samples, NS142 and NS153, increased to >99%.
- No additional recovery was obtained for cooperite in the presence of xanthate and remained at 94%.
- Palladoarsenide (NS147) gave a recovery of ~96%.
- Both merenskyite samples showed a good flotation response with SIBX addition, where NS143 and NS152, increased to >99%.
- The recovery for vysotskite increased to 95%.

In the presence of copper sulphate followed by xanthate addition:

- The recovery for sperrylite drops off marginally for NS145 (69%) and increased slightly for NS146 (8.5%).
- For both moncheite minerals the recovery drops off significantly compared to the xanthate only trials, i.e.; NS142 and NS153 gave recoveries of 48.5% and 41.3%, respectively.
- A slight drop in recovery (88%) was observed for cooperite.
- The recovery for palladoarsenide (NS147) dropped off to 67%.
- For merenskyite, the flotation kinetics dropped off sharply. However, the reduction in the ultimate recovery is not so significant, especially for merenskyite, NS152 compared to the xanthate only trials, i.e.; NS143 and NS152 gave recoveries of 87% and 96%, respectively.
- Vysotskite's recovery improved to 99%.

The effect of oxidation, size and/or pentlandite conditioning, copper sulphate and calcium ion concentration is summarised as follows:

- Oxidation of the minerals negatively affected the flotation performance of the Pt and Pd bismuth telluride samples but not the Pt and Pd telluride samples.
- The data showed that the recovery for both moncheite samples decreased with the decrease in the size fraction size.
- Conditioning of the minerals in the presence of pentlandite reduced the recovery of moncheite by around 47%.

University of Cape Town

- Lowering the copper sulphate concentration by an order of magnitude, from 5.00E-5M to 5.00E-6M, improved the recovery of moncheite (NS153) from 48% to 93%.
- Increasing the calcium ion concentration in the synthetic water did not negatively affect the flotation response of the $PdTe_2$ (NS152) mineral.

University of Cape Town

CHAPTER 5

DISCUSSION

This research proposes that the floatability of the Pt and Pd arsenide, telluride and sulphide mineral species may be influenced by one or more of the following effects;

- Differing crystal structure and/or composition or surface structure and/or composition of the various Pt and Pd mineral species resulting in their being not hydrophobic or amenable to collector adsorption.
- The Pt and Pd mineral species readily oxidises and the oxidation products negatively affect their floatability.
- Oxidation products from other minerals and grinding media also affect the mineral surface composition and floatability by precipitation onto the mineral surfaces.
- The Pt and Pd mineral species may not be amenable to copper activation because they have differing crystal structures compared, for example, to sulphides like pentlandite as there is no sulphur atoms available in which copper may bond.
- Passivation of the mineral surfaces by Bi and Te oxide and hydroxide species may occur which would reduce the floatability of the Pt and Pd mineral species.
- Ion species in the pulp may affect mineral surfaces which impacts on the floatability of the Pt and Pd mineral species, e.g. Ca and Mg ions passivating the mineral surfaces.

The key questions that were addressed in this study were whether the Pt and Pd arsenide and telluride minerals either do not float or float slowly and, if so, what are the reasons contributing to this phenomenon and to interrogate the extent to which these results are similar to those obtained for the PGE sulphide minerals and link these flotation responses to the surface characteristics of the minerals.

The comparison between the Pt and Pd mineral species has highlighted significant differences between the minerals in question.

University of Cape Town

5.1 MINERALOGICAL CHARACTERISATION

EDS was used to characterise and check the homogeneity of the synthetic samples that were produced. XRD analyses were performed to determine the mineral phases present as well as to determine the crystal structure of the synthesised minerals and to compare the data obtained for the synthetic samples to those found in nature.

The XRD data has shown that for all the synthetic PGE mineral samples the phases that were expected to be present in the sample could positively be identified. None of the samples, however, were pure.

For the PGE sulphide minerals the XRD data has shown that sample NS144 was mostly pure cooperite, but an impurity was present which could not be identified and therefore quantification of this sample could not be achieved (Table 4.6). The EDS data, however, has shown a homogeneous product with the correct ratio of Pt:S viz. 86:14 (Table 4.1). The XRD data showed that NS148 was composed of 97% vysotskite and was one of the purest minerals synthesised in this study. The EDS data indicated that three phases were present; viz. two were minor phases with low sulphur content and the third contained the major phase with very similar Pd:S ratios (78:22) compared to the expected composition of Pd:S (77:23) (Table 4.1).

The XRD analyses for sperrylite confirmed the results obtained by EDS, which showed that there were Pt specks within the sperrylite phase for both samples (Tables 4.2 and 4.7). Sperrylite NS145 contained more of the Pt specks compared to sperrylite NS146 and these specks varied in purity with the Pt specks in NS146 contaminated with a higher percentage of arsenic. The palladoarsenide sample was difficult to quantify due to the poor diffractogram obtained, although, the majority of the mineral was identified as palladoarsenide. The difficulty in quantifying the mineral may be due to it being extremely fine grained which may also be attributed to the fact that the sample is extremely hard and therefore difficult to crush. The EDS data showed that there were two phases present; viz. the one phase was minor with a higher content of arsenic and the second contained the major phase with similar Pd:As ratios (74:26) compared to the expected composition of Pd:As (70:30) (Table 4.3).

University of Cape Town

The XRD analyses of the moncheite and merenskyite samples showed that samples NS142, NS153, NS143 and NS152 contained around 87% moncheite ($PtPd(BiTe)_2$), 76% moncheite (PtTe2), 97% merenskyite ($PdPt(BiTe_2)$) and 67% merenskyite ($PdTe_2$), respectively (Table 4.8). The EDS results for the PGE bismuth tellurides showed a large variation in composition (Tables 4.4 and 4.5). This variation in composition was acceptable as it is prevalent in the naturally occurring minerals (see Section 1.2.3). The EDS results for the PGE tellurides showed a lower concentration of tellurium for moncheite (PtTe2) with ratios of Pt:Te (58:42) and a higher concentration of tellurium for Pd for merenskyite ($PdTe_2$) with ratios of Pd:Te (72: 28) in composition (Tables 4.4 and 4.5).

For all the synthetically prepared minerals except palladoarsenide, there was good agreement between the measured and calculated crystal structures and they corresponded well to the information contained in the ICSD database. However, the data has not shown that the hydrophobicity of the synthesised Pt and Pd mineral species are influenced by the crystal planes and/or morphology of the minerals. Therefore these results do not highlight or explain the varying results obtained between the minerals during the surface analyses and microflotation testwork.

University of Cape Town

5.2 SURFACE CHARACTERISATION AND FLOTATION BEHAVIOUR OF THE PGE MINERALS

The observations made in the surface analysis experiments, viz. zeta potential determinations, ToF-SIMS and XPS measurements and their relationship to the flotation behaviour of the samples has particular interest in this study.

5.2.1 The role of the xanthate collector in the floatability of the PGE minerals

Xanthates are the most commonly used sulphydryl collectors in the flotation of the valuable minerals. They have long been successfully employed in the mineral processing industry to separate sulphides from gangue minerals such as silicates. The selectivity is attributed to the reagent structure, which incorporates a functional group with specific

affinity for one and/or more cations present on the mineral surfaces. As discussed in Section 1.5, these collectors adsorb on sulphides through a mixed potential mechanism which involves the anodic oxidation of the collector and cathodic reduction of surface oxygen. The anodic oxidation of xanthate either involves xanthate chemisorption, metal xanthate formation or catalytic oxidation to dixanthogen all of which are dependent on the minerals involved (Yoon and Basilio, 1993).

Due to the lack of reliable equilibrium constant values in the literature for sodium isobutyl xanthate species, ethyl xanthate was used to demonstrate possible xanthate speciation. It was assumed that the ethyl and isobutyl species would behave similarly due to their related molecular structure. However, due to the higher insolubility of sodium isobutyl xanthate compared with ethyl xanthate, the formation of the dimer may occur at a lower E_h (*i.e.* under less oxidising conditions) than for ethyl xanthate. A calculation of the speciation of ethyl xanthate at pH 9 was performed for a range of E_h conditions and is shown in Figure 5.1 (Malysiak, 2003). E_h is referenced to the standard hydrogen electrode (SHE).

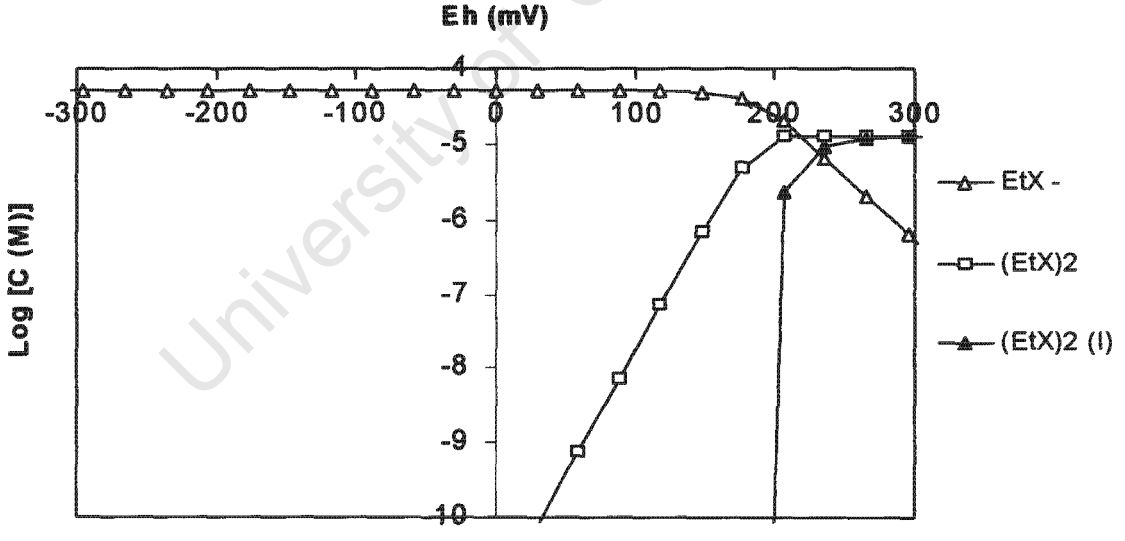

Figure 5.1: Speciation diagram for ethyl xanthate (EtX) at pH 9.

For the PGE mineral species the E_h values measured during the study were above 200mV, which would therefore favour the formation of dixanthogen (Vermaak et al., 2004).

University of Cape Town

To confirm the speciation of xanthate, testwork was performed on the Pt mineral species where these minerals were conditioned for 5 minutes in the presence of xanthate (SIBX) at a concentration of 5.00E-04M. The samples were analysed using PHI TRIFT IV^{NT} ToF-SIMS fitted with an Au source which has three Au clusters (Au_1, Au_2 and Au_3). A 30kVAu_3-400µm bunched beam was used for the dixanthogen trials. The Au_3 cluster was used for these analyses as it is more sensitive for organic molecules due to the low dose of primary ions used to bombard the surface of the sample. The cold stage facility (cooling of introduction and analytical chamber) on the instrument was also used so that the samples could be kept frozen during analysis as dixanthogen is volatile under high vacuum. The results in Figure 5.2 have shown conclusively the presence of dixanthogen on all the Pt mineral species except for sperrylite NS146, which correlates well with the surface analyses and microflotation data presented in the thesis. This is a most important observation in the context of this investigation.

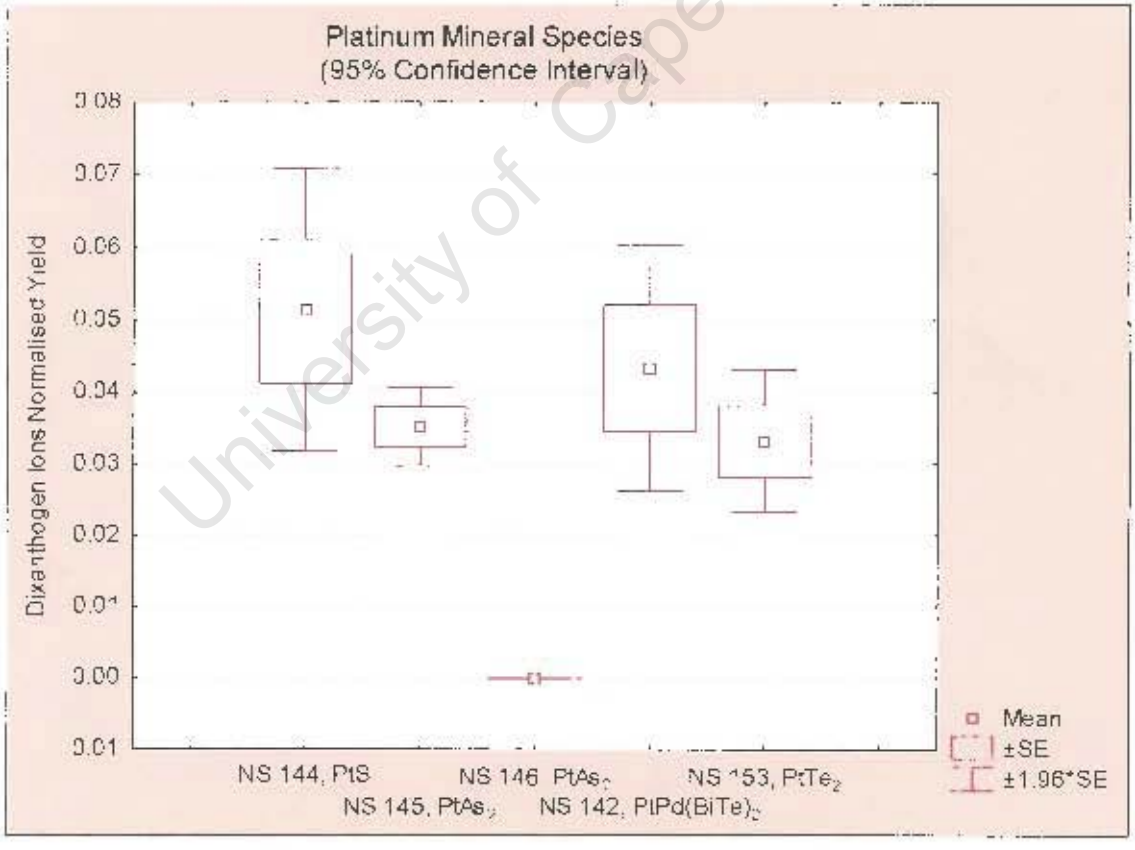

Figure 5.2: Dixanthogen ions normalised yield for the Pt mineral species at pH 9.

University of Cape Town

The ToF-SIMS and XPS data showed xanthate adsorption for both PGE sulphide mineral species (Figures 4.21 and 4.23). The adsorption of xanthate and dixanthogen onto the base metal sulphide minerals has been studied extensively compared to such sparse information for the PGE minerals. For example, Hodgson and Agar (1989) investigated the adsorption of xanthate at pH 9 onto the pyrrhotite and pentlandite surfaces. They concluded that the product forming on the minerals was $Fe(OH)_2X$. Unlike chemisorption, no electron transfer was considered to arise through the adsorption of xanthate on the surface. The collector was adsorbed through coulombic attraction with cationic iron (III) site generated through oxidation of the mineral surface as illustrated in the following reactions:

$$FeS + 2H_2O \rightarrow Fe(OH)[S]^+ + 2H^+ + 2e \quad (21)$$

$$Fe(OH)[S]^+ + X^- \rightarrow Fe(OH)[S]X \quad (22)$$

Xanthate then oxidised to dixanthogen through the reduction of oxygen at the pyrrhotite surface

$$2X^- \rightarrow X_2 + 2e \quad (23)$$

$$O_2 + 2H_2O + 4e \rightarrow 4OH^- \quad (24)$$

Dixanthogen formation was considered to take place adjacent to the oxidised pyrrhotite surface and be physisorbed via the alkyl groups of the Fe(OH)[S]X complex. Dixanthogen was the species that conferred hydrophobicity on the surface of pyrrhotite and oxygen was required to promote the bubble contact. In the case of pentlandite it was concluded that the collector directly chemisorbed on to the nickel sites (pH 9). The addition of xanthate reduced the degree of oxidation of the pentlandite surfaces. Dixanthogen is formed from chemisorbed xanthate on the pentlandite surface according to the following reactions

$$Ni + X^- \rightarrow NiX + e \quad (25)$$

University of Cape Town

$$NiX + X^- \rightarrow Ni(X)_2 \rightarrow NiX_2 + e \quad (26)$$

The formation of dixanthogen would occur concurrently with the adsorption of xanthate on pentlandite during the oxidation process and enhance hydrophobicity. From the above literature and the ToF-SIMS data presented in this study, it can be reasonably concluded that at the conditions prevailing in this study both xanthate and dixanthogen are present on the surfaces of the minerals studied (except NS146).

The microflotation results showed that the addition of xanthate did not result in any additional recovery for cooperite which remained at 94% when compared to the case where 'no reagents' were added (Figure 4.43). The recovery of vysotskite, however, did improve by an additional 30% to 95% in the presence of xanthate (Figure 4.44). The cooperite results indicated that the best flotation response was obtained without the addition of a collector. In 1987, Hayes et al. reported that sulphide minerals which are amenable to collectorless flotation form metal-deficient sulphides and/or elemental sulphur on the mineral surfaces. For collectorless flotation to take place the minerals should be exposed to some form of mild oxidation so that elemental sulphur, and/or metal deficient lattice, and/or polysulphide are present on the mineral surfaces, which would induce hydrophobicity. However, the identity and stability, under both thermodynamic and kinetic controlled regime and the involvement of the hydrophobic species given in collectorless flotation have been topics of considerable debate and there is still no single acceptable interpretation.

University of Cape Town

The addition of xanthate for the PGE arsenide minerals has been shown to yield high recoveries of one sample of $PtAs_2$, viz. NS145, and of the Pd_2As sample (NS147) and yet did not increase the poor recovery of sperrylite sample NS146 (Figures 4.45, 4.46 and 4.47).

With respect to the platinum samples (NS145 and NS146) the only major difference between the two essentially pure fully liberated mineral samples is the deportment of pure

specks of surface Pt which are abundant in the case of sample NS145 and essentially absent in the case of sample NS146. This characteristic of Pt occurrence correlates well with the flotation behaviour and hence it is not unreasonable to speculate that these Pt specks are playing a role in the flotation behaviour of the samples.

ToF-SIMS clearly showed that xanthate adsorbed to a much greater extent on sample NS145 than NS146 (Figures 4.25 and 5.2). This difference is also reflected in the ToF-SIMS analyses with respect to sulphur (Figure 4.26). In terms of the flotation response, addition of SIBX to sample NS145 resulted in a recovery of 74% whereas in the case of NS146 there is virtually no recovery of the mineral (Figures 4.45 and 4.46). The ToF-SIMS results thus correlate well with the flotation recovery results. It has been shown that xanthate forms a type of covalent bond with gold and it is possible that this is the case with Pt as well (Smart, 2006). In the presence of xanthate, it is known that platinum floats very readily and this would also support the hypothesis that it is the presence of the pure Pt specks which result in NS145 being so much more hydrophobic in the presence of SIBX than NS146. These specks may act as favourable sites for reaction with xanthate and thus promote hydrophobicity.

Thus it is difficult to explain conclusively the different responses of the two samples to xanthate treatment other than to refer to the only major difference between the two samples, viz. the greater abundance of Pt specks in NS145 which are associated with high recoveries. It should also be noted that in the case of NS146 the Pt specks have a tenfold greater concentration of arsenic than in the case of NS145. Thus it can be deduced that the arsenic may in some way inhibit the formation of dixanthogen. Even if dixanthogen is formed on the Pt specks the ratio of hydrophilic surface to hydrophobic surface is too low to induce sufficient hydrophobicity on the mineral surface (Shackleton et al. 2007).

In the case of palladoarsenide the high recovery of the mineral after xanthate treatment correlates well with the ToF-SIMS results with respect to xanthate coverage (Figures 4.27, 4.28 and 4.49). It is, however, not logical to extrapolate the argument in the case of $PtAs_2$

University of Cape Town

to the Pd_2As case since the BSE micrograph for the latter shows that there are no highly pure Pd specks present compared to the Pt specks in the case of sample NS145. It can only be speculated that the solid state properties of Pd_2As are more conducive to the electron transfer reaction involved in the formation of dixanthogen from xanthate ions. This is an interesting solid state physics question which deserves greater investigation in a subsequent study.

For the Pt and Pd telluride samples, the ToF-SIMS experiments have also clearly shown that xanthate was present on the surface of all the telluride samples studied (Figures 4.30 and 4.36). The ToF-SIMS has also shown the presence of dixanthogen on the Pt mineral species (Figure 5.2). Vermaak et al., (2004) has shown the presence of dixanthogen on the Pd-Bi-Te mineral species. The XPS experiments also found that xanthate had adsorbed on the surface of the moncheite and merenskyite samples, as indicated by there being 0.6% S on NS142, 0.7% S on NS143, 3.8% S on NS153 and 1.2% S on NS152, with higher values for the samples in which there is no bismuth present. In terms of the flotation response, the addition of SIBX to the PGE telluride samples resulted in >99% recovery in the microflotation studies (Figures 4.50, 4.51, 4.57 and 4.58). This was relative to the natural floatabilities obtained after 20 minutes microflotation of between 40-50% for moncheite and between 60-75% for merenskyite. In all cases the rates of flotation were high with essentially final recoveries being obtained after 7 minutes.

The zeta potential results for the PGE sulphide and telluride mineral species have shown that when xanthate is added there is hardly an effect on the zeta potential values over the pH range 6-10 (Figures 4.11, 4.12, 4.16 - 4.19) indicating little or no xanthate adsorption on the mineral surfaces. The PGE arsenide minerals on the other hand show a small shift in the zeta potential versus pH curves to more negative values (Figures 4.13 - 4.15) which would indicate either xanthate adsorption onto the mineral surfaces or that the slightly more negative charge observed may be due to electron transfer from xanthate ions to the sperrylite surface during the formation of dixanthogen. However, this trend to a slightly more negative charge occurs in both NS145 and NS146. It can be reasonably deduced from the results presented above that the presence or absence of xanthate species on the

University of Cape Town

surface does not or hardly affects the surface charge of the minerals. This is an important observation when seen in the context of much literature showing the effect of xanthate on the zeta potential of especially base metal sulphides. It is important to point out that most of the studies on base metal sulphide minerals have been carried out in a simple electrolyte and thus the double layer compression will not be affected. For this study the double layer compression occurs since synthetic water with an ionic strength of 3.5E-02M was used throughout the study.

The ToF-SIMS, XPS and microflotation data did not correlate with the zeta potential results with respect to xanthate adsorption and therefore the zeta potential measurements did not prove to be a good indicator of flotation behaviour compared, for example, with what is often observed to be the case with the base metal sulphide minerals. This can be explained by the formation of dixanthogen (Figure 5.2), which is a neutral species and does not alter the minerals surface charge.

It is well known that poor recoveries can often be ascribed to either the effect of inadequate liberation of the mineral or to particle size effects. With respect to liberation, self-evidently the samples used in the present study are fully liberated in terms of their separation from gangue which is obviously absent. The tests in which the samples of sperrylite were further comminuted are, however, revealing. In order to ascertain the cause of the variable flotation response between the two sperrylite samples, i.e. NS145 and NSA146, mineralogical analyses were carried out using the Mineral Liberation Analyser (MLA). The MLA examination of the +38 -38µm size fractions of the first flotation concentrate (2 minutes of flotation in the presence of SIBX) and tailings samples for each sperrylite sample (Figures 5.3, 5.4, 5.5 and 5.6) has shown that there is a difference in the size distribution between the two mineral samples during crushing prior to flotation, i.e. NS145 is more friable than NS146, so the size distribution of the +38 -38µm size fraction is finer for NS145 tailings compared with NS146 tailings (Figures 5.4 and 5.6). As seen in these Figures, and as discussed earlier, there is also a difference in the population of the Pt specks between the sperrylite samples investigated.

University of Cape Town

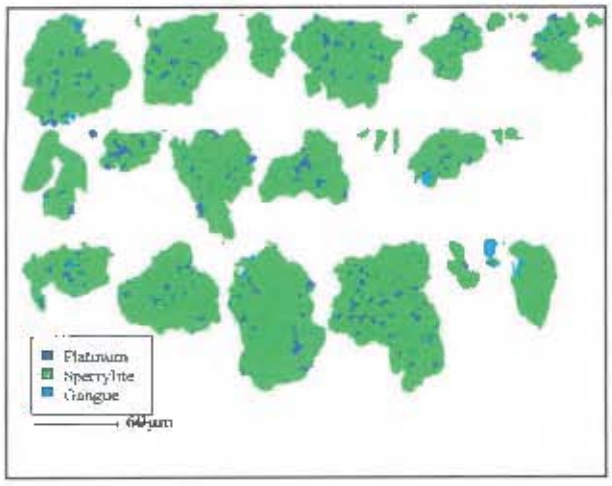

Figure 5.3: Sperrylite NS145 concentrate mineral map

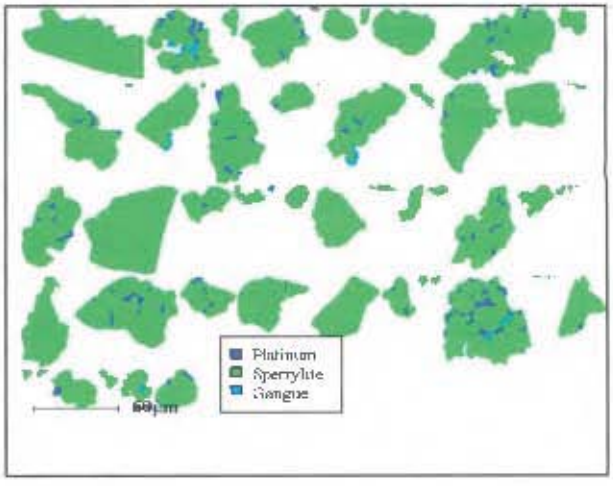

Figure 5.4: Sperrylite NS145 tailings mineral map.

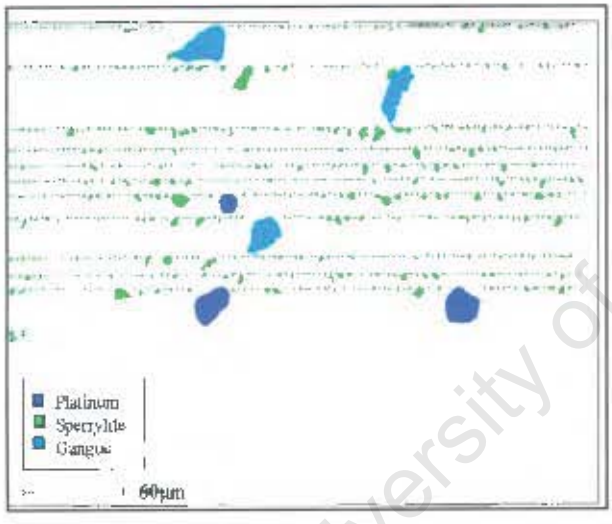

Figure 5.5: Sperrylite NS146 concentrate mineral map.

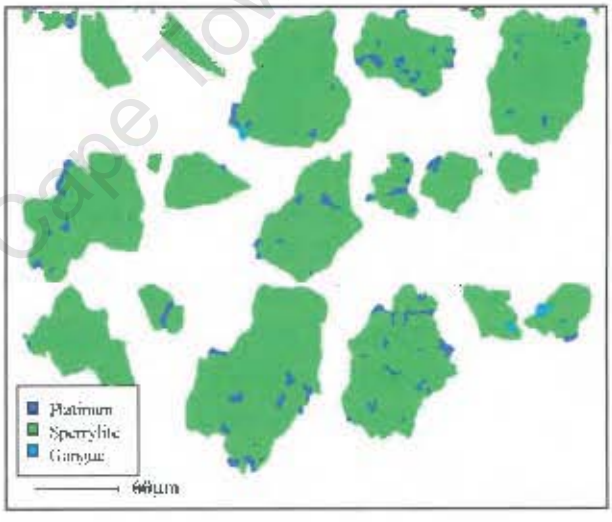

Figure 5.6: Sperrylite NS146 tailings mineral map.

University of Cape Town

The above results have also alluded to possible reasons for the respective decreases and increases in the flotation recovery observed for NS145 and NS146 samples, respectively, for the -38µm size fraction when compared to the +38 -106µm material (Figure 4 39). It is well know that fine particles have a reduced flotation rate and thus the total recovery observed will be lower at a given residence time compared to the relatively coarser size fractions. This phenomenon clearly plays a role when comparing the recovery of the -38µm (42%) to the +38 -106µm size fraction (74%) for sample NS145 On the other

hand, the increase in the recovery observed for NS146, for the -38µm size fraction, may be attributed to a higher degree of liberation of Pt specks in this finer size fraction which led to an increase in the recovery from 1.9% for the coarse size fraction to 37% for -38µm size fraction.

In summary, in terms of the flotation response, the addition of SIBX to all PGE samples resulted in recoveries of between 74% and 99% except for sperrylite NS146. The ToF-SIMS data has clearly shown that the active species for flotation was dixanthogen. In the case of sperrylite NS146 there is virtually no recovery of the mineral which is consistent with the ToF-SIMS and XPS results which shows low xanthate and no dixathogen surface coverage. It is difficult to explain conclusively the different response obtained for sperrylite NS146 compared to all the other PGE samples to xanthate treatment other than to refer to the two major differences; viz. firstly, the greater abundance of Pt specks in NS145 which are associated with high recoveries. It should also be noted that in the case of NS146 the Pt specks have a tenfold greater concentration of arsenic than in the case of NS145, and secondly, that the arsenic in some way may inhibit the formation of dixanthogen or even if dixanthogen is formed on the Pt specks the ratio of hydrophilic surface to hydrophobic surface is too low to induce sufficient hydrophobicity on the mineral surface. This observation clearly indicates the importance of platinum group mineral composition and distribution during the formation of these minerals in geological time. When a large body of mafic magma is emplaced in the earth's crust, slow cooling takes place. Silicate, oxide and sulphide minerals crystallize and sink to the bottom of the magma chamber to form texturally distinctive layers. The magma thus changes composition continuously until solidification is complete. As a result, elements such as the platinum group metals, nickel and copper when in the presence of a sulphide phase, can become sufficiently enriched to form mineralised horizons at predictable levels within the intrusion. A prime example of such a body of igneous rock is the Bushveld Complex of South Africa (Buchanan, 1988). At lower temperatures the platinum group elements become immicible with the base metal sulphides and therefore crystallize as separate platinum group minerals associated with sulphides. Subsequent alteration processes could further impact on the platinum group mineral composition and distribution (Schouwstra, 2007).

University of Cape Town

5.2.2 The role of copper sulphate in the floatability of the PGE minerals in the presence of xanthate

The influence of copper sulphate on the flotation behaviour of the synthesised minerals is of significant interest. As is well known copper sulphate is widely used as an activator of base metal sulphide minerals. Its role in these cases has been extensively reviewed by Finkelstein (1997). In the case of base metal sulphides, the role of copper sulphate is generally interpreted to involve redox reactions between the Cu^{2+} and the sulphide resulting in the formation of Cu^{+} and S(ox) in the presence of xanthate ions, Cu(I)-X complexes are formed (Hodgson and Agar, 1989). It is also widely believed that $CuSO_4$ may affect the behaviour of the froth phase.

To highlight the possible interactions between copper and xanthate ions and the subsequent effect on copper and xanthate speciation, the speciation diagrams for a solution containing 5.00E-05M SIBX and copper ions at pH 9 as a function of E_h are shown in Figure 5.7. E_h is referenced to the standard hydrogen electrode (SHE).

University of Cape Town

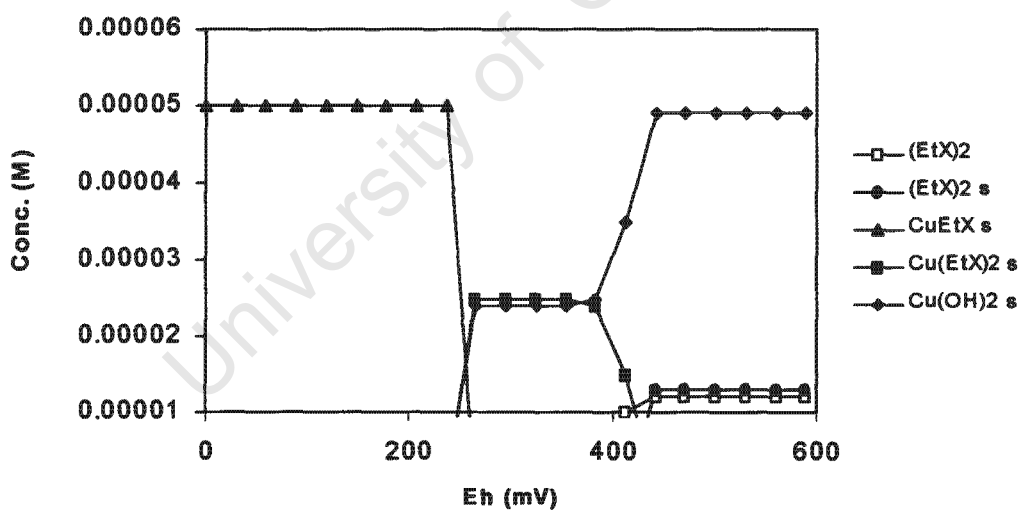

Figure 5.7: Speciation diagrams at pH 9 for 5.0E-05 M ethyl xanthate and copper.

At pH 9, three competing processes are likely to be occurring in terms of adsorption of copper (II) ions from solution. This could occur due to chemical adsorption (oxidation-reduction reaction during which Cu^{2+} ion oxidises the sulphur of PGE sulphides and is

itself reduced to Cu^{1+}), or in the case of PGE sulphide, arsenide and telluride minerals electrostatic attraction (attraction between the mineral surface and copper due to opposite charges) and/or $Cu(OH)_2$ precipitation (non-selective process at alkaline pH). The predominant copper-xanthate species present at pH 9 is likely to be a mixture of $Cu(OH)_2$ and either Cu(I) and/or Cu(II) xanthate species. Since the system is kinetically controlled, copper ions in solution will adsorb readily onto the sulphide ions on the PGE sulphide surfaces before any equilibrium concentration of the copper hydroxy species is reached. Residual xanthate ions in solution will then react with the precipitated $Cu(OH)_2$ colloids, which are likely to be converted to hydrophobic Cu(I)-X colloids according to the following mechanism:

$$2Cu(OH)_2 \rightarrow 2Cu(II)X_2 \rightarrow 2Cu(I)X + X_2 \qquad (26)$$

The copper speciation diagram at pH 9 for a solution containing 5.00E-05M copper (II) ions is shown in Figure 5.8. At oxidising E_h values (*i.e.* above 0 mV) the concentration of copper (II) ions in solution is approximately equal to the concentration of $Cu(OH)_2$ species in solution which is 7.9E-07M. The remainder of the copper (II) ions added, i.e. 4.92E-05M from an initial solution concentration of 5.00E-05M, would then be present as $Cu(OH)_2$ precipitate, assuming no adsorption onto the mineral surfaces, which would drive the equilibrium in the direction of $Cu(OH)_2$. $Cu(OH)_2$ precipitate would first appear at about pH 7 (Figure 5.9). Although the data in Figure 5.9 were determined at an E_h of 300 mV, the onset of $Cu(OH)_2$ is not considered to be strongly dependent on E_h (Gerson, personal communication). At low pH (<6) the positive copper (II) ion species predominate and at high pH (>6), the precipitation of $Cu(OH)_2$ would lead to a marked decrease in zeta potential observed above pH 8, due to the fact that $Cu(OH)_2$ does not carry charge.

University of Cape Town

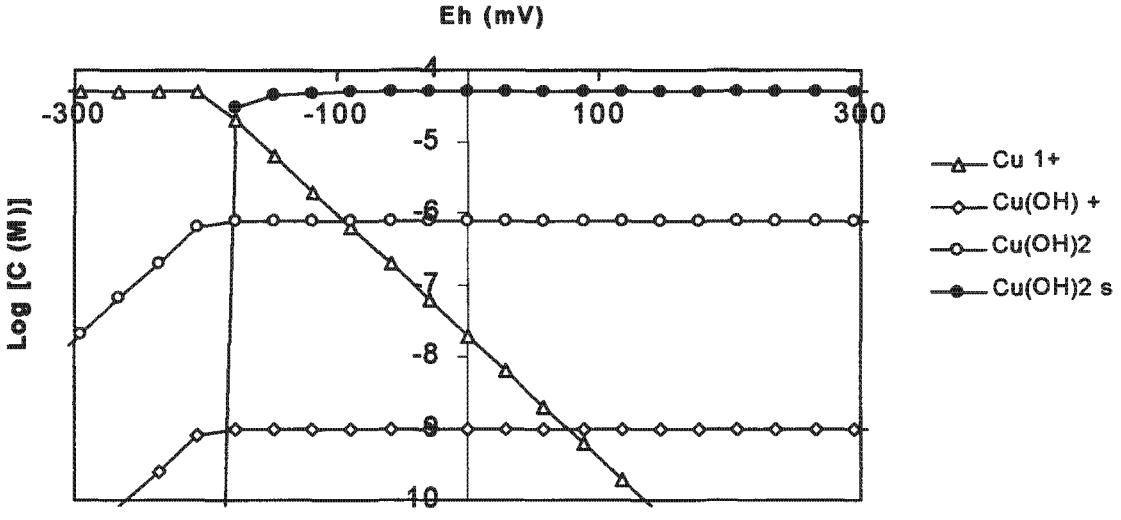

Figure 5.8: Copper speciation diagram for pH 9 over a range of E_h conditions.

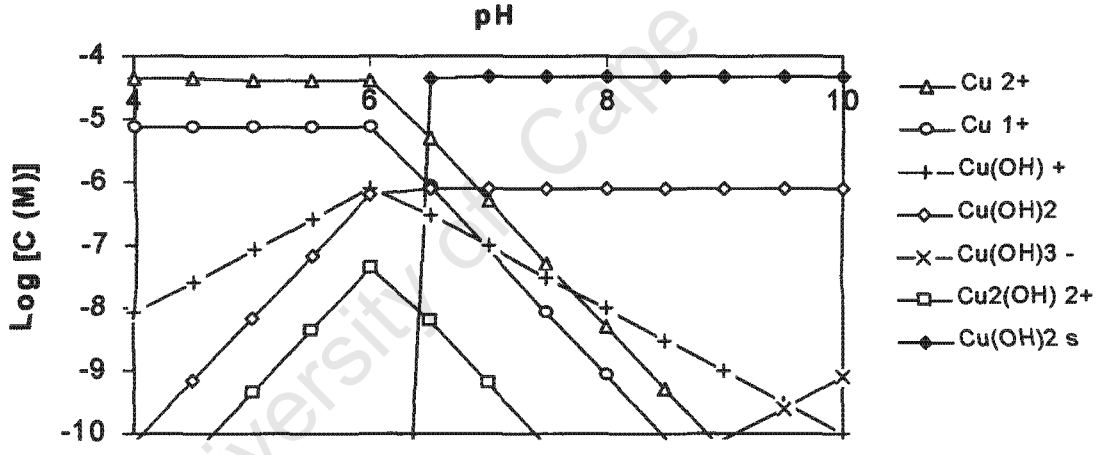

Figure 5.9: Copper speciation for copper concentration of 5.00E-05M as a function of pH at constant E_h of 300 mV.

At alkaline pHs, the interpretation of copper adsorption is largely dependent on an understanding of the speciation behaviour of copper. These show that at pH=9 copper exists predominantly in the hydroxide form as either cuprous or cupric hydroxide.

Copper sulphate has also been shown to be able to inadvertently activate gangue minerals. Numerous investigations have been carried out to investigate this phenomenon

University of Cape Town

(e.g. Malysiak, 2003; Nagaraj and Brinen, 1995). The data obtained during those studies revealed that unlike xanthate adsorption, copper ion adsorption is non-selective, i.e. adsorption onto sulphide as well as siliceous minerals has been observed. The possible mechanisms for copper ion adsorption and inadvertent activation have been considered by many researches and are discussed below.

Fuerstenau (1976) reported that adsorption of copper ions onto the quartz surfaces may be a result of hydrogen bonding between adsorbed hydrogen ion and the copper hydroxy complex (Figure 5.10).

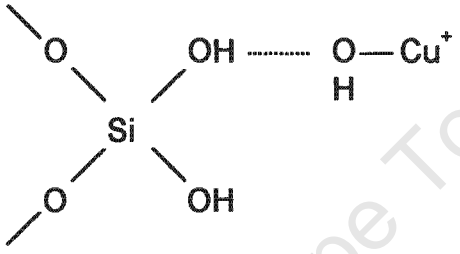

Figure 5.10: Hydrogen bonding (Copper Ions).

He also proposed that an alternative mechanism could be the adsorption of the copper hydroxy complex by the formation and splitting out of water (Figure 5.11).

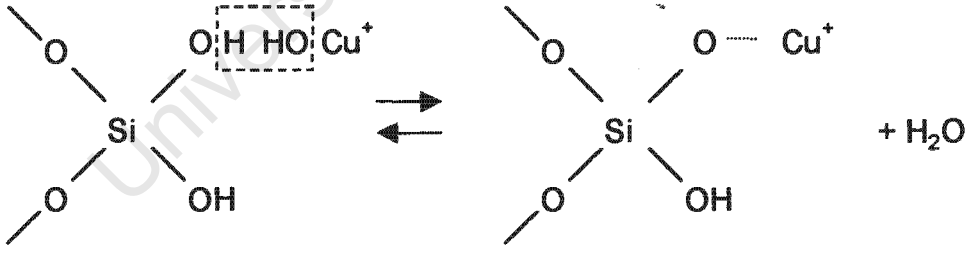

Figure 5.11: Hydroxy complex formation (Copper Ions).

The third possible mechanism involved nucleation and growth of a hydroxide precipitate at the surface. These adsorption mechanisms would result in a more positive mineral surface charge. It is assumed that these mechanisms will play a role in copper ion adsorption for the siliceous minerals.

University of Cape Town

Nagaraj and Brinen (1996), using XPS, found that copper was present as Cu^{1+} rather than Cu^{2+} after collector treatment of copper activated pyroxene. This suggested that a chemical reaction was occurring during the adsorption of xanthate onto the copper activated silicate surfaces, which involved the formation of Cu(I)-X complexes. The second possible mechanism could have been electrostatic attraction between positively charged copper species and negatively charged xanthate ions. A schematic representation of the xanthate interaction with the copper ion activated silicate mineral surfaces is given in Figure 5.12.

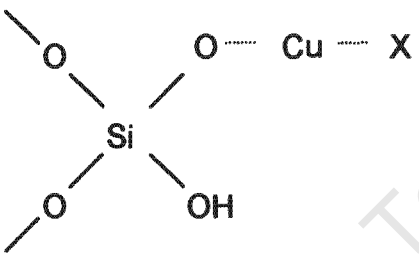

Figure 5.12: Schematic representation of xanthate adsorption onto copper activated silicate mineral.

University of Cape Town

In the case of siliceous gangue minerals where a chemical reaction between copper species and the gangue mineral is unlikely to occur, it is generally assumed that activation occurs as a result of an interaction between the precipitated copper hydroxide, which exists as a colloidal or ionic species, and the xanthate ion. Smart (2005) has proposed that such a reaction results in the formation of cuprous xanthate. It is also then proposed that the redox reaction is accompanied by oxidation of xanthate ions to dixanthogen which renders the gangue hydrophobic. In a study evaluating the effect of the inadvertent activation of pyroxene, for example, it was shown that the recovery of pyroxene increased from 5% when treated only with SIBX to 77% when treated sequentially with copper sulphate and SIBX (Shackleton et al., 2003).

In the present study, the minerals being floated are fully liberated samples of platinum or palladium arsenide, telluride and sulphide. It is not appropriate to suggest that the mechanism proposed for sulphide minerals, which involve well-known chemical

interactions with the sulphide surface layer, can be used to explain the observation made in the present instance for the PGE arsenides and tellurides. Arguably, the observations made in the case of the relatively inert surface of the siliceous gangue minerals may be of greater relevance here although this does not imply at all that the PGE mineral surfaces are chemically inert. Thus an explanation for the behaviour of the copper sulphate may be related to interactions between copper hydroxide species such as $Cu(OH)^+$ or $Cu(OH)_2$ and the xanthate. If the redox reaction proposed in the case of the activation of siliceous gangue minerals is to be considered then it should follow that the dixanthogen formed would result in an enhanced recovery. However, counter-intuitively, it was repeatedly observed that the addition of copper sulphate either hardly influenced recovery in the case of sperrylite (NS145) and vysotskite (NS148) or in fact caused the recovery to decrease in the case of palladoarsenide (NS147), both moncheite samples (NS142 and NS153), both merenskyite samples (NS143 and NS152) and cooperite (NS144) samples. In the absence of any further experimental data, it is presently only possible to speculate on why this should be the case.

The zeta potential measurements all showed significant reductions in the negative charge of the surfaces after the addition of copper sulphate except for palladoarsenide. At pH=6 the copper exists predominantly in the Cu^{2+} state and so it can be assumed that these ions serve to partially neutralise the negative surface. Although Cu^{2+} can be hydrolysed to form $Cu^{2+}(H2O)_x$ species which would inhibit interference with the surface. The zeta potential versus pH changes are, however, relatively modest in the case of moncheite and not present in the case of palladoarsenide but quite significant in the case of sperrylite, merenskyite, cooperite and vysotskite where the zeta potential increased by between 12 - 18mV. At pH=10 the zeta potential is close to zero and this may simply be due to a deposition of $Cu(OH)_2$ colloids, the dominant copper sulphate species at this pH, on the surface thus essentially masking the surface charge. Confirmation of the fact that the dominant effect of adding copper sulphate was simply to cause $Cu(OH)_2$ species to block access of xanthate to the surface was obtained in the experiments carried out at concentrations of copper sulphate an order of magnitude lower (Figures 4.32, 4.33 and 4.52). These experiments showed as expected a much lower concentration of copper on

University of Cape Town

the surface but also a concomitantly higher concentration of xanthate on the surface due to a higher availability of surface active sites. Consistent with these observations, the flotation recovery for the case where a lower copper concentration was employed was markedly higher. When SIBX is added after the addition of copper sulphate, the zeta potential becomes more negative to varying extents on the different samples. Both ToF-SIMS and XPS also show that this treatment results in less xanthate on the surface than when only SIBX was added for most cases.

Copper activation of cooperite follows the well-established mechanism as observed for other base metal sulphides in which the copper is reduced to Cu(I) on adsorption. The classical activation mechanism seen with cooperite does not appear to be operating for vysotskite. This may be partly due to the highly oxidised state of these surfaces before the copper addition.

Furthermore for both sperrylite samples (NS145 and NS146) and palladoarsenide (NS147) the XPS results show that when copper is added, approximately 20%, 33% and 13%, respectively, of the copper is already in the Cu^{1+} oxidation state without the addition of xanthate. When xanthate is added to the arsenide copper treated minerals, all the remaining Cu^{2+} species is converted to Cu(I)xanthate species. Even though the Cu(I)xanthate species were formed this did not result in a good flotation response.

The effect of the presence of bismuth in the behaviour of the minerals is interesting. In the case of moncheite ($PtPd(BiTe)_2$), NS153, the XPS has data shown that copper sulphate/xanthate treatment results in 36% of the existing copper being present in the Cu^{1+} state. For moncheite ($PtTe_2$), NS142, however, the equivalent value is only 6%. The zeta potential of NS153 under the same conditions is also much less negative than NS142. In addition, the ToF-SIMS also showed a lower Cu ions surface coverage for NS153 compared to NS142. A significant conversion of Cu(II) to Cu(I) can be also associated with the formation of CuX. It could thus be inferred that the presence of Bi in NS142 may somehow inhibit the electron transfer reaction which reduces Cu^{2+} to Cu^{1+} which seems to occur fairly readily on $PtTe_2$ (NS153). It also appears that the presence of

University of Cape Town

Bi in the lattice of the mineral and Cu on the surface affects the adsorption of xanthate as seen in the XPS results where a 10 fold lower %S is observed for NS142 compared to NS153 (Table 4.18) (Shackleton et al. 2007). This lower xanthate concentration observed on the mineral surface may also contribute to the lower conversion of Cu^{2+} to Cu^{1+} as xanthate adsorption is the driving force for the conversion to take place. All these observations however do not in any way predict the hydrophobicity of the treated samples. Both NS142 and NS153 only show approximately 40% recovery after copper sulphate/xanthate treatment and so the possible effect of the formation of CuX, as indicated by XPS, on the surface charge provides little insight into the ultimate hydrophobicity of the mineral samples and their flotation performance. What is clear from these experiments is that the presence of copper sulphate in synthetic water, added as an activator for the base metal sulphide minerals, is deleterious to the recovery of moncheite. As proposed above this is probably due to the deposition of $Cu(OH)_2$ colloids which inhibit access of xanthate ions to the surface. The effect on merenskyite is less detrimental and in fact although the rate of flotation is significantly lower when copper sulphate is used the final recoveries after 20 minutes are close to 100%. This may be due to the fact that less copper was adsorbed onto the Pd mineral surfaces due to the extensive oxidation observed during the XPS analyses (Table 4.19). As seen for moncheite the lower copper concentration (5.00E-06M) hardly affected the flotation response (Figure 4.52). Again, however, zeta potential is a poor predictor of flotation behaviour other than showing that when the zeta potential becomes relatively less negative the samples are also relatively less hydrophobic as indicated by the microflotation tests.

The xanthate concentrations on the surface in the absence or presence of copper are not significantly different and hence the mere presence of xanthate species on the surface is not an indicator of floatability. It can therefore only be concluded that it is the chemical nature of the xanthate and not the mere presence of a xanthate species on the surface which is crucial to promoting flotation. When copper is absent it has been shown (Figure 5.2) that the xanthate is readily converted to dixanthogen resulting in the high recoveries observed (Vermaak et al., 2004). As already stated, in the presence of copper ions, however, XPS tests on moncheite and merenskyite suggest that part of the xanthate is

University of Cape Town

converted via a redox reaction with Cu(II) to Cu(I)X which, however, appears not to contribute significantly to rendering the surface hydrophobic. This is particularly demonstrated in the case of moncheite where the greater the amount of Cu(I) the less the increase in flotation recovery relative to that observed in the absence of reagents.

In the case of sperrylite (NS145) and vysotskite (NS148), it is possible that the redox reaction involving precipitated copper hydroxide and SIBX is kinetically controlled and that the mineral surface either slows down the electron transfer process or indeed in the case of palladoarsenide (NS147), moncheite (NS142 and NS153), merenskyite (NS143 and NS152) and cooperite (NS144) may even inhibit such a redox reaction. It is beyond the scope of the present study to speculate on the relative conductivity properties of the samples such as the abundance of valence and/or conduction bands, etc., all of which could play a role in the ability of electrons to migrate in a surface reaction involving such solids.

A comparison of the XPS results for the PGE minerals have shown some interesting facts about the minerals studied. In general, all of the palladium minerals are highly oxidised after conditioning in synthetic water (Table 4.19). However, this fact did not seem to affect their flotation response, if anything, their flotation rates and recovery were higher compared to the Pt minerals. Surface concentrations of copper are low and inconsistent for the Pd minerals compared to the Pt mineral species. Most of the copper is present as hydrophilic Cu(II) even after xanthate addition. The classical activation mechanism seen with cooperite does not appear to be operating for the PGE arsenides, tellurides and even for vysotskite. This may be partly due to the highly oxidised state of these surfaces before copper addition. Xanthate adsorption, however, still occurs with and without copper conditioning.

The results may explain the differences observed between the Pt and Pd minerals with respect to flotation rates and recoveries. In general, in the presence of copper sulphate the Pd minerals display a lower copper surface coverage when compared to the Pt minerals (Tables 4.18 and 4.19). This may be attributed to surface oxidation products

University of Cape Town

which interfere with and reduce the adsorption of copper species on the surfaces of the Pd minerals. These oxidation products do not seem to affect the collector adsorption and therefore higher flotation rates and recoveries were observed.

In order to gain some insight into the nature of the bonding of the copper species to the mineral surface, tests were conducted in the presence of a complexing agent, ethylenediamine (EDA), which was added after $CuSO_4$ addition and after the addition of $CuSO_4$+SIBX, in an attempt to remove any of the weakly bound unconverted $Cu(OH)_2$ colloids.

The formation of the copper chelate involves bonding of the copper ion through covalent and coordination bonds with the electron-donor atoms of the functional group of the chelating reagent (Fuerstenau et al. 1999). This occurs by the exchange of water molecules, which are bound to the copper atom, for ligand molecules. EDA is a bidentate ligand, which when unprotonated, can form two coordinate covalent bonds with a metal atom through the lone pair electrons on both nitrogens. In its neutral form, it forms soluble complexes with both copper(I) and copper(II) ions: i.e. $Cu(EDA)^{2+}$, $Cu(EDA)_2^{2+}$ and $Cu(OH)(EDA)^{+}$. Copper-EDA species form at pH values much lower than those at which EDA is hydrolysed in water-EDA systems, reflecting their stability (Aksu and Doyle, 2000).

Figure 5.13 shows the E_h-pH diagram for the copper-water-EDA system and it can be seen that at pH 9, copper is complexed by two EDA ligands to give $Cu(EDA)_2^{2+}$ species at E_h >0.2 V. The E_h for the system studied was above 0.200 mV.

University of Cape Town

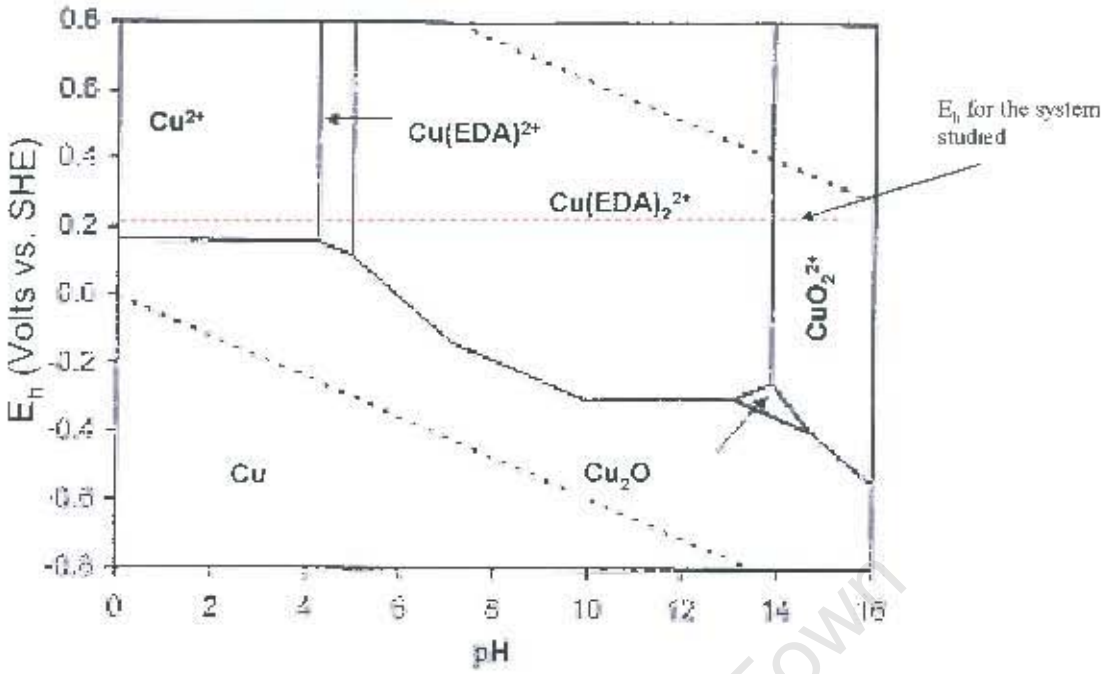

Figure 5.13: E_h-pH diagram for the copper-water-ethylenediamine (EDA) system at 25°C and 1 atm. Total EDA activity, $\{EDA_T\}$ = 1E-2M; Total dissolved copper activity, $\{Cu_T\}$ = 1E-6M, (Aksu and Doyle, 2000).

The ToF-SIMS data has shown that when EDA is added to the sperrylite system, in either sequence, viz. before or after xanthate addition, there is removal of copper from the surfaces of both samples (Figures 4.38 and 4.39). This suggests that the copper xanthate or hydroxyl species are not strongly bound to the mineral surface for both sperrylite samples. It is possible that copper is removed as a result of the preferential complexation with EDA in solution. For palladoarsenide the addition of EDA after $CuSO_4$ and prior to SIBX there is removal of the copper hydroxyl species. This reduction in the solution concentration of copper ions consequently causes copper species on the surface to undergo dissolution (O'Connor et al, 2006).

It is interesting to speculate on the role of the bismuth for the moncheite and merenskyite samples. There is little difference between the flotation behaviour of the samples with or without bismuth. The EDA data shows that the Cu(II) species are more readily removed from the Pt and Pd bismuth telluride surfaces compared to the more pure Pt and Pd telluride mineral species. It could thus be deduced that the copper xanthate binds more

University of Cape Town

strongly to the surface of the PGE telluride than to the PGE bismuth telluride. This is also consistent with the proposal that it is the dixanthogen, which it is postulated, is solely responsible for promoting flotation and that the only function of copper is to cause the formation of $Cu(OH)_2$ colloids which are not strongly bound to the surface but which may mask or inhibit the hydrophobic rendering effect of the dixanthogen (Shackleton et al. 2007). The Bi free samples NS153 and NS152 did not exhibit any reduction in surface copper with the addition of EDA for the $CuSO_4$+SIBX+EDA sequence which is consistent with Cu(I)X being more strongly bound than the $Cu(OH)_2$. It should however be noted that a lower copper surface coverage was observed on the moncheite NS153 mineral surface prior to the addition of EDA compared to the moncheite sample NS142. Palladoarsenide (NS147) did not exhibit any copper removal with the addition of EDA for the $CuSO_4$+SIBX+EDA sequence. It should be noted that a significantly lower copper surface coverage was observed on the palladoarsenide mineral surface prior to the addition of EDA compared to the other PGE minerals. The Pt and Pd sulphide minerals surface analysis showed that vysotskite (NS148) did not exhibit any copper removal with the addition of EDA for the either sequence while cooperite (NS144) did show copper removal in the sequence of $CuSO_4$+ EDA +SIBX.

In summary, the mechanisms of copper activation with the addition of SIBX appear to be distinctly different between the PGE sulphide, arsenide and telluride samples. Copper activation of cooperite follows the well-established mechanism of other mineral sulphides in which the copper is reduced to Cu(I) on adsorption. Adsorbed copper on the tellurides, however, is limited in surface concentration and predominantly Cu(II) with some limited Cu(I) only evident after xanthate adsorption. This lower degree of adsorbed copper (II) ions onto the PGE telluride mineral surfaces will result in a higher concentration in solution of copper ions and hence will result in a higher concentration of the thermodynamically favoured $Cu(OH)_2$ precipitate at alkaline pH (Figure 5.3). The hydrophilic precipitate [$Cu(OH)_2$] would not increase the mineral hydrophobicity but would reduce the number of surface sites available for xanthate adsorption and will result in the reduction of the floatability for the telluride minerals. For the arsenides, the main surface chemical mechanism contributing to sperrylite and palladoarsenide flotation is adsorption of

University of Cape Town

precipitated Cu(II) hydroxide (as colloidal and ionic species) followed by in situ reduction to Cu(I)xanthate. This reaction will be accompanied in the redox couple by oxidation of some xanthate ions to dixanthogen further adding to the hydrophobic species on the sperrylite and palladoarsenide surfaces. However, xanthate is still adsorbed without copper activation but in lower surface concentrations and therefore lower induced hydrophobicity. The sperrylite surface appears to remain unreacted through all of the conditioning steps as indicated particularly by the unchanged arsenic signals (as arsenide). Although Cu(I)xanthate species were formed on the arsenide minerals, this did not necessarily ensure a high recovery as was observed for sperrylite sample NS146.

5.2.3 Effect of oxidation on the floatability of the PGE minerals

Due to the good floatability obtained for both synthetic moncheite samples in the presence of xanthate further testwork was conducted with the aim of evaluating various conditions, which may have a deleterious effect on the flotation response of the synthetic minerals examined. It is well established (Smart et al., 2003) that the surface products of excessive oxidation (oxides and hydroxides) have a profound and generally negative effect on surface hydrophobicity. Mild oxidation however, appears to enhance the flotation of sulphide minerals (adsorption of collectors and the formation of hydrophobic sulphur species) and is often a requirement for self-induced flotation. On the other hand, excessive oxidation inhibits flotation.

5.2.3.1 Simulated oxidation

The effect of oxidation was examined on both moncheite samples [NS142-$PtPd(BiTe)_2$ and NS153-$PtTe_2$]. The oxidising conditions involved exposing the minerals to 100°C for 7 days with the purging of air at regular intervals. The results showed that the recovery of the platinum bismuth telluride sample, NS142, was negatively impacted on when exposing the sample to oxidising conditions compared to the platinum telluride sample, NS153, which was unaffected by the oxidising conditions. It can be inferred that this may be due to bismuth possibly being more susceptible to oxidation which is consistent with the relative oxidation potentials of the respective elements. Table 5.1 shows the electrochemical series at 25°C for the elements of interest to the

University of Cape Town

investigation [E° values from CRC Handbook of Chemistry and Physics (1985-1986)]. The data shows that Pt is the least oxidised and Bi is readily oxidised.

Table 5.22: Electrochemical series for Pt, Pd, Bi and Te.

Reaction	*E°, V*	
$Pt^{2+} + 2e \rightarrow Pt$	1.118	**Least oxidisable**
$Pd^{2+} + 2e \rightarrow Pt$	0.951	
$Te^{4+} + 4e \rightarrow Te$	0.568	
$Bi^{3+} + 3e \rightarrow Bi$	0.226	
$Pt(OH)_2 + 2e \rightarrow Pt + 2OH^-$	0.14	
$Pd(OH)_2 + 2e \rightarrow Pd + 2OH^-$	0.07	
$TeO_3^{2-} + 3H_2O + 4e \rightarrow Te + 6OH^-$	-0.57	
$Bi_2O_3 + 3H_2O + 6e \rightarrow 2Bi + 6OH^-$	-0.46	**Most oxidisable**

This is further supported by the ΔG values shown in Figure 5.14. The ΔG-diagram (Ellingham) shows the relative stability of Bi, Te, Pd and Pt oxides in decreasing order in terms of oxidation [ΔG values taken from Outokumpu HSC Chemistry® for Windows, Version 4.1, 1999].

University of Cape Town

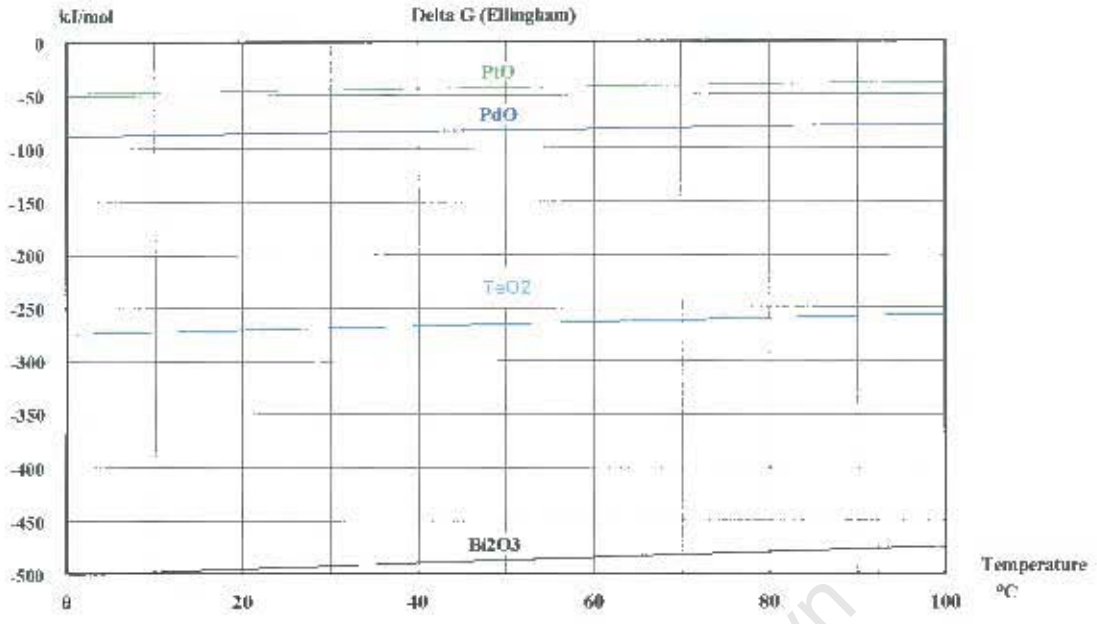

Figure 5.14: ΔG-diagram (Ellingham) showing the relative stability of Bi, Te, Pd and Pt oxides.

These results are also consistent with the results of Elvy (1996) who showed that the oxidation of the minerals in the Pd-Te-Bi system led to the formation of layers of tellurium and/or bismuth oxide covering the palladium-rich substrate. ToF-SIMS results have shown that both moncheite samples exhibit surface oxidation products and that these species were likely to be Bi(III) and Te(IV) oxides and hydroxides. Separate XPS results, where the telluride mineral were conditioned in synthetic water, have confirmed these oxidation products. This supports the proposal that bismuth is readily oxidised and that these oxidation products negatively affect the recovery of the PGE telluride minerals while tellurium does not appear to have an effect on the flotation response.

As stated in Section 4.2.3, it was noted that the Pd minerals species surfaces (PGE arsenide, telluride and sulphide) were significantly altered and showed heavily oxidised surfaces when compared to the Pt mineral species which showed minimal oxidation (Tables 4.18 and 4.19). It is interesting to note that the oxidation observed for the palladium mineral species did not detrimentally affect the recovery of these minerals; in fact, it appears as if the oxidation of the mineral surfaces enhanced the

University of Cape Town

hydrophobicity of the mineral species in the presence of xanthate. Smart et al., (2003) reported that xanthate may behave as a cleaning and dispersing agent, displacing the oxidised iron species from the pyrite surface. The interaction between the oxidation products and the sulphide mineral surface is generally weak (electrostatic and/or hydrophobic in nature) as sonication/decantation removes these oxidation products (Clarke, et al., 1995). It may be speculated that the oxidation products formed on the Pd mineral surfaces are only weakly attached to the surface and thus they can be more readily exchanged for xanthate species compared to the platinum minerals.

5.2.3.2 Bismuth and surface alteration

Testwork was conducted under the premise that bismuth oxidises readily and that therefore if the pure Pt or Pd telluride samples were ground with bismuth powder, a lower flotation response would be expected. As discussed in Section 5.2.3.1 the flotation kinetics of the samples with bismuth in the structure was lower compared to the pure PGE telluride samples; but the overall recovery was not negatively affected. The results showed that when samples of $PtTe_2$ and $PdTe_2$ were ground with bismuth powder the flotation rates as well as the overall recovery for both mineral samples is negatively affected, especially for the $PdTe_2$ sample (Figure 4.60). This result confirms the data results shown in Section 5.2.3.1 which suggested that bismuth was more susceptible to oxidation.

5.2.3.3 Oxidation from grinding environment

It was hypothesised that oxidation products from other minerals and grinding media would affect the mineral surface composition and floatability of the PGE minerals by the precipitation of oxide and hydroxide species onto the mineral surfaces.

Conditioning of moncheite in the presence of pentlandite reduced the flotation response of the +38 -38µm size fraction from >99% to 56%. This effect was not as profound when the pentlandite fraction was removed by screening and discarded prior to flotation as the flotation recovery was reduced to 73%. The ToF-SIMS data showed that the relative percent surface concentration of Fe and Ni increased while the

University of Cape Town

xanthate ion surface concentration decreased on the moncheite mineral surfaces (Figure 4.34).

In this study, it was interesting to observe the changes in the surface concentration of moncheite with respect to the nickel and iron ions. The nickel and iron speciation diagrams are given in Figure 5.15 and Figure 5.16, respectively. The diagrams show that the $Ni(OH)_2$, $NiOH^+$, $Fe(OH)_2$ and $FeOH^+$ species are the dominant species present at pH 9.

Based on the nickel and iron speciation diagrams, it is proposed that at pH 9, both iron and nickel are adsorbing onto the moncheite surfaces as iron and nickel hydroxy species, thus forming hydrophilic overlayers. The PGE minerals rest potentials are generally higher than that observed for the base metal sulphides and thus these overlayers of oxide, hydroxide and oxy-hydroxide are likely to be due to galvanic interactions. In a two component system, PGE minerals act as a cathode while sulphide minerals act as an anode and thus metal hydroxides migrate onto PGE mineral surfaces. It has been found that cathodic polarizations adversely affect the flotation response of minerals such as pyrrhotite (Adam and Iwasaki, 1984a) and chalcopyrite (Li and Iwasaki, 1992a). In addition the ToF-SIMS data also showed an increase in the relative percent surface concentration for Ca+Mg+Al+Si, which would also contribute to the passivation of the mineral surfaces

University of Cape Town

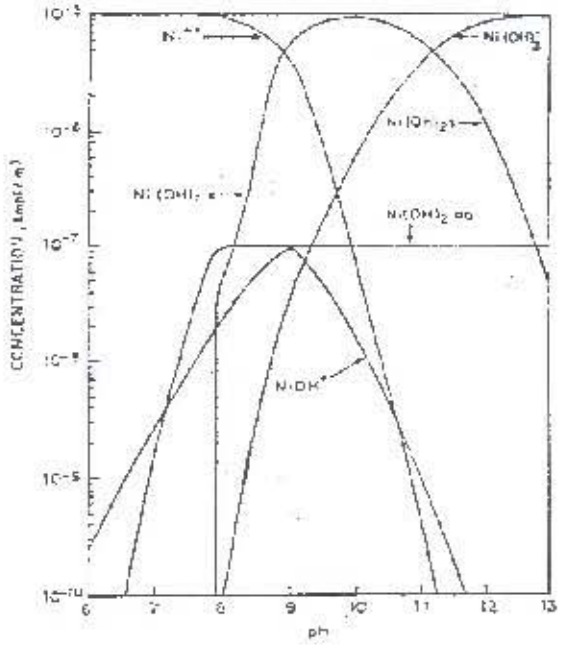

Figure 5.15: Speciation diagram for 1.00E-05M Ni^{2+} (Acar and Somasundaran, 1992).

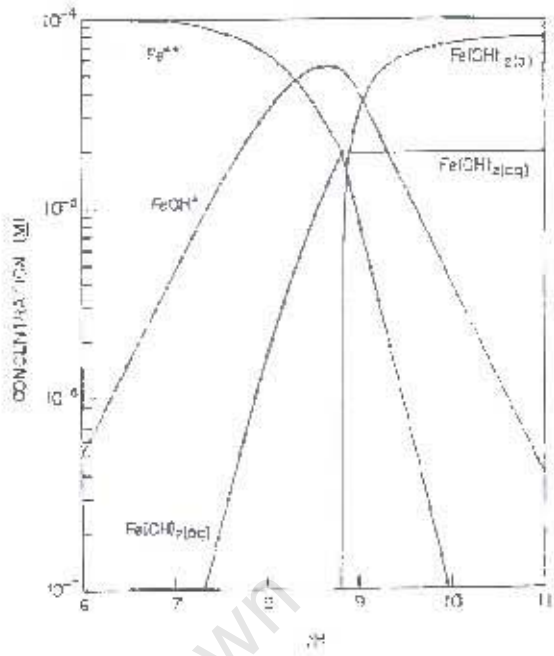

Figure 5.16: Speciation diagram for 1.00E-04M Fe^{2+} (Fuerstenau, 1976).

As expected, the testwork has shown that particle size plays a role in the flotation of the PGE telluride minerals. Subrahmanyam and Forssberg (1990) reviewed processing of fine particle and described the influence of particle size on the rate of recovery of minerals. In general, it was found that fine particles (<10µm) have low collision efficiencies with gas bubbles and are accessible to mechanical entrainment. Further grinding of the ore samples can have a twofold effect, viz. both to reduce particle size and to improve liberation. In the present study there is no gangue present and so the samples are essentially fully liberated. However, it was speculated that exposing fresh sites in the matrix of the mineral after further grinding could possibly improve recoveries. As shown in Figure 4.54, however, the effect of further grinding to finer particle sizes had the effect expected when floating fine particles, viz. a loss of recovery. This was the case for both samples of moncheite. The results showed that the recovery decreased with a decrease in particle size, the finer fraction, -10µm, giving the lowest recovery. However, when conditioned in the presence of pentlandite, the -10µm size fraction showed an improvement in flotation response (Figure 4.56). This is probably due to the pentlandite dissolution products being adsorbed onto the

University of Cape Town

PGE mineral surface and causing a neutral surface charge. This neutral charge will cause aggregation and it is well known that these larger aggregates would have a higher flotation response.

5.2.4 Effect of calcium ion concentration

Calcium ions found in process water can have a major impact on flotation of pentlandite and pyroxene minerals (Malysiak, 2003). The synthetic water formulation used during this study contained sodium, magnesium, calcium, bicarbonate, chloride, nitrate and sulphate ions. It is accepted that sulphide mineral surfaces in pulp, in the absence or presence of a collector, are energetically and chemically heterogeneous and contain a variety of active sites (Ralston, 1991). Ralston also pointed out that the most energetic sites are likely to be hydrophilic. Clusters of water molecules will adhere to these sites. Sulphide mineral surfaces typically consist of hydrophilic and hydrophobic patches and the relative population of each of these mineral sites would influence the sulphide mineral floatability. In the case of this study, all mineral surfaces came into contact with the ions in synthetic water prior to the addition of copper (II) and/or xanthate ions. Thus e.g. Ca^{2+} and Mg^{2+} ions, which are predominant at the pH range of interest (Figures 5.17 and 5.18) adsorb onto the active sites of all minerals.

University of Cape Town

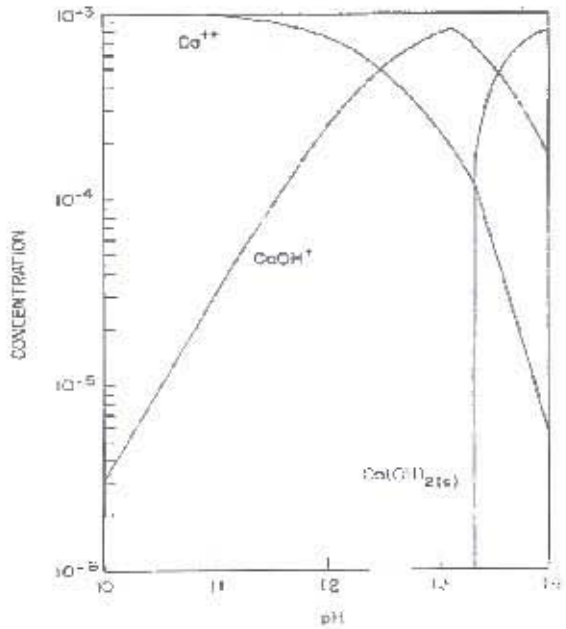

Figure 5.17: Speciation diagram for 1.0E-03M Ca^{2+} (Fuerstenau, 1976).

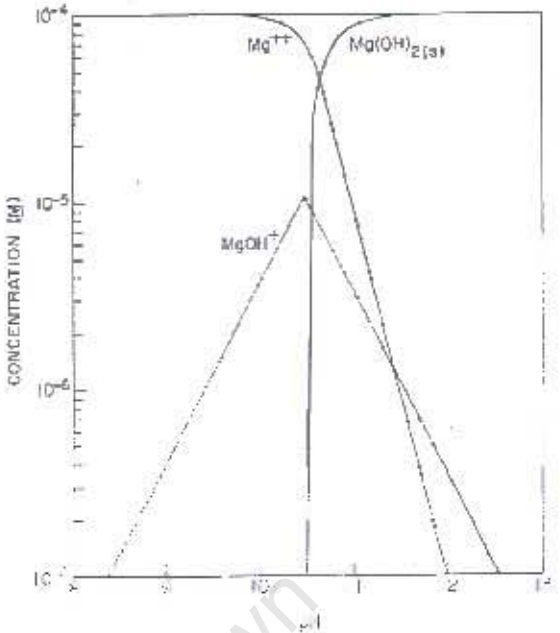

Figure 5.18: Speciation diagram for 1.00E-04M Mg^{2+} (Fuerstenau, 1976).

In the present study changing the calcium concentration in the synthetic water from 80ppm to 500ppm did not affect the flotation response of the $PdTe_2$ (NS152) mineral species. Subsequent ToF-SIMS and XPS analyses also showed that the ions found in synthetic water do not significantly affect the mineral surface characteristics of the PGEs at the concentrations tested and therefore do not have an influence on the flotation response of the minerals studied. However, it should be noted that the XPS results for cooperite showed considerable adsorbed Mg ion surface concentration, hence, the PtS may specifically adsorb Mg^{2+} from synthetic water but this did not seem to affect the flotation response.

5.2.5 Other collectors

Sperrylite sample NS146 has proved to be an extremely difficult sample to recover by flotation methodologies. Various collectors and combinations of collectors, activator and pH environments were screened in an attempt to improve the flotation response for sperrylite sample NS146.

University of Cape Town

The sample responded slightly better to the addition of Senkol 65 (Dithocarbonate) as the collector compared with SIBX. The dosage for Senkol 65 was 5.00E-05M. The highest recovery (20%) was obtained at double the Senkol 65 and SIBX concentrations (Figure 4.47).

In addition, microflotation testwork was carried out at pH 6 with $CuSO_4$+SIBX additions for NS146 and compared to the corresponding pH 9 trial. The results show that the recovery increased from 8.5% for the pH 9 trial to 15% for the pH 6 trial. This is probably due to a lower concentration of $Cu(OH)_2$ colloids resulting on the surface, which are predominant above pH 8. When carrying out the microflotation test at pH 10 with SIBX for NS146 the recovery was reduced to 0.59%, which may be due to the high concentration of hydroxide ions on the mineral surface which negatively affects xanthate adsorption due to competition for sites. This trend was also observed during the zeta potential determinations.

Since no significant improvements in sperrylite recovery was obtained using the above flotation conditions, further research is necessary in order to enhance the recovery of this mineral by flotation.

University of Cape Town

CHAPTER 6

CONCLUSIONS

The aim of this study was to investigate whether there was a difference in the floatability between the PGE sulphide, arsenide and telluride minerals and if so to what can these differences be ascribed. It had been suggested, from empirical observations on plants, that $PtAs_2$ (sperrylite) and $PtPd(BiTe)_2$ (moncheite) are poorly floatable minerals compared to the PGE sulphide species and that this accounts for a significant loss of PGE in flotation processes. Since it is difficult to obtain sufficient amounts of these minerals, the present study has investigated the surface characteristics and flotation behaviour of synthetic cooperite, vysotskite sperrylite, palladoarsenide, moncheite and merenskyite.

At the start of the study it was hypothesised that the difference in floatability of these PGE minerals may be due to a number of factors.

1. <u>The crystal structure and/or morphology of the PGE minerals affect the hydrophobicity of these minerals.</u>

   For all the synthetically prepared minerals except palladoarsenide, there was good agreement between the measured and calculated crystal structures and they corresponded well with the information contained in the ICSD database. However, the results of this research have not shown that the hydrophobicity of the synthesised Pt and Pd mineral species are influenced by the crystal planes and/or morphology of the minerals. Therefore these particular results do not highlight or explain the varying results obtained with these minerals during the surface analyses and microflotation testwork.

   The study of the arsenide minerals has shown, remarkably, that two samples of sperrylite which had virtually identical bulk compositions and crystallinity showed quite different flotation behaviour. Recoveries of greater than 70% were obtained in the case of NS145 whereas the highest recovery for NS146 sample was about 40% and this was only obtained after grinding to <38µm. There was a strong correlation between the appearance of Pt specks on the surface as observed in the EDS results and the recoveries of the two

University of Cape Town

samples, the sample having more such specks on the surface showing significantly greater recoveries. From this it could be deduced that it may be the presence of such free Pt specks which favours the flotation behaviour by providing appropriate sites for collector adsorption. This may be ascribed either to the effect of xanthate being covalently bonded to the surface or to the effect of dixanthogen being formed at the flotation conditions. This increase in recovery in the case of NS146 after grinding may be due to the exposure of new free Pt specks/sites.

In general, it has been shown that the PGE minerals float readily when treated with SIBX and the XPS and ToF-SIMS results showed clearly that xanthate is adsorbed on the mineral surfaces at a higher concentration compared to the copper activated minerals except for the sperrylite (NS146) and cooperite (NS144) samples. The ToF-SIMS data have clearly shown that the active species for flotation was dixanthogen.

2. Another hypothesis proposed for the lower floatability observed for the PGE mineral species was the presence of oxidation products (air induced oxidation) which would influence their floatability.

Platinum is a noble metal and is essentially non-oxidisable under normal conditions; hence, this is only likely to occur for the palladium mineral species. The zeta potential determinations have shown that the surface charge differs considerably between the Pt and Pd mineral species which may be due to the significant surface oxidation observed for the Pd minerals. There were, however, no clear correlations between the observations made of the surface charges of the minerals and their flotation behaviour. Oxidation of the PGE telluride minerals were shown to negatively affect the flotation performance of the bismuth-rich samples but not the pure Pt and Pd telluride samples which supports the hypothesis that bismuth is readily oxidised and that the oxidation products negatively affect the floatability of these minerals.

University of Cape Town

3. The poor floatabilities of the PGE mineral species [$PtTe_2$ and $PtPd(BiTe)_2$] may also be speculated to be a result of contact with oxidation products produced during grinding causing inadvertent depression due to precipitating ions, for example, from pentlandite, $NiOH^+$ and $FeOH^+$.

Conditioning of the minerals in the presence of pentlandite reduced the recovery of moncheite [$PtPd(BiTe)_2$] by around 47%. This was ascribed to pentlandite dissolution products (iron and nickel hydroxy species) forming overlayers on the mineral surfaces thereby inhibiting the adsorption of collector. This observation supports the hypothesis that oxidation products from other minerals and grinding media affect the mineral surface composition and floatability by precipitation onto the mineral surfaces. In addition, further grinding of moncheite [$PtPd(BiTe)_2$] conditioned with pentlandite showed a negative effect on recovery due to the fineness of the particle size distribution and there was no advantage gained from any possible exposure of fresh sites in the sample. However, the -10µm size fraction showed an improvement in flotation response which was probably due to the pentlandite dissolution products being adsorbed onto the PGE mineral surface and causing a neutral surface charge. This neutral charge would promote aggregation and these larger aggregates would have a higher flotation response.

4. It is widely known (Finkelstein, 1997) that copper sulphate is used as a promoter of the base metal sulphide minerals. It was speculated that similarly copper sulphate would promote the flotation of the PGE mineral species.

These tests were carried out in a frothless environment thus eliminating any effect copper sulphate may have on froth structure. There were no clear correlations between the observations made of the surface charges of the minerals and their flotation behaviour. Copper sulphate addition had the expected effect on zeta potential values but this did not correlate with the floatability of the minerals.

Copper sulphate, the standard activator used in concentrators for the recovery of PGMs by flotation, was found to have a negative effect on the recovery of all of the synthetic PGE

University of Cape Town

mineral samples, with the exception of vysotskite, when compared with the results obtained in the presence of xanthate on its own. Zeta potential, ToF-SIMS and XPS data have shown that PGE mineral surfaces are covered with $Cu(OH)_2$ precipitate in the presence of copper sulphate and that the surface coverage is largely Cu(II). When xanthate ions interact with the copper(II) species (colloidal and ionic) present on the surface of the minerals, the copper is slowly converted by an in-situ reduction to Cu(I)xanthate. The percentage conversion is low for the Pd arsenide, Pd sulphide and the PGE bismuth and pure telluride mineral samples compared to the situation with cooperite and both sperrylite samples where a 100% conversion from Cu(II) to Cu(I) was obtained. Although there were indications that Cu(I)X was formed this was associated with a lowering in flotation recovery. It is thus speculated that the negative effect of copper on the recovery of these minerals may be due to $Cu(OH)_2$ precipitation on the mineral surfaces occurring in patches and thus when xanthate ions are subsequently added, most of the active sites are already occupied by the hydrophilic $Cu(OH)_2$ which reduces the degree of xanthate adsorbing directly onto the vacant Pt and Pd mineral surface sites.

EDA additions have shown that the copper and copper xanthate species are not strongly bound to the mineral surfaces except for vysotskite. This observation confirms the copper speciation on the mineral surface thereby indicating that the copper is present on the surface as a result of the precipitation of $Cu(OH)_2$ colloids rather than a chemical reaction between the copper and metal ions in the PGE mineral structure.

5. Testwork was conducted to investigate the possibility that bismuth oxidises readily and these passivating layers of bismuth oxide and hydroxide may influence the flotation response.

The flotation rates of the samples with bismuth in the structure were lower compared to the pure PGE telluride samples; although the overall recovery was similar. For the $PtTe_2$ and $PdTe_2$ samples which were ground with bismuth powder the results showed that the flotation rates as well as the overall recovery for both mineral samples was negatively affected, especially for the $PdTe_2$ sample. This result supports the hypothesis that

University of Cape Town

bismuth being more susceptible to oxidation, yields oxidation products (Bi oxide and hydroxide species) which negatively affect the flotation response of the PGE telluride mineral species.

6. Finally it was proposed that the ion species such as Ca ions, present in the pulp may affect the mineral surfaces and influence the floatability of the Pt and Pd mineral species by forming passivating layers on the mineral surfaces.

   This hypothesis was not supported by the results obtained in this study as the calcium ions, which are always present in process water, did not negatively affect the flotation response of the $PdTe_2$ mineral species.

The aim of this study was to investigate whether there was a difference in the floatability between the PGE sulphide, arsenide and telluride minerals. The variation in their flotation performance was due to either their surface properties or the nature of the flotation reagents used. Although the minerals used were synthetic samples they have been shown in a separate study (Shamaila, 2007) to behave in a similar way to the naturally occurring minerals. Their flotation response on concentrators may be due to variations in their surface properties which result from the conditions prevailing during their formation in geological time.

It was also shown that the use of copper sulphate which is subsequently present on PGM flotation plants is not conducive to the flotation of PGE arsenide and telluride minerals. The addition of copper sulphate could thus be re-evaluated and added during the later stages of flotation. The PGE sulphides do not show any added benefit with the addition of copper sulphate. This is a complex problem; however, it should be borne in mind that the copper sulphate addition improves the recoveries of the base metal sulphides especially at lower pHs. The addition of xanthate showed a flotation recovery of at least 95% for all the minerals except sperrylite sample (NS146) despite the difference in their natural floatability. This research showed that it is not only the grain size distribution that plays a role in flotation but also the mineral surface chemistry. For example, for the same size distribution of +38 -38µm for the Pt mineral species, in the presence of xanthate, the order of flotation rate (in

University of Cape Town

decreasing order) was moncheite, cooperite followed by sperrylite and for the Pd mineral species, the order of flotation rate was merenskyite, palladoarsenide and vysotskite. The ions found in the synthetic water and at the concentrations used in the study did not affect the mineral surfaces and hinder flotation.

In conclusion it is clear that Pt and Pd arsenide and telluride minerals can be recovered in significant quantities using xanthate as the collector under the conditions tested.

University of Cape Town

CHAPTER 7

List of References

Abeidu, A.M. and Almahdy, A.M., 1980. Magnesia mixture as a result a regulator in the separation of pyrite from chalcopyrite and arsenopyrite. International Journal of Mineral Processing Vol.6, pp. 285.

Acar, S. and Somasundaran, P., 1992. Effect of dissolved mineral species on the electrokinetic behaviour of sulphides. Minerals Engineering, Vol. 5, No.1, pp. 27-40.

Aksu, Sedar and Doyle, Fiona M., 2000. Potential-pH diagrams for copper in aqueous solutions of various organic complexing agents. Electrochem. Soc. Proc., Vol 200-14, pp. 258-269.

Allison, S.A., Gold, L.A., Nicol, N.G. and Granville, A., 1972. A determination of the product of reaction between various sulphide minerals and aqueous xanthate solution, and a correlation of the products with electrode rest potentials. Metallurgical Transactions, B3, pp. 2613-2618.

Bannister, F.A. and Hey, M.H., 1932. Mineralogical Magazine, 23, 188.

Bergizov, V.D., Meshchankina, V.I. and Dubankina, L.S., 1974. Palladoarsenide, Pd2As, a new natural palladium arsenide from copper-nickel ores of the Oktybar deposits. Zapiski Vesesoyuznoe Mineralogicheskoe Obshchestvo, Vol, 103, pp. 104-107.

Benninghoven, A., 1975. Developmnets in secondary ion spectroscopy and applications to surface studies. Surface Science, 53, pp. 596-625.

Bradshaw, D.J. and O'Connor, C.T., 1996. Measurement of the sub-process of bubble loading in flotation. Minerals Engineering, Vol. 9, No. 4, pp. 443-448.

Brinen, J.S. and Nagaraj, D.R., 1994. Direct observation of a Pb-dithiophosphinate complex on galena mineral surfaces using SIMS. Surface and Interface Analysis, 21, pp. 874-876.

Buchanan, D.L., 1988. Platinum-group element exploration. Developments in Economic Geology, 26, pp 3.

University of Cape Town

Buckley, A.N. and Woods, R., 1991. Surface composition of pentlandite under flotation-related conditions. Surf. and Interface Anal., Vol 17, pp. 675-680.

Cabri, L. J., Laflamme, J.H.G., Stewart, J.M., Rowland, J.F. and Chen, T.T., 1975. New data on some palladium arsenides and antimonides. Canadian Mineralogist, Vol. 13, pp 321 – 335.

Cabri, L. J., 2002. The platinum-group minerals. In Cabri, L.J., Ed., The geology, geochemistry, mineralogy and mineral beneficiation of platinum-group elements. Canadian Institute of Mining, Metallurgy and Petroleum, Special Volume 54, pp 42, 59, 68, 72, 88 and 98.

Cawthorn, R.G., Merkle, R.K.W. and Viljoen, M.J., "Platinum-Group Element Deposits in the Bushveld Complex, South Africa" in "The Geology, Geochemistry, Mineralogy and Mineral Beneficiation of the Platinum Group Elements", CIM Special Volume 54, eds, Cabri, L.J., Canadian Institute of Mining, Metallurgy and Petroleum, 2002, pp 389 – 429.

Clarke, P., Fornasiero, D., Ralston, J. and Smart, R.St.C., 1995. A study of the removal of oxidation products from sulphide mineral surfaces. Minerals Engineering, Vol. 8, No.11, pp. 1347-1357.

CRC Handbook of Chemistry and Physics, 66th edition 1985-1986, Editor-in-Chief R.C. Weast, CRC Press, Inc. Boca Raton, Florida, pp D151-D155.

de Vaux, D., 1997. An introduction to Time of Flight Secondary Ion Mass Spectrometry. Anglo bi-annual operations director's technical seminar.

Elvy, S.B., Williams, P.A. and Buckley, A.N., 1996. XPS evidence for the incongruent surface oxidation of minerals in the Pd-Te-Bi system Surface and Interface Analysis. Vol. 95, pp 525-534.

Fairthorne, G, Fornasiero, D. and Ralston, J., 1997. Effect of oxidation on the collectorless flotation of chalcopyrite. Int. J. Miner. Process., 49, pp. 31-48.

University of Cape Town

Finkelstein, N.P. and Allison, S.A., 1976. The chemistry of activation, deactivation and depression in the flotation of zinc sulphide: a review. In Fuerstenau, M.C. (Ed.), A.M.

Finkelstein, N.P., 1997. The activation of sulphide minerals for flotation: a review. International Journal of Mineral Processing, 52, pp. 81-120.

Formanek, V. and Lauvernier, J., 1963. Beneficiation of cobalt arsenides of Bou-Azzer (Morocco) by gravity concentration and flotation. Proceedings, 6th International Mineral Processing Congress, Cannes, pp. 333 – 352.

Fornasiero, D and Ralston, J., 2006. Effect of surface oxide/hydroxide products on the collectorless flotation of copper-activated sphalerite. Int. J. Miner. Process., 78, pp. 231-237.

Forssberg, K.S.E. and Jonsson, H., 1981. Absorption of heavy metal ions on pyrrhotite. Scandinavian Journal of Metallurgy, Vol. 10, pp. 225-230.

Forssburg (Editor), Proc. XVI International Mineral Processing Congress. Stockholm, Elselvier, Amsterdam, pp. 1211-1232.

Fuerstenau, M.C., 1976. Flotation. A.M. Gaudin Memorial Volume, Volume 1, Published by American Institute of Mining, Metallurgical, and Petroleum Engineers, Inc., New York, pp. 148-196.

Fuerstenau, M.C., Palmer, B.R. and Gutierrez, B., 1977. Mechanisms of flotation of selected iron-bearing silicates. Society of Mining Engineers, Vol. 262, pp. 234-236.

Fuerstenau, D.W., 1982. Activation and flotation of sulphide minerals. In King R.P. (Ed.), Principles of Flotation, S.A. Inst. Min. Metall. , Johannesburg, pp. 188-198.

Fuerstenau, M.C., Misra, M. and Palmer, B.R., 1990. Xanthate adsorption on selected sulphides in the virtual absence and presence of oxygen, Part 2. Int. J. Miner. Process., 29, pp. 111-119 .

Gait, R. I. 1982. Sperrylite from the type locality. Mineralogical Record 13:159-60.

University of Cape Town

Gaudin, A.M., Fuerstenau, D.W. and Mao, G.W., 1959. Activation and deactivation studies with copper on sphalerite. Mining Engineering, SME, 11, pp. 430-436.

Gerson, Andrea R., Lange, Angela G., Prince, Kathryn E. and Smart, Roger S., 1998. The mechanism of copper activation of sphalerite. Applied Surface Science 5510.

Gerson, A., 2002. Personal Communication.

Glasstone, S., 1946. The solid state. Textbook of Physical Chemistry, Second Edition – Fifth Printing, D. Von Nostrand Company, Inc., Chapter V. pp. 379-380.

Goh, S.W., Buckley, A.N., Lamb, R.N. and Woods, R., 2006. The ability of static secondary ion mass spectrometry to discriminate submonolayer from multilayer adsorption of thiol collectors. Minerals Engineering, 19, pp. 571-581.

Grano, S.R., Ralston, J. and Smart, R. St.C. 1990. Influence of electrochemical environment on the flotation behaviour of Mt. Isa copper and lead zinc ore. International Journal of Mineral Processing, 30, 69-97.

Grano, S.R., Wong, P.L.M., Skinner, W., Johnson, N.W. and Ralston, J., 1996. Detection and control of calcium sulphate precipitation in the lead circuit of the Hilton concentrator of Mount ISA mines limited, Australia. Proceedings of the XIX IMPC, Vol. 3 (29), pp. 171-179.

Greoneveld Meijer, W.O.J., 1955. Synthesis, structures and properties of platinum metal tellurides. The American Mineralogist, Vol. 40, No. 7-8, pp 646-657.

Hayes, R.A., 1987. The effect of E_h on the collectorless flotation of sulphide minerals. M. Appl. Sci. Thesis, South Australian Institute of Technology, Adelaide, Australia.

Hey, P.V. and Malysiak, V., 2004. Mineralogical and metallurgical investigation of selected borehole core intersections from Pedra Branca, Brazil. Anglo Platinum Report - Platinum Project No 183.

University of Cape Town

Howell, D.A., McDonald, I. and Armitage, P.E.B., 2006. Platinum group mineral assemblages in the Platreef at the Sandsloot mine, northern Bushveld Complex, South Africa. Min. Mag. 70, 83-101.

Hodgson, M. and Agar, G.E., 1989. Electrochemical investigations into the flotation chemistry of pentlandite and pyrrhotite: Process water and xanthate interactions. Canadian Metallurgical Quarterly, Vol. 28, No.3, pp. 189-198.

HSC Chemistry® Chemistry for Windows, Version 4.1, 1999. Chemical reaction and equilibrium software with extensive thermochemical database, Outokumpu.

Hunter, R.J., 1993. Introduction to modern colloid science. Oxford University Press.

Iwaksaki, I., Weiblen, P.W., Reid, K.J., Ryan, P.J., Nakazawa, H. and Malicsi, A.S., 1986. Platinum group and arsenide minerals in copper-nickel sulphide bearing Duluth gabbro and their flotation recoveries. Transactions of the American Institute of Mining, Metallurgical and Petrolium Engineers, Society of Mining Engineers of AIME, Vol. 280 Pt A.

Kakovskii, I.A., 1957. Physical properties of some flotation reagents and their salts with ions of heavy non-ferrous metals. Proc. 2nd Int. Conf. Surface Activity, London, pp. 225-237.

Kakovskii, I.A. and Arashkevich, V.M., 1968. The study of properties of organic disulphides. Preprint, VIIIth I.M.P.C., Leningrad.

Kartio, I., Laajalehto, K., Suoninen, E., Karthe, S. and Szargan, R., 1992. Technique for XPS measurements of volatile absorbed layers: Application to studies of sulphide flotation. Surf. and Interface Anal., Vol. 18, 807-810.

Khmeleva, T.N., Chapelet, J.K., Skinner, W.M. and Beattie, D.A., 2006. Depression mechanisms of sodium bisulphate in the xanthate-induced flotation of copper activated sphalerite. Int. J. Miner. Process., 79. pp. 61-75

Knipe, S.W., Mycroft, J.R., Pratt, A.R., Nesbitt, H.W. and Bancroft, G.M., 1994. X-ray photoelectron spectroscopic study of water adsorption in iron sulphide minerals. Geochimica et Cosmochimica Acta, Vol. 59, No. 6, pp. 1079-1090.

University of Cape Town

Kristall, Z., Grano, S.R., Reynolds, K.and Smart, R. St.C. and Ralston, J., 1994. An investigation of sphalerite flotation in the Murchinson zinc concentrator. Fifth Mill Operators' Conference.

Laajalehto, K., Kartio, I., Kaurila, T. Laiho, T. and Suoninen, E., 1992. Investigation of copper sulphide surfaces using synchrotron radiated excited photoemission spectroscopy. Proceedings of ECASIA'95, Montreaux 9-13.

Legrand, D.L., Nesbitt, H.W. and Bancroft, G.M., 1997. Surface characterisation of pentlandite (Fe,Ni)S_8 by X-ray photoelectron spectroscopy. International Journal of Mineral Processing, Vol 51, pp. 217-228.

Legrand, D.L., Nesbitt, H.W. and Bancroft, G.M., 1998. X-ray photoelectron spectroscopic study of a pristine millerite, NiS, surface and the effect of air and water oxidation. Amer. Mineral. Vol. 83, pp 1256 - 1265.

Li, X. and Iwasaki, I, 1992a. Effect of cathodic polarization on the floatability of chalcopyrite in the absence of oxygen. Miner. Metall. Process., 9:1, pp. 1-6.

Mackenzie, J.M.W. and O'Brien, R.T., 1969. Zeta potential of quartz in the presence of nickel (II) and cobalt (II). Society of Mining Engineers, Vol. 244, pp. 168-173.

Malcovicky, M, Malcivicky, E. and Rose-Hansen, J., 1992. The phase system Pt-Fe-As-S at 850°C and 470°C. Neues Jahrbuch fur Mineralogie Monatshefte, Pt N10.

Malvern Instruments, 1996. PCS Training Manual, Issue 1.3.

Malysiak, V. 2003. Pentlandite – pyroxene and pentlandite – feldspar interactions and their effect on separation by flotation. Ph.D Thesis, Cape Town University, pp 123-128.

Merkle, R.K.W., Pikl, R., Verryn, S.M.C. and De Waal, D., 1999. Raman spectra of synthetic 'braggite' (Pt,Pd,Ni)S. Mineralogical Magazine, Vol. 63, No. 3, pp 363-367.

University of Cape Town

Monte, M.B.M., Dutra,A.J.B., Albuquerque, Jr., Tondo, L.A. and Lins, F.F., 2002. The influence of the oxidation state of pyrite and arsenopyrite on the flotation of an auriferous sulphide ore. Minerals Engineering, No.15, pp. 1113-1120.

Moulder, John F., Stickely, William F., Sobal, Peter E. and Bomben, Kenneth D., 1995. Handbook of X-ray Photoelectron Spectroscopy. reference book of standard spectra for identification and interpretation of XPS data. Pyhsical Electronics, Inc. USA.

Mycroft, J.R., Bancroft, G.M, McIntyre, N.S., Lorimer, J.W. and Hill, I.R., 1990. Detection of sulphur and polysulphides on electrochemically oxidised pyrite surfaces by X-ray photoelectron spectroscopy and Raman spectroscopy. J. Electroanal. Che, Vol. 292, pp. 139-152.

Mycroft, J.R., Nesbitt, H.W and Pratt, A.R., 1995. X-ray photoelectron and Auger electron spectroscopy of air-oxidised pyrrhotite: Distribution of oxidised species with depth. Geochimica et Cosmochimica Acta, Vol. 59, pp. 721-733

Nagaraj, D.R. and Brinen, J., 1996. SIMS and XPS study of the adsorption of sulphide collectors on pyroxene: a case for inadvert metal in activation. Colloids and Surfaces, A: Physicochemical and Engineering Aspects 116, pp. 241-249.

Nagaraj, D.R., Lewellyn, M.E., Wang, S.S., Mingione, P.A. and Scanlon, M.J., 1988. New sulphide and precious metals collectors: for acid, neutral and mildly alkaline circuits. XVI I.M.P.C., edited by E.Forssberg Elsevier Science Publishes B.V., Amsterdam

Nakazawa, H. and Iwasaki, I., 1986. Flotation behaviour of nickel arsenide. International Journal of Mineral Processing, Vol. 18, pp. 191 – 202.

Nesbitt, H.W., Bancroft, G.M., Pratt, A.R. and Scaini, M , 1998. Sulphur and iron surface states on fractured pyrite surfaces. American Mineralogist, vol. 83, pp. 1067-1076.

Nesbitt, H W. Schaufuss A.G., Scaini, M. and Bancroft, G.M., 2001. XPS measurement of fivefold and sixfold coordinated sulphur in pyrrhotite and evidence for millerite and pyrrhotite surface species. American Mineralogist, Vol. 86, pp. 318-326.

University of Cape Town

O'Connor, C.T., Bradshaw, D.J. and Upton, A.E., 1990. The use of dithiophosphates and dithiocarbamates for the flotation of arsenopyrite. Minerals Engineering, Vol. 3, No.5, pp. 447-459.

O'Connor, C.T., Malysiak, V. and Shackleton, N.J., 2005. The interaction of xanthates and amines with pyroxene activated by copper and nickel. Minerals Engineering, Vol.19, Issues 6-8, pp. 799-806.

O'Dea, A. R., Prince, K. E., Smart, R.St.C. and Gerson, A.R., 2001. Secondary ion mass spectrometry investigation of the interaction of xanthate with galena. Int. J. Miner. Process., 61, pp. 121-143.

Penberthy, C.J., Oosthyzen, E.J. and Merkle, R.K.W., 1999. The recovery of platinum-group elements from UG-2 chromitite, Bushveld Complex – a mineralogical perspective, Mineralogy and Petrology, Vol. 68, pp. 213-222.

Perry, D.L., Tsao, L. and Taylor, J.A., 1984. Surface studies of the interaction of copper ions with sulphide minerals. In Electrochemistry in Minerals and Metal Processing. Electrochemical Society, Pennington, pp. 169-184.

Piantadosi, C. and Smart, R.St.C., 2002. Statistical comparison of hydrophobic and hydrophilic species on galena and pyrite particles in flotation concentrates and tails from TOF-SIMS evidence. Int. J. Miner. Process., 64, pp. 43-54.

Pikl, R., De Waal, D., Merkle, R.K.W. and Verryn, S.M.C., 1999. Raman spectroscopic identification of synthetic "braggite" (Pt,Pd,Ni)S samples in comparison with synthetic cooperite. Applied Spectroscopy, Vol. 53, No. 8, pp 927-930.

Prestidge, C.A., Thiel, A.G., Ralston, J. and Smart, R.St.C., 1994. The interaction of ethyl xanthate with copper(II)-activated zinc sulphide: Kinetic effects. Colloids Surface, A. Physicochem. Eng. Aspects, 85, pp. 51-68.

Physical Electronics, 1997. ToF-SIMS Trift II Broshure.

Physical Electronics, 2006. ToF-SIMS, Web page: http//www.Phi.com.

University of Cape Town

Qiming, F., Shi, X. and Jin, C., 1993. The study of pulp electrochemical flotation separation of pyrite and arsenopyrite. XVIII International Mineral Processing Congress, Vol.3, Sydney, pp 767-770.

Ralston, J, 1991. E_h and its consequences in sulphide mineral flotation. Minerals Engineering, Vol. 4, Nos. 7-11, pp. 859-878.

Reich, F., 1997. The operators Guide for the 2100 TRIFT II ToF SIMS", Physical Electronics.

Schaufuß, Andrea G., Nesbitt, H. Wayne, Kartio, Ikka, Laajalehto, Kari, Bancroft, G. Michael and Szargan Rüdiger, 1998. Incipient oxidation of fractured pyrite surfaces in air. Journal of Electron Spectroscopy and related phenomena 96, 69-82.

Schouwstra, R.P., Kinloch, E.D. and Lee, C.A., 2000. A short geological review of the Bushveld Complex. Platinum Metals Review, 44, (1), 33-39.

Schouwstra, R.P., 2007. Personnel communication.

Schueler, B.W., 1992. Microscope imaging by time of flight secondary ion mass spectrometry. Microsc. Microanal. Microstruct. 3, pp. 119-139.

Shackleton, N J, Malysiak, V and O'Connor, C T., 2003. The use of amine complexes in managing inadvertent activation of pyroxene in a pentlandite-pyroxene flotation system. Minerals Engineering, 16, 9, 849-856.

Shackleton, N J, Malysiak, V and O'Connor, C T, 2007. The surface characteristics and flotation behaviour of the platinum and palladium arsenides. Inter. Jour. Miner. Proc. (Submitted for Publication).

Shackleton, N J, Malysiak, V and O'Connor, C T, 2007. The surface characteristics and flotation behaviour of the platinum and palladium tellurides. Minerals Engineering. (Submitted for Publication).

Shamaila, S., 2007. Rates of flotation recovery versus Platreef PGE telluride and arsenide speciation. Thesis to be submitted to UCT for M.Sc. in Chemical Engineering.

University of Cape Town

Sigbahn, K., 1990. From X-ray to electron spectroscopy and new trends. Journal of Electron Spectroscopy and Related Phenomena, 51. 11-36.

Smart, R. St.C and Judd, B. 1994. Improved Lasta filter and copper reflotation performance through surface analysis surveys and WMC's Olympic dam operation. Fifth Mill Operators' Conference, the Australasian Institute of Mining and Metallurgy, Publication Series 9/94.

Smart, Roger S. C, Skinner, William M. and Gerson, Andrea R., 1999. XPS of sulphide mineral surfaces: Metal-deficient, polysulphides, defects and elemental sulphur. Surf. and Interface Anal. 28, 101-105.

Smart, R. St. C. Jasieniak, M., Prince, K.E. and Skinner, W.M., 2000. SIMS studies of oxidation mechanisms and polysulphide formation in reacted sulphide surfaces. Minerals Engineering, Vol. 13, No. 8-9, pp 857-870.

Smart, R.S.C., Amarantidis, J., Skinner, W.M., Prestige, C.A., La Vanier, L. and Grano, S.R., 2003. Surface analytical studies of oxidation and collector adsorption in sulphide mineral flotation. In Solid-Liquid Interfaces, Eds. K. Wandelt, S. Thurgate, Topics Appl. Phys., 85, pp. 3-60.

Smart R. St. C., 2005. Personal Communication.

Smart R. St. C., 2006. Personal Communication.

Smart, Roger, McIntyre, Stewart, Bancroft, Mike and Bello, Igor. 2006. X-ray photoelectron spectroscopy presentation. Training course.

Subrahmanyam, T.V. and Forssberg, K.S. Eric, 1990. Fine particles processing: shear flocculation and carrier flotation – a review. International Journal of Mineral Processing, Vol. 30, pp 265-286.

Valdivieso, A.L., Escamilla, C.O., Song, S., Baez, I.L. and Martinez, I.G., 2003. Adsorption of isopropyl xanthate ions onto arsenopyrite and its effect on flotation. International Journal of Mineral Processing Vol. 69, pp. 175-184.

University of Cape Town

Van der Laan, G., Pattrick, R.A.D., Henderson, C.M.B. and Vaughan, D.J., 1992. Oxidation state variations in copper minerals studied with Cu *2p* X-ray adsorption spectroscopy. J.Phys. Che. Solids, Vol. 53, No. 9, pp. 1185-1190.

Vaughan, D.J., Becker, U. and Wright, K., 1997. Sulphide mineral surfaces: theory and experiment. International Journal of Mineral Processing, Vol. 51, pp. 1-14.

Vermaak, M.K.G., Venter, J.A. and Pistorius, P.C., 2004. Electrochemical studies of the interaction of ethyl xanthate with Pd-Bi-Te. International Platinum Conference 'Platinum Adding Value', The South African Institute of Mining and Metallurgy, pp. 167-172.

Vermaak, M.K.G., 2005, Fundamentals of the flotation behaviour of palladium bismuth tellurides. PhD Thesis, University of Pretoria, pp 39-43.

Vickerman, J.C., 2001. ToF-SIMS-An Overview. ToF-SIMS surface analysis by mass spectrometry. Ed. J.C. Vickerman and D. Briggs, Chapter 1, pp1-94.

Viljoen, M.J. and Schürmann, L.W., "Platinum Group Minerals" in "The Mineral Resources of South Africa", Handbook 16, Sixth Edition, eds. Wilson, M.G.C. and Anhaeusser, C.R., Council for Geoscience, South Africa, 1998, pp 532 – 568.

Volyanskii, B.E., Ostorozhaya, E.E., Geonya, N.I., Gorshtein, A.E. and Illyuvieva, G.V., 1985. Sulphydryl collector reaction with the surface of sperrylite. The Soviet Journal of Non-Ferrous Metals, Issue 1, pp. 88-90.

Wang, X., Forssberg, K.S.E. and Bolin, N.J., 1989. Thermodynamic calculations on iron-containing sulphide mineral flotation systems. I. The stability of iron-xanthate. International Journal of Mineral Processing, 27, pp. 1-19.

Wang, X.H., Jiang, C.L. Xuan, D. and Forssberg, E. 1992. An electrochemical study of selective separation of Cu (II) activated pyrite and arsenopyrite. Proc. Electrochem. Soc., Vol. 92-117, pp. 235-258.

Weast, R.C., CRC Handbook of Chemistry and Physics, 62nd Edition, 1982, CRC Press, Florida, pp B78-B79.

University of Cape Town

WebElements™ *"Source: WebElements [http://www.webelements.com/]"*

Wesseldijk, Q.I., Reuter, M.A., Bradshaw, D.J. and Harris, P.J., 1999. The flotation behaviour of chromite with respect to the beneficiation of UG2 ore. Minerals Engineering, Vol. 12, No. 10, pp. 1177-1184.

Yan, D.S. and Hariyasa, 1997. Selective flotation of pyrite and gold tellurides. Minerals Engineering, Vol. 10, No. 3, pp. 327-337.

Yoon, R.H., Basilio, C.I., Marticorena, M.A., Kerr, A.N. and Stratton-Crawley, R., 1995. A study of the pyrrhotite depression mechanism by diethylenetriamine. Minerals Engineering, Vol. 8, No. 7, pp. 807-816.

Zackwieja, Joseph B., McCarron, John J., Walker, Grayson W. and Buckley, Alan N., 1989. Correlation between the surface composition and collectorless flotation of chalcopyrite. Journal of Colloid and Interface Science. Vol. 132, No. 2.

University of Cape Town

APPENDIX A: Copper and Xanthate Surface Coverage Calculations

It is instructive to carry out semi-quantitative exploratory calculations of estimates of the particle surface coverage by various reagents. The case of copper sulphate and xanthate used during the study is shown below as an example.

Mineral Surface Area Determined Using BET Method:

Cooperite NS144:	$0.077\ m^2/g = 0.077 \times 10^{20}\ Å^2/g$
Vysotskite NS148:	$0.068\ m^2/g = 0.068 \times 10^{20}\ Å^2/g$
Sperrylite NS145:	$0.04\ m^2/g = 0.04 \times 10^{20}\ Å^2/g$
Sperrylite NS146:	$0.06\ m^2/g = 0.06 \times 10^{20}\ Å^2/g$
Palladoarsenide NS147:	$0.26\ m^2/g = 0.26 \times 10^{20}\ Å^2/g$
Moncheite NS142:	$0.2\ m^2/g = 0.20 \times 10^{20}\ Å^2/g$
Moncheite NS153:	$0.22\ m^2/g = 0.22 \times 10^{20}\ Å^2/g$
Merenskyite NS143:	$0.13\ m^2/g = 0.13 \times 10^{20}\ Å^2/g$
Merenskyite NS152:	$0.14\ m^2/g = 0.14 \times 10^{20}\ Å^2/g$

Copper Surface Coverage:

Cu Concentration:	$5 \times 10^{-5}\ mol.dm^{-3}$
Grams of Cu in 250 cm^3 (cell volume):	8×10^{-4}
Number of Cu Moles:	$8 \times 10^{-4}/63.5 = 1.2598 \times 10^{-5}$
Number of Cu Atoms:	$1.2598 \times 10^{-5} \times 6.023 \times 10^{23} = 7.5878 \times 10^{18}$

Gaudin et al. (1959) assumed that the possible copper uptake for sphalerite was one ion for each 20.8 $Å^2$. Assuming that the same copper surface area is relevant for each of the PGE minerals uptake, the required surface area for pseudo-monolayer coverage would be:

$$7.5878 \times 10^{18} \times 20.8\ Å^2 = 1.5783 \times 10^{20}\ Å^2/g$$

This implies that 20.5, 23.21, 39.46, 26.31, 6.07, 7.89, 7.17, 12.14 and 11.27 pseudo-monolayers of copper could be formed on cooperite NS144, vysotskite NS148, sperrylite NS145, sperrylite NS146, palladoarsenide NS147, moncheite NS142, moncheite NS153, merenskyite NS143 and merenskyite NS152, respectively

University of Cape Town

Xanthate Surface Coverage:

Xanthate Concentration:	5×10^{-5} mol.dm^{3}
Grams of Xanthate in 250 cm^3:	1.9×10^{-3}
Number of Xanthate Moles:	$1.9 \times 10^{-3}/149 = 1.2752 \times 10^{-5}$
Number of Xanthate Atoms:	$1.2752 \times 10^{-5} \times 6.023 \times 10^{23} = 7.6805 \times 10^{18}$

Bradshaw (1997) assumed that the possible thiol collector uptake for pyrite is one ion for each 37 Å^2. Assuming that the same xanthate surface area is relevant for the pentlandite-pyroxene and pentlandite-feldspar mixture uptake, the required surface area for pseudo-monolayer coverage would be:

$$7.6805 \times 10^{18} \times 37 \text{ Å}^2 = 2.8418 \times 10^{20} \text{ Å}^2/\text{g}$$

This implies that 36.91, 41.79, 71.04, 47.36, 10.93, 14.21, 12.92, 21.86 and 20.30 pseudo-monolayers of xanthate could be formed on cooperite NS144, vysotskite NS148, sperrylite NS145, sperrylite NS146, palladoarsenide NS147, moncheite NS142, moncheite NS153, merenskyite NS143 and merenskyite NS152, respectively.

University of Cape Town

APPENDIX B: Zeta Potential Determination Procedure

A detailed zeta potential determination procedure used throughout the study is shown below. This procedure was used to ensure accuracy and repeatability of zeta potential data.

- Crush 0.3 g of a mineral sample to 100% -25µm in an agate mortar and pestle.
- Add 240 cm^3 of synthetic water.
- Stir well and split into 4 beakers (60 cm^3).
- Adjust pH to 6, 8 and 10 with Na_2CO_3 or HCl.
- Condition for 20 minutes.
- Measure electrophoretic mobility, (volume used +/- 10 cm^3).
- Add reagent, e.g. copper sulphate (5.00E-05M), and condition for 5 minutes.
- Measure electrophoretic mobility.

University of Cape Town

APPENDIX C: Microflotation Test Procedure

The microflotation test procedure, given below, was followed during the study in order to obtain reproducible data.

- For a single mineral study, weigh 2 grams of a mineral sample after crushing and screening (+38 -38µm size fraction). Add the mineral sample to 50 cm^3 of synthetic water adjusted to the desired pH.
- Transfer the solution to the microflotation cell and fill the cell to just below the overflow lip.
- Circulate pulp with peristaltic pump, set at 60 rpm / 1 min.
- Condition for 1 minute, add reagents as required and condition for the time required.
- Top up the cell volume to 250 cm^3, put cone in place and introduce the air (5 cm^3/min) through a syringe at the base of the cell.
- Remove the syringe and collect flotation products after:
  - 2 min - 1st Conc.
  - 4 min - 2nd Conc.
  - 6 min - 3rd Conc.
  - 10 min - 4th Conc.
  - 20 min - 5th Conc.
- Collect tailings sample.
- Filter each product on weighed filter paper and rinse with deionised water adjusted to the desired pH.
- Dry under argon if ToF-SIMS analysis is required.
- Weigh dried product and calculate recoveries obtained.
- Conditioning times used during the study:
  - SIBX: 2 min
    $CuSO_4$: 5 min
  - EDA: 5 min

University of Cape Town

APPENDIX D: Example of ToF-SIMS Analysis Spreadsheet

A typical ToF-SIMS automated spectra evaluation report is shown below. The intensities obtained would be normalised for the elements of interest and presented as the normalised yield.

AUTOMATED SPECTRA EVALUATION REPORT

Grain Number	#Si	#Al	#Si+o	#Si+o+h	#Na	#Ca	#Mg	#Ai	#Fe	#Fe+o	#Fe+o+h	#Cu	#Cu+o+h	#Cr	#C5+#C9+o+	#S
02425p.tdc	3225	143	3	20	243	1176	4621	740	1837	38	15	20	3	65	0	573
02426p.tdc	3877	84	6	24	951	720	4909	759	1734	33	24	22	5	52	1	550
02427p.tdc	2868	315	4	7	110	411	3671	508	1049	18	5	15	4	25	0	56
02428p.tdc	14703	305	44	41	1127	2650	17779	3485	6084	118	78	76	12	218	0	80
02429p.tdc	3722	46	0	1	69	399	3908	443	997	9	0	6	1	40	0	2
02430p.tdc	4087	589	5	26	611	484	6022	731	1086	28	4	18	6	31	0	190
02431p.tdc	527	11	0	1	31	72	798	92	174	1	5	3	1	5	0	15
02432p.tdc	1597	211	0	0	37	70	2025	147	244	5	0	5	0	11	0	0
02433p.tdc	1482	55	1	0	52	59	1474	170	186	2	0	1	0	13	0	0
02434p.tdc	2838	74	4	10	145	1625	3728	397	1521	18	25	10	3	42	*	172
02435p.tdc	1598	35	0	0	69	184	1575	232	320	3	0	4	0	16	0	0
02436p.tdc	155	3	1	1	10	28	225	34	57	1	0	0	1	0	0	1
02437p.tdc	5111	187	14	43	408	1136	7429	1114	2439	49	49	29	10	86	0	225
02438p.tdc	39694	2774	65	113	1165	1406	49502	5618	11945	277	204	89	12	346	0	372
02439p.tdc	16567	236	16	21	1002	1327	22756	1622	3892	114	36	37	6	112	0	67
02440p.tdc	4056	263	4	4	206	145	5577	367	754	26	7	2	2	19	0	6
02441p.tdc	6387	52	4	3	477	790	8137	1627	1745	48	16	6	2	80	0	6
02442p.tdc	3618	731	1	4	330	186	4854	1004	2016	30	20	11	2	43	0	0
02443p.tdc	7865	219	5	8	234	116	9910	403	1121	37	12	2	2	19	1	1063
02444p.tdc	418	11	0	3	119	334	741	130	67	2	0	3	0	12	0	0
02445p.tdc	3548	19	0	1	90	118	4795	264	478	8	0	3	0	12	0	577
02446p.tdc	5300	37	0	2	463	478	7544	971	836	22	7	8	1	48	0	690
02447p.tdc	1589	24	2	0	186	240	2545	389	174	3	0	1	0	21	0	56
02448p.tdc	1811	168	7	2	192	360	2446	208	635	4	1	13	0	25	1	60
02449p.tdc	10023	1143	22	40	460	644	15042	2319	3929	71	65	30	5	110	1	384
02450p.tdc	15966	161	9	22	1091	1127	22503	1823	3456	67	33	27	6	80	0	144
02451p.tdc	21737	1146	33	62	1093	1073	31219	3082	7134	144	92	47	17	247	0	145
02452p.tdc	1988	85	5	6	192	363	3154	467	617	15	10	10	1	22	0	114
02453p.tdc	4062	1048	21	36	1825	778	6709	1113	3503	57	48	29	13	81	0	1
02454p.tdc	5458	183	9	17	286	574	7776	796	1480	32	6	13	4	47	0	8
02455p.tdc	814	12	5	4	45	117	1098	100	219	6	15	7	1	17	0	80
02456p.tdc	286	4	0	1	22	22	361	42	68	3	1	2	1	3	0	67
02457p.tdc	464	13	3	1	32	51	606	63	157	8	4	1	*	7	0	1
02458p.tdc	4552	138	9	6	281	205	6808	486	1454	27	18	11	6	26	0	129
02459p.tdc	2183	34	2	11	970	1099	3451	1670	385	7	4	7	*	14	0	417
02460p.tdc	6727	280	13	37	402	1135	11225	1348	2474	45	52	35	11	114	2	127
02461p.tdc	8563	266	11	20	1668	1254	13637	2027	2920	84	39	22	10	109	1	222
02462p.tdc	7366	764	3	14	223	311	10311	1150	2219	42	8	13	3	78	0	168
02463p.tdc	18177	1018	26	30	802	916	25317	2197	5071	131	71	34	6	201	0	214
02464p.tdc	11873	3079	50	106	8796	2616	18575	2967	8507	131	106	75	14	223	0	222
02465p.tdc	15580	441	25	39	1474	2293	22994	2898	4320	106	46	45	7	154	2	86
02466p.tdc	5726	103	7	11	268	190	8062	700	1287	53	16	10	4	65	0	80
02467p.tdc	147	1780	13	21	124	188	188	80	3879	26	35	61	3	12	3	1080
02468p.tdc	560	5905	30	132	950	2194	936	166	9085	101	82	115	8	27	87	9491
02469p.tdc	156	837	4	5	38	828	251	53	2350	10	4	20	3	6	57	3225
02470p.tdc	234	541	38	15	138	65	32	510	845	3	4	16	1	5	2	73
02471p.tdc	4	94	1	0	2	181	0	9	197	3	0	0	0	7	0	0
02472p.tdc	276	2585	18	46	225	442	94	40	3827	43	21	43	3	10	22	1370
02473p.tdc	1399	3671	29	37	60	1042	1172	267	9826	89	39	80	4	26	79	6964
02474p.tdc	610	6865	45	41	494	1636	533	148	9730	82	44	119	6	17	145	8091
02475p.tdc	822	4571	17	43	216	257	996	151	3061	38	7	26	0	10	71	2895
02476p.tdc	0	5	0	0	0	5	0	0	0	0	0	0	0	0	2	262
02477p.tdc	568	3441	18	24	55	3088	886	95	6983	58	5	59	3	22	49	3362
02478p.tdc	588	4889	13	35	71	1642	655	118	5620	50	13	145	8	19	44	4125
02479p.tdc	652	4781	21	18	81	309	579	165	7002	80	5	111	2	10	58	4101
02480p.tdc	1560	14463	116	163	294	1118	1392	533	27775	258	403	317	16	112	4	3196
02481p.tdc	1108	5210	37	71	329	2974	957	214	10031	90	96	156	10	35	1	1005
02482p.tdc	212	2632	26	44	87	681	209	60	4413	42	31	60	2	28	1	656
02483p.tdc	261	3702	24	35	135	878	304	90	6311	72	79	86	6	71	8	1062
02484p.tdc	72	1417	6	5	66	50	60	16	1256	12	0	24	2	5	15	3290
02485p.tdc	456	2641	26	32	78	675	310	77	5310	55	143	57	5	30	11	1102
02486p.tdc	108	2310	26	18	44	566	177	56	4272	34	29	60	1	8	8	1097
02487p.tdc	67	48	2	2	106	103	11	228	121	17	32	3	3	26	0	18
02488p.tdc	1268	7174	41	71	267	552	1057	372	13237	117	186	141	5	27	24	7423
02489p.tdc	1470	10737	73	104	544	4837	1435	549	16754	160	77	171	5	43	77	2312
02490p.tdc	101	309	1	0	19	59	62	17	476	4	3	6	0	2	9	307
02491p.tdc	319	2027	9	10	115	648	354	63	2359	17	6	35	3	12	42	1755
02492p.tdc	409	2779	32	50	50	146	110	106	3686	83	85	58	5	28	120	6425
02493p.tdc	272	943	1	0	9	55	70	26	1389	8	0	32	3	5	130	8061
02494p.tdc	0	0	0	0	0	0	0	0	0	0	0	0	3	0	74	3169
02495p.tdc	0	3	0	0	0	0	0	0	0	0	0	0	3	0	54	1205

University of Cape Town

APPENDIX E: XPS Spectra and interpretation for each of the platinum and palladium sulphide, arsenide and telluride mineral species.

The full set of spectra are attached for each sample including selected curve fitting for Cu, Te, Bi, Pt, S, O, C signals.

Note in the C 1s spectra for each sample that the charge compensation can be different on each surface. The C 1s peak should be referenced to uncharged hydrocarbon at 284.8 eV and all other spectra for the sample corrected for this shift.

Sample NS 144: Cooperite PtS.

NS144-1. Synthetic water conditioning.

- The survey spectrum shows Pt, S, O and C with a **S/Pt ratio close to 1.5**. There also appears to be considerable adsorbed (or impurity) **Mg ion surface concentration** on this sample. The peak near 50 eV is difficult to attribute to any other species and corresponds closely to the Mg 2p BE. **Hence, the PtS may specifically adsorb Mg^{2+} from synthetic water**. Similar evidence for measurable Na, Ca, bicarbonate, Cl, and nitrate ion concentrations could not be found.
- The C 1s adsorbed hydrocarbon signal is at 282.3 eV.
- The oxygen concentration on this surface is relatively low suggesting only **limited oxidation.** This is consistent with the S 2p region which does not show any significant sulfate speciation near 168 eV.
- The S 2p spin-orbit components (doublet) are not consistent with a single species. The $2p_{3/2}$:$2p_{1/2}$ ratio should be 2:1 for a single species but the fit for 2 components in the figure is near 1.5:1. It therefore seems likely that more than one species is present on this surface after synthetic water conditioning and some surface reaction. This conclusion is also consistent with the S/Pt ratio of 1.5. A suggested fit is shown in the figure with the second doublet ($2p_{3/2}$ at 163.6 eV corrected) corresponding to a higher order polysulfide S_n^{2-} with n>2.
- The Pt signals is observed at 72.0 eV (corrected) corresponding to Pt(II).

NS144-2. Copper activation.

- This sample has much higher adsorbed Cu at 1.6% compared with NS 142 at 0.8%.
- **The Cu 2p region analysis shows that almost all of the copper is present as Cu(II) ions. There is no significant evidence of the Cu(II) satellite near 940 eV. Adsorption of the Cu(II) has followed the classical mechanism of local reduction with oxidation of adjacent sulfide sites.**
- **The S 2p fits now suggest a significant contribution from a polysulfide of lower order (n~3) consistent with the local oxidation of the S.** These fits are indicative only since the overall envelope is not sufficiently differentiated to be confident of the position of the second doublet.
- There is no observable change to the Pt or O signals.

University of Cape Town

NS144-3. Xanthate with copper activation.

- **The Cu concentration remains at 1.6 % and there is now a distinct increase in the S concentration from 19% to 24% after xanthate addition.**
- Cu remains almost entirely as Cu(I) after xanthate addition. The Cu(I) complex is the most stable xanthate form.
- The S2p again suggests additional species in the envelope but it is not possible to discriminate the contributions from polysulfides and xanthate.
- Again, there is no change in Pt spectra but the O 1s spectrum appears broader.
- The C 1s spectrum does not provide reliable evidence of xanthate adsorption making it difficult to estimate the adsorbed concentration.

NS144-4. Xanthate without copper activation.

- These spectra are closely similar to NS144-3 but with no Cu signal and lower %S (22%) compared with copper activation.
- There may be a higher proportion of additional species (polysulfides, xanthate) compared to the main doublet but the curve fit is not reliable for this estimation.

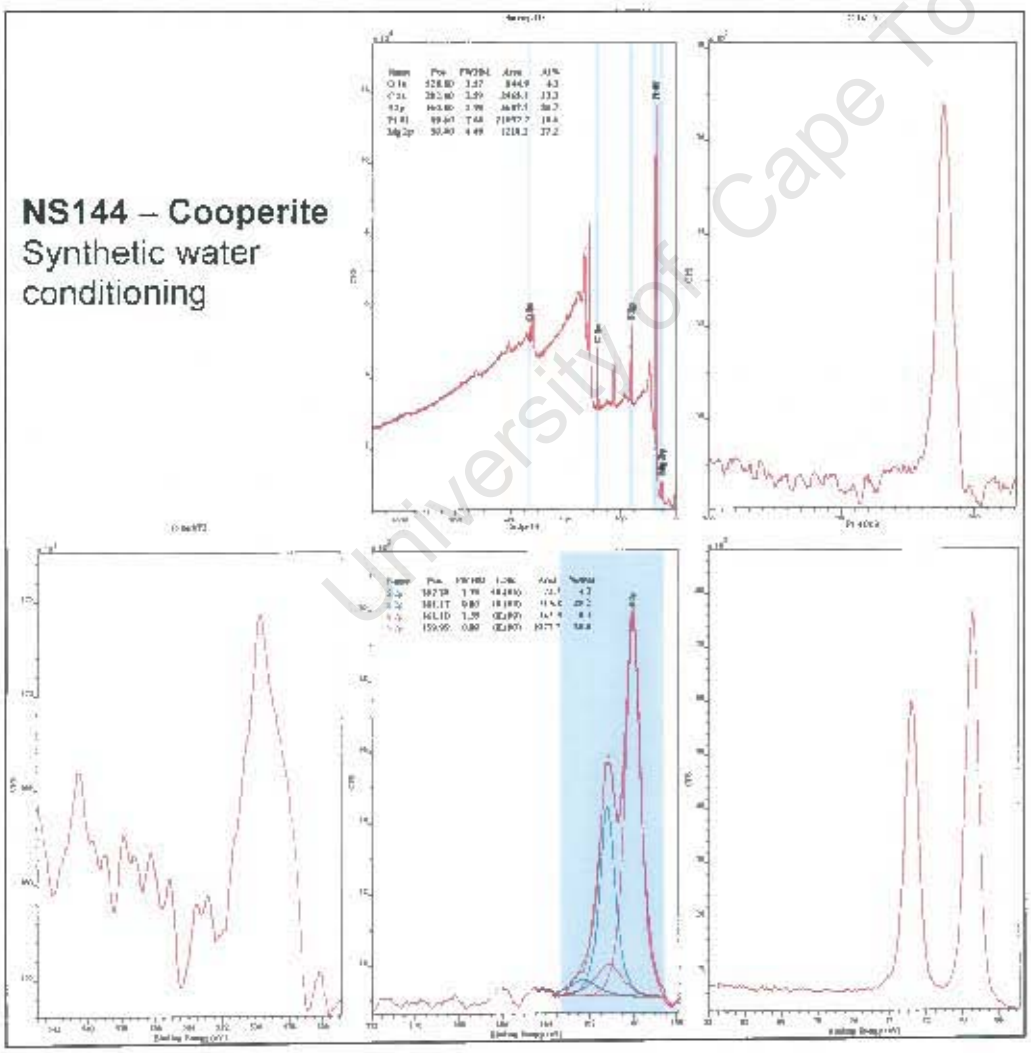

University of Cape Town

NS144 – Cooperite
Copper activation

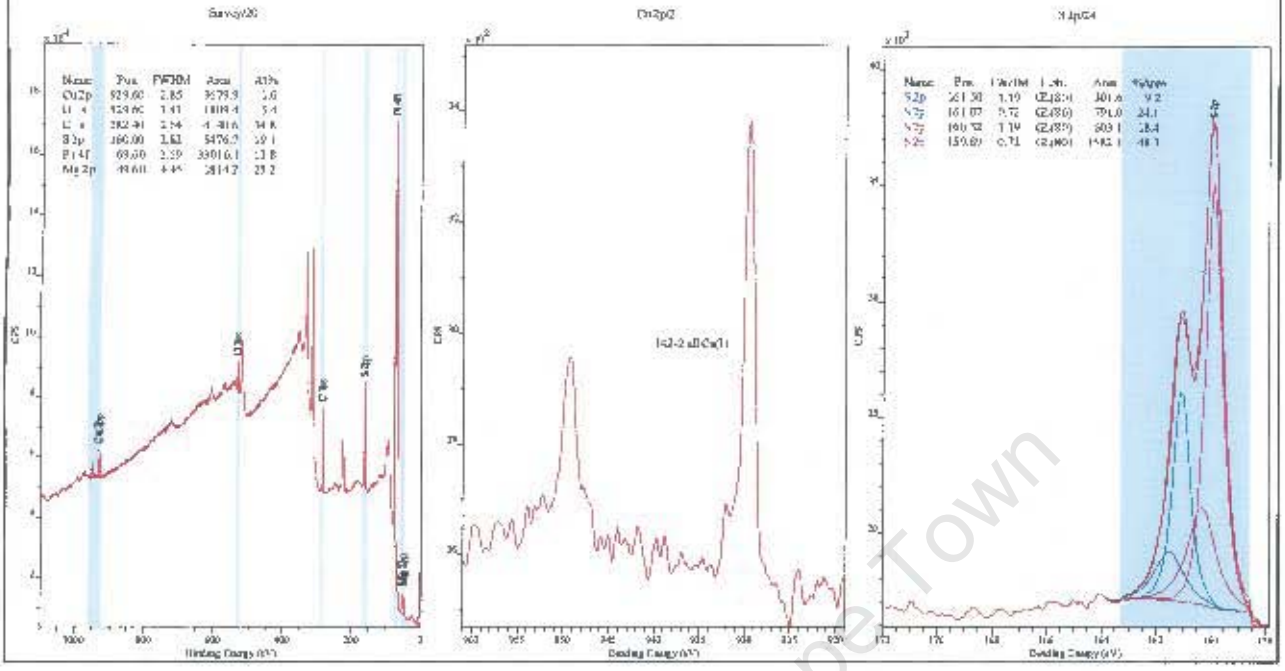

University of Cape Town

NS144 – Cooperite
Xanthate with copper activation

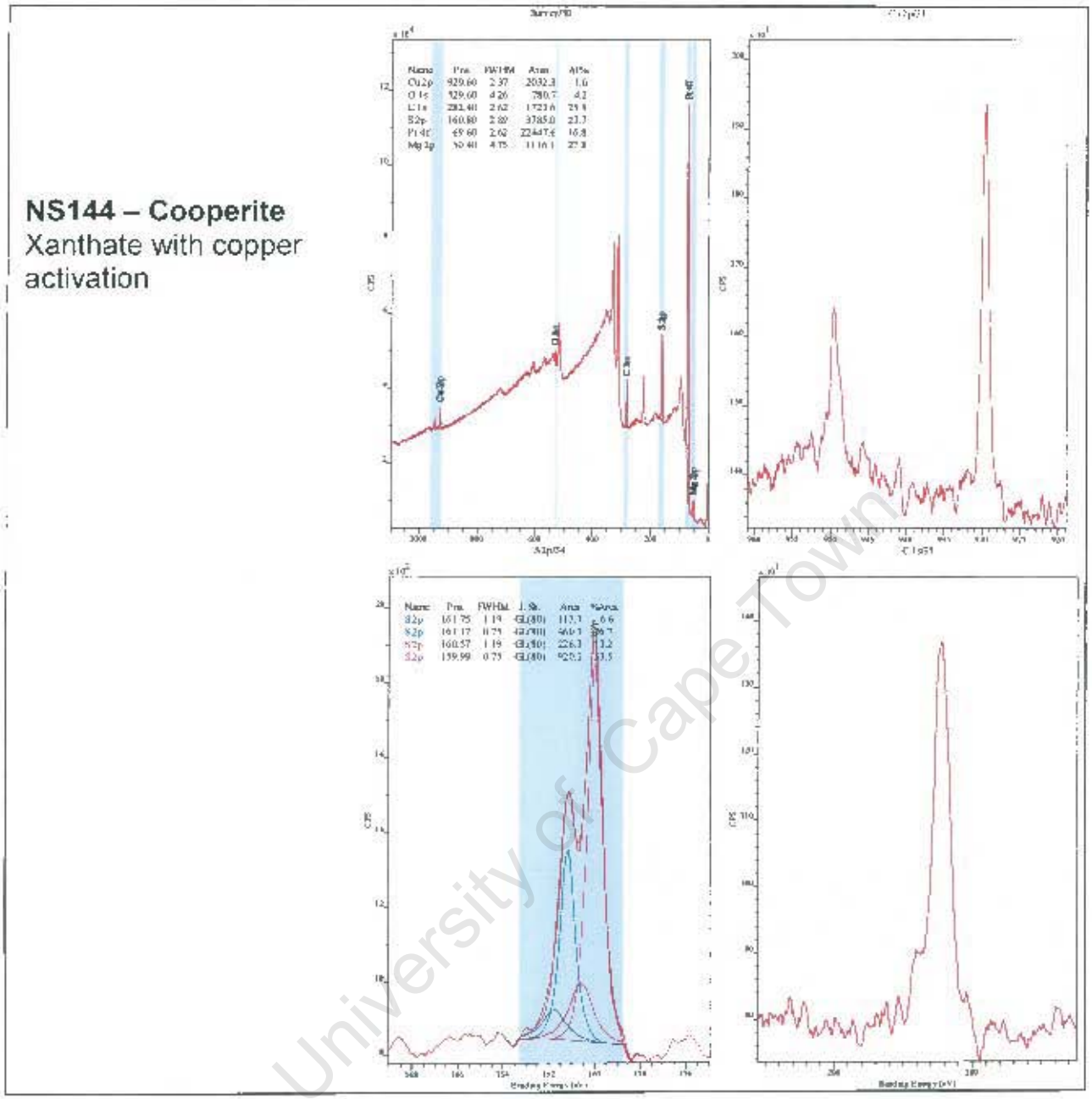

University of Cape Town

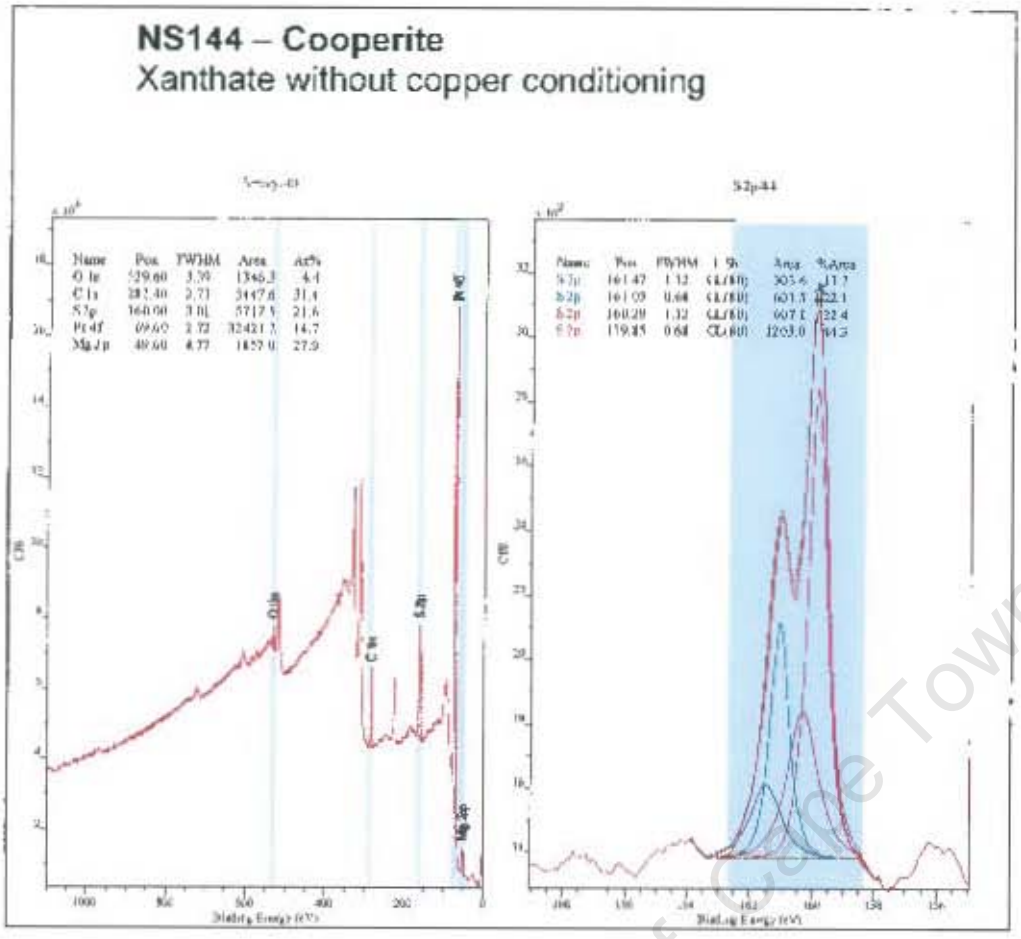

Sample NS 148: Vysotskite PdS.

NS148-1. Synthetic water conditioning.

- The survey spectrum shows Pd, S, O, C and very minor Te (0.5%) with a **S/Pd ratio close to 1.7. The surface is heavily oxidized (49% O).**
- Synthetic water formulation contains Na, Mg, Ca, bicarbonate, Cl, nitrate and sulfate ions. None of these are significantly detected. **These ions do not appear to be strongly adsorbed from the synthetic water.**
- The C 1s adsorbed hydrocarbon signal is almost uncharged at 285.0 eV.
- The oxygen appears to be largely associated with the Pd species which shows two components: unoxidised PdS at 335.7 eV (18%); and oxidized PdO at 336.6 eV (82%). The corresponding O 1s signals are dominated by the 533 eV component likely to be from a covalent PdO.
- The S 2p region gives a doublet with the lowest BE corresponding closely to a sulphide S^{2-} species (S $2p_{3/2}$ 161.5 eV). It does not show any significant sulfate speciation due to oxidation near 168 eV. The S 2p spin-orbit components (doublet) are not consistent with a single species. The $2p_{3/2}$:$2p_{1/2}$ ratio should be 2:1 for a single species but the fit for 2 components in the figure is near 1.6:1. The spacing of the S $2p_{3/2}$ to S $2p_{1/2}$ doublet should be 1.8 eV and this is not correct here or in subsequent curve fits. It

University of Cape Town

therefore seems likely that more than one species is present on this surface after synthetic water conditioning and some surface reaction. This conclusion is also consistent with the S/Pt ratio of 1.7. A suggested fit is shown in the figure with the second doublet ($2p_{3/2}$ at 163.6 eV corrected) corresponding to a higher order polysulfide S_n^{2-} with n>2.

- There may be some additional component near 164 eV corresponding to elemental sulphur.
- The minor Te is also oxidized to TeO_2-like species.

NS148-2. Copper activation.

- This sample also has relatively low adsorbed Cu at 1.0%.
- The C 1s adsorbed hydrocarbon signal is almost uncharged at 284.7 eV.
- **In contrast to PtS (100% Cu(I)), the Cu 2p region analysis of PdS shows that only 35% of the copper is present as Cu(I) ions.**
- **The S 2p fits now suggest a significant contribution from a polysulfide of lower order (n~3) with S $2p_{3/2}$ near 162.8 eV consistent with the local oxidation of the S.** These fits are indicative only since the overall envelope is not sufficiently differentiated to be confident of the position of the second doublet.
- There is no observable change to the Pdt or O signals.

NS148-3. Xanthate with copper activation.

- **The Cu concentration remains at 1.1 %.**
- The C 1s adsorbed hydrocarbon signal is slightly charged at 285.1 eV.
- Cu becomes predominantly Cu(I) (78%) after xanthate addition. The Cu(I) complex is the most stable xanthate form.
- The S2p again suggests additional species in the envelope but it is not possible to discriminate the contributions from polysulfides and xanthate.
- **The Pd signal shows a significant increase in the PdS component from 12 to 31% of the signal possibly indicating surface cleaning by the adsorbing xanthate.**
- Although there is an increase in C concentration, the C 1s spectrum does not provide reliable evidence of xanthate adsorption making it difficult to estimate the adsorbed concentration.

NS148-4. Xanthate without copper activation.

- These spectra are closely similar to NS148-C but with no Cu signal and only slightly lower %S compared with copper activation.
- There may be a higher proportion of additional species (polysulfides, xanthate) compared to the main doublet but the curve fit is not reliable for this estimation.
- **The Pd signal shows a less significant increase in the PdS component from 12 to 18 % of the signal cf. 31% for NS 148-C.** This may indicate less surface cleaning due to less xanthate adsorption.

University of Cape Town

NS148 – Vysotskite
Synthetic water conditioning

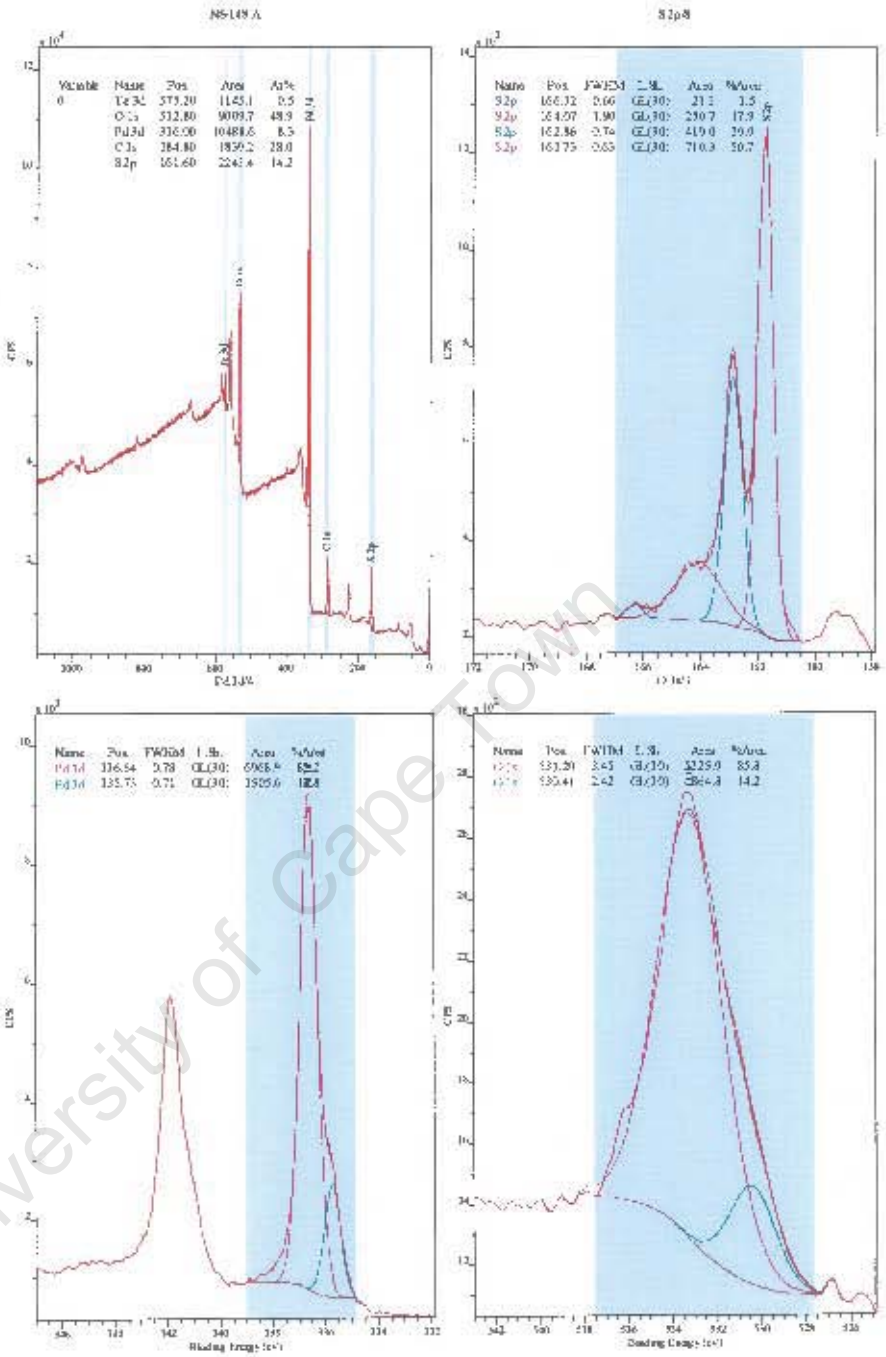

University of Cape Town

NS148 – Vysotskite
Copper activation

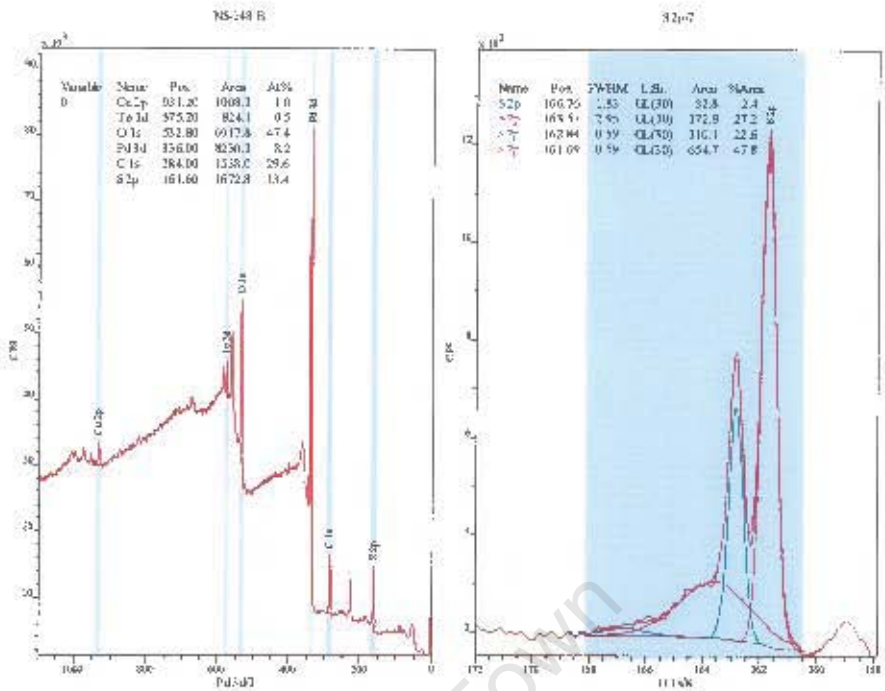

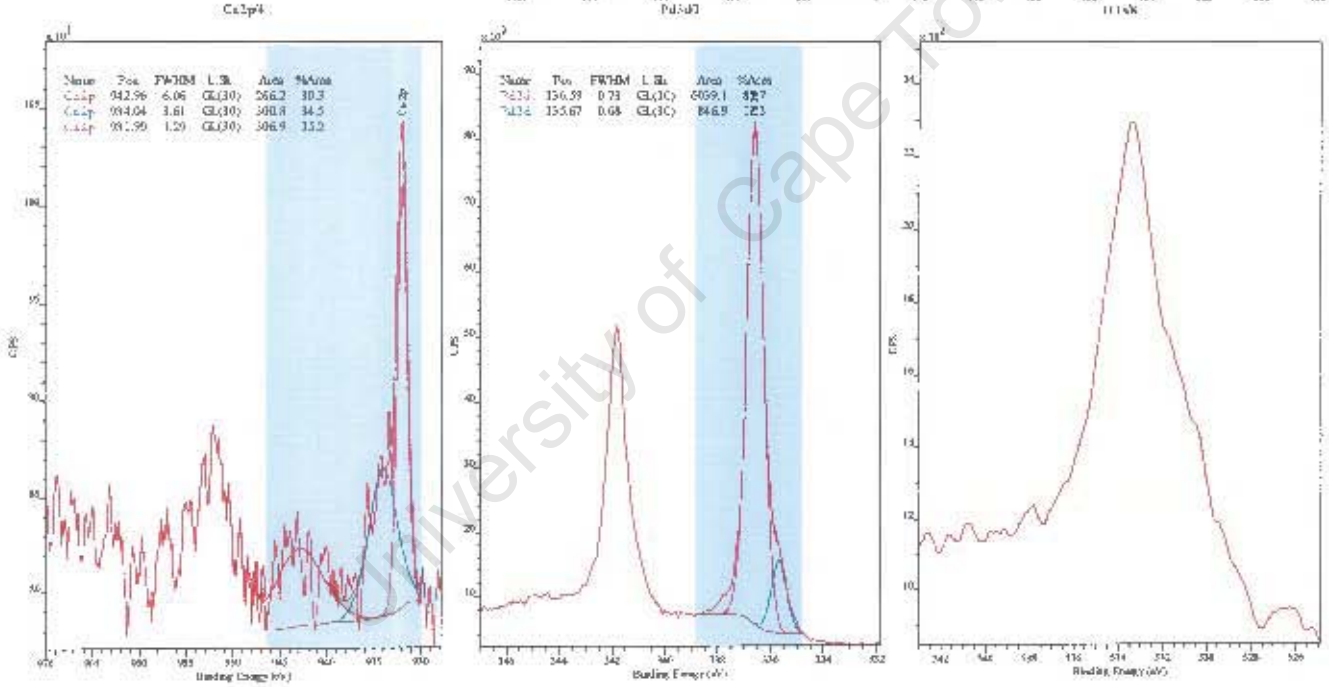

University of Cape Town

NS148 – Vysotskite
Xanthate with copper activation

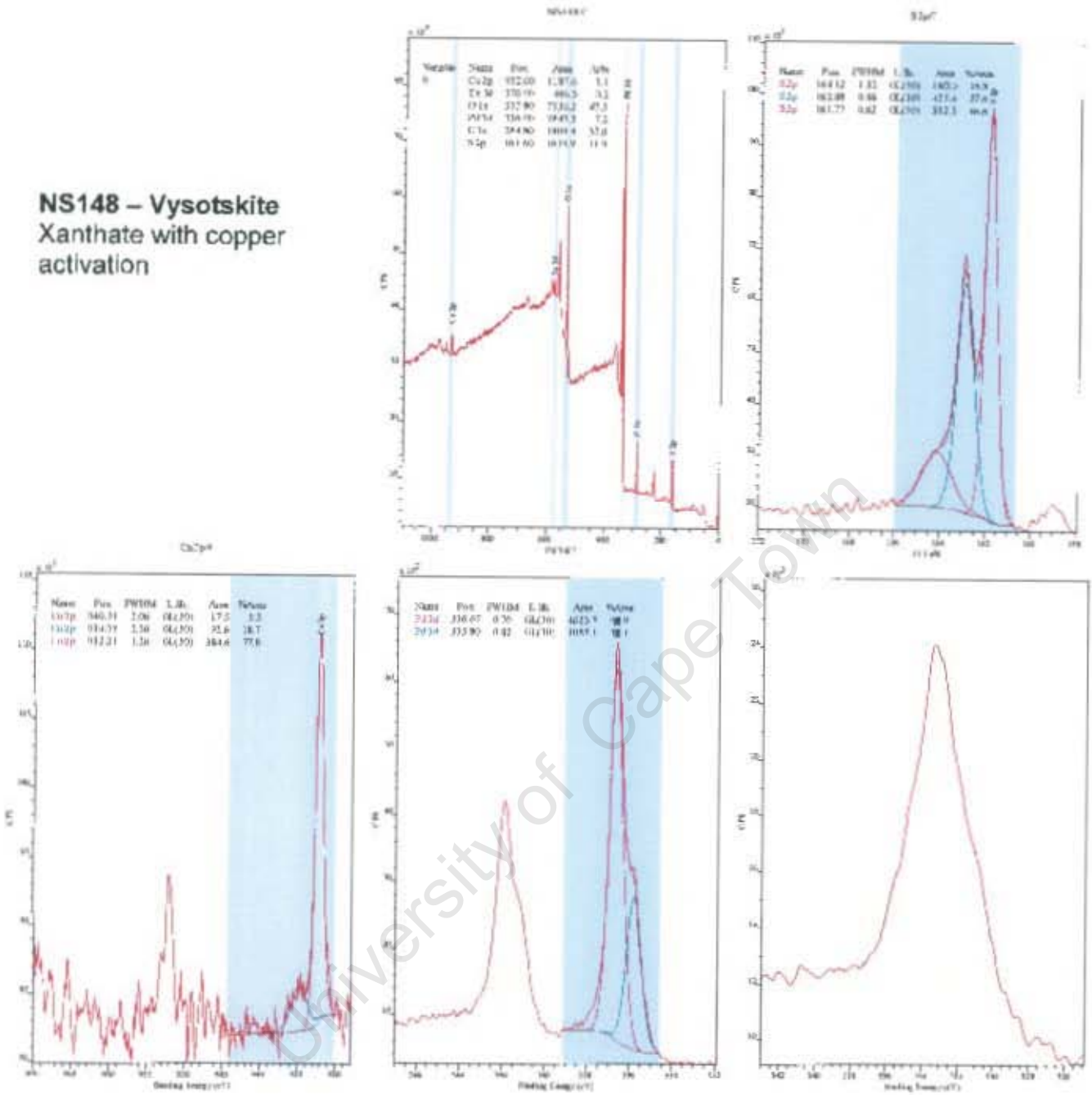

University of Cape Town

NS148 – Vysotskite
Xanthate without copper activation

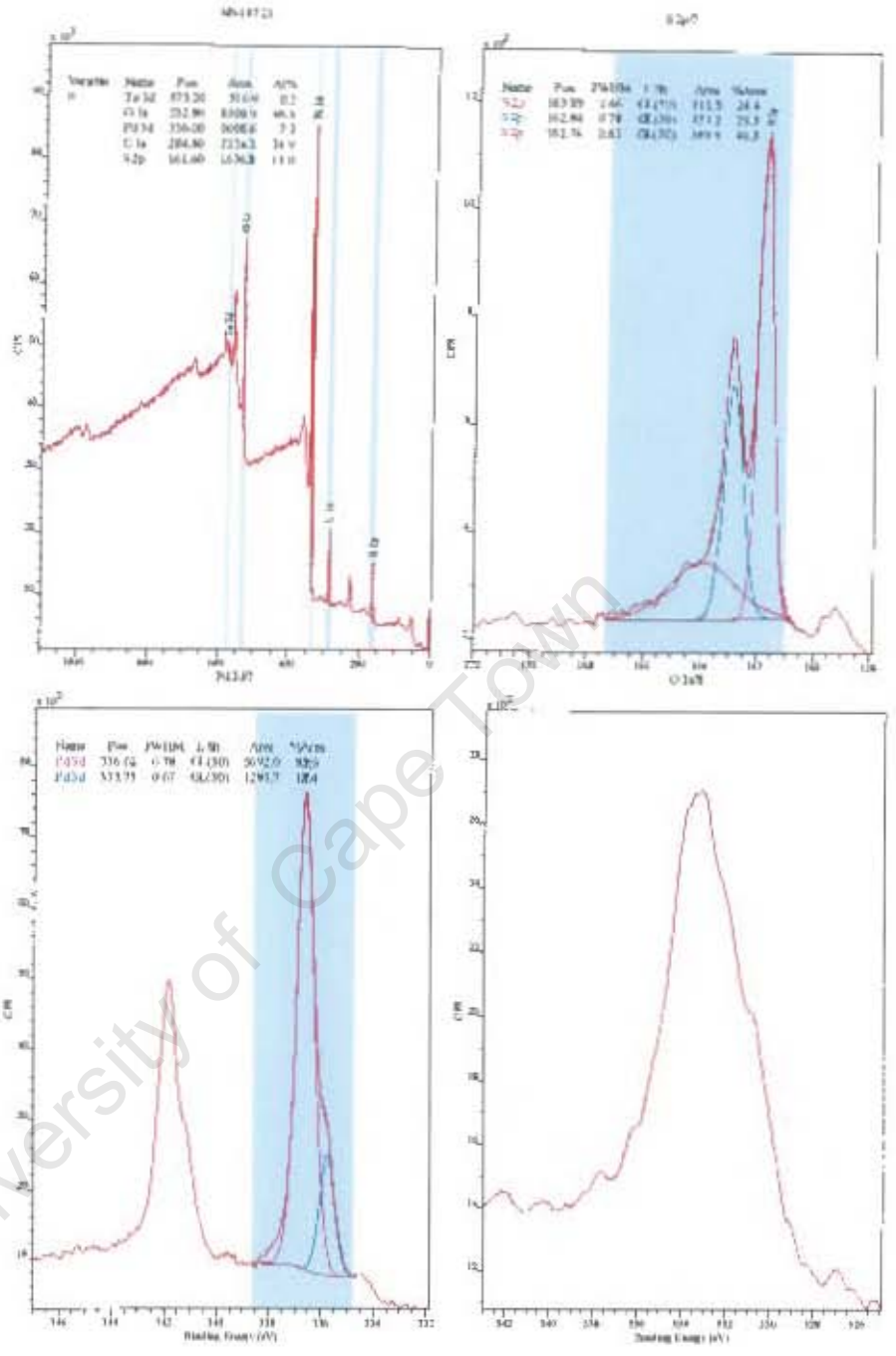

NS145-Sperrylite $PtAs_2$.

NS145-2. Synthetic water conditioning.

- This Amandelbult water formulation contains Na, Mg, Ca, bicarbonate, Cl, nitrate and sulfate ions. None of these are significantly detected although the S of sulfate is difficult to resolve from the Bi signals near 164eV. **These ions do not appear to be strongly adsorbed.**
- There is no significant change in atomic %s or As or C signals.

University of Cape Town

- There may be some minor shift in Pt intensities to the lower BE Pt metal signals and to lower BE O 1s signals possibly due to removal of fine adherent particles after dry grinding.

NS145-3. Copper activation.

- Copper is detected in the survey spectrum at 3.5%. This is a relatively high %; 1.5% is usually sufficient for effective copper activation in plant sample.
- The Cu 2p region shows that the large majority of this copper is as Cu(II). The curve fit gives a ratio **of Cu(II):Cu(I) of ~5:1**. Hence, the formation of precipitated, probably colloidal, $Cu(OH)_2$ is the main species identified on the sperrylite surface.
- There appears to be a further minor increase in the low BE Pt(0) signals and narrowing of the O 1s signal to lower BE.
- There are no significant changes in the C, As or Bi (S) regions.

NS145-4. Xanthate addition after copper activation.

- Copper is still present at 3.2% of the surface composition.
- **The chemical state of the copper has changed dramatically from >80% Cu(II) to 100% Cu(I) as seen in the Cu 2p spectra.**
- There are no significant changes in the Pt or As spectra, i.e. no significant reaction with the copper ions.
- There is now a significant addition to the S 2p region near 164eV (overlapped with the Bi impurity) when compared with this region before xanthate addition.
- There are also additional intensity increase in higher BE C 1s near 287eV (i.e. –C-O-) and O 1s near 532.6eV both corresponding to components of the xanthate molecule. **Strong adsorption of xanthate as Cu(I)xanthate species can be confirmed by these changes.**

NS145-5. Xanthate addition without copper activation.

- Comparison of the spectra with NS145-4 shows that there are additions to the S 2p, O 1s and C 1s regions but that these intensity increases are not as large. A visual estimate suggests ~60% but this would require more extensive high resolution measurement and advanced curve fitting to confirm.
- There is again no significant change in Pt or As signals.

University of Cape Town

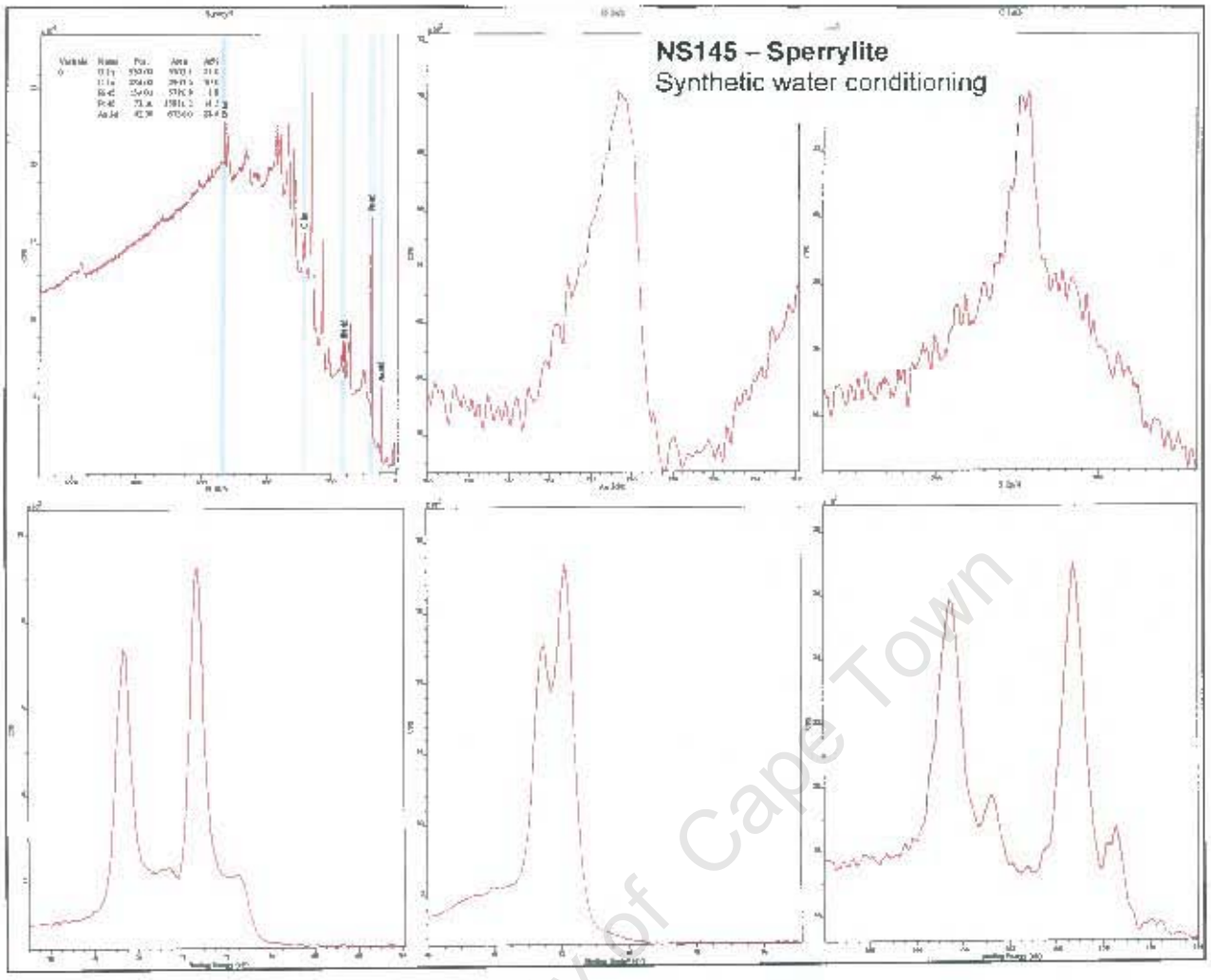

University of Cape Town

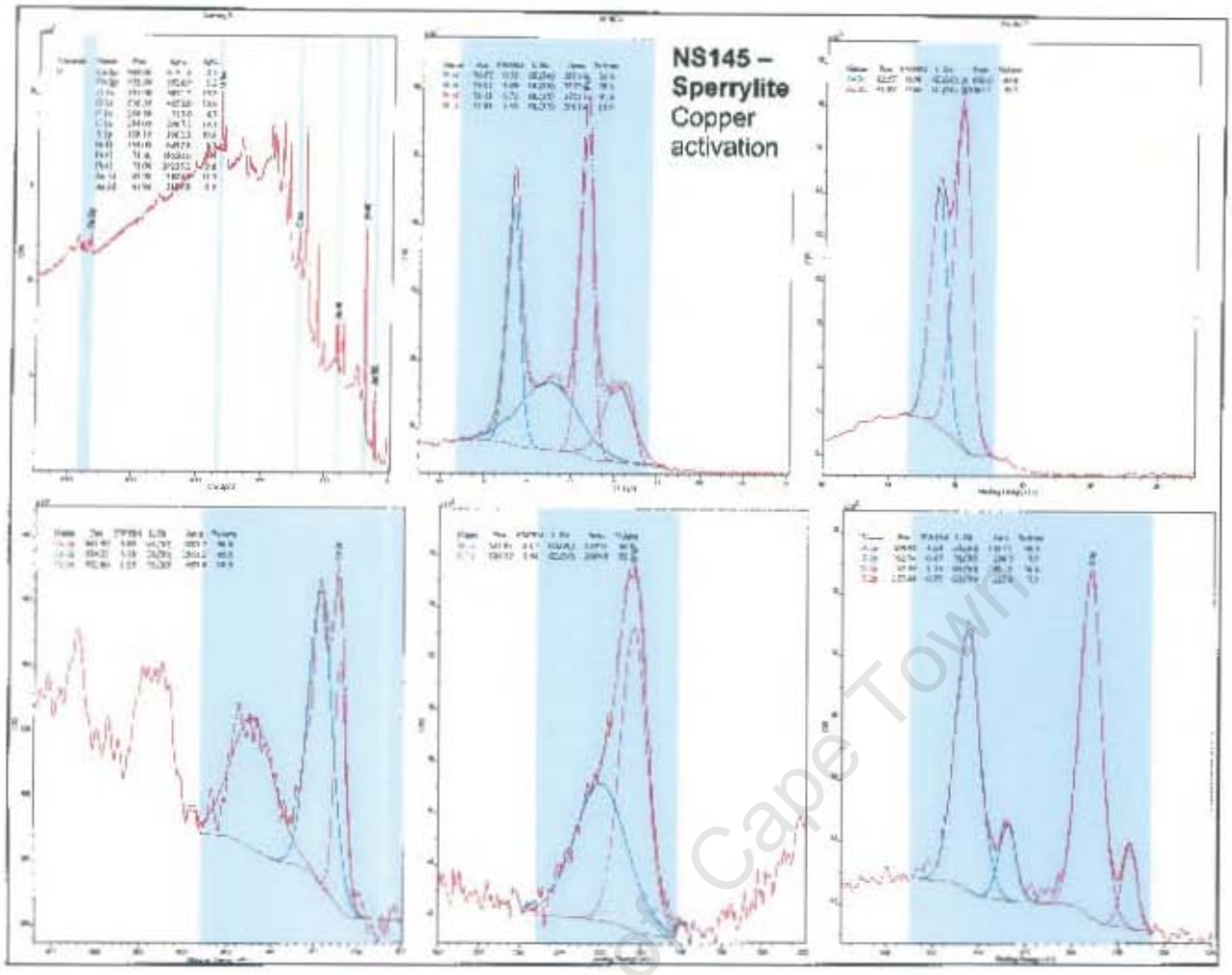

University of Cape Town

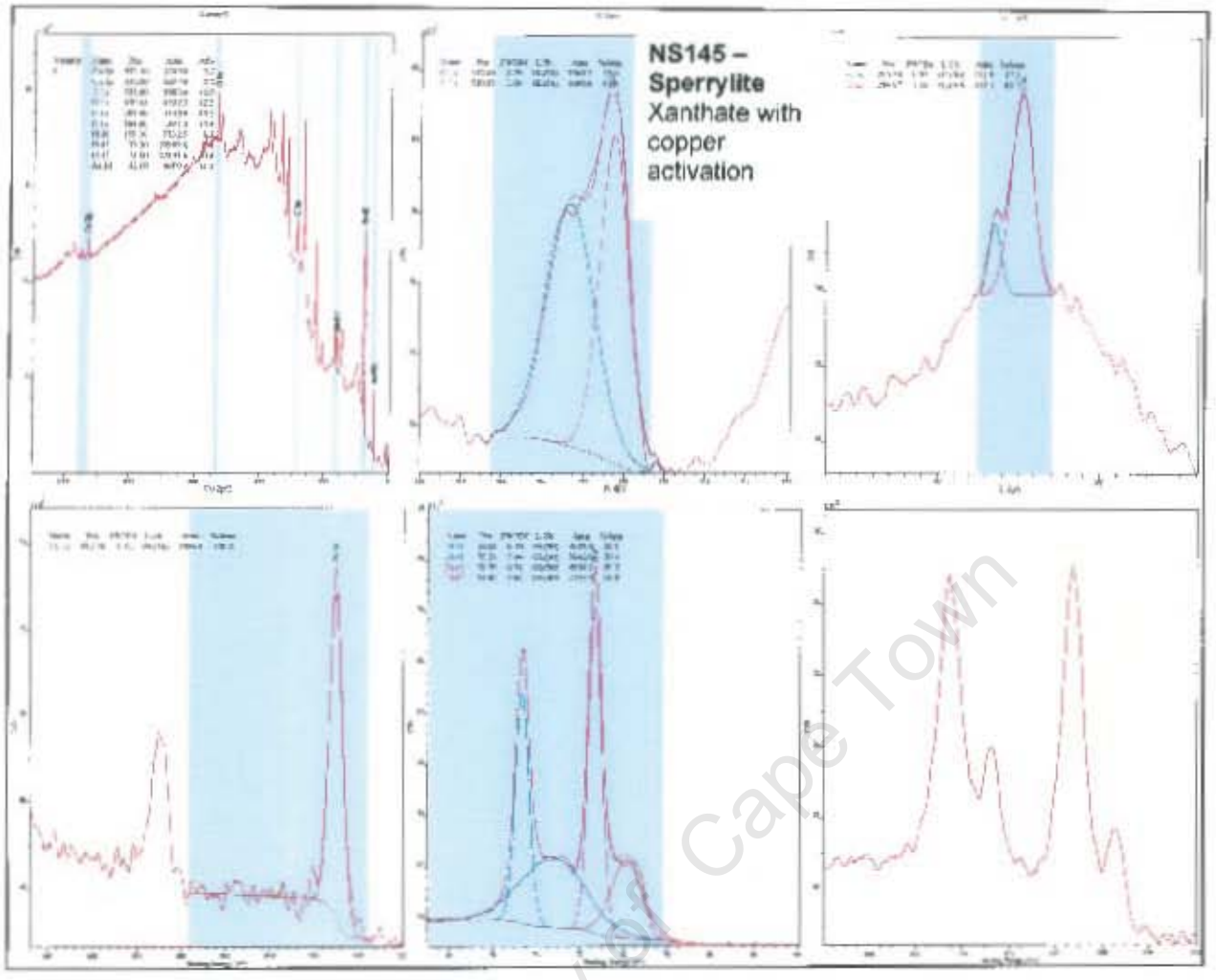

University of Cape Town

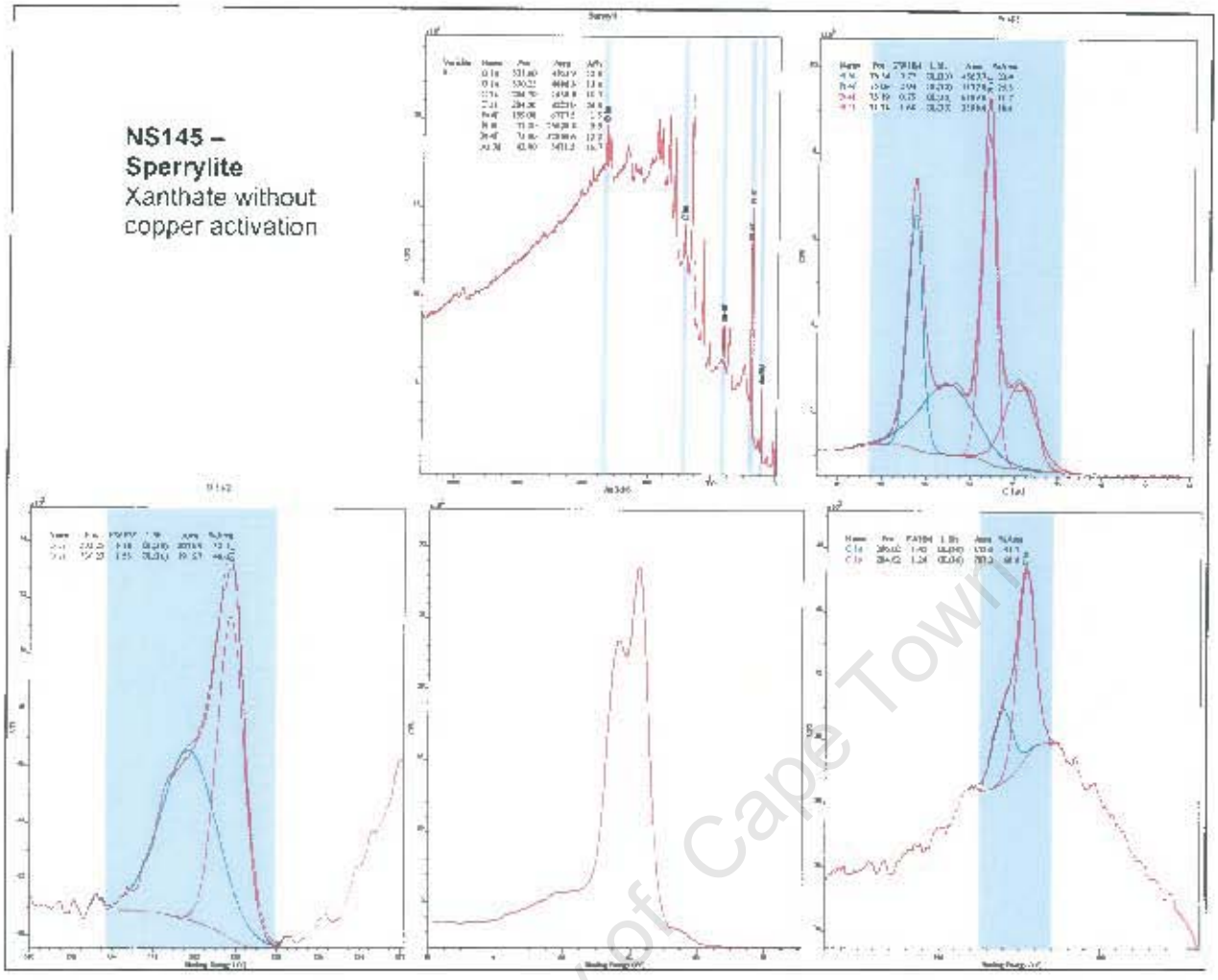

NS146-Sperrylite $PtAs_2$

NS146-2. Synthetic water conditioning..

- There is some adsorbed Na and fewer hydrocarbons possibly due to minor differences in washing effectiveness for this sample. There may also be some minor increase in the S 2p region due to adsorbed sulfate for the same reason.
- The same increase in low BE Pt signals is observed as for NS145-2

NS146-3. Copper activation.

- This sample has higher adsorbed Cu at 4.6%.
- **The majority of the copper is still present as Cu(II) ions but the Cu(II):Cu(I) ratio in this sample is lower at ~2:1** from the curve fit suggesting some initial reaction with the surface. However, this may be due to charging of the colloidal Cu(OH)2 precipitates, moving their BEs to higher values near 934eV, with some uncharged Cu(II) adsorbed contributing the peak near 932eV. Both forms would contribute to the shake-up satellite near 942eV. Resolution of this possibility would require more analysis.
- There is again a minor increase in the lower BE Pt components and possibly in the S 2p region but no observable change in the As states.

University of Cape Town

NS146-4. Xanthate with copper activation.

- There is distinct addition to the S 2p, O 1s and C 1s regions as for NS145-4 showing strong adsorption of xanthate.
- Cu is present at 3.7% and again almost entirely as Cu(I) after xanthate addition. There may be some minor (<5%) contributions from Cu(II) in the Cu 2p spectrum near 934 and 942eV but it is difficult to resolve this from the background.
- Again, no change in Pt or As spectra.

NS146-5. Xanthate without copper activation.

- These spectra are closely similar to NS145-5 with distinct but lower xanthate adsorption compared with copper activation.

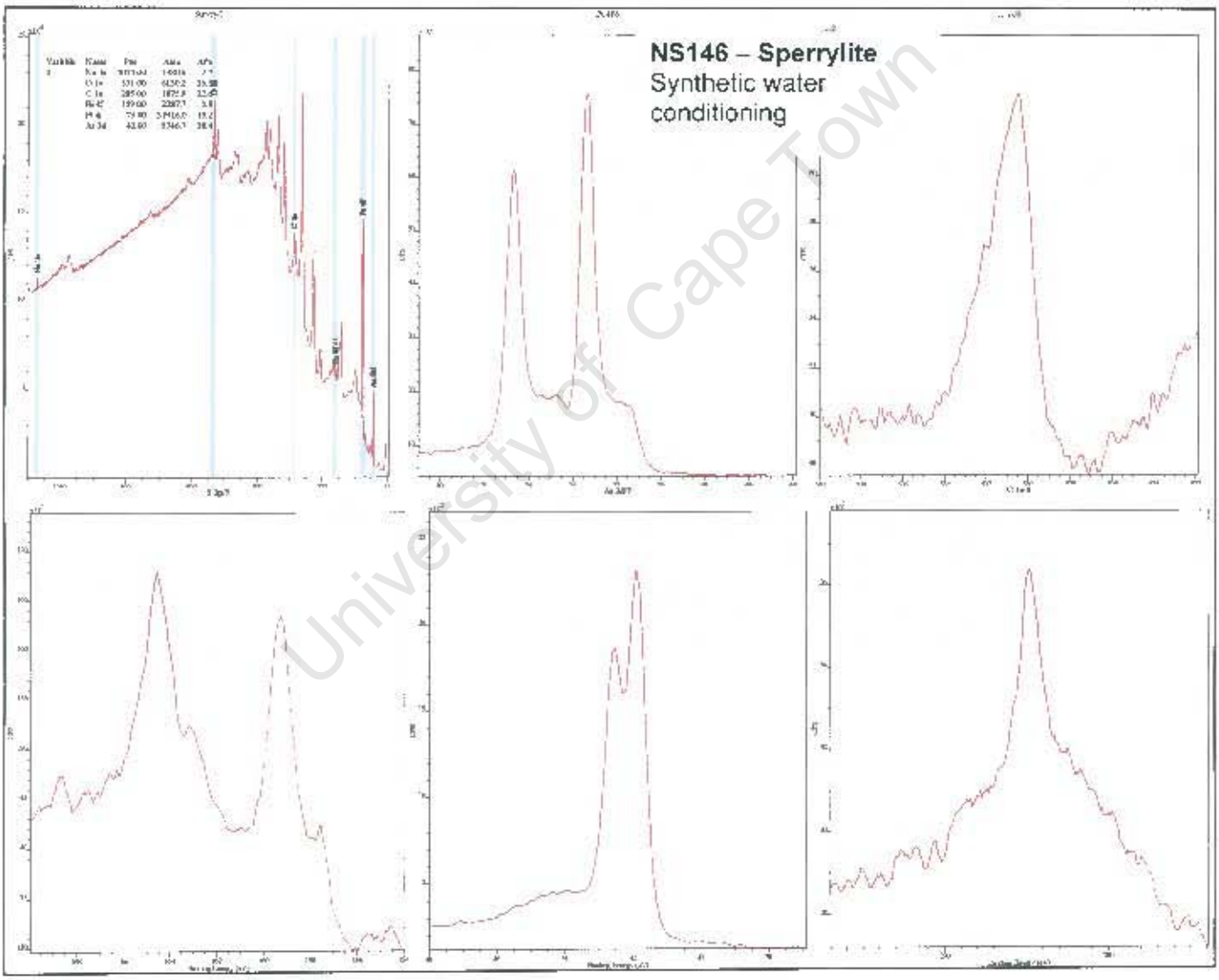

University of Cape Town

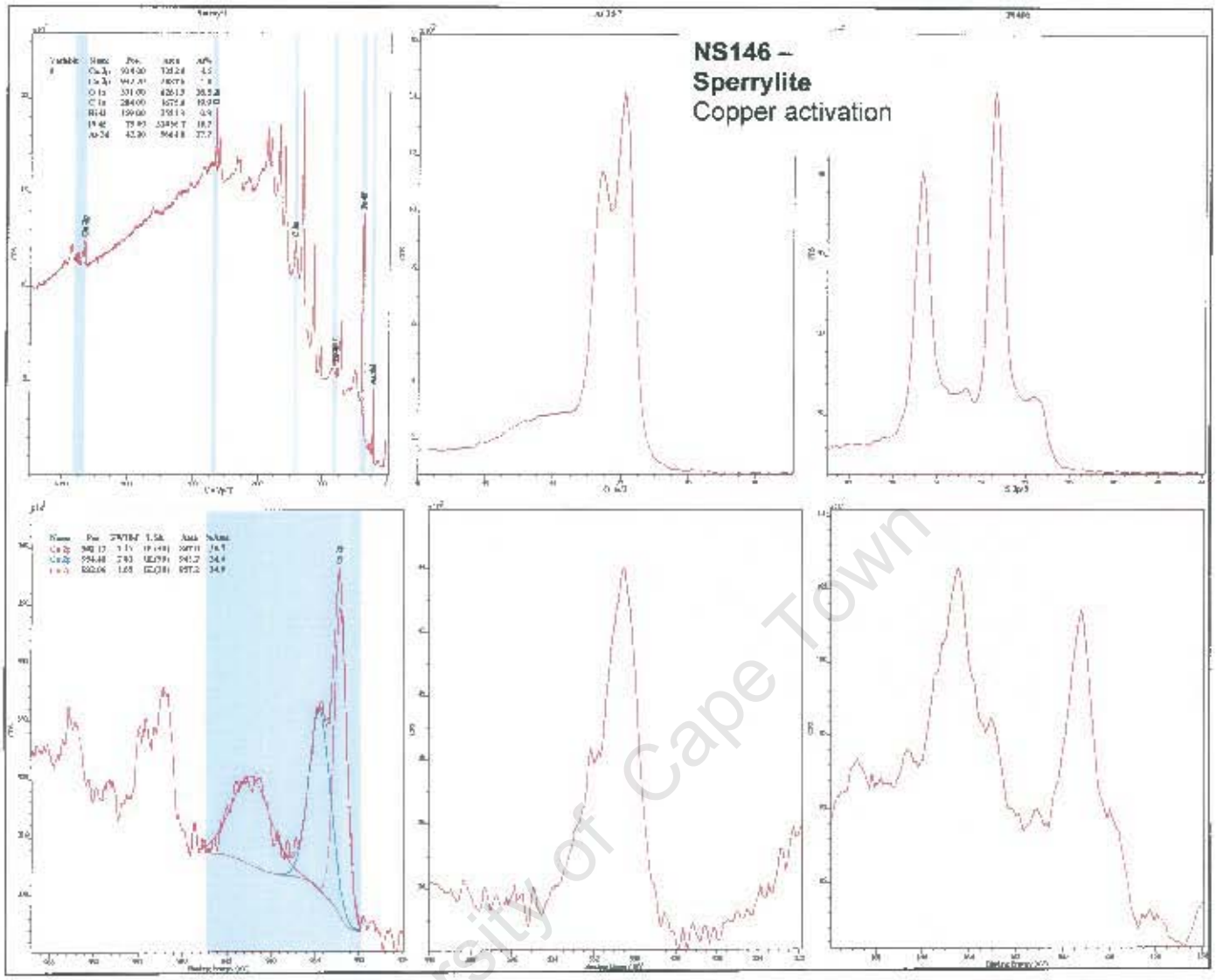

University of Cape Town

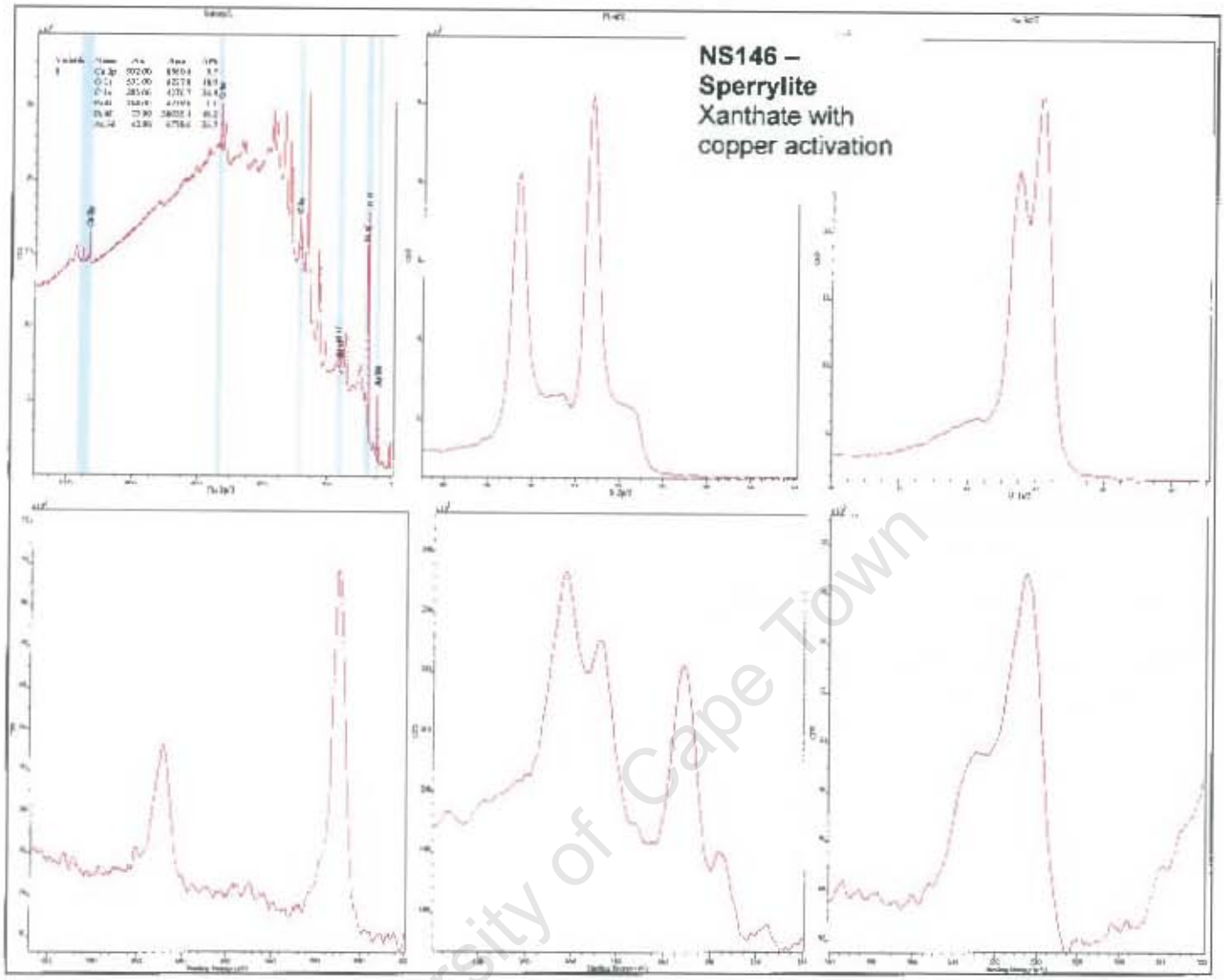

University of Cape Town

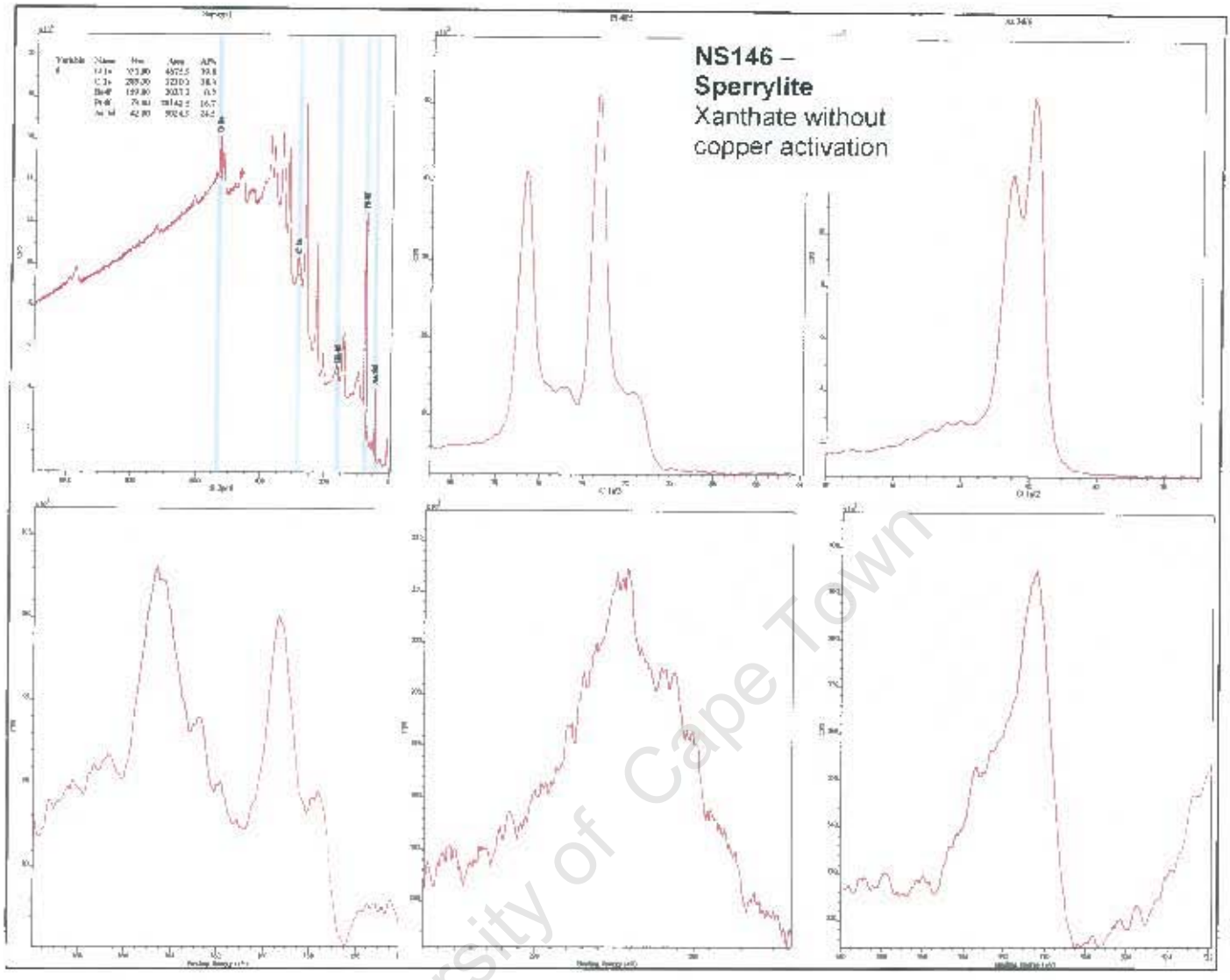

Sample NS 147: synthetic Pd_2As.

In this sample, the survey concentrations are likely to have underestimated the Pd concentrations by ~10% due to overlapping signals. There are also unassigned signals near 400 eV (N?), 433 and 460 eV.

NS147-1. Synthetic water conditioning.

- The survey spectrum shows Pd, As, O, C, minor Te (0.1%) and trace Pt with a **Pd/As ratio close to 1.3. The surface is very heavily oxidized (58% O).**
- The (Amandelbult) Standard Plant Water formulation contains Na, Mg, Ca, bicarbonate, Cl, nitrate and sulfate ions. None of these are significantly detected. **These ions do not appear to be strongly adsorbed from the synthetic water.**
- The C 1s adsorbed hydrocarbon signal is substantially overcompensated in charge correction at 283.9 eV.

University of Cape Town

- The oxidation appears to be partly associated with the Pd species which shows two components: unoxidised PdAs at 335.0 eV (16%); and oxidized PdO or $Pd(OH)_2$ at 336.6 eV (83%).
- The As 3d signal also shows oxidation with the arsenide at 41.2 overlapped with an oxidized species (As(I)?) near 42.3 eV (72%) and an oxidized As(III) species at 44.1 eV (28%) corresponding to AsO_2^- or As_2O_3.
- The corresponding O 1s signal has both oxide/hydroxide component near 530.4 eV (56%) and a 532.1 eV component (44%) likely to be from covalent PdO, AsO_2^- or As_2O_3.

NS147-2. Copper activation.

- This sample has relatively low adsorbed Cu at 1.2%.
- The C 1s adsorbed hydrocarbon signal is again substantially overcompensated in charge correction at at 283.8 eV.
- **As with PtS, the Cu 2p region analysis of this sample shows that only 13% of the copper is present as Cu(I) ions.**
- **The Pd now appears to be entirely oxidized PdO or $Pd(OH)_2$ at 336.6 eV.**
- The As 3d signal also shows more oxidation with less arsenide and oxidized As(I) at 42.3 eV (43%), and a very broad peak possibly including both the oxidized species at 44.1 eV (28%), corresponding to AsO_2^- or As_2O_3 and a higher BE component at 45.7 eV corresponding to As(V) species.
- The corresponding O 1s signal has much less oxide/hydroxide component near 530.4 eV (12%) and much more 532.6 eV component (88%) likely to be from covalent PdO, AsO_2^- or As_2O_3.
-

NS147-3. Xanthate with copper activation.

- **The Cu concentration is reduced to 0.2% which is unlikely to be effective and is too low to reliably speciate.**
- The C 1s adsorbed hydrocarbon signal is now uncharged at 284.8 eV.
- **Nevertheless, both the S2p and S 2s regions (2.0%) again show xanthate adsorption.**
- The Pd remains entirely oxidized PdO or $Pd(OH)_2$ at 336.6 eV.
- The As 3d signal also shows more oxidation with less arsenide at 41.7 eV (28%), the oxidized species at 42.4 eV (33%) and a higher BE component at 45.2 eV corresponding to As(V) species (39%).
- The corresponding O 1s signal also has much less oxide/hydroxide component near 530.4 eV (7%) and much more 532.6 eV component (93%).

NS147-4. Xanthate without copper activation.

- These spectra are closely similar to NS147-C (but with no Cu signal) and similar 2.5%S.
- The C 1s adsorbed hydrocarbon signal is at 284.4 eV.
- The S 2p signal at 162.5 eV corresponds closely to the xanthate BE.
- The Pd remains entirely oxidized PdO or $Pd(OH)_2$ at 336.6 eV.

University of Cape Town

- The As 3d signal again shows more oxidation with less arsenide at 41.9 eV (15%), the oxidized species at 42.7 eV (27%) and a higher BE component at 45.7 eV corresponding to As(V) species (58%).
- The corresponding O 1s signal is closely similar to 147-C with much less oxide/hydroxide component near 530.4 eV (7%) and much more 532.6 eV component (93%).
- Estimates of relative S 2s concentrations could not be obtained due to overlaps in this region.

University of Cape Town

NS147 – Palladoarsenide
Synthetic water conditioning

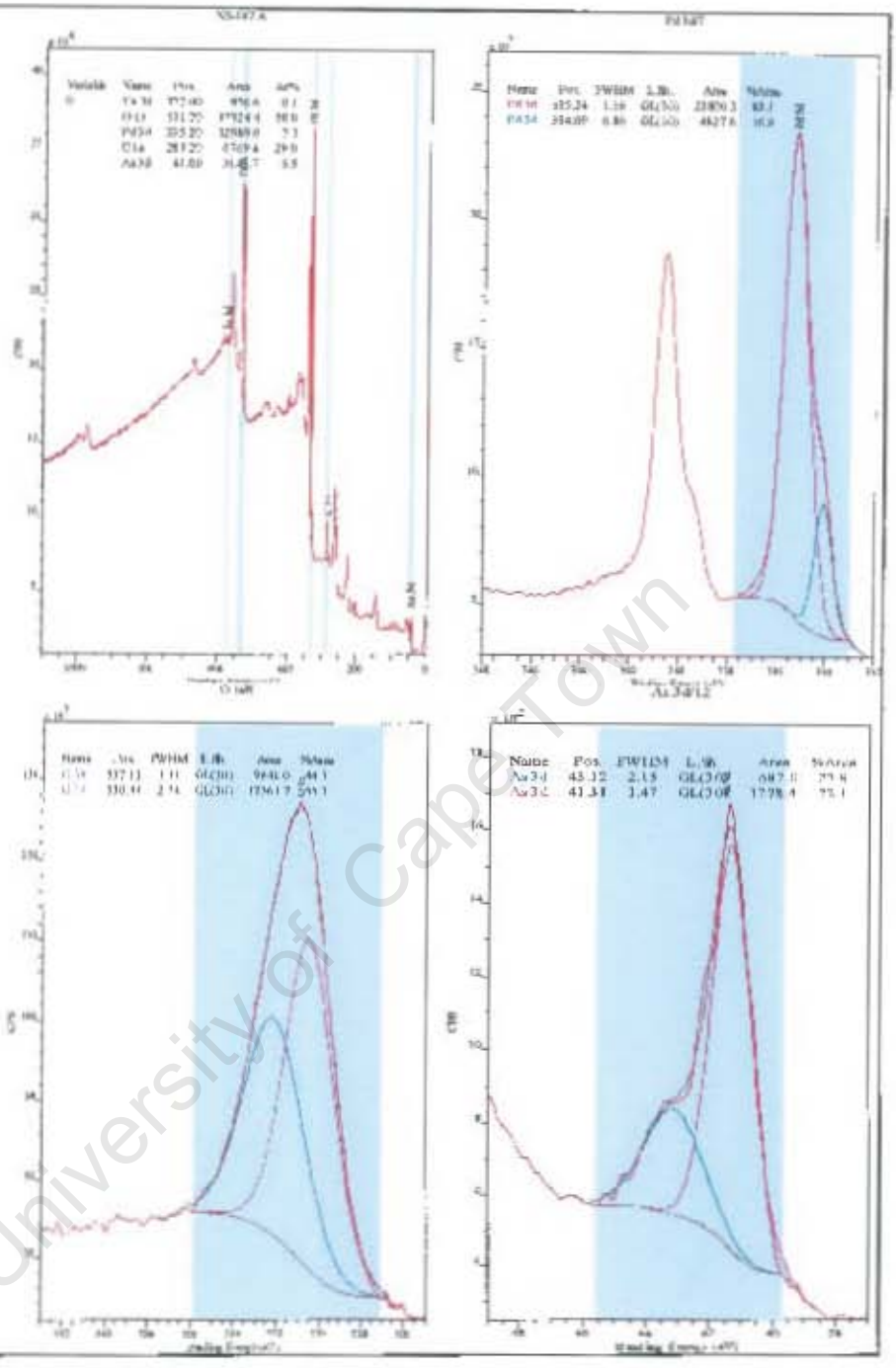

University of Cape Town

NS147 –
Palladoarsenide
Copper activation

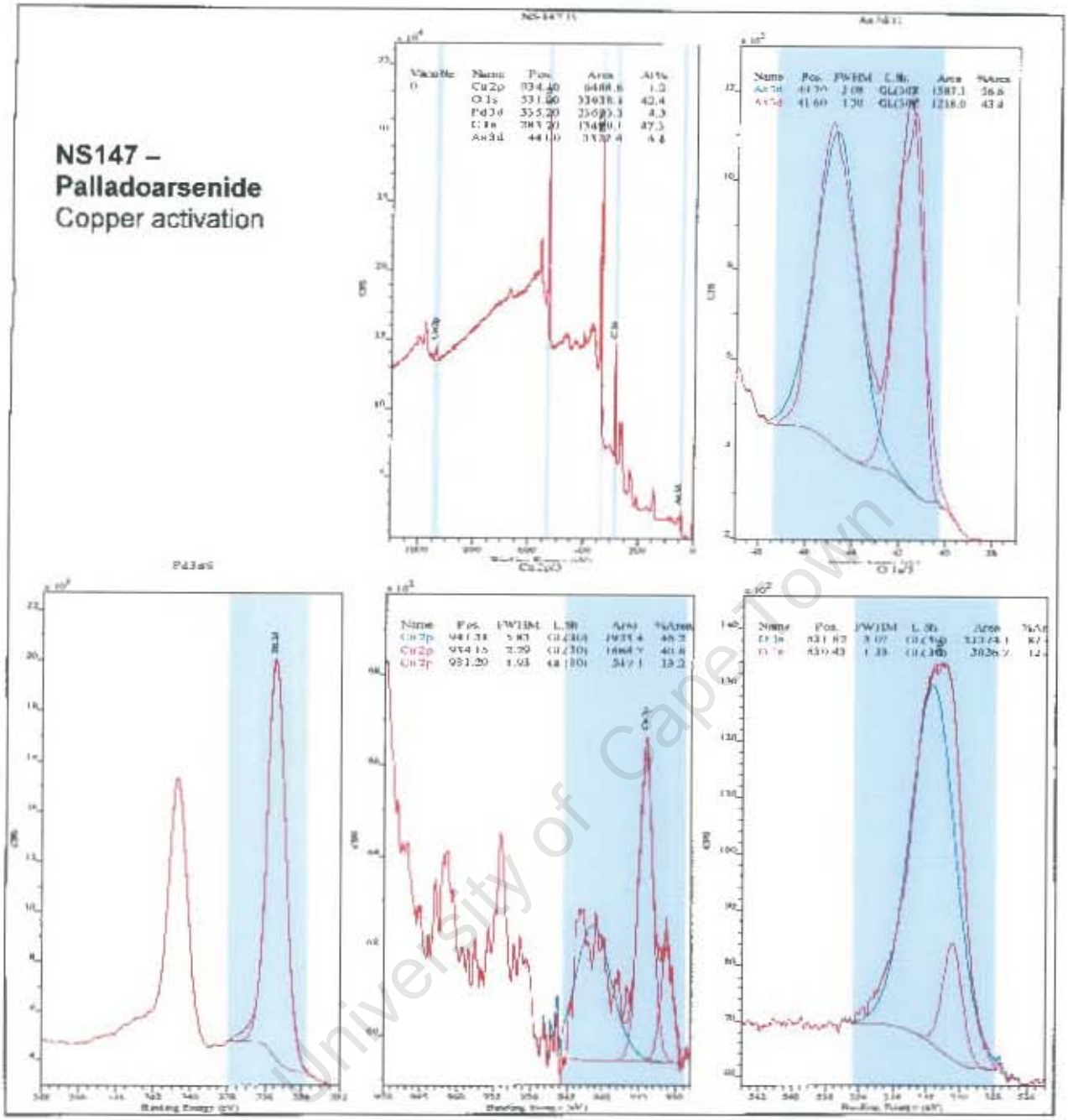

University of Cape Town

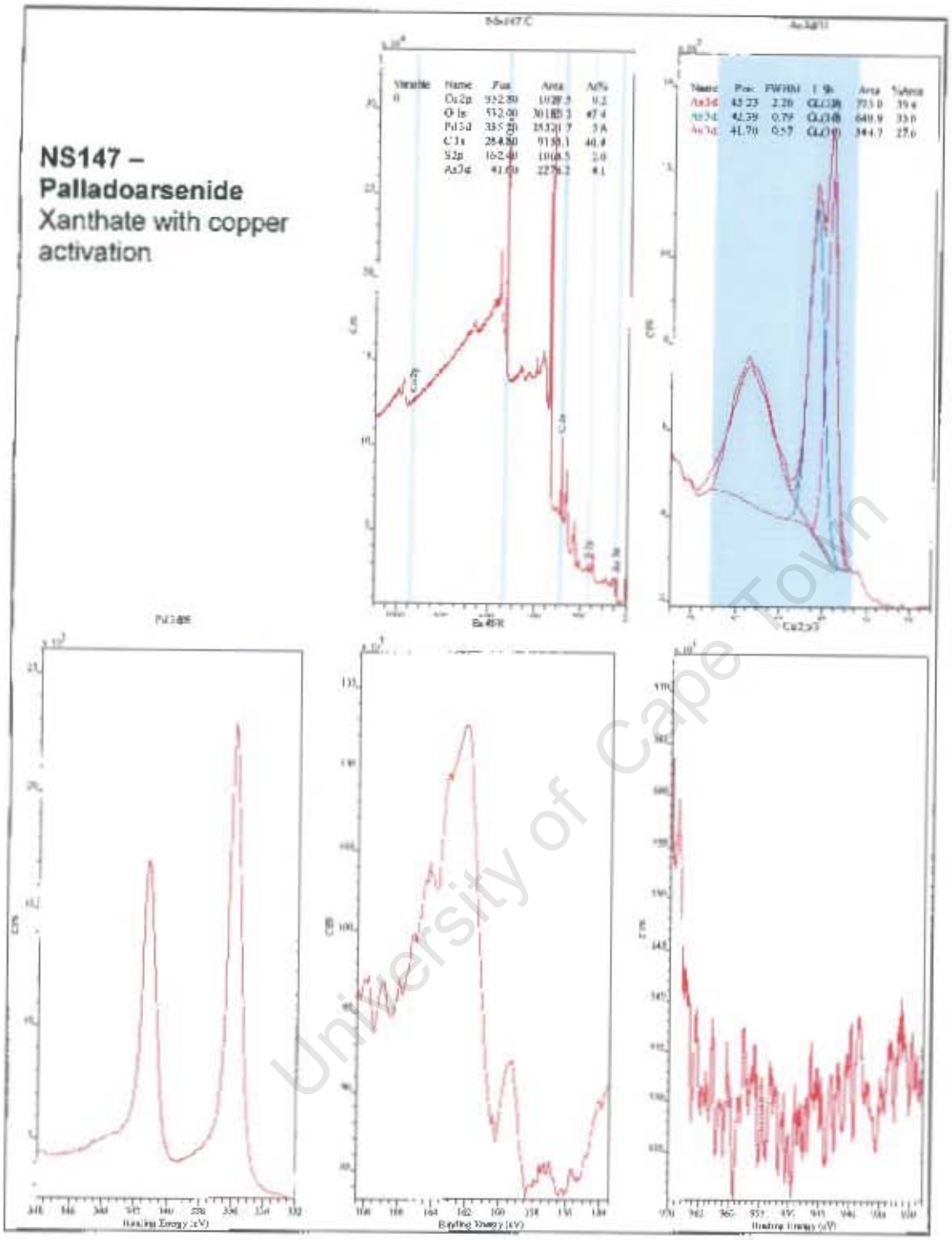

University of Cape Town

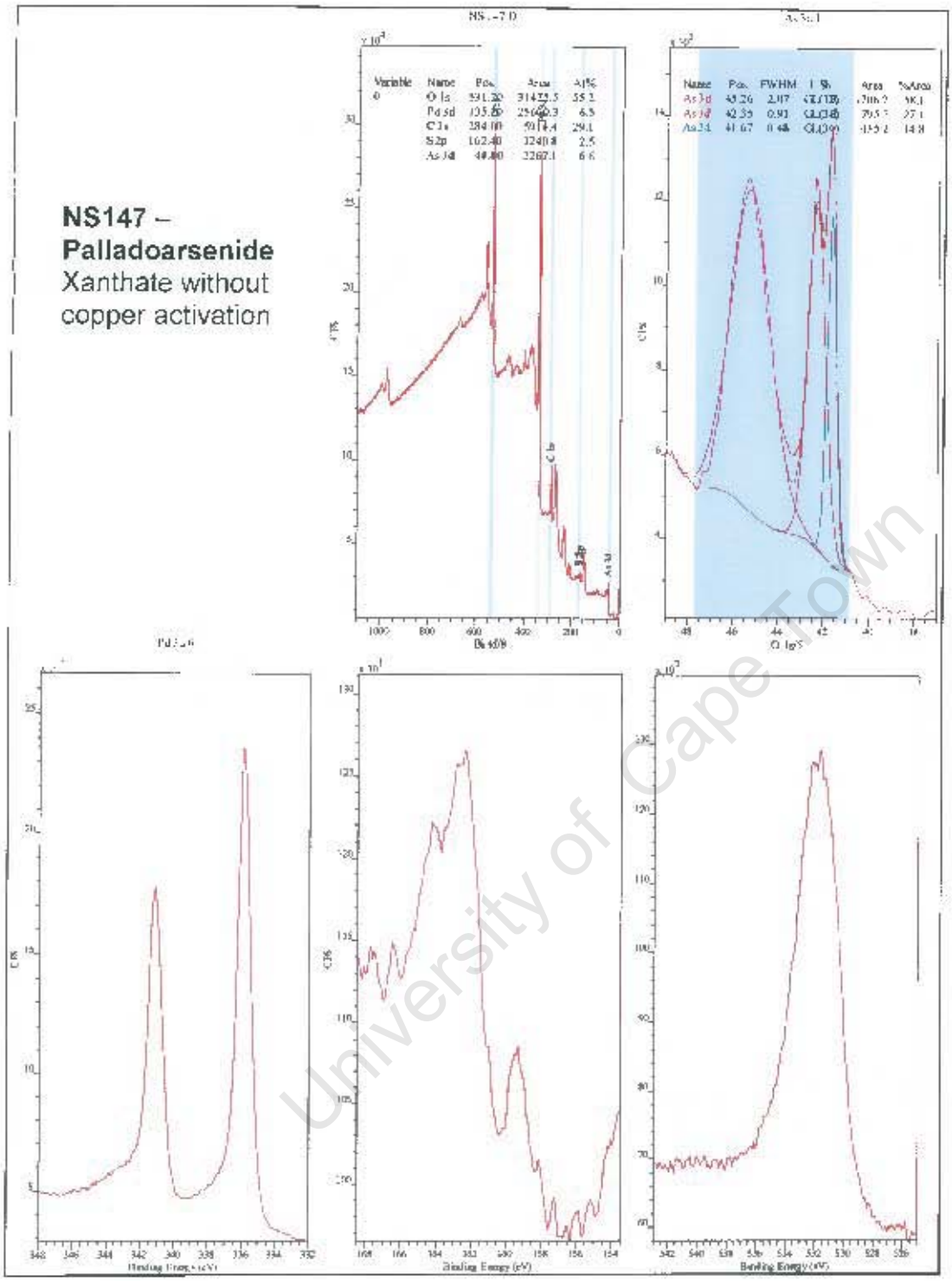

Sample NS 142: Moncheite $PtPd(BiTe)_2$.

NS142-1. Synthetic water conditioning.

- The elemental percentages (survey spectrum; error +-10% of each) indicate **Pt, Te, Bi and Pd** with some oxygen and carbon species.

University of Cape Town

- The symthetic water formulation contains Na, Mg, Ca, bicarbonate, Cl, nitrate and sulfate ions. None of these are significantly detected although the S of sulfate is difficult to resolve from the Bi signals near 164eV. There may be minor Mg surface concentration (Mg 2p overlapped with Pt 4f) but there is no significant evidence of Mg 2s signal. **These ions do not appear to be strongly adsorbed from the synthetic water.**
- No Cu or S (as S 2s signal) is detected.
- The Te $3d_{5/2}$ signal has 2 components at 573.2 and 575.7 eV likely to be from a telluride **and an oxidized species (e.g. TeO_4 ion or $Te(OH)_2$)** respectively.
- This is consistent with the O 1s signal with both oxide and hydroxide components at 529.9 and 531.2 eV resp.
- The Bi 4f signal, overlapped with the S 2p region, appears to have both oxidized Bi(III) (158.2 eV) and more reduced Bi (I) or Bi(0) (157.2 eV) components **again indicating some surface oxidation**.
- The Pt $4f_{7/2}$ signal appears to be **Pt(II) at 72.3eV.** There is no significant indication of more than one chemical state for the Pt.
- The Pd surface concentration is small and the Pd 3d is overlapped with the strong Pt 4d doublet. The Pd 4p was used for quantitation but was too weak for reliable speciation.
- The C 1s appears to be ubiquitous hydrocarbon contamination uncharged at 284.9 eV.

NS142-2. Copper activation.

- Copper is detected in the survey spectrum at 0.8%. **This is a relatively low surface concentration for activation**; 1.5% is usually sufficient for effective copper activation in plant samples.
- The C 1s hydrocarbon is shifted to 283.9 eV.
- The Cu 2p region shows that almost all of this is in the form of Cu(II). The curve fit gives **99% Cu(II)**. Hence, the formation of precipitated, probably colloidal, $Cu(OH)_2$ is the main species identified on this surface. No significant reduction to Cu(I) has occurred in the adsorption process.
- There are no significant changes in the speciation of the Te, O, Bi or Pt signals. There does not appear to have been significant interaction of the adsorbed Cu with these species.

NS142-3. Xanthate addition after copper activation.

- Copper is still present at 0.7% of the surface composition and a small signal is detected (0.3%) in the S 2s region corresponding to some xanthate adsorption.
- **The chemical state of the copper has changed slightly from 99% Cu(II) to 94% Cu(II) with 6% Cu(I) as seen in the Cu 2p spectra. Hence, the addition of the xanthate has reduced some of the Cu(II) with corresponding production of some oxidized dixanthogen. However, the surface concentrations of both Cu(I) and xanthate S are low.**
- There are again no significant changes in the Te, O, Bi or Pt spectra, i.e. no significant reaction with the copper or xanthate ions.

University of Cape Town

- The C 1s appears to be ubiquitous hydrocarbon contamination uncharged at 285.0 eV. There is no obvious increase in the higher BE shoulder near 288 eV that might correspond to the carbon atoms from the small adsorbed xanthate concentration.

NS142-4. Xanthate addition without copper activation.

- No Cu is detected in the survey spectrum but **a small S 2s concentration (0.6%) is recorded.** This survey concentration estimate carries a large uncertainty. The more direct comparison is probably the area estimates from the S 2s regions. For the copper-xanthate system, the area estimate is 240 c/s compared with the xanthate alone at 370 c/s. The curve fits will show, however, that both estimates from this small concentration are subject to background selection with probably >20% error.
- Comparison of the spectra with NS142-3 shows that there may be additions to the high BE shoulders in the O 1s and C 1s regions but that these intensity increases are not large.
- There is again no significant change in Te or O signals but obvious broadening of the Bi and Pt signals. This may be due to charge broadening since the C 1s is shifted to 528.3 eV but, if so, it has affected the Pt and Bi sites more than the Te or O sites.

University of Cape Town

NS142 –
Moncheite
Synthetic water conditioning

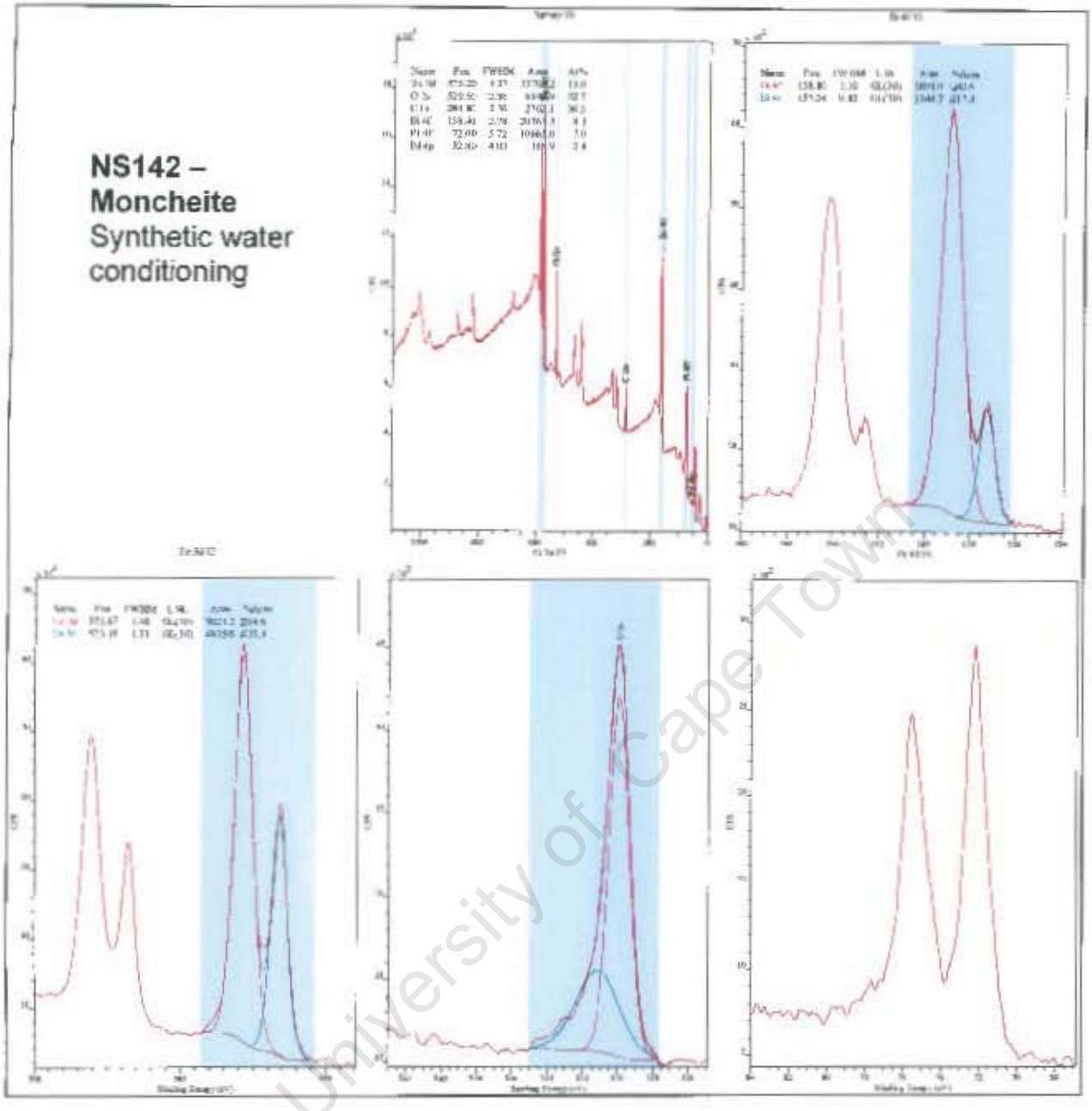

University of Cape Town

NS142 –
Moncheite
Copper activation

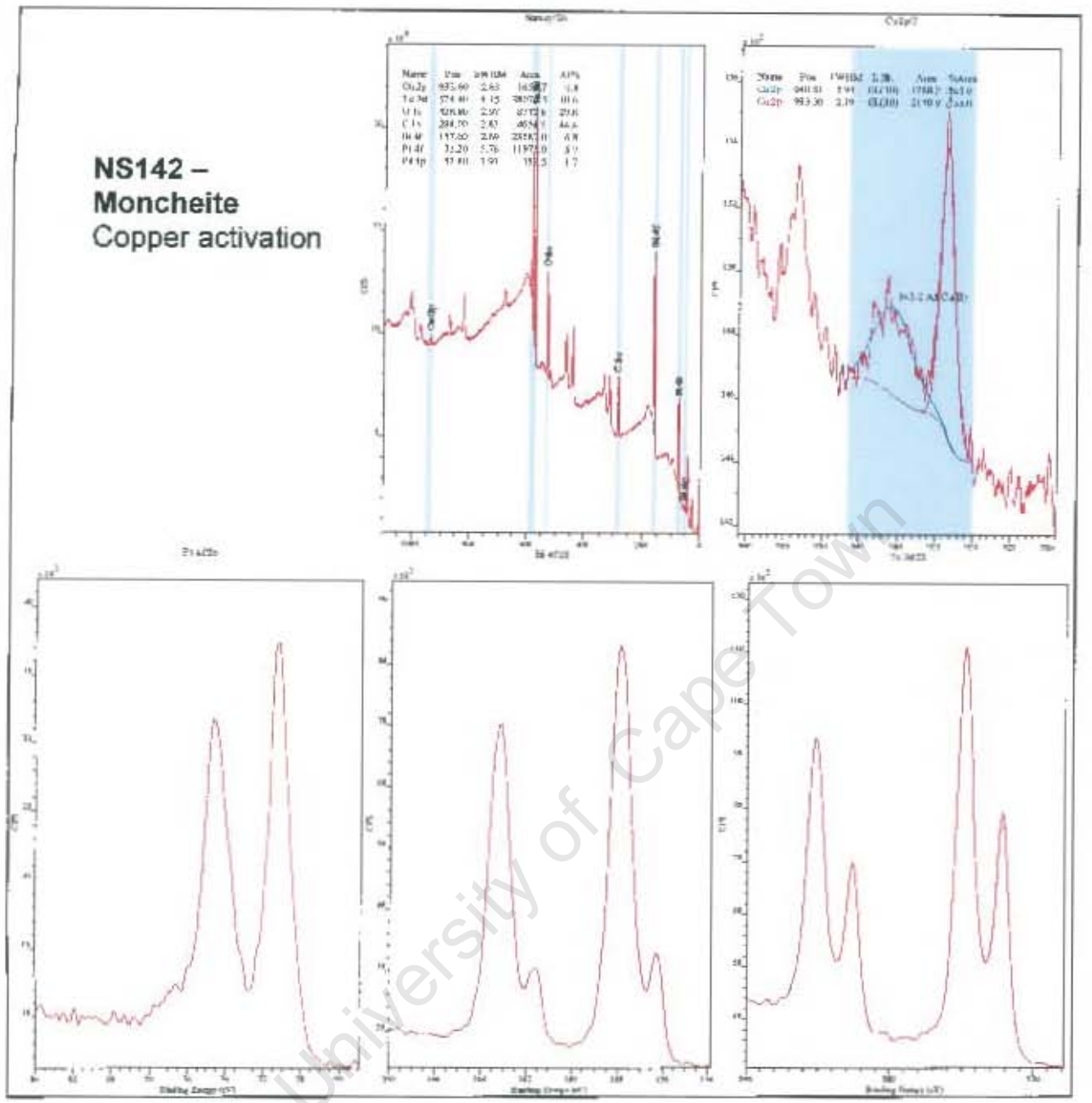

University of Cape Town

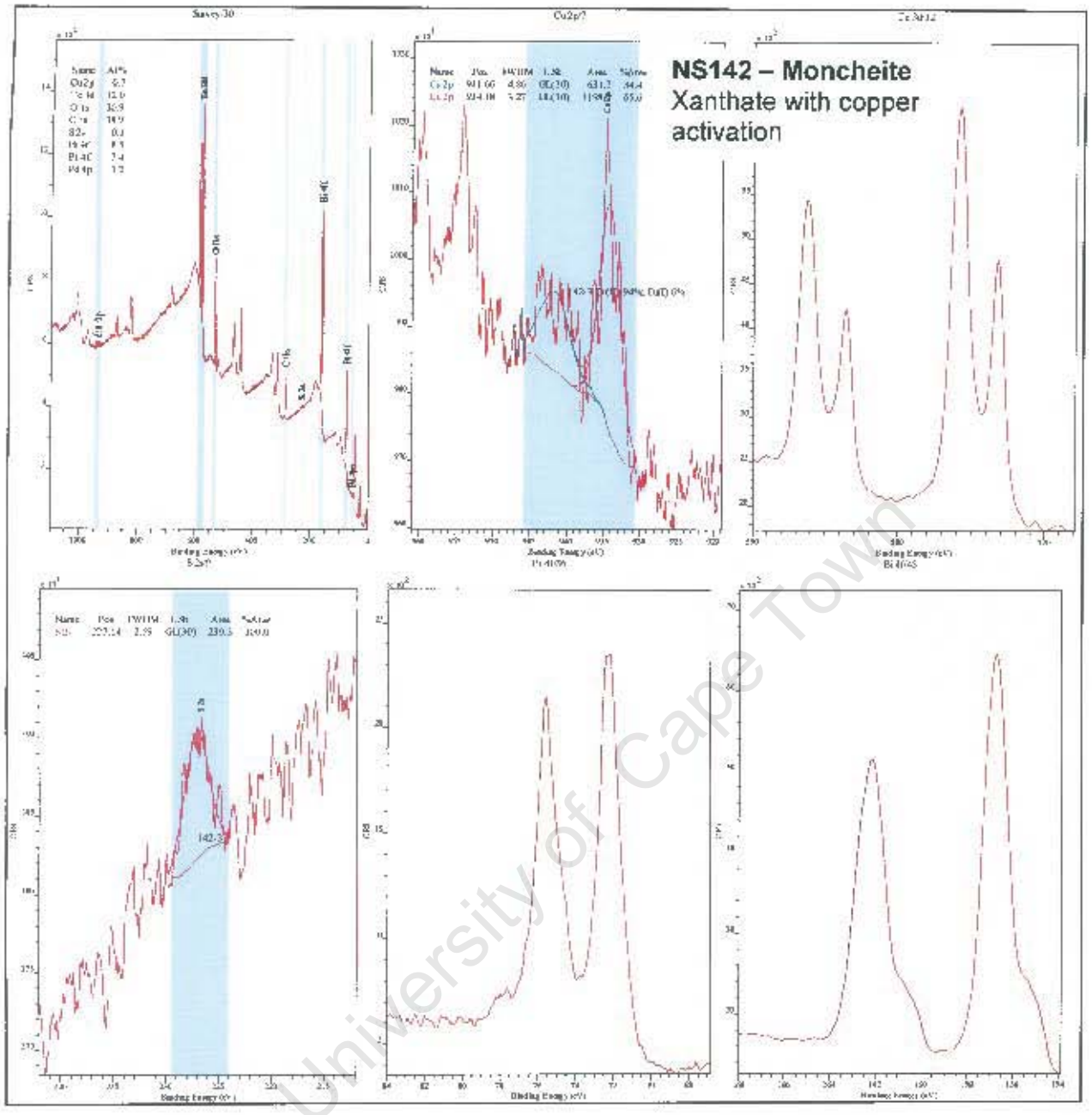

University of Cape Town

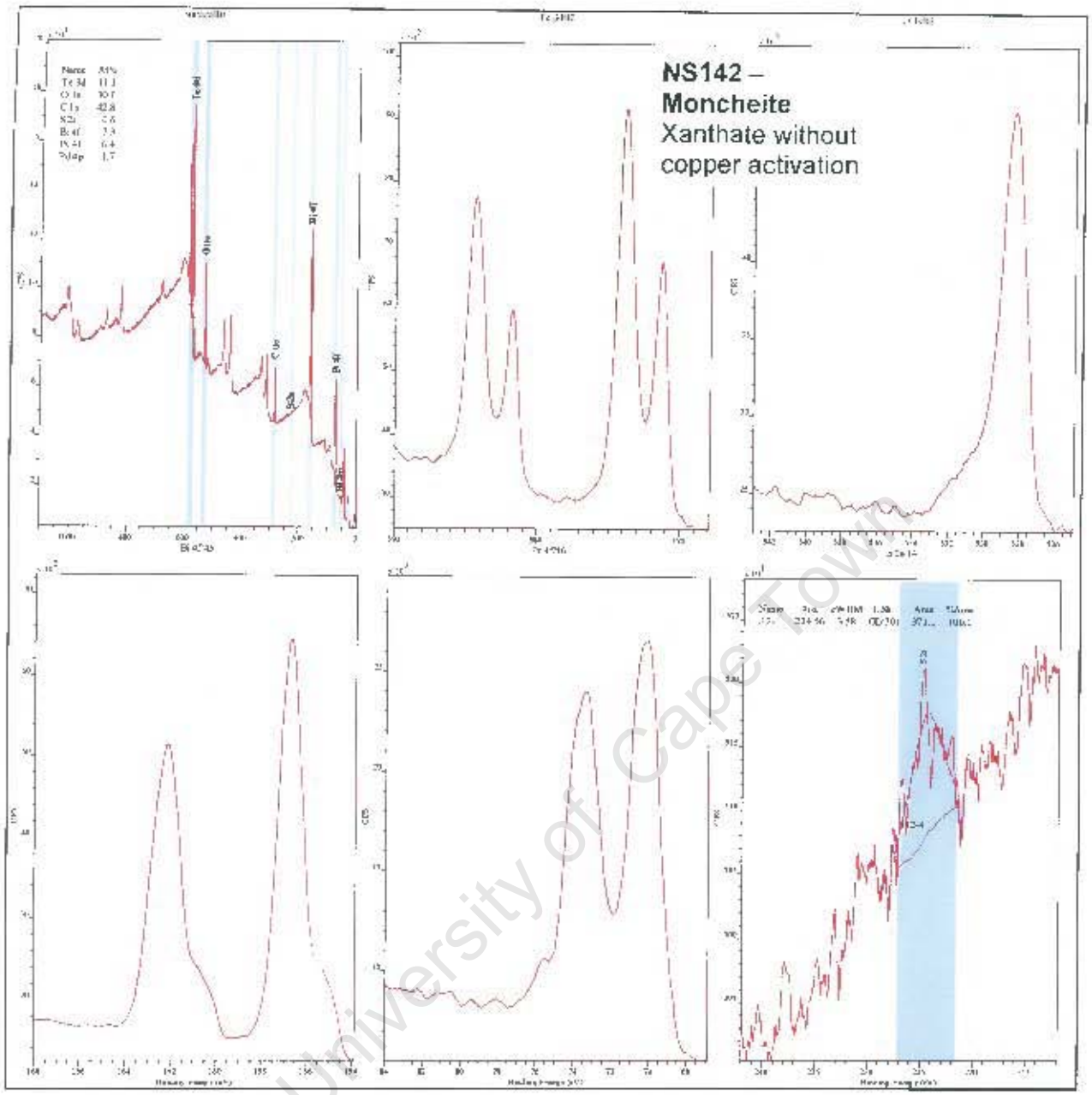

University of Cape Town

Sample NS 153: Moncheite $PtTe_2$

NS153-1. Synthetic water conditioning.

The elemental percentages (survey spectrum; error +-10% of each)) indicate **Pt and Te** with some oxygen and carbon species. The %O in this surface is much less (~2/3) than for Sample 142.

- None of the SYNTHETIC WATER ions are significantly detected. There may be minor Mg surface concentration (Mg 2p overlapped with Pt 4f) but there is no significant evidence of Mg 2s signal. **These ions do not appear to be strongly adsorbed from the synthetic water.**

- No Cu or S is detected.
- The C 1s, like Sample 142, appears to be ubiquitous hydrocarbon contamination uncharged at 284.9 eV.
- The Te $3d_{5/2}$ signal, like Sample 142, has 2 components at 573.2 and 575.7 eV likely to be from a telluride and an oxidized species (e.g. TeO_4 ion or $Te(OH)_2$) respectively. **But the ratio of these two species is very different between 142 (35:65) and 153 (60:40). Hence, this sample appears to be less oxidized after synthetic water reaction.**
- The O 1s signal has both oxide and hydroxide components at 529.9 and 531.2 eV resp.
- The Pt $4f_{7/2}$ signal still appears to be **Pt(II) at slightly higher BE of 72.8eV.** There is no significant indication of more than one chemical state for the Pt.

NS153-2. Copper activation.

- **Copper is detected in the survey spectrum at 1.0%. This is still a relatively low surface concentration for activation.**
- The C 1s hydrocarbon is uncharged at 284.8 eV.
- The Cu 2p region shows that all of this is in the form of Cu(II). The curve fit gives **100% Cu(II)**. Hence, the formation of precipitated, probably colloidal, $Cu(OH)_2$ is the main species identified on this surface. No significant reduction to Cu(I) has occurred in the adsorption process.
- There are no significant changes in the speciation of the Te, O or Pt signals. There does not appear to have been significant interaction of the adsorbed Cu with these species.

NS153-3. Xanthate addition after copper activation.

- Copper is still present at 0.7% of the surface composition and **a new S 2p signal is detected (2.8%) near 163 eV BE corresponding to xanthate adsorption**. The higher BE broad peak above the S 2p from the xanthate is from a Te 4s signal which overlaps any sulfate signal.
- The C 1s appears to be ubiquitous hydrocarbon contamination slightly charged at 285.2 eV. There is an obvious increase in the higher BE shoulder near 288.5 eV that might correspond to the carbon atoms from the adsorbed xanthate concentration.
- The O 1s spectrum also has an obvious high BE addition probably from the C-O-S groups of the adsorbed xanthate.
- **The chemical state of the copper has changed from 100% Cu(II) to 64% Cu(II) with 36% Cu(I) in distinct forms as seen in the Cu 2p spectra. The separation of the two Cu(I) and Cu(II) contributions to the main peak is probably due to differential charging of the more insulating $Cu(OH)_2$. Hence, the addition of the xanthate has reduced much more of the Cu(II) with corresponding production of oxidized dixanthogen. However, the surface concentrations of both Cu(I) and xanthate S are low.**
- There are significant changes in the Te and Pt spectra. The Te $3d_{5/2}$ component at 575.7 eV likely to be from an oxidized species (e.g. TeO_4 ion or $Te(OH)_2$) has reduced in relative intensity. **Hence, this sample appears to be have less oxide/hydroxide after xanthate addition. This is consistent with the well-known ability of**

University of Cape Town

collectors to displace attached oxidation products from surfaces in competitive adsorption (Smart et al., 2003).

- The S 2p peak is broad and undifferentiated suggesting more than just the xanthate species but it may also be due to differential charge broadening.
- The Pt $4f_{7/2}$ has shifted slightly to lower BE (72.5 eV) after xanthate adsorption.

NS153-4. Xanthate addition without copper activation.

- No Cu is detected in the survey spectrum but **a distinct S 2p concentration (3.8%) is recorded.**
- Comparison of the spectra with NS153-3 shows that there is again addition to the high BE shoulder in the O 1s regions consistent with xanthate adsorption. However, this is not obvious in the C 1s spectrum.
- The Te $3d_{5/2}$ component at 575.7 eV likely to be from an oxidized species (e.g. TeO_4 ion or $Te(OH)_2$) has reduced in peak intensity and broadened. **Hence, this sample also appears to be have less oxide/hydroxide after xanthate addition. This is consistent with the well-known ability of collectors to displace attached oxidation products from surfaces in competitive adsorption (Smart et al., 2003).**
- The S 2p peak is again broad and undifferentiated suggesting more than just the xanthate species but it may also be due to differential charge broadening as seen in the Te and O spectra.
- Comparing the relative intensities of the xanthate S with and without copper activation **suggests that more xanthate is adsorbed in this no-copper case.** A fit to the complete S 2p envelope gives 960 c/s for 153-3 with 1780 c/s for this 153-4 sample. This is consistent with the %S from the survey spectrum.

University of Cape Town

NS153 –
Moncheite
Synthetic water conditioning

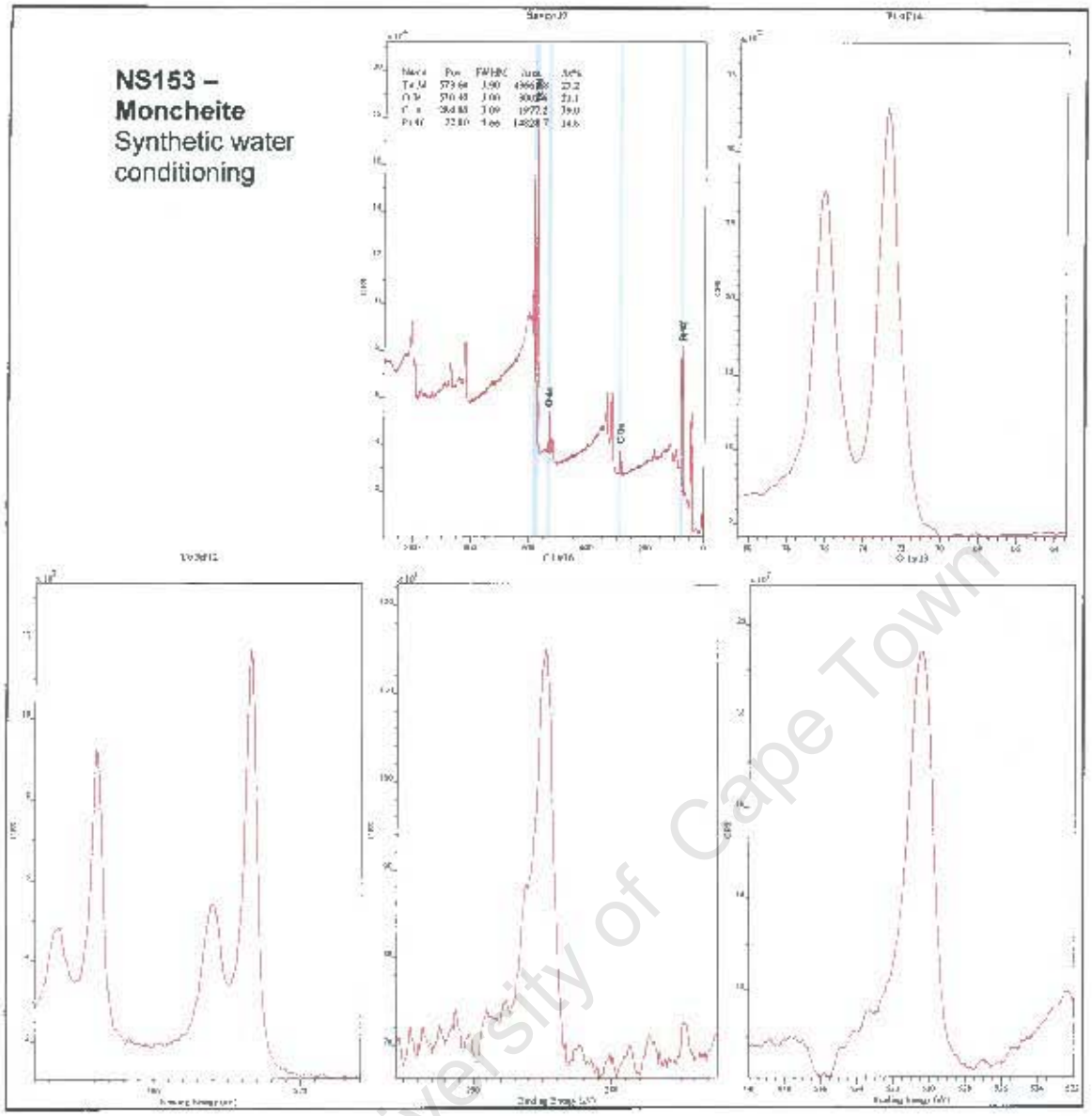

University of Cape Town

NS153 –
Moncheite
Copper activation

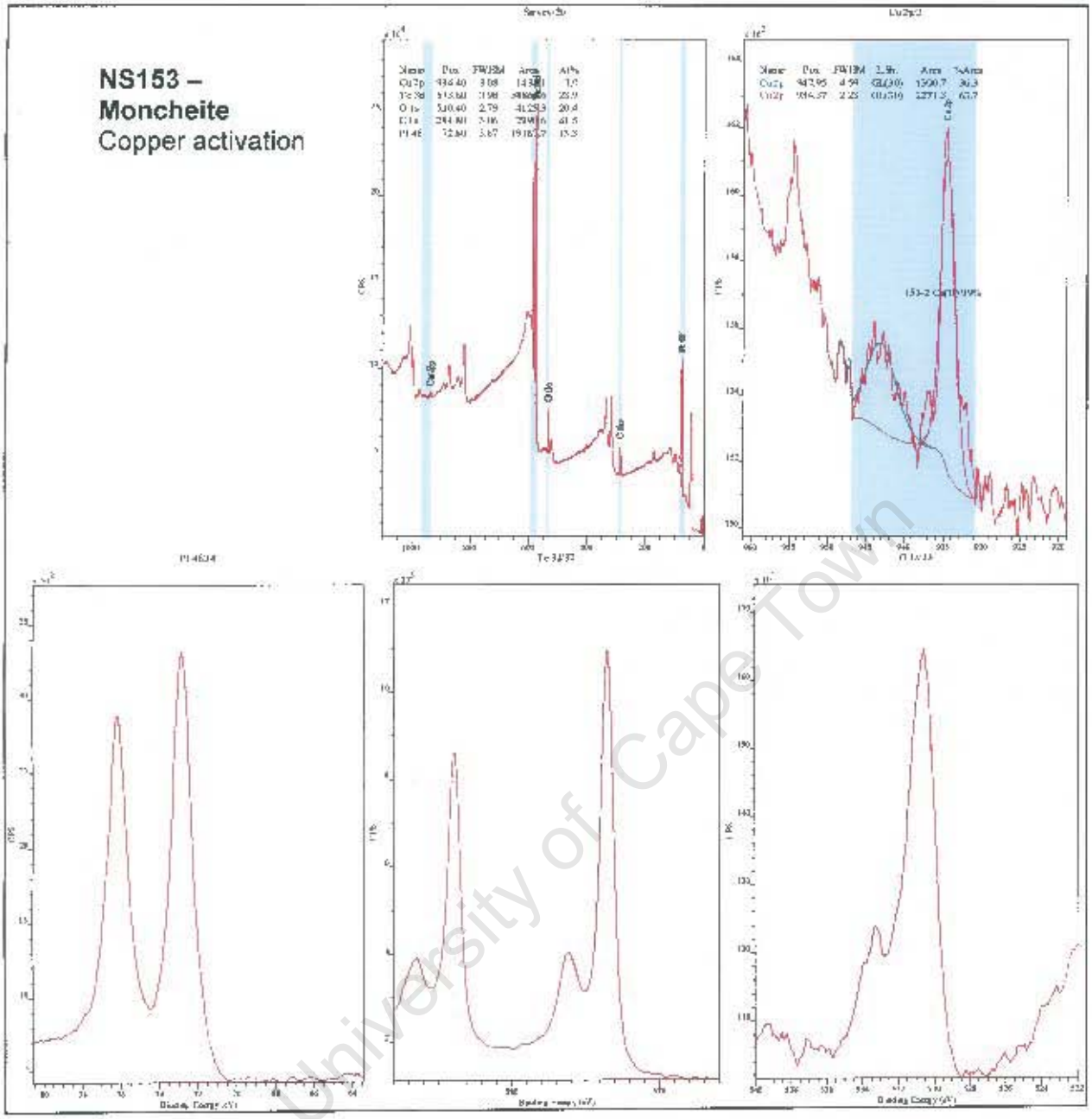

University of Cape Town

NS153 – Moncheite
Xanthate with
copper activation

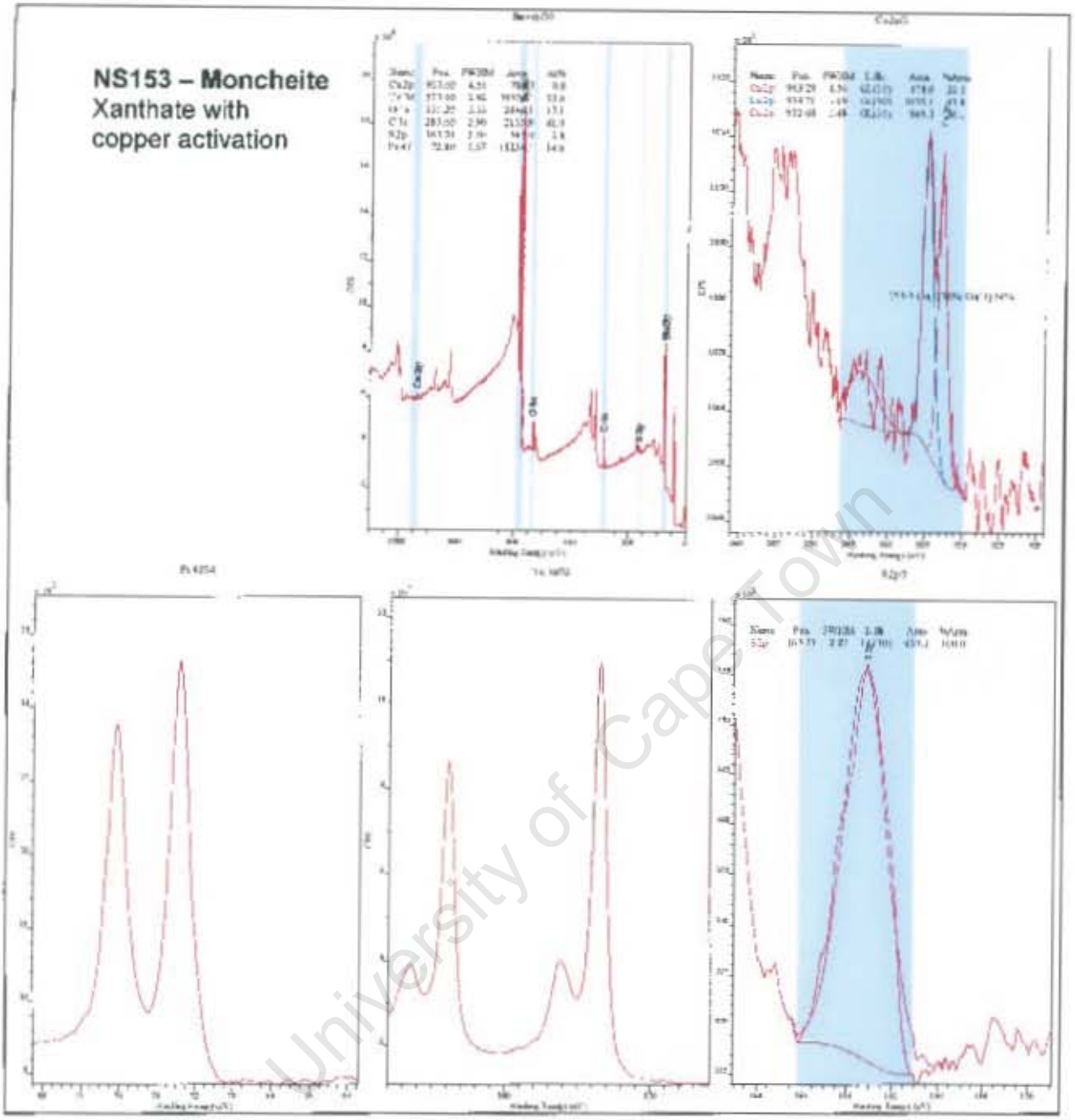

University of Cape Town

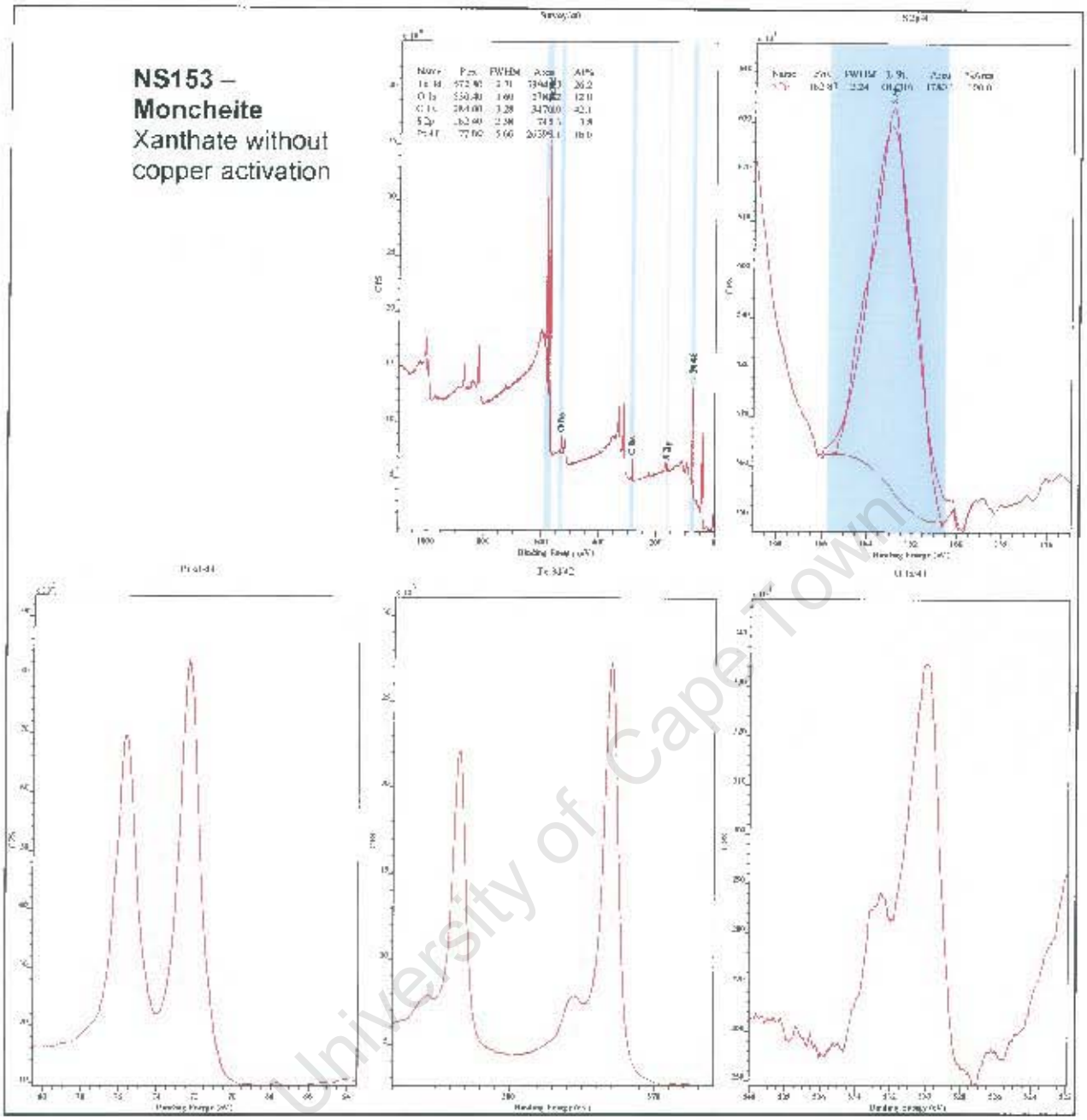

Sample NS 143: Merenskyite $PdPt(BiTe)_2$.

The survey spectra compositions have errors of ±10% in each estimate. In this sample, these values are likely to have underestimated the Bi concentrations and overestimated Pt concentrations by similar percentages due to overlapping signals.

NS143-1. Synthetic water conditioning.

The elemental percentages indicate extensive oxidation of these surfaces with predominantly oxidized Te species and low concentrations of exposed **Pd, Bi and Pt** (and hydrocarbon

University of Cape Town

species). Surface exposure of Bi and Pt is surprisingly low, obscured by the oxidized Te species.

- The (Amandelbult) Standard Plant Water formulation contains Na, Mg, Ca, bicarbonate, Cl, nitrate and sulfate ions. None of these are significantly detected. **These ions do not appear to be strongly adsorbed from the synthetic water.**
- No Cu or S (as S 2s signal) are detected.
- The C 1s appears to be ubiquitous hydrocarbon contamination uncharged at 284.7 eV.
- The Te $3d_{5/2}$ signal has 2 components at 573.0 and 576.0 eV likely to be from a telluride (44%) **and an oxidized species (e.g. TeO_4 ion or $Te(OH)_2$)** (56%) respectively.
- This is consistent with the O 1s signal with both ionic oxide and hydroxide or covalent oxide components at 530.0 and 532.6 eV resp.
- The Bi 4f signal appears to have three components: oxidized Bi(V) as in BiO_3 (159.0 eV) (72%), Bi(III) as in Bi_2O_3 (157.1 eV) (25%) and minor more reduced Bi as in $PdPtBi_2$ (156.1 eV) (3%) **again indicating extensive surface oxidation**.
- The weak Pt $4f_{7/2}$ signal appears to be Pt(II) at 72.3eV but not as the oxide PtO (74.2 eV). There is no significant indication of more than one chemical state for the Pt. This signal does not change through the conditioning sequence.
- The single Pd $3d_{5/2}$ signal is at 336.0 eV corresponding to an oxidized species like PdO. This signal also does not change through the sequence.

NS143-2. Copper activation.

- Copper is detected in the survey spectrum at **1.1%. This is a relatively low surface concentration for activation**; 1.5% is usually sufficient for effective copper activation in plant samples but it needs to be as Cu(I) species.
- The lower oxygen concentration is probably due to the higher hydrocarbon contamination on this surface.
- The C 1s hydrocarbon is uncharged at 284.7 eV.
- The Cu 2p region shows that almost all of this is in the form of Cu(II). The curve fit gives **87% Cu(II)**. Hence, the formation of precipitated, probably colloidal, $Cu(OH)_2$ is the main species identified on this surface.
- There are no significant changes in the speciation of the Te, O, Pd, Bi or Pt signals. **There does not appear to have been significant interaction of the adsorbed Cu with these species.**

NS143-3. Xanthate addition after copper activation.

- Copper is still present at 0.9% of the surface composition and **a small signal is detected (1.1%) in the S 2s region corresponding to some xanthate adsorption.**
- **The chemical state of the copper has changed slightly from 87% Cu(II) to 70% Cu(II) with 30% Cu(I) as seen in the Cu 2p spectra. Hence, the addition of the xanthate has reduced some of the Cu(II) with corresponding production of some oxidized dixanthogen. However, the surface concentrations of both Cu(I) and xanthate S are low.**
- There is a relative increase in the O 1s signal near 532 eV corresponding to xanthate oxygen species.

University of Cape Town

- There are again no significant changes in the Te or Pt spectra, i.e. no significant reaction with the copper or xanthate ions.
- There is a slight increase in the Bi signal corresponding to the $PtPd(BiTe)_2$ surface possibly indicating some surface cleaning action of the xanthate, i.e. oxidised product removal.
- The C 1s appears to be ubiquitous hydrocarbon contamination almost uncharged at 284.6 eV. There is no obvious increase in the higher BE shoulder near 288 eV that might correspond to the carbon atoms from the small adsorbed xanthate concentration.

NS143-4. Xanthate addition without copper activation.

- No Cu is detected in the survey spectrum but **a small S 2s concentration (0.7%) is recorded.** This survey concentration estimate carries a large uncertainty. The more direct comparison is probably the area estimates from the S 2s regions. For the copper-xanthate system, the area estimate is 361 c/s compared with the xanthate alone at 319 c/s. The curve fits will show, however, that both estimates from this small concentration are subject to background selection with probably >20% error.
- The C 1s appears to be ubiquitous hydrocarbon contamination at 284.6 eV.
- The Te signal has a relative increase in the low BE component corresponding to the telluride species indicating surface cleaning. This is consistent with the lower O%.
- Comparison of the spectra with NS142-3 shows that there may be additions to the high BE shoulders in the O 1s and C 1s regions but that these intensity increases are not large.
- There is again no significant change in Pd or Pt signals.

University of Cape Town

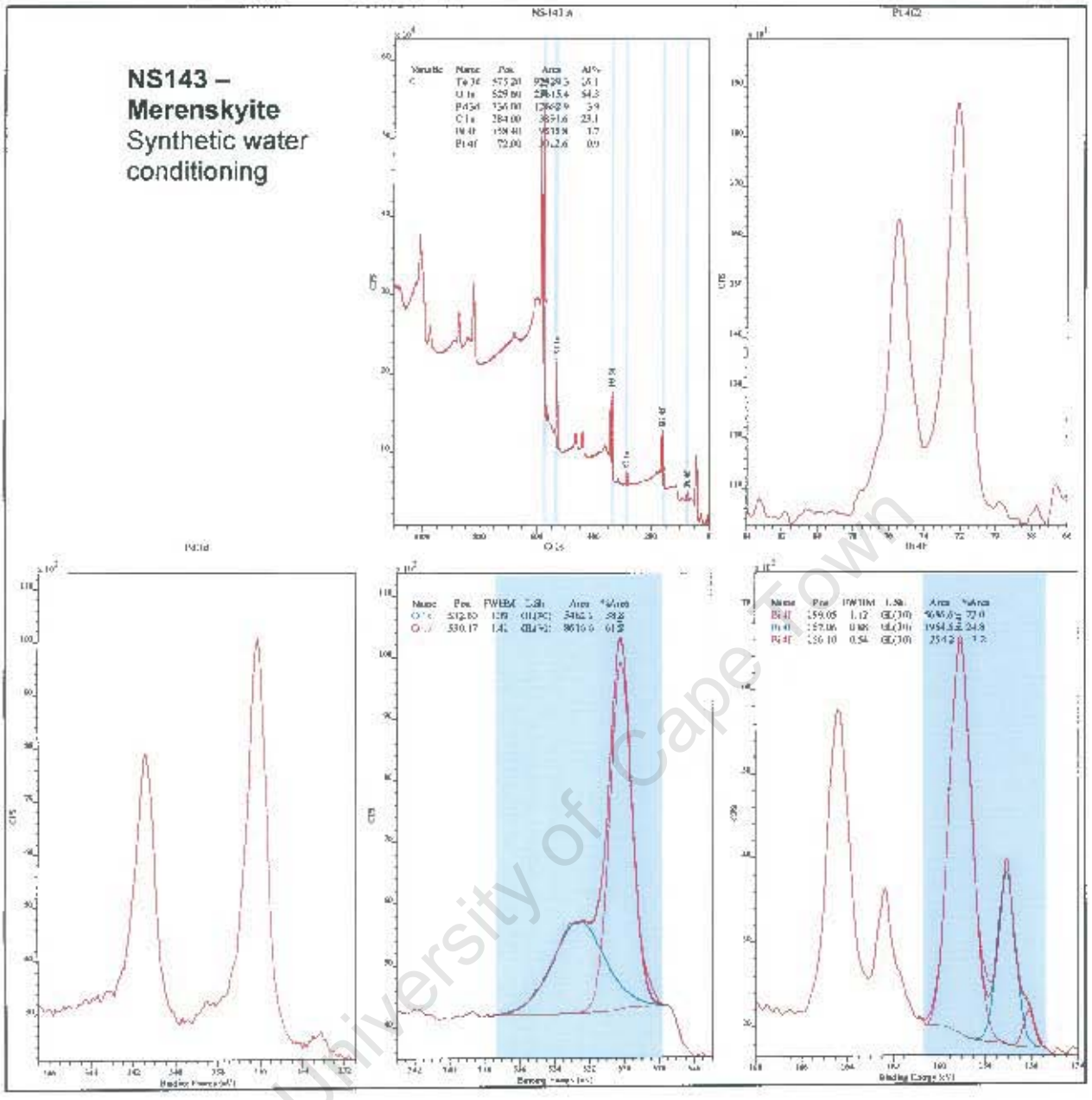

University of Cape Town

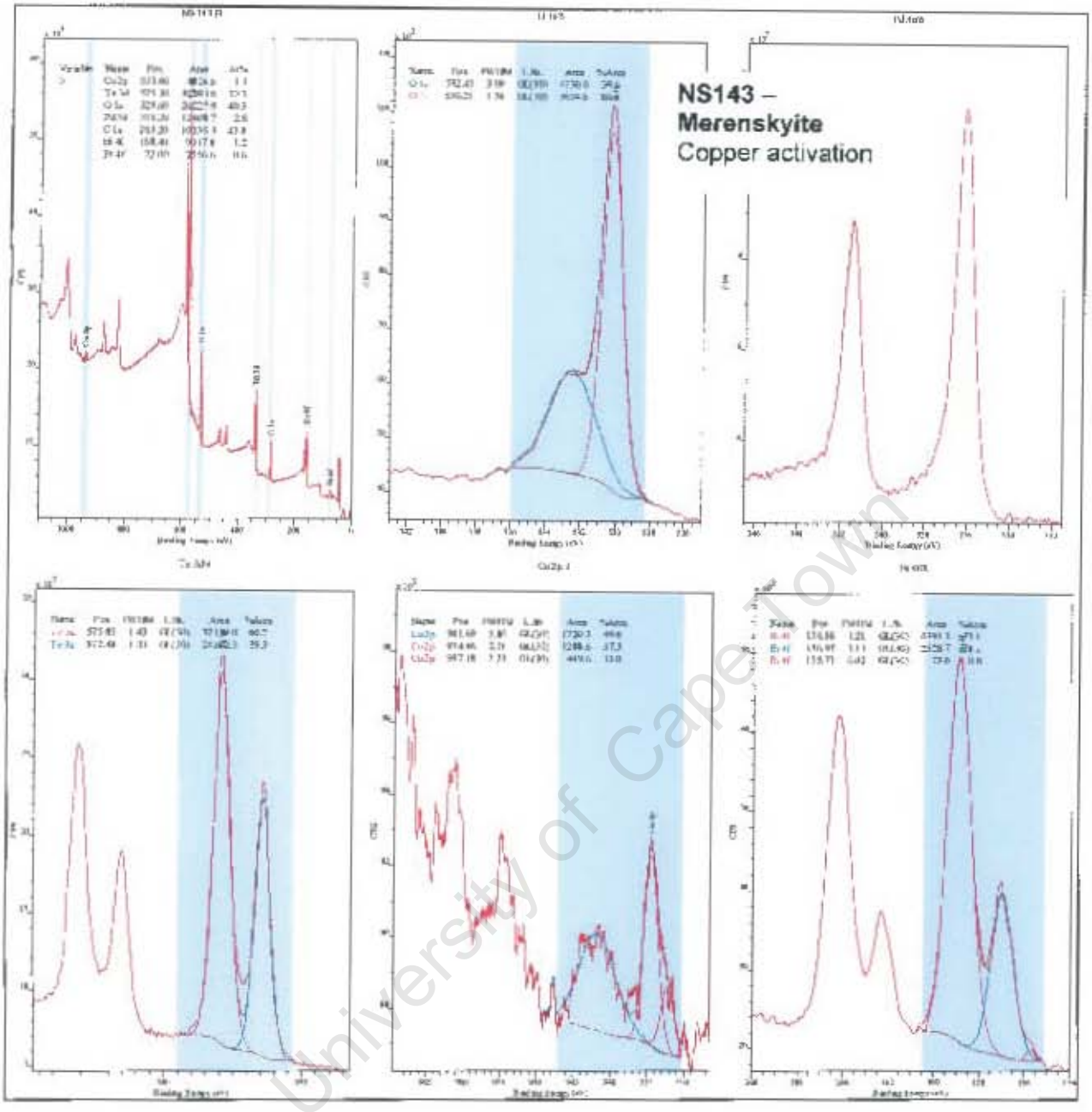

University of Cape Town

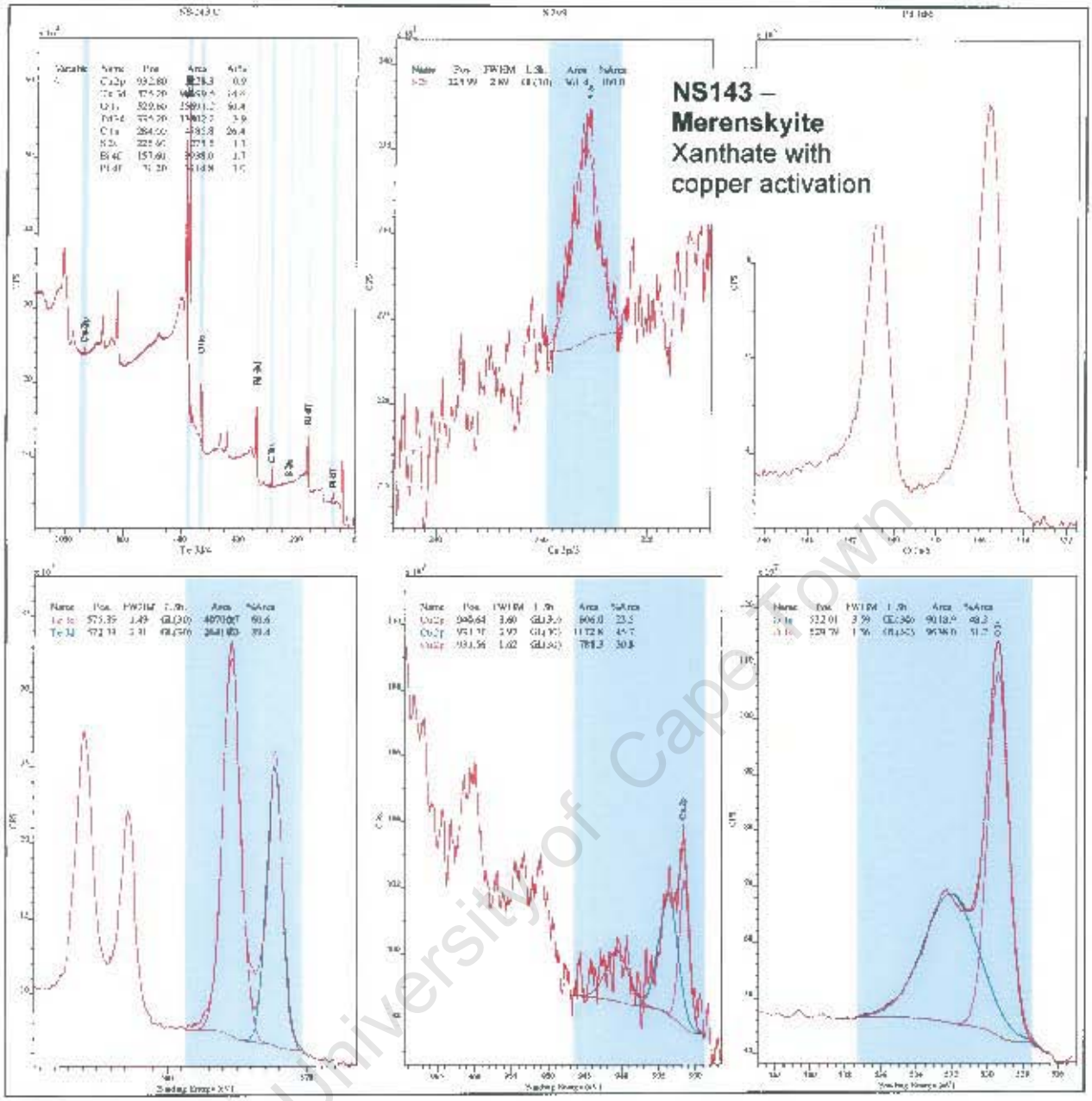

University of Cape Town

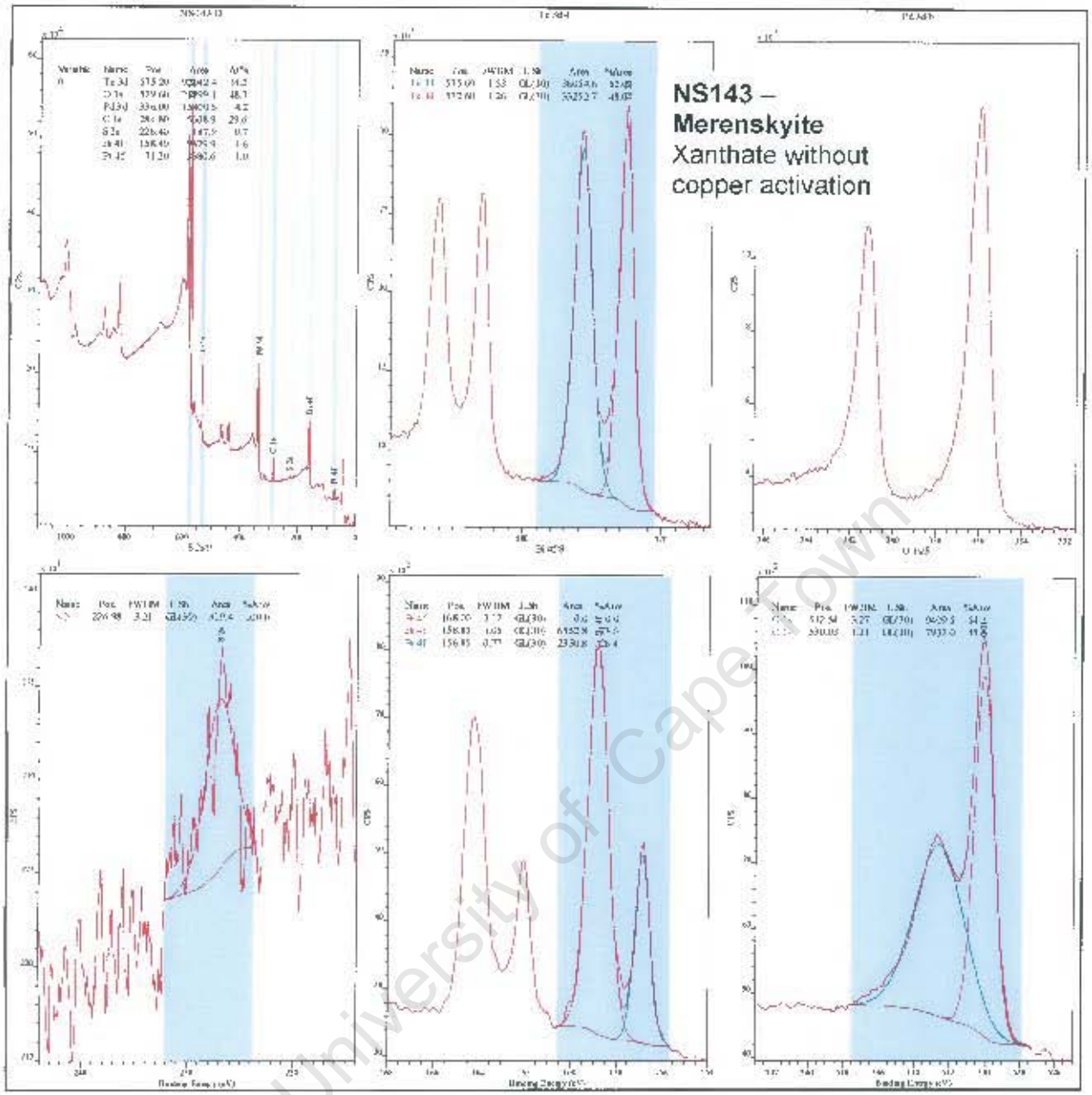

University of Cape Town

Sample NS 152: Merenskyite $PdTe_2$

NS152-A. Synthetic water conditioning.

- The elemental percentages (survey spectrum; error +-10% of each)) indicate **Pd and Te** with some oxygen and carbon species only but again the sample is heavily oxidised (59% O) in this surface.
- None of the synthetic water ions are significantly detected. **These ions do not appear to be strongly adsorbed from the synthetic water.**
- No Cu or S is detected.

- The C 1s appears to be ubiquitous hydrocarbon contamination with possibly two charge states at 284.3 and 286.0 eV.
- The Te $3d_{5/2}$ signal has 3 components at 572.8, 573.5 and 576.0 eV likely to be from a telluride (56%), possibly charged telluride areas (33%), **and an oxidized species (e.g. TeO_4 ion or $Te(OH)_2$)** (11%) respectively.
- This is consistent with the O 1s signal with both ionic oxide and hydroxide or covalent oxide components at 530.2 (7%) and 533.0 (93%) eV resp.
- The single Pd $3d_{5/2}$ signal is at 336.0 eV corresponding to an oxidized species like PdO. This signal also does not change through the sequence.

NS152-B. Copper activation.

- **Copper is not detected in the survey spectrum or in the high resolution scan. It does not appear to adsorb to this mineral or is covered by oxidized products.**
- The C 1s hydrocarbon is at 284.4 eV now with a single charge state.
- The Te $3d_{5/2}$ signal has a distinct increase in the component at 576.0 eV likely to be from **an oxidized species (e.g. TeO_4 ion or $Te(OH)_2$)** (11 to 20%).
- There is also an increase in the lower BE O 1s signal likely to be associated with ionic oxide or hydroxide species.
- There are no significant changes in the speciation of the oxidized Pd signals.

NS152-C. Xanthate addition after copper activation.

- Copper is still not detected in the survey composition above about 0.1%.
- **New weak S 2p and S 2s signals are detected (0.8%) corresponding to xanthate adsorption**. The higher BE broad peak above the S 2p from the xanthate is from a Te 4s signal which overlaps any sulfate signal but the S 2s is a single peak which makes any sulfate unlikely.
- The C 1s appears to be ubiquitous hydrocarbon contamination slightly charged at 285.1 eV. There is a small increase in the higher BE shoulder near 288.5 eV that might correspond to the carbon atoms from the adsorbed xanthate concentration.
- The O 1s spectrum also has an obvious high BE addition (86% to 95%) probably from the C-O-S groups of the adsorbed xanthate. (The apparent reduction in O% is probably due to the increased C contamination in this sample.)
- There are significant changes in the Te spectra. The Te $3d_{5/2}$ component at 575.7 eV likely to be from an oxidized species (e.g. TeO_4 ion or $Te(OH)_2$) has reduced in relative intensity (20% to 10%). **Hence, this sample appears to be having less oxide/hydroxide after xanthate addition. This is consistent with the well-known ability of collectors to displace attached oxidation products from surfaces in competitive adsorption.**
- There are no significant changes in the speciation of the oxidized Pd signals.

NS152-D. Xanthate addition without copper activation.

- **Distinct but weak S 2p and S 2s spectra (1.2%) are recorded.**
- The C 1s appears to be ubiquitous hydrocarbon contamination at 284.6 eV.

University of Cape Town

- Comparison of the spectra with NS152-C shows that there is again addition to the high BE shoulder in the O 1s regions consistent with xanthate adsorption. This is also obvious in the C 1s spectrum.
- The Te $3d_{5/2}$ component at 575.7 eV likely to be from an oxidized species (e.g. TeO_4 ion or $Te(OH)_2$) is again reduced in peak intensity and broadened. **Hence, this sample also appears to be having less oxide/hydroxide after xanthate addition.**
- There are no significant changes in the speciation of the oxidized Pd signals.
- Comparing the relative intensities of the xanthate S 2s with and without copper activation **suggests that less xanthate is adsorbed in this no-copper case.** A fit to the complete S 2p envelope gives 480 c/s for 152-C with 130 c/s for this 152-D sample. These estimates are probably not sufficiently accurate to be reliable.

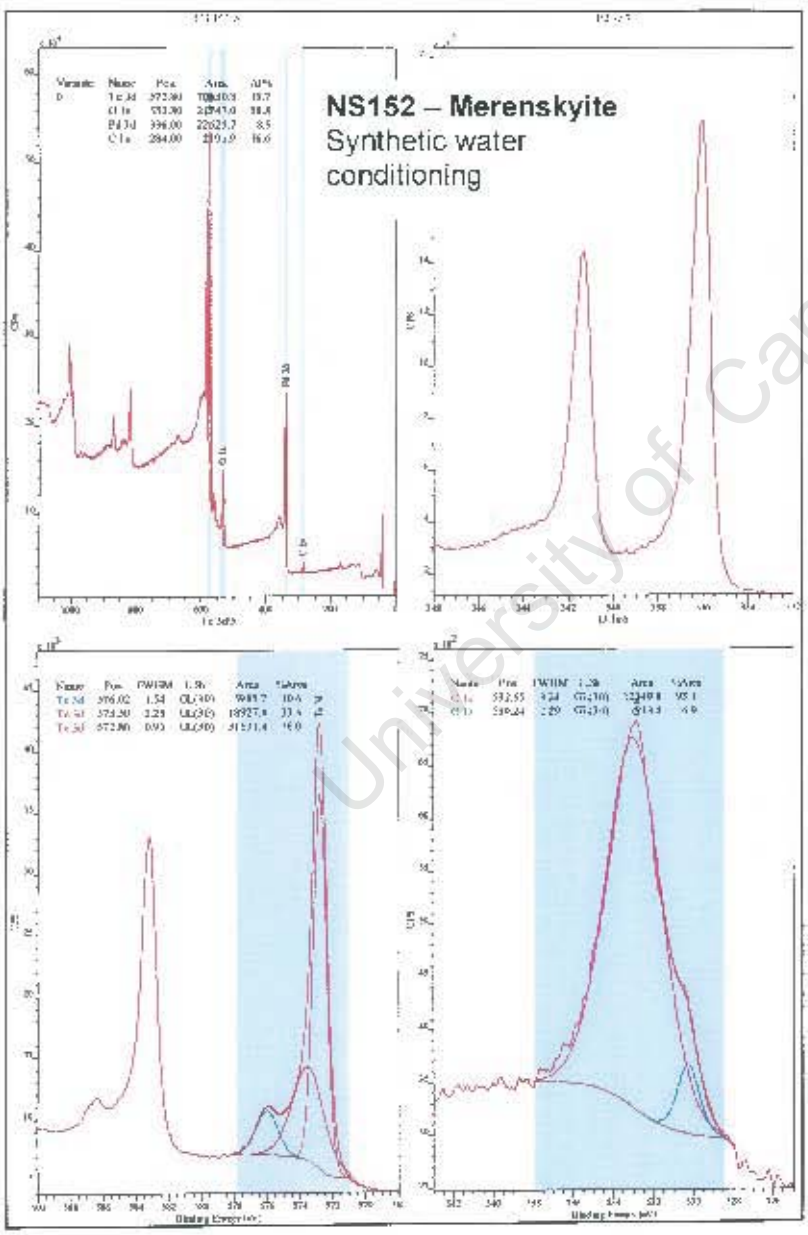

University of Cape Town

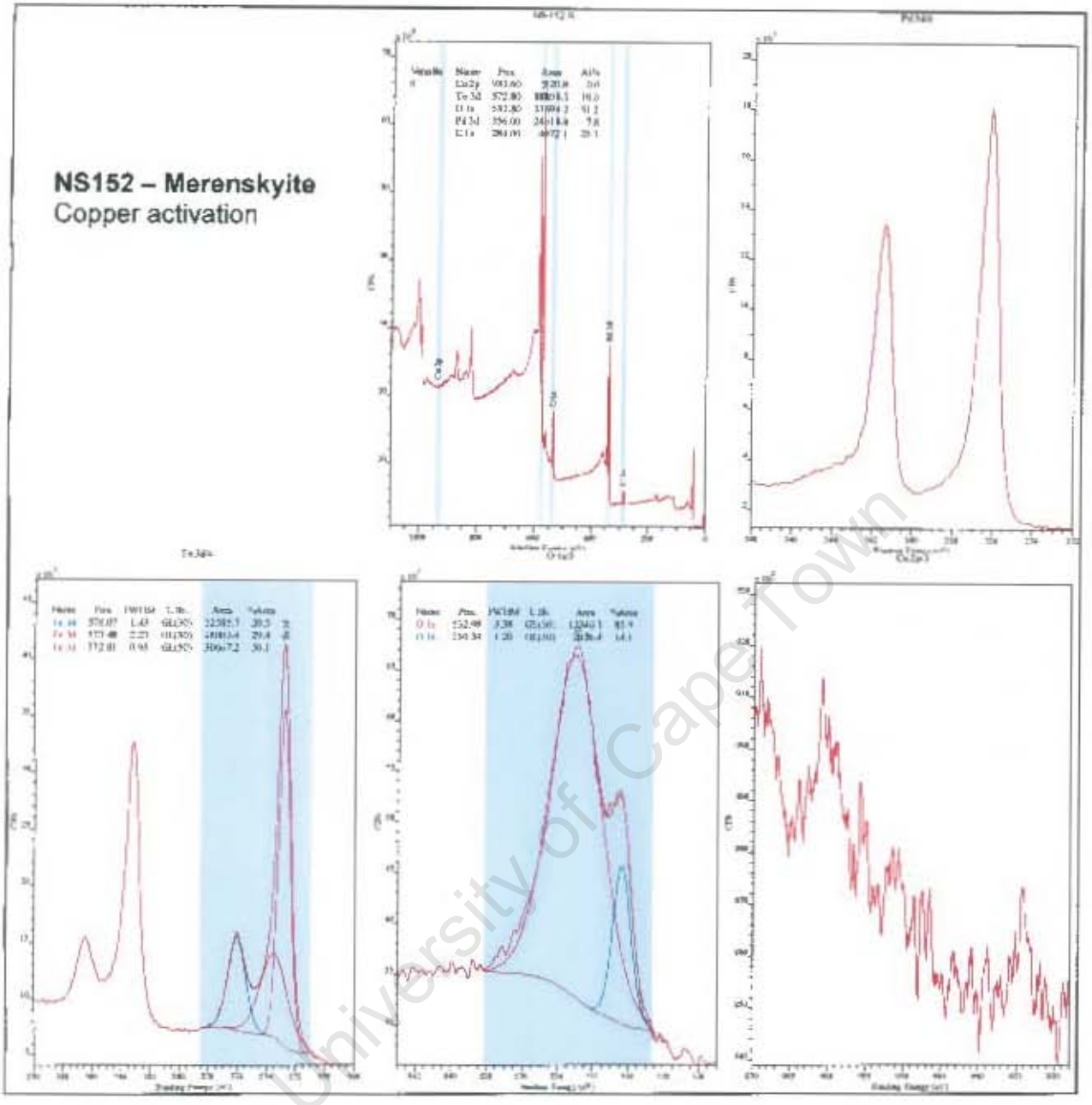

University of Cape Town

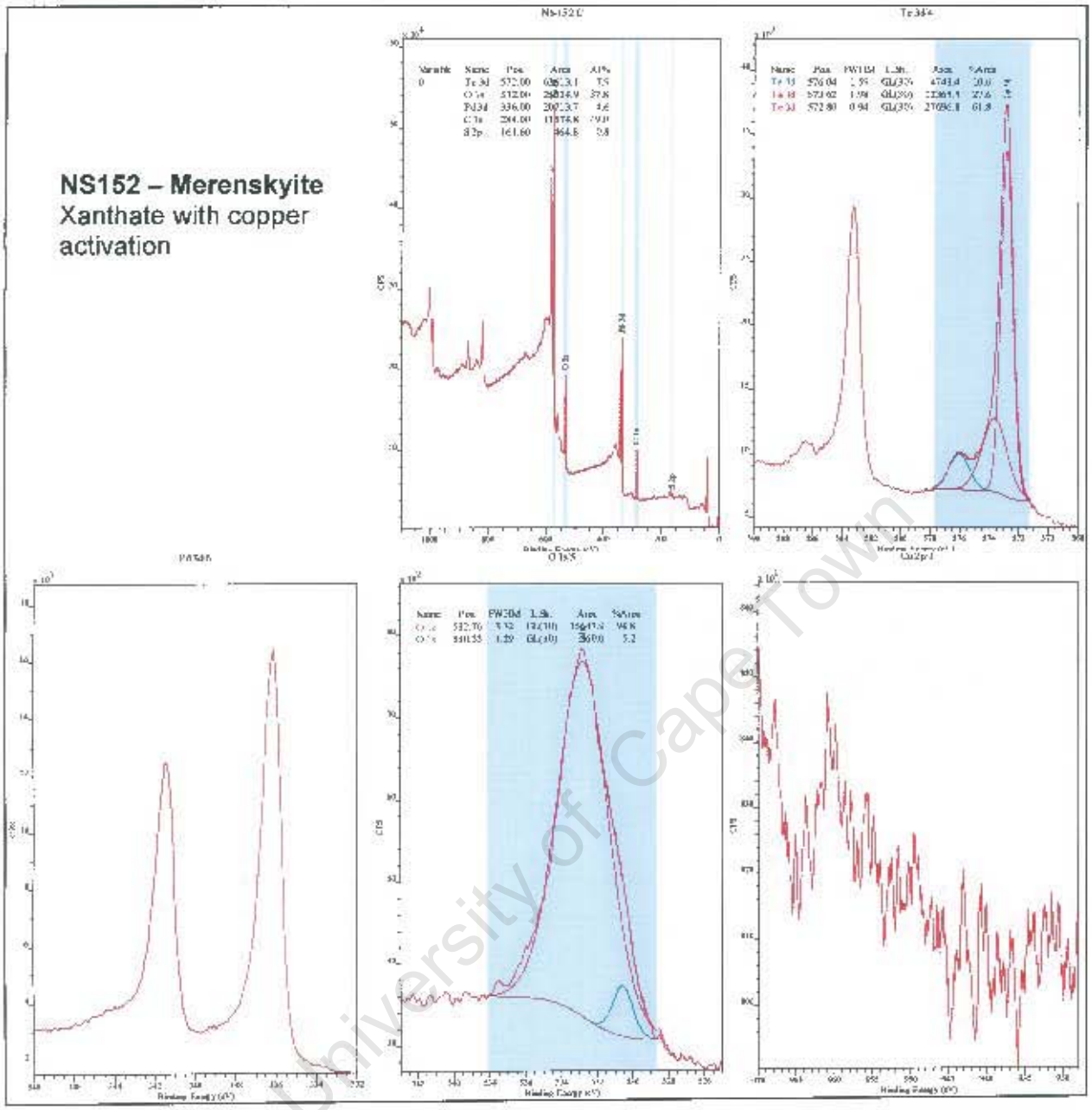

University of Cape Town

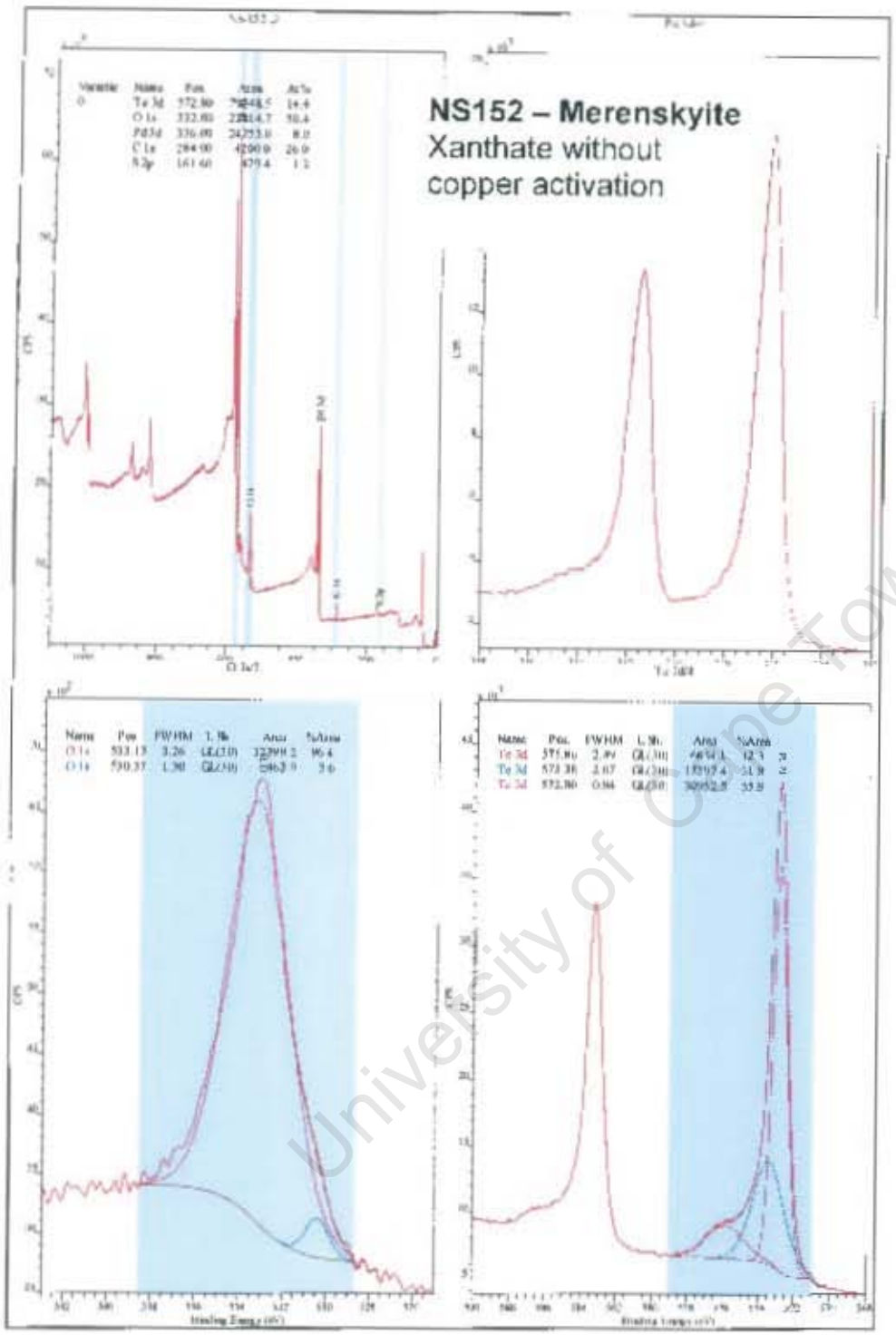

University of Cape Town